Development of Next Generation Methanol Synthesis Catalysts

Elaine Margaret Vass

PhD Thesis

Department of Chemistry

University of Glasgow

June 2005

June 2005

Summary

Copper and cerium containing alloys have been investigated previously for methanol synthesis and were found to be surprisingly active. After a pre-treatment in synthesis gas the alloys were highly active for the production of methanol from carbon monoxide and hydrogen. Investigation of the catalysts suggested that the active species involved a lanthanide hydride or small copper particles in close contact with a lanthanide oxide. However the initial high activity at low temperatures exhibited by the catalysts decreased rapidly in the presence of water or carbon dioxide. Attempts to improve the long-term stability of the catalysts were unsuccessful.

As a consequence, the main aim of this project was to re-visit the area of copper and cerium containing catalysts for use in the methanol industry. The goals were not only to prepare more robust copper/cerium catalysts, but also to further investigate the species that contributed to the high activity of the copper/cerium intermetallic catalysts.

Initially a series of copper and cerium catalysts supported on silica or alumina were prepared. The preparation method was chosen so as to maximise the metal dispersion over the support. Alternative precursors were explored in the early stages of the investigation; however for simplicity nitrate precursors were selected for the preparation process. The resulting catalysts were characterised using a variety of techniques, to gain a greater insight into the nature of the catalysts surface. This was combined with the use of *in-situ* techniques to determine changes to the surface during reaction conditions. A range of techniques were used including: Solid State UV-Vis-NIR Spectroscopy, BET Surface Area Analysis, *in-situ* Raman Spectroscopy, Temperature Programmed Reduction (TPR), X-Ray Diffraction (XRD) and chemisorptions. Characterisation of the catalysts showed marked differences between each of the individual components on the support compared with the combined cerium and copper/supported catalysts.

Methanol decomposition was used to investigate the activity of the prepared catalysts. Ideally, for the catalysts to behave similarly to the Cu/Ce alloy catalysts, they would have to decompose methanol to produce predominantly carbon monoxide and hydrogen. However, on closer examination of these catalysts it was found that the presence of cerium in the catalysts led to an increase in the carbon dioxide:carbon monoxide ratio.

As the effect of cerium on the copper/silica catalysts appeared to increase CO_2 production, a study was carried out to investigate the active species of the copper/cerium alloy catalysts. One of the species considered to contribute towards the high activity of the alloy catalysts was cerium hydride. However as an individual component its effects on methanol synthesis were never fully investigated.

A cerium hydride was prepared and a number of its properties were examined using small, highly reactive molecules. The results showed that adsorbed hydrogen was reactive, readily available for exchange with deuterium and able to catalyse hydrogenation reactions. The cerium hydride selectively hydrogenated carbon to carbon double and triple bonds in preference to carbon to oxygen multiple bonds. Moreover, the presence of carbon monoxide or carbon dioxide did not poison the cerium hydride. The hydride reacted irreversibly with methanol to produce methane and hydrogen. Experiments using deuterated reactants confirmed that the hydrogen (or deuterium) absorbed by the cerium metal is available for exchange.

Due to increasing interest in the water-gas shift reaction for the production of hydrogen for fuel purposes and its uses in industry, the copper/cerium mixed catalysts were examined for use in the water gas shift reaction. In general the mixed metal catalysts were found to be highly active for conversion of carbon monoxide from the reaction mixture. However on closer examination, surface oxygen appeared to have a strong influence on catalytic activity. Further experiments were used to determine the extent to which surface oxygen influenced the reaction products. Addition of cerium to copper-containing catalysts reportedly has the advantage of reducing the 'pyrophoricity' observed when reduced shift catalysts are exposed to air/oxygen. As a result of this investigation, it was found that the addition of cerium to copper-containing catalysts was able to reduce the temperature exotherm produced when the catalyst was treated with oxygen.

During the course of the study, changes in reactivity of the silica-supported catalysts were observed which led to re-examination of a selection of the catalysts for their activity towards methanol decomposition and the hydrogenation of 1,3-butadiene. The changes in activity were attributed to aging of the catalysts.

Acknowledgements

I would like to thank the staff and students in the Chemistry department who have helped during this thesis. In particular I would like to thank my supervisor, Prof. Jackson for his guidance and patience over the last three years. Dr. Kelly (Johnson Matthey Catalysts) for his industrial input and advice, Colin Ranson for carrying out copper surface area tests at JM Catalysts and Malcolm Kett for training on the Raman spectrometer. In addition, members of the catalysis and surface science group at the University of Glasgow consistently helped with constructive questions and advice at seminars and presentations.

Help from the technical and support staff of the Chemistry department also proved invaluable during the course of my studies; in particular I would like to thank Ron Spence and Andy Monaghan, William McCormack, Gayle Nicholson and Arlene Douglas (Glass Workshop), Kim Wilson (Microanalysis), Stuart McKay (Computer Support), Michael Beglan (Environmental Chemistry Department, AAS) and Bill Higgison (Earth Sciences Department, XRD).

I would like to thank the members of the catalysis group (including Arran Canning, Elaine Gelder, Elaine Opara, Kenneth Hindle, Sreekala Rugmini, Sharon Burns and David Williams) who have not only provided assistance in the lab, but also made it such an enjoyable and interesting place to work. Finally, I would like to thank my family, without their constant encouragement and support I may never have finished.

Declaration

The work contained in this thesis, submitted for the degree of Doctor of philosophy, is my own work, except where due reference is made to other authors. No material within has been previously submitted for a degree at this or any other university.

Elaine M. Vass

Elaine M. Vass

Contents

List of Figures

List of Tables

1 INTRODUCTION

1.1 Catalyst Development

Catalysts were first developed in the early 19th century and the first large scale catalytic process was the production of ammonia from nitrogen and hydrogen (Haber process) [1]. The first synthetic methanol plant was commissioned by BASF in 1923. Since their initial development for industry, design of new catalysts was driven by reduction in operating conditions such as reaction temperature and pressure. This was combined with the need to reduce waste production for more environmentally friendly processes. Hence catalyst selectivity towards the desired product was also crucial. Industrially, the main driving force for catalyst development is a reduction in operating costs. The UK chemical industry has a trade surplus of ~£4 billion and 80% of the products require a catalytic process during the production stages (CIA figures, 1999). Competition within industry encouraged research into improving current catalysts, while developing novel catalysts for new and old reaction processes. Particular attention is given to improving the selectivity, activity and life of catalysts. Improvements in surface science techniques have led to an improved understanding of catalytically active species and reaction mechanisms. An increased understanding of the processes involved in catalysis is being applied to future catalyst designs.

1.1.1 Selectivity

Selectivity of catalysts is crucial for industrial scale reactions. Commercial catalysts must be highly selective for both environmental and monetary purposes. High selectivity towards the desired product minimises the formation of unwanted side-products. One example of the importance of having highly selective catalysts is within the synthesis gas industry. Many commercially important chemicals are developed from synthesis gas, which is normally composed of hydrogen and carbon monoxide/carbon dioxide. Synthesis gas can be produced by oxidising coal with steam or by burning methane [1]. The products generated from synthesis gas depend not only on the reaction conditions but also the choice of catalyst as shown in figure 1.1.1. Therefore with careful selection of catalyst, the desired product can be formed while minimising formation of unwanted side products.

Figure 1.1.1. Catalytic reactions of synthesis gas (adapted from ref [1], pg 3).

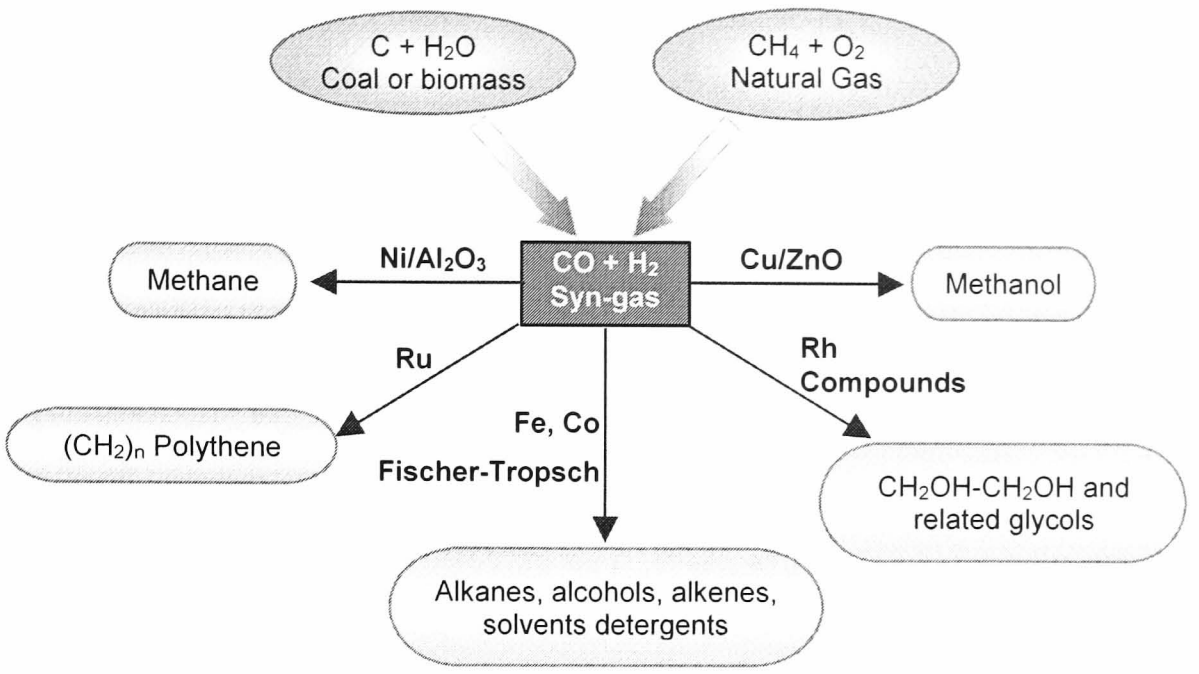

The choice of active metal for a catalyst depends upon the reaction and in many cases is governed by the strength of adsorption of the reactant and product with the metal. Examples of the uses of different catalysts for a variety of industrial processes are shown in table 1.1.1.

Table 1.1.1. Choice of metal for industrial catalysts [2].

Catalysts	*Processes*
Fe	Ammonia synthesis
Pd, Pt	Hydrogenation
Co, Ni, Pd, Pt, Cu	Hydrogenation, steam reforming, catalytic reforming, methanol synthesis, low temperature shift (LTS)
Fe_3O_4	High temperature shift (HTS)
Ag	Methanol oxidation to formaldehyde
SiO_2/Al_2O_3, zeolites	Catalytic cracking, hydrocracking

1.1.2 Activity

The activity of catalysts is used as a measure of the effectiveness of a catalyst, i.e. its ability to convert feedstock into products. Activity is often measured by the rate of the reaction, activation energy of the reaction or more commonly, using the turnover frequency (TOF). Simply stated, the turnover frequency is the number of times that the

overall catalytic reaction takes place per catalytic site per unit time for a given set of reaction conditions [1]. The turnover frequency can be expressed as:

$$TOF = \frac{\text{Number of molecules of a given product}}{\text{Number of active sites x Time}}$$

For a typical heterogeneous reaction, involving the catalytic transformation of small molecules in the temperature range of 373 to 737 K and pressures of up to a few bars, turnover frequencies fall between 10^{-2} and 10^{2} s^{-1} [1]. In industry catalysts are chosen in order to have the maximum activity of feedstock conversion, combined with a high selectivity towards the desired product.

1.1.3 Lifetime

The lifetime of a catalyst is an important factor when designing catalysts for industrial applications. Commercially, catalysts should maintain high activity for as long as possible. Typical industrial catalysts and their expected lifetimes are shown in table 1.1.2.

Table 1.1.2. Average lifetime of typical catalysts in industrial processes [2].

Process	*Typical Catalyst*	*Life (Years)*	*Common cause of decay: catalyst property affected*
Ammonia Synthesis	$Fe/Al_2O_3/CaO/K$	5-10	Slow sintering: activity
Methanol Synthesis	$CuO/ZnO/Al_2O_3$	2-8	Slow sintering: activity
Low Temperature Shift	$Cu/ZnO/Al_2O_3$	2-6	Slow poisoning, sintering accelerated by poisoning: activity
High Temperature Shift	Fe_3O_4/Cr_2O_3	2-4	Slow sintering, pellet breakage: activity, pressure drop
Steam Reforming	$Ni/CaO/Al_2O_3$	2-4	Sintering, occasionally C formation, ring breakage: activity, pressure drop
Ammonia Oxidation	Pt Alloy Gauze	0.1-0.5	Surface roughness, loss of Pt, poisons: selectivity

In practice catalysts rarely maintain their initial activity throughout their lifetime. There are several factors, which can deactivate a catalyst leading to a shorter lifetime. These include physical decay of the catalyst, poisoning by impurities in the feed gas or catalyst and poisoning by reaction products. Ideally, catalyst particles should be chosen with sufficient mechanical strength to withstand the reaction conditions. However

deterioration of the catalysts can lead to plugging of pores, channelling, increase in pressure drop and irregular bed performance. Fouling can occur as a result of deposition of reactor debris on the catalyst particles. The deposits can include scale, rust and other corrosion products. As a result, catalyst pores are blocked resulting in a loss of surface area.

Reaction temperature can have a strong effect on catalyst lifetime. Care has to be taken to ensure that the operating temperature of a process is below the temperature at which sintering or volatization of the active component can occur. Sintering is the process whereby at elevated temperatures metal particles agglomerate and form larger particles, thereby reducing the metal surface area (figure 1.1.2). At the Tammann temperature ($0.5T_m$, where T_m is the melting point of the metal or oxide in absolute units) bulk metal or metal oxide lattices have enough thermal energy to migrate within the crystallite to form larger particles. Even at $0.3T_m$, the Huttig temperature, surface atoms have enough energy to overcome weaker surface crystal forces and become mobile. Metal sintering can be reduced by a number of factors including the use of high surface area catalysts, by including additives in the catalyst and by careful selection of reaction temperature. Hence helping to maintain a high dispersion of metal particles.

Figure 1.1.2. Sintering of an active component on a support material.

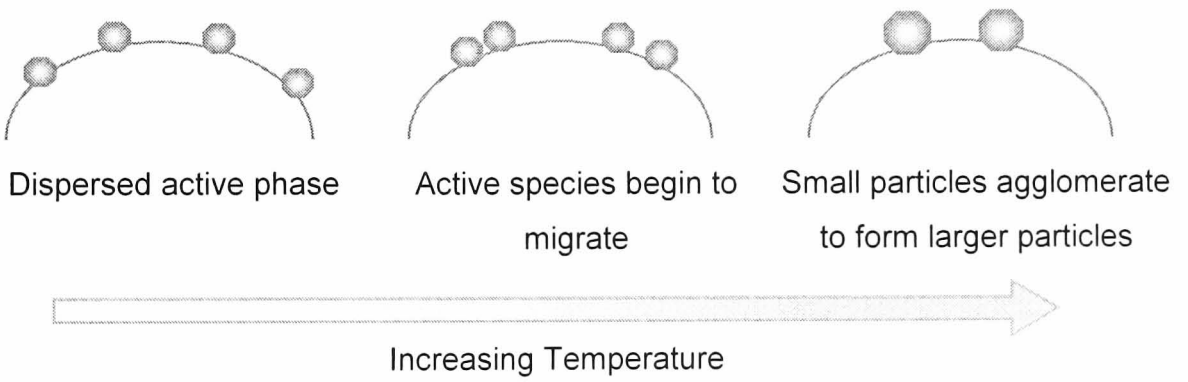

High temperatures can also enhance the formation of surface compounds for example; at high temperature metal/alumina catalysts can form metal aluminates. All components of the catalyst must be maintained in their most active form during reactions. Increased temperatures can lead to phase changes, which can reduce surface area of the support or reduce the activity of the active component.

Catalysts can also be poisoned by the presence of impurities in reactant gases. A poison is any agent, which reacts permanently with an active site, i.e. strong adsorption of ion/molecule with active site. Typical poisons in the petroleum industry are compounds containing sulphur, nitrogen, phosphorus or arsenic, whereas ammonia synthesis catalysts are readily poisoned by carbon dioxide in the feedstock.[3].

After complete deactivation, conversion and formation of products becomes so low that the catalyst must be replaced or regenerated. Regenerated catalysts are rarely as active as the original components and eventually, with repeated regeneration the catalysts become less effective and in some cases it becomes more economical to replace the catalyst. In the case of copper-based catalysts, regeneration is not practical, as the high temperature required to desorb poisons such as sulphur would cause sintering of the copper crystallites and/or the support [4]. However in the case of catalysts containing precious metals it is more economical to regenerate the catalyst or recover the metal.

1.1.4 Preparation

Dowden [5] described in detail the processes involved in the catalyst design process, including choice of metal, support, additives and consideration of mechanism and side reactions. A major factor influencing surface area and metal dispersion is the preparation technique. A variety of techniques are used to synthesise catalysts, including impregnation, co-precipitation, molten fusion, knitted gauze and skeletal. The most common methods for industrial scale preparation are co-precipitation and wet impregnation. The chosen method can affect the catalyst's physical characteristics such as hardness, density, porosity, pore volume, pore size, pore distribution, particle size and particle shape.

Due to their low surface areas, few unsupported catalysts are used in industry. However, precious metal gauzes are still used in the production of nitric acid from ammonia [6]. Highly dispersed metal is not required for the reaction as the rate of reaction using unsupported Pt-based gauze is fast. Fused catalysts are rare in industry; their main use is in the ammonia synthesis process [2]. A fused catalyst is formed by fusion of magnetite (Fe_3O_4) with promoters, for use in the ammonia synthesis process. The porosity of fused catalysts is generated by reduction of Fe_3O_4 to iron metal. The removal of the oxygen component leaves a porous iron structure with a higher surface

area than would have been achieved from reduction of the metal. Typically the catalyst is triply promoted with calcium, potassium and alumina [7]. Although fusion creates good interaction between the components, the catalysts produced often have low surface areas and require further activation. In addition, the absence of a support can reduce the resistance of the catalyst to poisoning.

Skeletal catalysts are prepared from alloys, which are treated with acid or base to leach out one of the components to leave a skeletal structure. The product is a high surface area porous metal. The active components of these catalysts can include iron, cobalt, nickel copper or silver. The leached component of the alloy can include aluminium, zinc, silicon and magnesium. Traces of the leached compounds remaining in the final catalyst improve catalyst stability. Raney Nickel™ catalysts are still used as hydrogenation catalysts [8] on a laboratory scale and by the tonne in industry. The advantages of the catalysts are that they can be used under mild reaction conditions. The disadvantages are that the catalysts produced are sensitive to poisons and can be readily deactivated at higher temperatures.

Supports are not only useful for improving the active metal surface area, but can adsorb poisons and improve the thermal stability of the catalyst. Supported catalysts are normally prepared by impregnation or co-precipitation. In some cases both methods can be combined to produce a single catalyst. Impregnation is the simplest and most direct technique for catalyst preparation [9]. Impregnated catalysts are prepared by mixing a metal salt solution with a pre-formed support, followed by drying to remove excess solvent. The process is called incipient wetness impregnation if the volume of the solution is equal to the pore volume of the support. The drying step results in the crystallisation of the metal salt on the pore surface [3]. The distribution of the active species on the support can vary, depending on the reaction conditions. Factors that can be changed include: type and concentration of precursor salt, solvent, temperature, type of support and contact time with support [10]. The various distributions possible are shown in figure 1.1.3.

Figure 1.1.3. Distribution of active species on support [10].

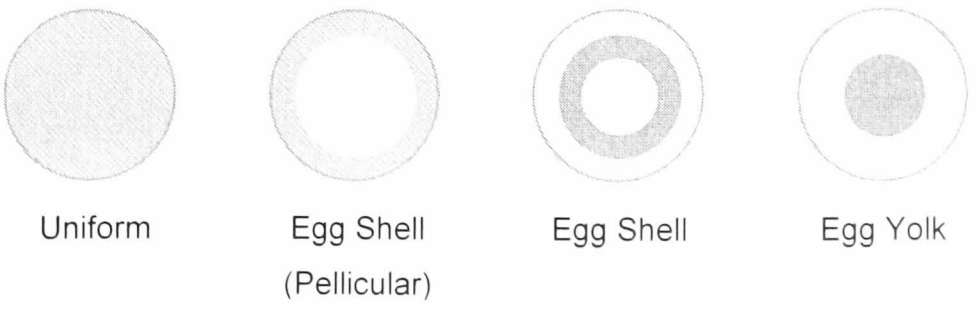

There are several advantages to preparing catalysts by impregnation. When using precious metals, the metal is well dispersed and there is no loss of material within the support phases. With impregnation the support can be prepared separately, allowing for higher temperature treatments than would be possible if the active metal was already incorporated on the support. When preparing alkali-doped catalysts it is convenient to use impregnation, as the washing step of a precipitation preparation would remove the alkali salt. The disadvantage of impregnation techniques is that there is limit to the quantity of active phase that can be deposited onto the support.

The co-precipitation technique requires the simultaneous formation of the support and active phase. The general reaction can be illustrated by the following equation:

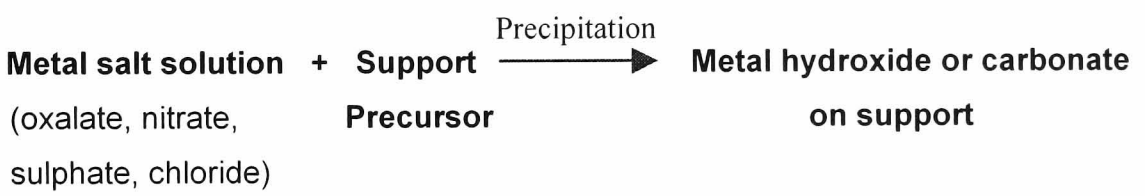

There are a number of steps in the precipitation process, as shown in figure 1.1.4. Catalyst preparation is complicated by the number of variables involved during the formation stages. For example, changes to the concentration of reactant solutions, as well as changes to the pH and temperature of the reaction mixture are factors which strongly influence the structure of the final catalyst.

Figure 1.1.4. Steps in the preparation of catalysts by co-precipitation.

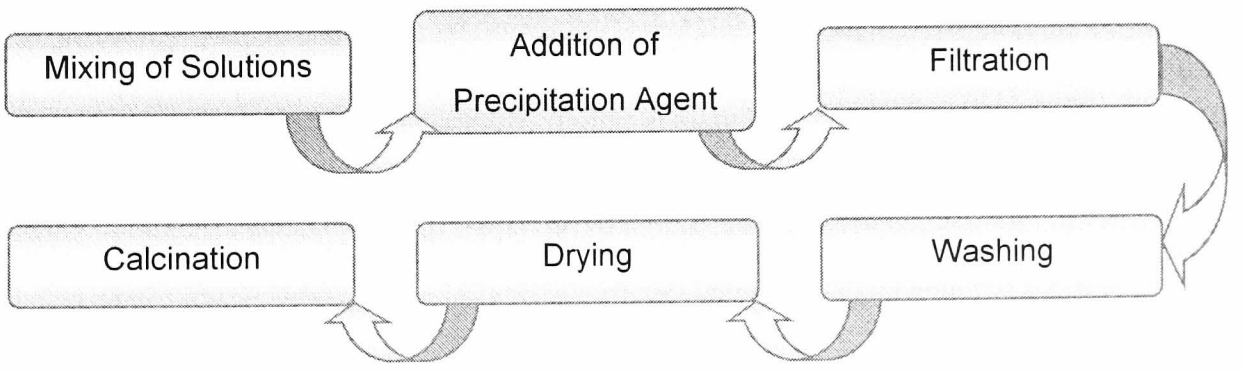

Co-precipitation of catalysts may also include an ageing step after precipitation or washing of the catalyst. Typically, catalysts with metal loadings higher than 10-20% are prepared by co-precipitation. In addition to the suitability of co-precipitation methods for formation of catalysts with high metal loadings, a further advantage is that this method enhances the interaction between the different components of the catalyst,

for example between the active phase and support phases. An example of an industrial catalyst prepared by co-precipitation is the methanol synthesis catalyst.

1.1.5 Supports

Supported catalysts are more commonly used in industry. The support is normally unreactive and provides beneficial properties such as increasing active metal dispersion and catalyst surface area. It can also improve thermal stability of the catalyst and reduce the effects of sintering. The support provides the catalyst with its final shape and mechanical strength. Supports can also be used to adsorb small amounts of impurities, hence reducing catalyst deactivation. Some of the different types of support available are carbon, silica, alumina, titania, zirconia and ceria. Among the most common forms of support are oxides. The choice of support can effect the physical properties of the final catalyst such as hardness, density, pore volume, pore size, pore distribution, particle size and particle shape [11]. Examples of some of the different properties of supports can be seen by examining some of the oxide supports such as alumina, silica and ceria.

Alumina is an amphoteric support, which can exist in a number of different forms. The starting materials are normally aluminium trihydroxides ($Al(OH)_3$) of which the most common crystallite forms are Gibbsite and Bayerite. Subsequent forms of alumina are formed by dehydration of the material to produce firstly oxyhydroxides (AlO(OH)) then further dehydrated to the transition aluminas ($Al_2O_3.xH_2O$, $0<x<1$) [10].

Figure 1.1.5. Changes in structure of alumina during heating [10].

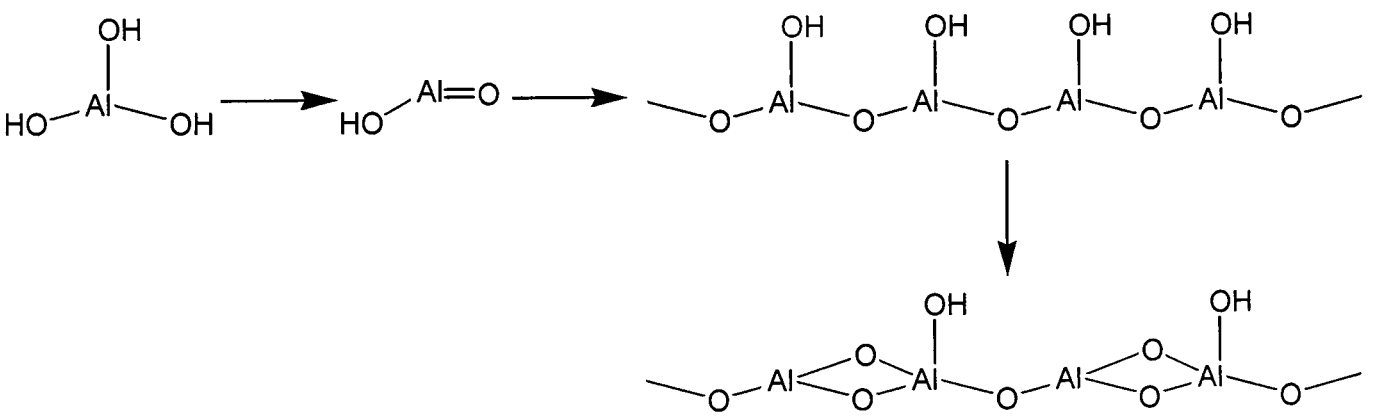

On complete dehydration, corundum (α-alumina) is formed. Transitions to different forms of alumina begin at nearly 450 K and continuous changes in phase occur up to

approximately 1400 K at which point the product is α-alumina [12, 13]. The transition aluminas (γ-, η-, δ- and θ-alumina) are most frequently used for catalytic applications. Properties of the transition aluminas such as surface area and porosity vary widely between the different forms of alumina. The most commonly used form is γ-alumina, which is used for hydrocarbon conversion (petroleum refining) [14-16], alcohol dehydrogenation [17-19], oxidation of organics [20, 21] and oxidation of carbon monoxide and hydrocarbons [22, 23].

Silica is produced by reacting an alkali metasilicate (e.g. sodium silicate with SiO_2/Na_2O = 3.22) and an acid such as HCl [3]. The solution forms a gel, which is washed to remove Na^+ before drying the catalyst. The structure of silica supports is the result of condensation of silanol groups to produce polymeric siloxanes, as shown in figure 1.1.6.

Figure 1.1.6. Changes in silica structure during heating [10].

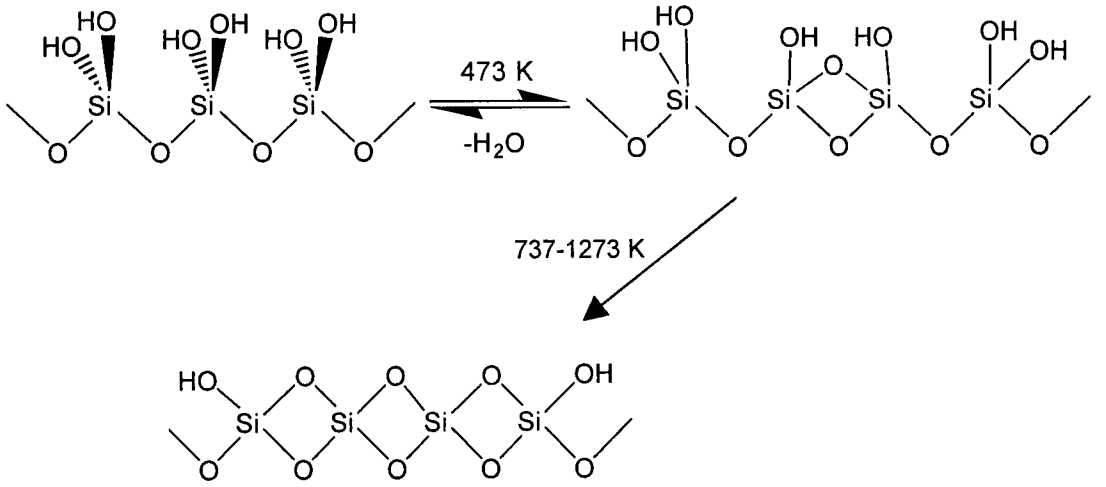

The support is an amorphous material composed mainly of non-ordered SiO_4 tetrahedra [3, 24]. The tetrahedra are arranged in rings [25]. The rings contain *n* silicon atoms linked by oxygen atoms. The rings can range from 3 to 8-membered [25], however it has been reported that porous silicas contain mainly 3-membered rings [26]. Silica supports are acidic in nature [10]. Similarly to alumina supports, dehydration of the surface at high temperature reduces the concentration of surface hydroxyls [27]. After drying silica gels, the surface area of the final material can range from 200-800 m^2g^{-1}, however pore size/volume is strongly dependent upon the drying conditions. A second preparation of silica involves the hydrolysis of tetraethoxysilane with aqueous ammonia. Particle size can range from 10-500 nm and is dependent upon the

preparation conditions. By using low concentrations of tetraethoxysilane, smaller, spherical particles can be formed [28].

Two well-known catalyst supports, which are commercially available, are Cabosil and Aerosil. The support is formed by flame hydrolysis of $SiCl_4$. This preparation technique forms a finely divided non-porous silica (particle size 5-40 nm and surface area of 50 to 400 m^2g^{-1}) [29]. Kieselguhr is a naturally occurring form of silica [10]. The silica contains 70 to 90 % of SiO_2, with 0.2-0.7 μm pores and a surface area ranging from 15-40 m^2g^{-1}. Although of lower purity and surface area than other forms of SiO_2 available, kieselguhr is used to support nickel for large-scale reactions.

A recent review by Trovarelli [30] summarised some of the main catalytic properties and uses of ceria. The morphology of ceria crystallites is strongly dependent upon the preparation conditions, i.e. choice of metal salt precursor and catalyst pre-treatment [31]. Increased temperature during calcination of ceria results in a loss of microporosity and a decrease in specific surface area [32]. Ceria is an amphoteric material and unlike alumina and silica is a partially reducible oxide. At high temperatures (above 1100 K [33], or lower temp in the presence of a transition metal [34]) Ce^{4+} (CeO_2) can be reduced to Ce^{3+} (Ce_2O_3). Although reduction to the Ce_2O_3 form requires high temperatures, removal of surface capping oxygen can begin at the lower temperature of 770 K [33]. The presence of two forms of cerium in the support can lead to the formation of surface and bulk vacancies. Sub-oxides retain the fluorite structure of CeO_2 even after considerable loss of oxygen [30]. However, the sub-oxides are readily re-oxidised to CeO_2 on exposure to an oxidising environment [35-37]. As well as being used as a support, ceria can be added to a support such as silica or alumina. Ceria is used predominantly as an oxidation catalyst [38, 39] and is a component of automotive catalysts (Three Way Catalysis) [40, 41].

1.2 Catalysis within the Methanol Industry

Methanol is produced on a tonnage scale and has a wide variety of uses. In 2001, the main uses for methanol were broken down into 34% formaldehyde production, 28% methyl tertiary butyl ether, 7% acetic acid and 31% various other chemicals/solvents/fuel additives [42]. More recently, methanol has been considered in the search for clean fuels. Methanol is being investigated as an alternative source for

the transportation and storage of hydrogen. Due to the varied uses of methanol, demand for this compound has continued to rise.

Figure 1.1.7. Industrial uses of methanol in 2001 [42].

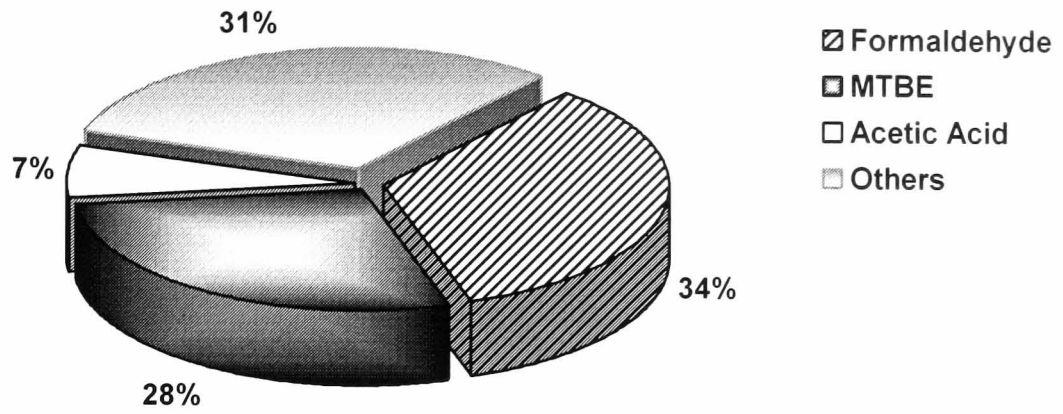

1.2.1 Methanol Synthesis Process

The methanol synthesis process has undergone many changes since it was first introduced on an industrial scale in 1923. The main improvements achieved have been driven by the reduction of investment costs, which dominate the production cost of methanol. The production of methanol occurs in a number of steps as shown in figure 1.1.8. There are six main stages in the synthesis process: feed gas purification, steam reforming, heat recovery (steam generation), compression, methanol synthesis and distillation.

Figure 1.1.8. Schematic of an industrial methanol synthesis process [Provided by JM Catalysts].

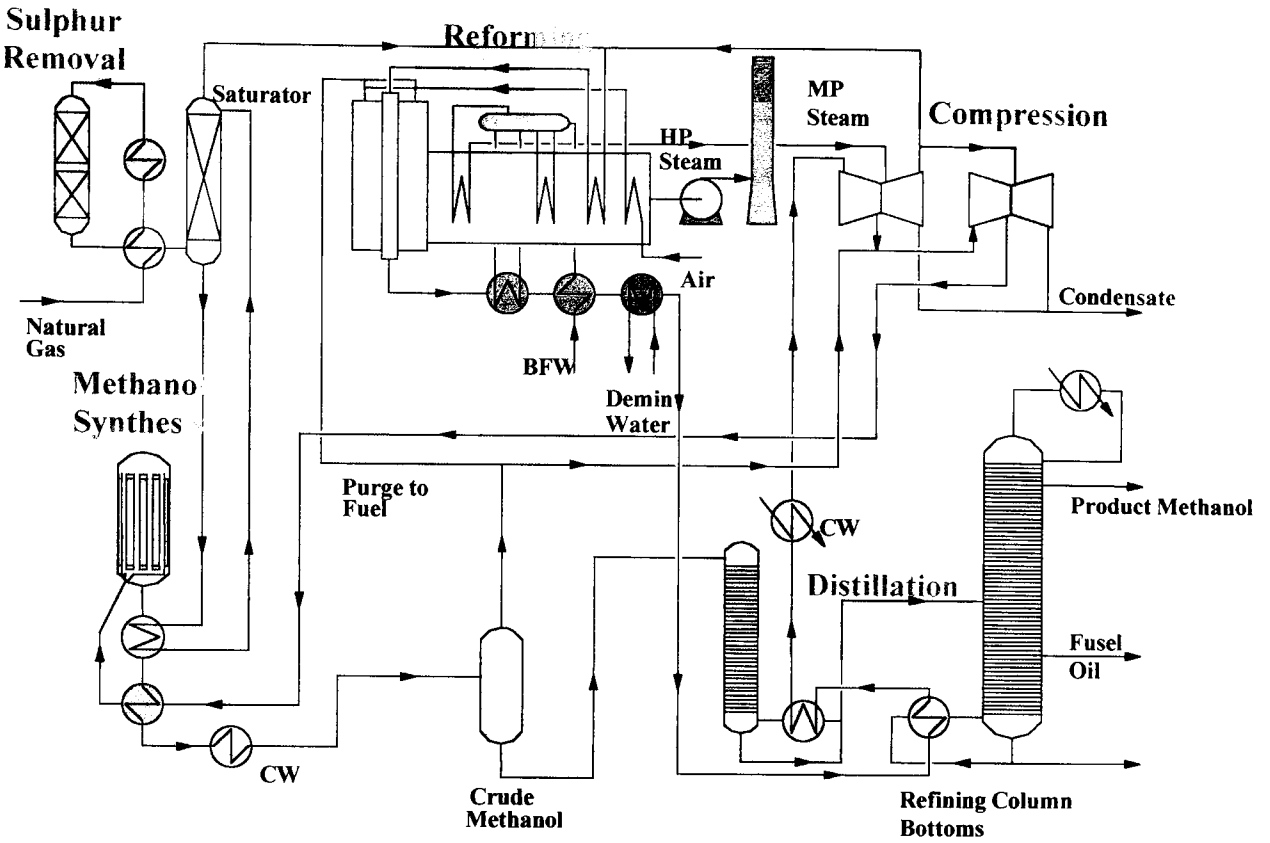

Natural gas has low sulphur content, containing compounds such as hydrogen sulphide, carbonyl sulphide or mercaptans. Hence, the first step of the process is to remove the sulphur containing compounds using an absorbent such as zinc oxide. This prevents poisoning of the reforming or methanol synthesis catalysts. Steam is introduced into the gas feed by the saturator. The next step is the steam reforming (or partial oxidation) of methane from natural gas [43].

Once formed the synthesis gas (a mixture of carbon monoxide, carbon dioxide and hydrogen) is compressed from approximately 20 to 80 bar before being fed into the methanol synthesis loop. Unreacted gas is recycled around the loop, where it is mixed with fresh synthesis gas. The crude methanol produced is purified by distillation through two columns. The first column removes light impurities such as ethers, esters, acetone, lower hydrocarbons and dissolved synthesis gas. The second column removes water, higher alcohols and higher hydrocarbons.

The route to methanol production is complicated by a number of factors, for example the low conversion of synthesis gas to methanol. Low conversion to methanol in industrial plants is due to a trade-off between reaction kinetics and the position of equilibrium [2]. High pressure and low temperature favour increased conversion to

methanol. However, the rate of production of methanol can be slow at low temperatures. Hence, by using a catalyst active at low temperatures, methanol can be produced under milder conditions. Typically in a low-pressure reactor only 15-20% of the synthesis gas is converted in each pass [44]. Unreacted gases have to be recycled and looped back into the reactor. Methanol synthesis is a strongly exothermic reaction (See equations 1 and 2). Therefore, heat exchangers are used to control the excess heat produced during reaction.

(1) $CO + 2H_2 \longrightarrow CH_3OH$ $\quad \Delta H° = -91\ kJmol^{-1}$

$\Delta G° = -25.34\ kJmol^{-1}$

(2) $CO_2 + 3H_2 \longrightarrow CH_3OH + H_2O$ $\quad \Delta H° = -49.5\ kJmol^{-1}$

$\Delta G° = 3.30\ kJmol^{-1}$

The water gas shift reaction is favourable under the reaction conditions for methanol synthesis and may consume the water produced by reaction (2) to favour methanol production from carbon dioxide.

(3) $CO + H_2O \longrightarrow CO_2 + H_2$ $\quad \Delta H° = -41.1\ kJmol^{-1}$

$\Delta G° = -28.6\ kJmol^{-1}$

Over the years, there has been considerable interest in the role of carbon oxides in methanol synthesis [2, 45], i.e. whether methanol is produced from carbon monoxide or carbon dioxide. It is possible to produce methanol from either carbon oxide as the starting material, but the rate of reaction with carbon monoxide is greatly increased by the presence of carbon dioxide in the feed stream. Radiotracer and kinetic studies have shown that methanol is produced from carbon dioxide rather than carbon monoxide using conventional methanol synthesis catalysts [2, 46].

The selectivity towards methanol synthesis improves at lower temperatures. Higher alcohols and hydrocarbons require higher activation energy than for methanol formation [47]. As a result, low temperature processes are favoured as they have higher selectivity towards methanol production. Higher copper surface area is linked with an increase in catalytic activity within groups of catalysts [48]. Although the general rule is true, values of methanol synthesis activity can vary for the same copper surface area.

depending on the support material, which has been chosen. Deactivation of methanol decomposition catalysts is due to a number of factors including sintering, poisoning and carbon deposition on the catalyst surface. However, the main source of deactivation is thermal sintering of the copper species [4].

Overall improvements in the methanol synthesis process are composed of elements of catalyst system improvements and reactor improvements. Consideration has to be given to the recycling of unreacted gases, controlled production of heat and ensuring a high selectivity towards methanol.

1.2.2 Commercial Methanol Synthesis Catalyst

The first commercial catalyst for methanol synthesis was developed in 1923 by BASF chemists and remained virtually unchanged for over forty years [2]. The catalyst used was a zinc oxide/chromium oxide catalyst. It was relatively poison resistant and was able to operate with synthesis gas containing sulphur and chlorine. At the same time, copper catalysts were also tested, but were readily poisoned under the same conditions. Synthesis gas was produced from coal gasification and contained a number of impurities such as sulphur and arsenic containing compounds, which readily deactivated catalysts containing copper [45]. Even under laboratory conditions copper-based catalysts deactivated. However the zinc oxide/chromium oxide catalysts were resistant to the poisons. Hence methanol was produced industrially using zinc/oxide chromium catalysts at high temperatures (593-723 K) and pressures (250-350 bar).

In the 1960's, there was a change in the source of synthesis gas, which shifted from coal or liquid to gaseous hydrocarbons (such as steam reforming of naphtha or methane). The change in synthesis was combined with improved technology for removing impurities from synthesis gas. The reduction in impurities such as sulphur and chlorine containing compounds enabled the use of copper based catalysts for methanol synthesis. However, problems remained with stability, which were only overcome by the development of the copper/zinc oxide/alumina catalyst in 1966 by ICI [2, 45]. As it had a much higher activity than the previous catalyst, reaction conditions could be much milder. Hence, the low-pressure catalyst was operated at 35-55 bar pressure and temperatures of 473-573 K. As the reaction was carried out at lower temperatures and pressures, it was more cost effective and rapidly replaced the high-pressure process.

Industrial methanol synthesis catalysts are prepared by a co-precipitation technique [49]. The pH during the precipitation process strongly influences the composition and particle size of the final catalyst. Ideal metal composition of the catalyst is achieved at a pH near 7 [2]. Each of the components of the $Cu/ZnO/Al_2O_3$ has a specific role in the methanol synthesis process. Copper is considered to be the active site for methanol synthesis. Zinc oxide is used as a 'poison soak' to adsorb any poisons present in the feed stream [45]. It was also found to improve the copper dispersion of the catalyst and reduce copper sintering. The main role of alumina in the catalyst is as a stabiliser, it was found to be a more effective stabiliser than chromia [50], which was used in the original high temperature process. Alumina can be prepared with high surface area and was found to be more effective than zinc oxide at minimising copper sintering. In addition, the reaction of the basic zinc oxide and alumina neutralised the surface acidity of the alumina, preventing the formation of dimethyl ether [45]. The composition of the catalyst can vary depending on the catalyst manufacturer. In general, the proportion of copper oxide can range from 40 to 80%, ZnO from 10 to 30% and Al_2O_3 from 5 to 10% [42]. Additives such as MgO may also be added to improve the performance of the catalyst by reducing copper sintering [42].

The low-pressure methanol synthesis process is still favoured in a market of 35 million metric tons production capacity and 28 million tons demand (1999 figures) [42]. For over 20 years, alternative catalysts have been investigated, but as yet none have proved as economical as the current process. Indeed the majority of changes, which have occurred in the methanol synthesis industry in the last 10-15 years, have been due to changes in reactor design rather than to the main catalyst components [42].

1.2.3 Methanol Synthesis Mechanism over Copper Based Catalysts

In depth studies have been made to determine the mechanism of the methanol synthesis process over the commercial $CuO/ZnO/Al_2O_3$ catalyst. By studying each of the individual components of the catalyst it was discovered that both zinc oxide and copper were active for methanol synthesis from carbon dioxide independently. In the commercial catalyst, the active component was thought to be copper as the copper loading correlated well with the catalyst activity [51]. Although methanol was derived solely from carbon dioxide, carbon monoxide was found to be necessary to maintain a reduced form of copper.

The proposed mechanism over the commercial catalyst [51] involved the dissociative adsorption of carbon dioxide onto copper to form a symmetric carbonate. This was then hydrogenated to form a bidentate formate (the longest lived intermediate in methanol synthesis). Subsequently the bidentate formate was hydrogenated to a methoxy species and desorbed from the surface as methanol. Hydrogenation of the bidentate formate is thought to be the rate determining step of the methanol synthesis process. The role of carbon monoxide in the feed is to maintain a more reduced copper surface than would be possible with just hydrogen. The state of the catalyst surface was found to be strongly dependent upon the reaction gas mixture [52]. The study of the commercial catalyst [51] also investigated a carbon monoxide/hydrogen feed for methanol synthesis. Although no intermediates were identified, it was suggested that the likely intermediate was a weakly bound formyl species and that this process would play a minor role in the presence of carbon dioxide in the feed.

Over the commercial catalyst alternative mechanisms involving the junction effect theory or a synergetic interaction between the copper and zinc oxide components, were largely discounted [51]. Temperature programmed desorption studies of a methanol synthesis catalyst showed only formate species desorbed from copper sites and not zinc oxide [53]. Hence the reaction occurred predominantly on the copper surface.

More recent reviews generally support the theory of synergetic effects between the active copper species and the support [44, 54]. However, in most cases the formation of a formate species is accepted as one of the main steps in the methanol synthesis mechanism [54]. With copper/zinc oxide catalysts in particular, some of the differences in results by different authors have been attributed to the variations in testing conditions [55]. Furthermore, it has been suggested that over a range of copper/silica catalysts, methanol was produced from carbon monoxide via a bifunctional reaction [56]. The group proposed that copper sites alone were not responsible for the synthesis activity and that surface hydroxyls may have played a role in the synthesis process.

For example, over a Cu/ZnO catalyst it is proposed that methanol is formed via a bifunctional mechanism [44, 57, 58]. It is assumed that the carbon dioxide is hydrogenated on the copper sites to yield methanol and water and that subsequent gas phase transport from the copper sites leads to the displacement of relatively stable

species from ZnO. Several variations of this bifunctional mechanism exist and most require the spillover of materials from one component to another.

Research has suggested that hydrogen spillover plays an important role in methanol synthesis. The definition of hydrogen spillover is "the migration of atomic hydrogen from a metal crystallite onto the support" [59]. Studies into this phenomenon have shown that hydrogen spillover increases with greater metal dispersion and that atomic hydrogen spillover is faster on fully hydroxylated/hydrated surfaces due to greater hydrogen mobility [59, 60]. There are a number of different materials which can behave as hydrogen acceptors including: irreducible oxides, partially reducible oxides and related systems, oxides capable of forming bronzes, reducible oxides not forming bronzes and carbon [61].

Investigations have been carried out into the role of hydrogen spillover during the formation of methanol from CO/H_2 and CO_2/H_2 over Cu/ZrO_2 catalysts [62]. For CO_2 hydrogenation, it was found that the hydrogen required for the hydrogenation of zirconia-bound carbonaceous species is provided by spillover of hydrogen atoms produced by dissociative adsorption of hydrogen on copper. In the case of CO hydrogenation, CO adsorbs on the zirconia to form formate species, which then undergo sequential hydrogenation to form methoxy species [62]. The products are removed from the surface by reductive elimination or hydrolysis. It was suggested that a possible role for the ZnO of commercial catalysts was as an atomic hydrogen reservoir and for promoting hydrogen spillover [60]. More recently, the spillover effect of the Cu-ZnO system was described as minimal when compared with the effect of ZnO on the creation of a Cu-O-Zn site [63]. Although Nakamura and co-workers [63] observed spillover, they concluded that it was not the main role of zinc oxide. Further studies have suggested that hydrogen can be 'locked in' to the copper species [46]. The hydrogen is adsorbed onto the copper then can be absorbed below the copper surface. Once an oxide surface layer forms on the copper this prevents release of the hydrogen unless ~40% of the oxide layer is first removed [46]. This process leads to a restructuring of the copper surface and is thought to play a role in the synthesis mechanism.

Therefore, although a great deal of research has investigated the mechanism of copper-based methanol synthesis catalysts, investigations continue to investigate the extent of support and additive effects.

1.2.4 Active Site for Methanol Synthesis

A great deal of investigation has been undertaken to determine the active sites of the catalyst in order to identify the effect of the different components on the copper/zinc oxide/alumina catalyst. The main source of controversy is the oxidation state of the copper species during reaction, whether it is Cu^0 or Cu^+. Although there is evidence for both species on methanol synthesis catalysts, it has been suggested recently that Cu^+ is the active site for methanol synthesis [44]. It was found that in the presence of carbon dioxide and with a large fraction of the Cu^0 surface covered by oxygen containing species that activity towards methanol synthesis was independent of Cu^0 surface area. It was also stated that anything, which stabilizes the presence of Cu^+ indiscriminately enhances the activity of the catalyst [44]. Hence, the role of ZnO in the catalyst was thought to contribute to catalyst activity. However it has also been shown that the reaction mixture strongly affects the surface oxygen coverage which in turn affects the catalyst activity [52].

Although the conditions for the methanol synthesis reaction favour carbon deposition, the main source of deactivation of copper species in commercial methanol synthesis catalysts is due to thermal sintering [4].

1.2.5 Alternative Methanol Synthesis Catalysts

A variety of alternative catalysts have been developed for use in methanol synthesis. They fall into three main categories: skeletal copper catalysts, copper intermetallic compounds and precious metals. However a fourth group, which examines copper/lanthanide oxide catalysts for use in hydrogenation processes, is increasingly being investigated.

1.2.5.1 Skeletal Copper Catalysts

Leaching alloys of copper/zinc/aluminium with a caustic solution, e.g. sodium hydroxide, produces Raney Copper™. This three-component system is a porous structure of copper, contaminated with both alumina and zinc oxide. The role of aluminium is to create Raney Copper™ catalysts with high surface area, whereas zinc is added for stability. Addition of zinc oxide was crucial to the rate of the methanol synthesis reaction, however copper was considered to be the active site, as for the commercial catalyst [64]. The catalysts were both active and selective for methanol synthesis [47]. Activity was found to be dependent upon alloy composition and leaching conditions. The optimum range of composition for the alloy was: 30-36% copper, 50% aluminium and 14-20% zinc [65]. After partial leaching of the catalyst the optimum composition of the activated catalyst was in the range of: 75-90% copper, 4-8% aluminium and 5.7-15% zinc [47].

Deactivation of skeletal catalysts in a poison free environment was attributed to copper crystallite sintering. The stability of the catalyst was found to rise with increasing ZnO content [66], hence improving its long-term activity. Although this type of catalyst shows high activity towards methanol synthesis, it is still not as effective as the current co-precipitated $Cu/ZnO/Al_2O_3$ catalyst. A more recent study of skeletal catalysts highlighted the importance of the formation of Cu-ZnO active sites for the formation of methanol from carbon dioxide and hydrogen [67]. The catalysts were more selective towards methanol and increasing the content of ZnO reduced the rate of the reverse water gas shift reaction [67].

1.2.5.2 Copper/Lanthanide Intermetallic Catalysts

Novel copper/lanthanide catalysts were prepared for use in the methanol synthesis reaction. At the beginning of the 1980's, research was carried out into copper and thorium [68] alloys (or copper and lanthanide alloys [69]), which yielded effective catalysts on exposure to synthesis gas. Under the testing conditions utilised, the alloy derived catalysts were considerably more active than their analogues prepared by co-precipitation or a commercial methanol synthesis catalyst [47]. The catalysts were highly active and their activity was attributed to the ability to generate both the active component and support on the atomic scale [47]. The disadvantage of the thorium/copper alloys was that during the activation procedure expansion of the catalyst

occurred [68]. This had an adverse effect on the gas flow through the catalyst bed; hence further development of the catalyst would be required before the catalysts could be applied to an industrial scale process.

Due to the problems associated with handling radioactive material such as thorium (α-particle emitter; half life ~1.4 x 10^{10} years), attempts were made to replace thorium with a different lanthanide metal [69]. However, initial catalysts developed by France and Wallace [69] were not only less active than the thorium containing catalysts, but also less selective. Higher alcohols and 20-50% water were present in the products.

However research into copper-lanthanide systems continued and in the late 1980s, Jennings, Lambert, Nix and Owen developed highly active methanol synthesis catalysts based on copper/lanthanide (or actinide) intermetallic compounds [70-72]. The intermetallic compounds were prepared by electron-beam melting of the constituent metals, i.e. copper with cerium, neodymium, lanthanum or thorium [72]. Compounds were prepared in an inert atmosphere due to the risk of combustion of the metals. The alloys were activated *in-situ*, by heating in a synthesis gas mixture.

When compared with commercial $Cu/ZnO/Al_2O_3$ catalysts, copper/lanthanide alloy catalysts were far more active towards methanol synthesis [72]. *In-situ* XRD studies suggested that lanthanide/intermetallic hydrides were present in the catalysts [73]. No crystalline copper was detected and methanol synthesis was thought to involve copper as ions or as very small aggregates (<10 Å) in close association with a lanthanide oxide [71, 72].

The formation of a formate intermediate (i.e. Cu-O-CH-O-Ce) at the periphery between copper clusters and the cerium oxide support in Cu/CeO_2 was suggested as the reason for the high activity of Ce-Cu alloy catalysts for methanol synthesis from carbon monoxide and hydrogen [74]. It was thought that the hydrogenolysis of peripheral formate should be facile on consideration of the bond energies [74]. It was suggested that this mechanism would have similarities to the mechanism of Pd/support catalysts [74].

A study using labelled $^{14}CO_2$ showed that methanol was produced predominantly from carbon monoxide over the intermetallic catalysts [75]. Hence, the mechanism of methanol synthesis was very different to that of commercial catalysts. In fact, carbon dioxide was found to deactivate copper/lanthanide alloy catalysts. Even very low levels of carbon dioxide (<1%) caused catalyst deactivation [72]. A typical synthesis gas feed for methanol production would contain approximately 7% carbon dioxide. The deactivation of the catalysts was caused by the formation of carbonates and was irreversible for copper/cerium catalysts [70]. In addition, self-poisoning occurred during the activation process due to the reverse water-gas shift reaction.

Ternary alloys were investigated and although they were slightly less active, addition of a third metal such as Al, Zn or Ti enhanced the catalysts resistance to poisoning [75]. Therefore increasing the stability of the catalyst.

There were many advantages to copper/lanthanide intermetallics, such as increased activity at low temperatures and the ability to produce anhydrous methanol directly [72]. However, a complicated preparation technique, as well as rapid deactivation, made the process unsuitable for conversion to an industrial process. The initially high catalyst activity lasted only a few hours even at low temperatures. One author suggested that the loss in activity was due to the highly active sites formed by the alloys being destroyed [4]. This was possibly due to agglomeration of the copper clusters to copper metal crystallites of similar size to those of conventional copper catalysts.
Incorporation of cerium as an additive into a copper/zinc oxide catalyst was found to have a detrimental effect on methanol synthesis activity [47]. This suggested that the alloy formation and subsequent activation were crucial steps in producing the enhanced methanol synthesis activity observed for the intermetallic catalysts.

1.2.5.3 Precious Metals

Precious metals including platinum, palladium, rhodium and iridium have been examined as methanol synthesis catalysts. However, the use of precious metal catalysts has a number of disadvantages. The high cost of precious metals, low reaction rate and formation of methane at higher temperatures has prevented their application on an industrial scale [47]. In general, selectivity towards methanol was poor, with the exception of palladium catalysts.

Palladium supported catalysts have been investigated as both methanol synthesis and decomposition catalysts [76, 77]. The support was shown to have a major influence over the activity of the catalyst [77-79]. An investigation of support effect showed that the activity of a 3% Pd/support catalyst increased in the order: $Pd/SiO_2 < Pd/Al_2O_3 < Pd/TiO_2 < Pd/ZrO_2$ [80]. Some of the most active catalysts are promoted by group I and II elements, such as the promotion of a Pd/silica catalyst by $CaCl_2$ [81]. More basic supports were found to encourage selectivity towards methanol. This was believed to be due to the alkali/alkaline earth metal stabilising formate intermediates, by increasing the basic nature of the surface oxygen [82]. Pd/CeO_2 catalysts were examined and found to be highly active for methanol synthesis [79, 83]. The active sites for methanol synthesis were thought to be the boundaries between the palladium and cerium oxide that are chemically in contact with each other. EXAFS spectra confirmed the close interaction of metal and support, as a Pd-O-Ce species was observed [79]. Although the cerium oxide was thought not to participate directly in the catalysis, the metal to support interaction remained crucial to the catalyst activity [79].

Palladium catalysts are active over temperatures ranging from between 453 and 573 K and a wide range of pressures [47]. On a weight of catalyst basis, copper/zinc catalysts are more active than palladium catalysts. However, when compared by the number of active sites, the palladium catalysts compare well with the commercial catalysts [47]. The main disadvantages of palladium catalyst are the low reaction rate and the cost of precious metal. These factors would increase the initial costs of running a plant; hence precious metals have not yet become a commercially viable route to methanol synthesis.

1.2.5.4 Copper/Lanthanide Oxide catalysts

The use of lanthanide oxides as promoters to supports or as supports themselves is increasing. Cu/CeO_2 catalysts prepared by a variety of methods were found to produce active methanol synthesis catalysts. Unlike commercial catalysts which produce methanol predominantly from carbon dioxide and hydrogen, methanol is produced solely from carbon monoxide and hydrogen over ceria-supported copper catalysts [84]. Although the activity of the Cu/CeO_2 catalyst was similar to that of a commercial catalyst at 30-50 K lower reaction temperature, the activity was unstable. *In-situ* studies showed that after reduction, copper metal and CeO_2 were the main species present [84]. However, after reaction, the intensity of the copper peak decreased and peaks for Cu_2O

and CuO were observed. Hence, oxidised copper particles were present even in a reductive reaction gas. This was most likely due to the interaction with cerium oxide. The group [84] thought that copper was not directly oxidised by the cerium oxide, but that oxidation took place in the presence of the carbon monoxide. Under reductive reaction conditions it is likely that the interaction between the metal and the support controls the oxidation state of the copper during the reaction. A similar process was observed with Pd/CeO_2 catalysts [85].

Preparation of a series of copper-oxide catalysts for hydrogenation was carried out by Sakata and co-workers [86]. A number of lanthanides were investigated as supports, with the resulting catalysts being active for methanol synthesis at temperatures between 473 and 523 K. Preparation and calcination treatments strongly influenced the catalytic activity of the catalysts. The most active catalyst was composed of a homogeneous mixture of copper metal and ytterbium oxide, where fine ytterbium oxide particles were homogeneously dispersed in the copper metal [86]. By changing the lanthanide oxide, the activity of the catalyst was enhanced. In particular, ytterbium showed the highest methanol synthesis activity from carbon monoxide and hydrogen, with carbon dioxide and methane only observed in the initial stages of the reaction [86].

1.2.6 Methanol Decomposition

The principle of microscopic reversibility states that the least energy pathway of a reaction will be followed in microscopic detail if the process is reversed. Our interest in methanol decomposition was to use the reverse reaction to examine the forward reaction. Due to the principle of microscopic reversibility, it was hoped that it might be possible to use methanol synthesis catalysts as decomposition catalysts. As a result, catalysts that decomposed selectively to CO and H_2 would follow the same mechanism as the copper/lanthanide intermetallics, which showed high activity towards methanol synthesis. However, formation of CO_2 or water would imply that the catalysts do not follow the same route as the intermetallic compounds, as these products would have poisoned the copper/lanthanide catalysts.

However, there are a number of difficulties in assuming that the reverse reaction will be a reliable test for the synthesis reaction. For example, testing has shown that methanol synthesis catalysts are among the least successful catalysts tested for methanol

decomposition. Another example is the ammonia synthesis reaction, which has very different types of catalysts from the decomposition reaction. Hence direct comparisons with the synthesis and decomposition reactions must be made with caution.

1.3 Water-Gas Shift Reaction

1.3.1 Water-Gas Shift Reaction in Industry

Although reported as early as 1888, the importance of the water-gas-shift reaction (WGSR) was not fully appreciated until the development of the Haber process for the manufacture of ammonia [2]. Then the need for a high purity source of hydrogen drove the initial development of shift catalysts. The catalytic shift reaction was able to remove unwanted carbon monoxide as well as producing hydrogen. When used in combination with the steam reforming of hydrocarbons, the shift reaction produces hydrogen and may have a role in future energy technologies [87]. The shift reaction is a process, which enables the conversion of carbon monoxide and water to carbon dioxide and hydrogen. The shift process can be carried out at high or low temperature, depending on the choice of catalyst.

Figure 1.1.9 shows both high and low temperature processes used in the early stages of ammonia synthesis from natural gas [88]. The first stage of the process is feedstock purification, to remove impurities such as chlorine and sulphur containing compounds, which can reduce catalyst lifetime and affect the activity and/or selectivity of the catalyst. Steam reforming is main hydrogen producing step and occurs in two stages, using nickel oxide catalysts. After reforming, carbon monoxide is converted to carbon dioxide by the shift reactors. The carbon dioxide is removed from the gas stream by scrubbing. The methanation step converts any residual traces of carbon oxides back to methane. The resultant gas is then compressed and used to produce ammonia.

Figure 1.1.9. Schematic of ammonia synthesis process [89].

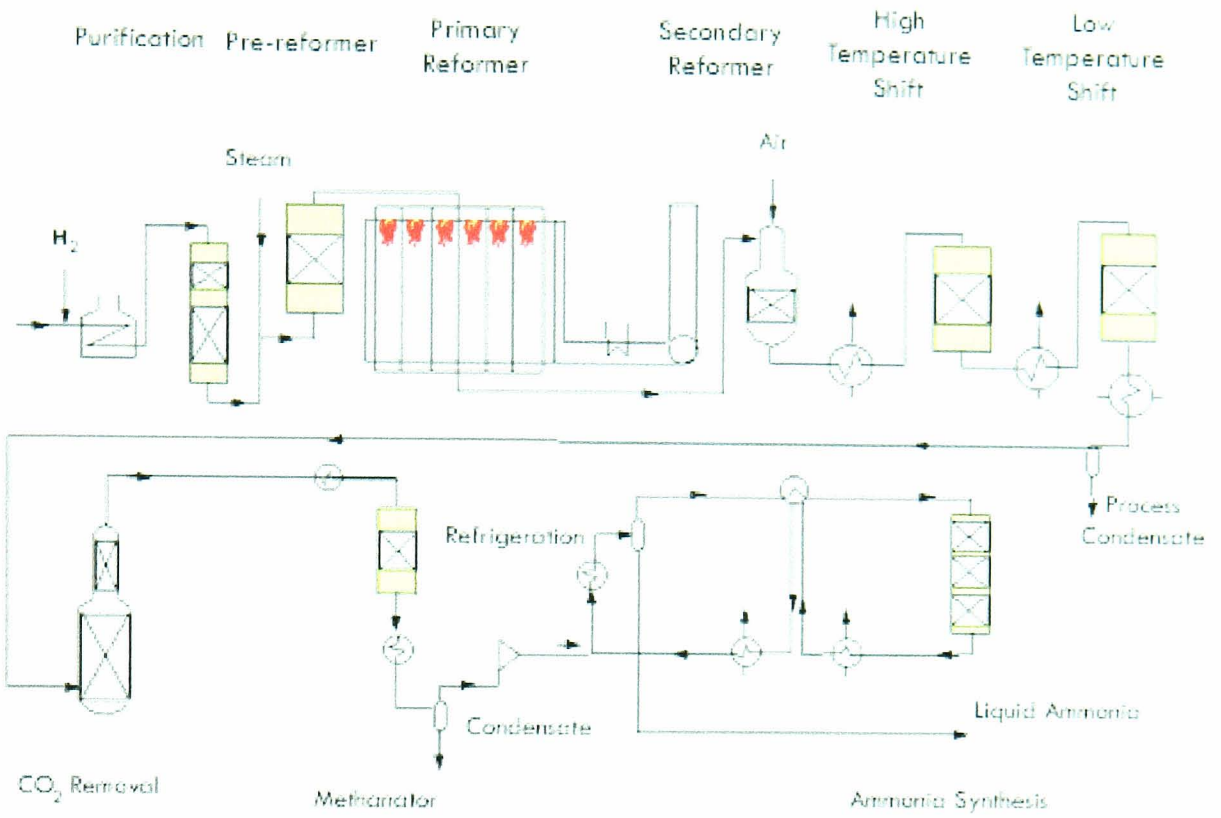

The high temperature shift reaction has been carried out using catalysts composed of iron and chromium oxides for more than 70 years. Fresh unreduced catalysts are composed of 90-95 % haematite (Fe_2O_3) and 5-10 % Cr_2O_3 [2]. High temperature shift catalysts are prepared by co-precipitation, followed by washing (to remove sulphur-containing compounds), ageing then calcination. The catalysts are reduced using synthesis gas to produce magnetite (Fe_3O_4) and Cr_2O_3. The iron oxide is active for the shift reaction and addition of chromium oxide stabilizes the iron oxide crystallites. The catalysts were resistant to poisoning; hence they could be used with feeds containing sulphur compounds (such as those derived from coal or fuel oil). More recent developments of high temperature catalysts have been in pellet design and minimising the sulphur content of the catalysts. The iron oxide and chromium oxide catalysts were highly selective for the water gas shift reaction. By controlling the reaction conditions to avoid formation of iron metal, the production of methane from carbon monoxide/dioxide by the methanation reaction was prevented. The optimum operating temperature for high temperature catalysts was between 623 and 723 K. The high temperature shift process was able to reduce the concentration of carbon monoxide to between 1 and 4% of the exit gases.

In the 1960's, improvements to the purity of feed-stream gases meant that copper based catalysts could be considered as shift catalysts. The benefit of using copper was that it could operate at lower temperatures (473-523 K), thereby giving equilibrium concentrations of less than 0.3% carbon monoxide in the exit gas. The copper-based catalysts were highly active and selective for the water-gas-shift reaction however, the main difficulties experienced with these catalysts were the ease with which they could be poisoned and/or sintered at higher temperatures. In practice, the high temperature catalyst (Fe_3O_4/Cr_2O_3) is followed by a low temperature copper-based shift catalyst to reduce the levels of carbon monoxide in the exit stream to between 0.1and 0.3 %.

The most active low temperature WGS catalyst is a co-precipitated $CuO/ZnO/Al_2O_3$ catalyst. Addition of Al_2O_3 to Cu/ZnO catalysts increased the stability of the copper crystallites against sintering while enhancing the mechanical strength of the catalysts. The copper oxide content of the catalysts normally ranges from 30-40%, similar to methanol synthesis catalysts. However, Chinchen *et al* [90] found that there was no common intermediate for the water gas shift and methanol synthesis reactions, although the major components of both catalysts are copper oxide, zinc oxide and alumina. Selectivity of modern low temperature shift catalysts can be as high as 99.9 % towards the formation of carbon dioxide and hydrogen. Promotion of shift catalysts with alkali metals has been found to drastically reduce the formation of by-products such as methanol. Inclusion of compounds such as potassium oxide [91, 92] or caesium oxide [93-95] was found to have a positive effect on the activity of copper-containing catalysts for both the forward and reverse water gas shift reactions.

Although several reports exist [96, 97] which suggest that there is a direct link between copper surface area and activity towards the shift reaction, one report suggests that catalyst preparation can also influence catalytic activity [98]. There is reportedly no general correlation between catalyst activity and copper surface area [98]. Hadden and co-workers [98] found that although the composition of the catalysts were similar, small changes to the preparation conditions were enough to alter the catalyst activity. By preparing two sets of $Cu/ZnO/Al_2O_3$ catalysts, a linear relationship was observed between copper surface area and catalyst activity [98]. However the two different groups of catalyst prepared had distinctly different copper surface area to activity relationships [98].

1.3.2 Water-Gas Shift Mechanism

Two types of mechanism have been proposed for the water-gas-shift reaction, an adsorptive (or formate) and a regenerative (or redox) mechanism. In the adsorptive mechanism the reactants adsorb onto the catalyst surface, react to form intermediates such as formates, decompose to form products then desorb from the surface. In the regenerative mechanism the surface undergoes successive oxidation and reduction cycles by water and carbon monoxide respectively. Hence, the corresponding products of hydrogen and carbon dioxide are produced. Experimental evidence has shown that the water-gas-shift reaction over both Fe_3O_4/Cr_2O_3 and $Cu/ZnO/Al_2O_3$ catalysts is likely to proceed via the regenerative mechanism [2]. A microkinetics study of the WGS reaction by Fishtik and Datta [99] indicated that the formate mechanism was dominant at low temperatures whereas the redox mechanism was dominant at high temperatures. Similar mechanisms are proposed for the water-gas-shift reaction over metal/ceria catalysts [100, 101]. For the ceria mediated redox process the mechanism is given as [101]:

(4) $* + CO \longrightarrow *\text{-}CO$

(5) $*\text{-}CO + 2CeO_2 \longrightarrow Ce_2O_3 + CO_2 + *$

(6) $H_2O + Ce_2O_3 \longrightarrow H_2 + 2CeO_2$

Carbon monoxide is adsorbed onto the transition metal sites (*) before reacting with oxygen from ceria, which is then re-oxidised by water.

By the formate mechanism, geminal hydroxyl groups on the surface of the partially reduced ceria react with carbon monoxide to produce formates. Addition of water decomposes the formate to form carbon dioxide and hydrogen, which desorb from the surface.

1.3.3 Equilibrium and Thermodynamics

The water-gas-shift reaction is a moderately exothermic reaction:

(7) $CO + H_2O \longrightarrow CO_2 + H_2$ $\qquad \Delta H^\circ = -41.1 \text{ kJ mol}^{-1}$

The equilibrium constant varies with temperature so low temperatures favour high conversions. Under low temperature shift conditions methanation of both carbon monoxide and carbon dioxide are thermodynamically very favourable.

(8) $CO + 3H_2 \longrightarrow CH_4 + H_2O$ $\Delta G^\circ = -142.1$ kJ mol^{-1}, $\Delta H^\circ = -206.2$ kJ mol^{-1}

(9) $CO_2 + 4H_2 \longrightarrow CH_4 + 2H_2O$ $\Delta G^\circ = -152.5$ kJ mol^{-1}, $\Delta H^\circ = -164.9$ kJ mol^{-1}

These reactions are unfavourable side reactions as they not only use up hydrogen, but the exothermic nature of the reactions could cause sintering of the catalyst if the temperature of the catalyst bed increases. However, copper-based catalysts do not show methanation activity [2].

Another problem with conventional catalysts is that reduced, low-temperature shift catalysts are potentially pyrophoric.

(10) $Cu + \frac{1}{2}O_2 \longrightarrow CuO$ $\Delta H^\circ = -157.2$ kJmol^{-1}

Hence, uncontrolled oxidation in air can result in an increase in catalyst bed temperature of between 800 and 900 K. Ruettinger and co-workers [102, 103] have looked at the use of base-metal catalysts with a precious metal (such as Rh, Pd or Pt) for the water-gas shift reaction. The advantages of the new catalysts were: no loss of catalyst activity after exposure to air, lower exotherm than a conventional Cu/ZnO catalyst and that they could be reactivated after exposure to water or low temperature steam. However, the beneficial properties observed were due to a number of factors including, lower metal loading and a different support compared with conventional $Cu/ZnO/Al_2O_3$ catalysts. The resulting lower exotherm from the catalyst bed when exposed to air or water suggests that the catalyst particles may not have reached a temperature at which sintering would occur. Hence re-activation would be more facile.

1.3.4 Recent Applications of Shift Catalysts

Although both high-temperature and low-temperature shift processes are still used for large-scale production of hydrogen, more recent work has focussed on water gas shift (WGS) catalysts for use within the automotive and fuel cells industries. Due to difficulty in scaling down the LTS or HTS processes, non-conventional WGS catalysts

are being developed for small-scale applications. One group of catalysts that are of considerable interest are transition metal/ceria catalysts [104-108].

Although ceria alone is not very active as a water-gas shift catalyst, addition of a transition metal greatly enhances its reactivity. This may be due to the metal enhancing reduction of the surface shell of the ceria. This forms active geminal hydroxyl groups which are thought to be the active site for the WGS reaction [107]. There is also evidence for the oxidation of the ceria support of Pd/ceria catalysts by carbon dioxide [106]. This is a thermodynamically favourable reaction under the experimental conditions used:

(11) $Ce_2O_3 + CO_2 \longrightarrow 2CeO_2 + CO \quad \Delta G^\circ = -85.8\ kJmol^{-1}$

It was suggested that water could replace carbon dioxide as the oxidant as this was a thermodynamically favourable reaction. Similar reactions were used to investigate the properties of Rh/ceria catalysts for the WGS [108]. The results showed that oxygen from the ceria was able to migrate to the rhodium surface and react with adsorbates (e.g. CO) on rhodium at temperatures greater than 400 K [108]. Although ceria plays a crucial role in WGS catalysts, there is still a great deal of discussion regarding the mechanism of the reaction over ceria containing catalysts.

1.4 Project Aims

The main reactions that will be considered in this study, are the synthesis/decomposition of methanol, the water gas shift reaction and the reactivity and properties of cerium hydride. All of these reactions are linked by their prospective uses within the methanol industry. Perhaps more important is that the results of the methanol decomposition reaction provide an insight as to the suitability of copper/cerium based catalysts for the methanol synthesis process. As well as improving the hydrogenation ability of a catalyst, hydrides are of interest for their storage capacity. The storage of hydrogen for mobile power applications is a field of increasing research.

The aim of this project is to investigate the area of copper/cerium catalysts for use within the methanol industry. Initially, catalysts containing copper and cerium components will be prepared and carefully characterised. The catalysts will be

examined for reactivity as methanol decomposition catalysts. By using the reverse reaction to investigate the forward reaction, it will be possible to identify any similarities to the early work surrounding copper/rare-earth alloys as methanol synthesis catalysts [70-72].

The second stage of the project will be to examine the properties of cerium hydride, a component thought to play a role in the synthesis of methanol from copper/cerium alloy catalysts [73]. The reactivity and properties of the hydride will be explored to determine any beneficial properties, which could be utilised within the methanol industry.

Finally, the copper/cerium/support catalysts will be investigated as water gas shift catalysts. As pyrophoricity is a problem with copper containing shift catalysts, the exotherm on exposure to oxygen will be examined for a series of copper/support and copper and cerium/support catalysts to determine any beneficial effects on addition of cerium.

2 EXPERIMENTAL SECTION

The following chapter describes the experimental apparatus and techniques utilised throughout the course of this study. Included are any calibration graphs and equations, which were used during the treatment of the results. The actual results and discussion of results are described in chapter three.

2.1 Catalyst Preparation

Sixteen of the catalysts examined were prepared at the University of Glasgow, while two of the catalysts studied were prepared at Johnson Matthey Catalysts. The catalysts prepared in Glasgow were all prepared by impregnation techniques. Different types of impregnation were used to produce highly dispersed, supported metal catalysts with metal w/w loadings of between 1 and 10%.

2.1.1 Materials

Two catalyst supports were chosen, silica and alumina. The silica used was C-10 Grace Silica (beads), which had a surface area of 296 $m^2 g^{-1}$ and pore volume of 1.1 $cm^3 g^{-1}$. While the alumina trilobe extrudates (supplied by Johnson Matthey Catalysts) were a low acidity support with a surface area of 104 $m^2 g^{-1}$ and a pore volume of 0.52 $cm^3 g^{-1}$. The following metal precursors were used:

- Copper (II) nitrate hemipentahydrate, 98%.
- Copper (II) acetate, 98%.
- Copper (II) ethylenediamine, (for preparation see section 2.1.2 and characterisation see section 3.1.1).
- Cerium (III) nitrate hexahydrate, 99%.
- Cerium (III) acetate hydrate, 99.9%.

Unless otherwise stated, all of the metal salts were purchased from Aldrich.

Cerium metal powder (> 40 mesh) of 99.9% purity (Alfa Aesar) was utilized. The metal was ampuled under argon and impurities were determined as calcium (200 ppm), magnesium (20 ppm), iron (10 ppm), silicon (10 ppm) and copper (3 ppm). Copper

metal powder of -40 mesh was 99.5% pure (Aldrich). For the methanol decomposition reactions either distilled AnalR methanol (>99.8%, BDH Lab Supplies) or methyl-d_3 alcohol-d (99.8 atom % D, Aldrich) was used. Distilled water was used in both catalyst preparation and for use in pulsed reactions.

The gases supplied by BOC Gases Ltd were: high purity hydrogen (99.995% minimum), helium (99.997%), oxygen free nitrogen (99.998% minimum), air (99%), pureshield argon (99.998% minimum), carbon monoxide (99.99% research grade), carbon dioxide (99.999% research grade), oxygen (99.6%), 2% hydrogen/nitrogen, 2% oxygen/argon, 1,3-butadiene (99%), trans-2-butene (99%), but-1-ene (99%), butane (99.5%), propyne (99.5%), propene (99%) and propane (99%). Deuterium gas (>99.8%) was supplied by Linde Gas UK. Dimethylether (99+%) and methane (99.0%) were supplied by the Aldrich Chemical Company. Helium gas for the experiments on glass rig 2 was treated by using two traps in sequence (Chrompack Gas-Clean Oxygen filter and Chrompack Gas-Clean Moisture filter) before the gases entered the system. The remaining gases were used without further purification.

2.1.2 Preparation of Copper (II) Ethylenediamine

The copper (II) ethylenediamine complex was prepared by adding ethylenediamine (0.083 mol, 5.5 cm^3) drop-wise to a warm solution (approx. 323 K) of copper nitrate (0.041 mol, 10.0 g) in 150 cm^3 of methanol (similar to preparation used in references [109] and [110]). The solution was stirred constantly on a hot plate and a purple precipitate formed immediately. After addition of ethylenediamine was complete, the solution was cooled in an ice bath and Buchner filtration was used to remove the excess liquid. The solid was transferred to a round bottom flask and dried *in vacuo* for 4 hours. The yield of the compound was near 83%.

2.1.3 Wet Impregnation

A metal salt solution was prepared using 150 cm^3 of distilled water. The weight of precursor used was dependent upon the w/w loading of metal required. The solution was added to 100 g of support material. Loadings of between 1 and 10% of metal (w/w) were prepared. The metal salt solution and support mixture was evaporated to dryness on a Buchi rotary evaporator (water bath at 353 K for approximately 30 mins).

The catalyst was then transferred to a drying dish and was dried either at room temperature or in an oven at 333 K for one week.

Dried catalysts were ground in a mortar and pestle then sieved to separate different particle sizes. Hence, three sizes of catalyst were available for testing, beads (as prepared), granules (250-450 microns) and fine powder (<250 microns).

2.1.4 Spray Impregnation

To improve the metal dispersion of the catalyst a spray impregnation technique was employed. As the pore volume of silica was ~1 $cm^3 g^{-1}$, the metal solutions were made by dissolving the required salt(s) in only 80 cm^3 of water. When more than one precursor was loaded onto the support, co-impregnation was used i.e. one solution containing multiple metal salts was loaded onto the support. The solution was transferred to a Degussa SG-1 sprayer. Fine jets of solution were sprayed onto 100 g of the support, which was spinning in a Pascall Lab Mixer. The catalysts did not require rotary evaporation as only the minimum volume of water had been added. Each catalyst was dried at 333 K in an oven for one week.

The dried beads/trilobes of catalyst were ground and sieved into three fractions, beads (as prepared), granules (250 to 450 microns) and fine powder (<250 microns).

2.1.5 Catalysts Prepared

As preparation conditions for the catalysts were improved throughout the course of the study, variables such as precursor salt, nominal metal loading, drying temperature, impregnation technique and support differed for each catalyst. Conditions for the formation of the catalysts prepared during this study are shown in table 2.1. The catalysts are named as XY/support where X is the nominal metal loading (w/w %) and Y the metal nitrate used as a precursor. Catalysts prepared using a different precursor or dried at room temperature are followed by the precursor and/or drying temperature in brackets.

Table 2.1. Catalyst preparation conditions and nomenclature.

Sample	*Nominal Metal Loading (% w/w)*			*Precursor*	*Impregnation*	*Support*	*Drying Temp (K)*
	Cu	*Ce*	*Pd*				
5Cu/Silica (293 K)	5	0	0	Nitrate	Wet	Silica	293
5Cu/Silica (WetImpreg)	5	0	0	Nitrate	Wet	Silica	333
10Cu/Silica (293 K)	10	0	0	Nitrate	Wet	Silica	293
10Cu/Silica	10	0	0	Nitrate	Wet	Silica	333
5Ce/Silica	0	5	0	Nitrate	Wet	Silica	333
10Ce/Silica	0	10	0	Nitrate	Wet	Silica	333
5Cu/Silica	5	0	0	Nitrate	Spray	Silica	333
5Cu5Ce/Silica	5	5	0	Nitrate	Spray	Silica	333
5Cu/Silica (en)	5	0	0	Ethylene-diamine	Spray	Silica	333
5Cu/Silica (ac)	5	0	0	Acetate	Wet	Silica	333
10Cu5Ce/Silica	10	5	0	Nitrate	Spray	Silica	333
10Cu5Ce0.05Pd/Silica	10	5	0.05	Nitrate	Spray	Silica	333
5Cu1Ce/Silica	5	1	0	Nitrate	Spray	Silica	333
5Ce/Alumina	0	5	0	Nitrate	Spray	Alumina	333
5Cu/Alumina	5	0	0	Nitrate	Spray	Alumina	333
5Cu5Ce/Alumina	5	5	0	Nitrate	Spray	Alumina	333

2.2 Pulse-Flow Micro-Reactor

The main characterisation and testing techniques were carried out using one of two pulse-flow micro-reactors. Both systems were almost identical and differed only by the mass spectrometer and gas chromatograph connected to each rig.

2.2.1 Glass Rigs (2 and 3) and Reactor

The glass rig (figure 2.1) was composed of glass bulbs connected to a manifold, which could be evacuated by the rotary pump (Edwards Rotary Pump, Max vacuum ~13.3 Pa (~10^{-2} torr)), a sample loop through which aliquots of gas could be inserted into the carrier gas, the reactor and a spiral trap. The 2 litre bulbs were used to store oxygen, carbon monoxide and hydrogen gas at just below atmospheric pressure. Additional gases could be connected to the manifold via extra cone sockets.

Figure 2.1. Diagram of glass lines 2 and 3.

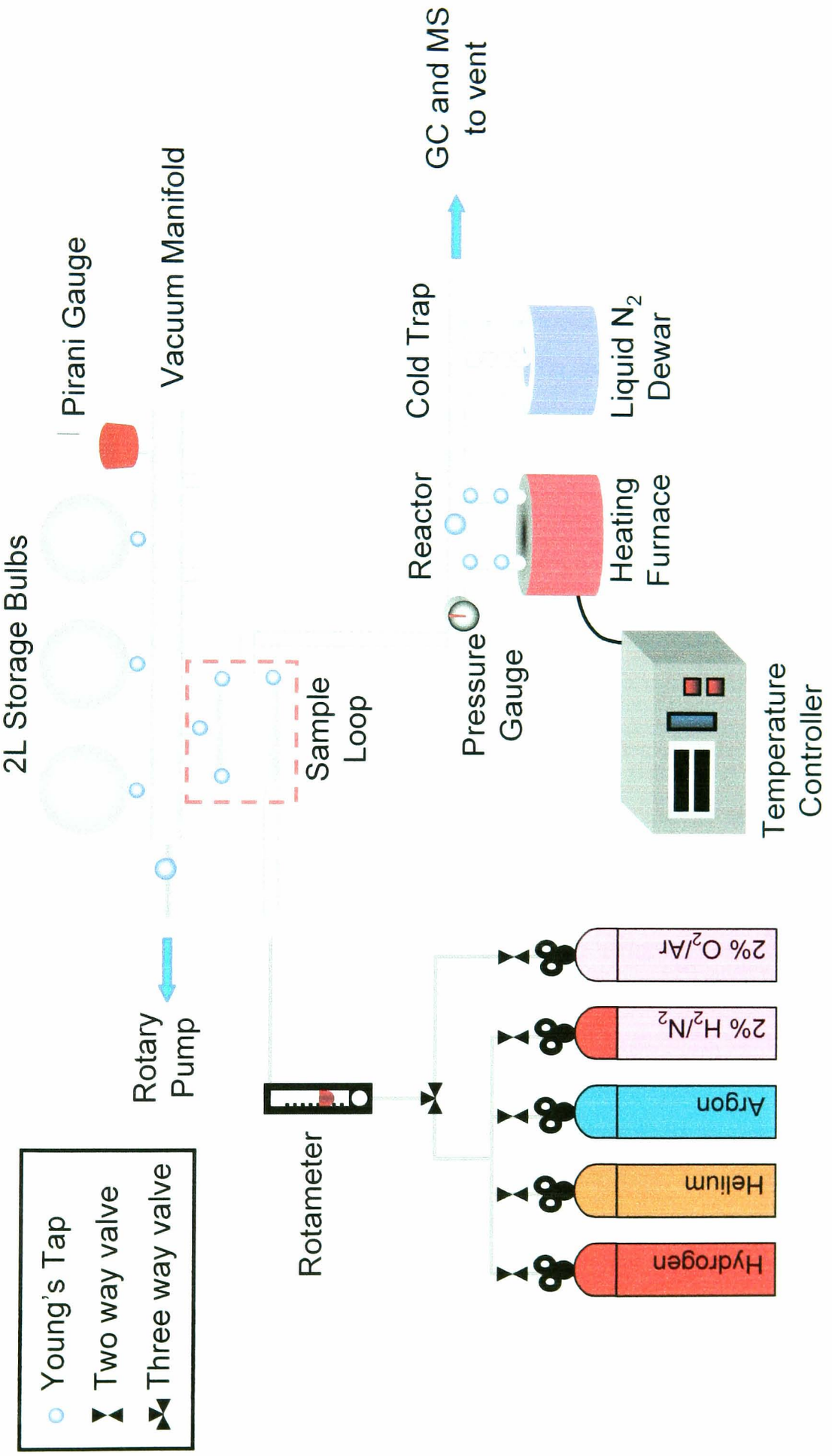

Figure 2.2. Diagram of reactor vessel.

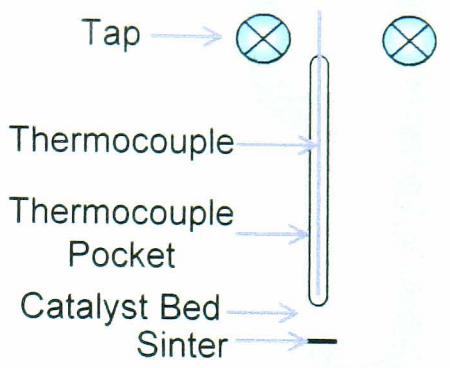

U-shaped reactors (figure 2.2) containing sample were attached to the rig using black wax to seal the cone and socket connections. The use of black wax ensured that a gastight seal was achieved. The thermocouple measured the temperature, which was controlled by a DMG temperature controller attached to a furnace. The thermocouple was placed inside the thermocouple pocket, which reached the top of the catalyst bed. As well as Pyrex reactors, quartz reactors were also available for use at high temperatures. The granules of catalyst (mesh 250-450 microns) were loaded into the reactor and placed on a fine sinter.

2.2.2 Gas Chromatograph and Mass Spectrometer

An on-line gas chromatograph (GC) and mass spectrometer (MS) were used to analyse the exit gases. On both rigs the gas chromatograph had a Thermal Conductivity Detector (TCD) and two columns. The TCD measures changes in conductivity between the gas, which passes through a reference side of the detector, and the gas that has passed through the glass line then GC column before re-entering the detector (figure 2.3). Hence, any changes in gas composition cause a change in the conductivity of the gases. This causes a change in the output signal, which appears as a peak on the integrator. The Porapak Q column was used to separate condensable gases such as carbon dioxide, water and methanol whereas a Molecular Sieve 5A column was used to separate non-condensable gases such as hydrogen, methane and carbon monoxide. Specific GC conditions varied depending on the reaction.

Figure 2.3. Schematic showing gas route through apparatus.

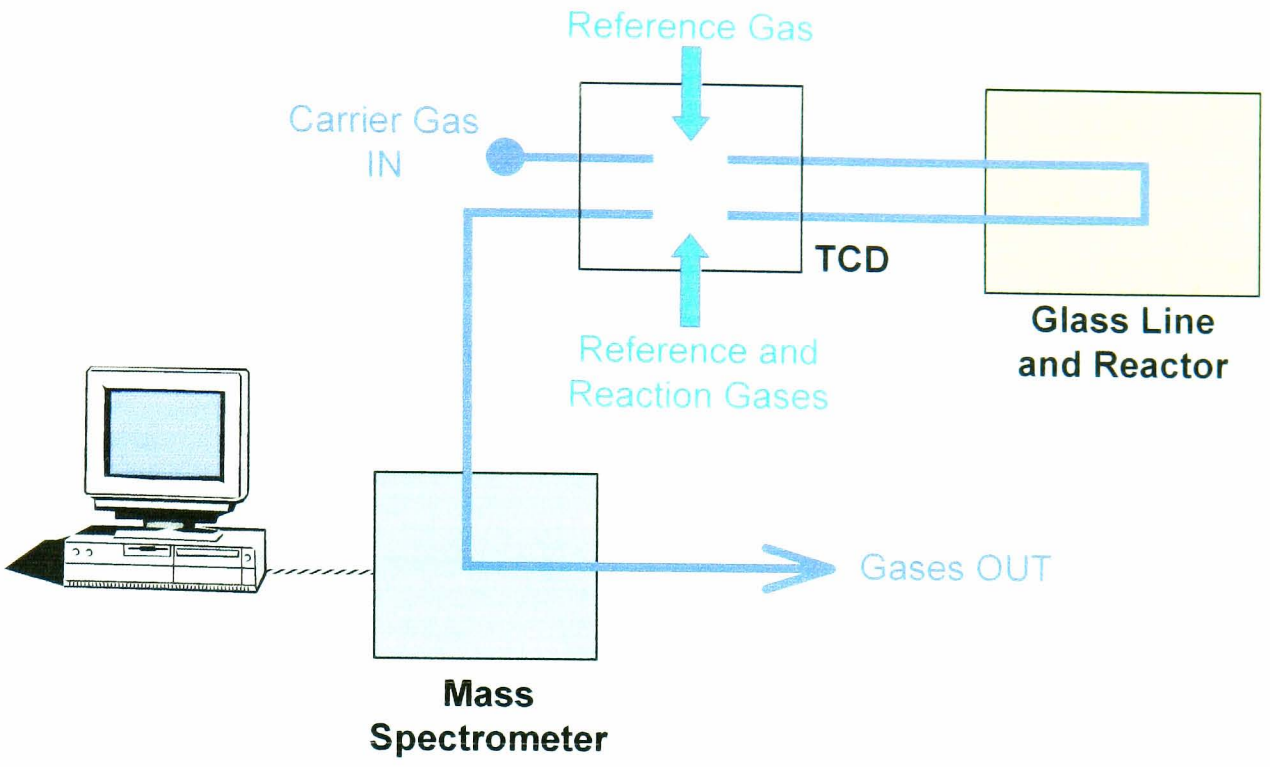

A quadrupole mass spectrometer (QMS) was connected to the gas line after the column had separated the gases. Hence, the gases were analysed by both GC and MS. The mass spectrometer was used in the MID mode. This mode follows the ionisation current of up to 20 mass to charge ratios (m/e) against time. The apparatus for each of the rigs is shown in table 2.2.

Table 2.2. Apparatus and sample loop volume for glass rigs 2 and 3.

Component	*Glass Rig 2*	*Glass Rig 3*
Mass Spectrometer	Genesys Quadstar 422 (ESS)	ESS MS
Gas Chromatograph	Pye 104 or Pye Unicam PU 4550	Shimadzu GC-14A
Sample Loop Volume (cm^3)	8.62	6.98

2.2.3 Pulse-Flow Mode

The pulse-flow micro-reactor can be used in either pulse-flow or continuous mode. In pulse mode aliquots of reactant gas (approx. 20 μmol) are inserted into a carrier gas such as helium using the sample loop (figure 2.4). As the sample loop has a set volume, the pressure of gas can be varied to change the number of moles of gas pulsed over the catalyst. This pressure was measured by a pirani gauge, which has a digital output. The

pressure of gas can be increased by opening the tap from the reactant gas or decreased by opening the tap to the vacuum pump to lower the pressure.

Figure 2.4. The two positions of the sample loop during pulse-mode operation.

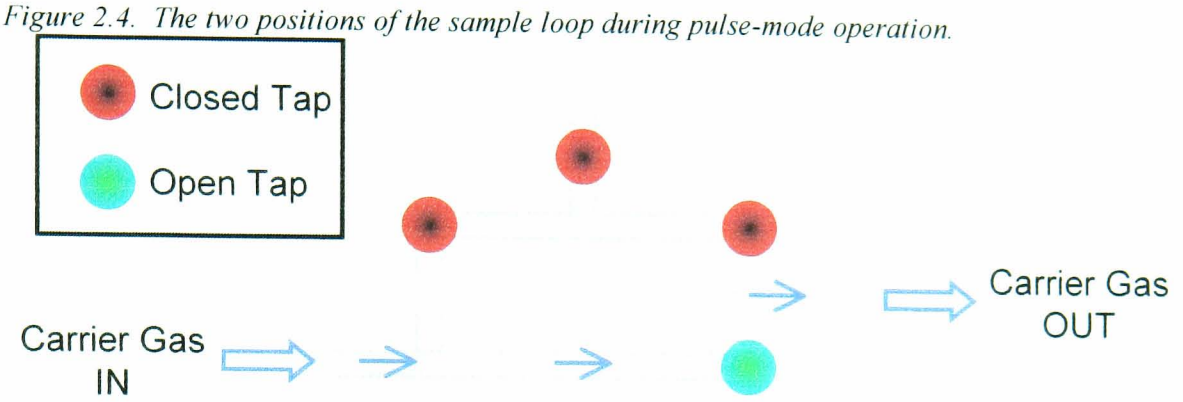

Pulse-mode operation was used to carry out both characterisation and reaction experiments. The sample loop was filled with gas from the manifold, while the carrier gas continued to flow through the bypass (position a). The position of the taps was then changed to direct the carrier gas through the sample loop (position b). Evacuating the sample loop and re-filling it with reactant gas allowed the process to be repeated. Hence, as many pulses as required could be inserted to the carrier gas to pass through the catalyst bed.

To pulse liquid vapour into the system, the following method was used. A vessel containing the liquid was attached to the rig. The liquid was evacuated several times to remove air. The tap to the pump was closed and the tap to the sample opened. The vapour from the liquid was allowed to fill the manifold until the required pressure had been reached. Literature vapour pressures for methanol and water are 1.3×10^4 Pa (100 torr at 294.1 K) and 2.3×10^3 Pa (17.5 torr at 293 K) respectively[111].

2.2.4 Calibrations

For each of the gases used during a reaction, calibrations were carried out. Pulses of varying size of the gas were pulsed into the gas line, by-passed the reactor and were analysed by GC. By plotting peak area against number of moles, the gradient of the line can be used to calculate the number of moles of gas/vapour produced in the product gases. Calibration graphs were plotted for the reactants and products of the methanol decomposition reaction, propyne hydrogenation and water-gas-shift reactions, which were analysed by GC.

The following examples of calibrations were carried out on Glass Rig 3, using the Schimadzu GC-14A gas chromatograph.

Methanol Decomposition

GC Settings:	TCD Temp	423 K	TCD Current	150 mA
	Column Temp	393 K	Carrier Gas (Flow)	He (40 cm^3 min^{-1})

The reactant and product gases followed by GC were methanol, carbon monoxide, carbon dioxide, methyl formate (MF) and dimethylether (DME).

Figure 2.5. Methanol decomposition calibration graph.

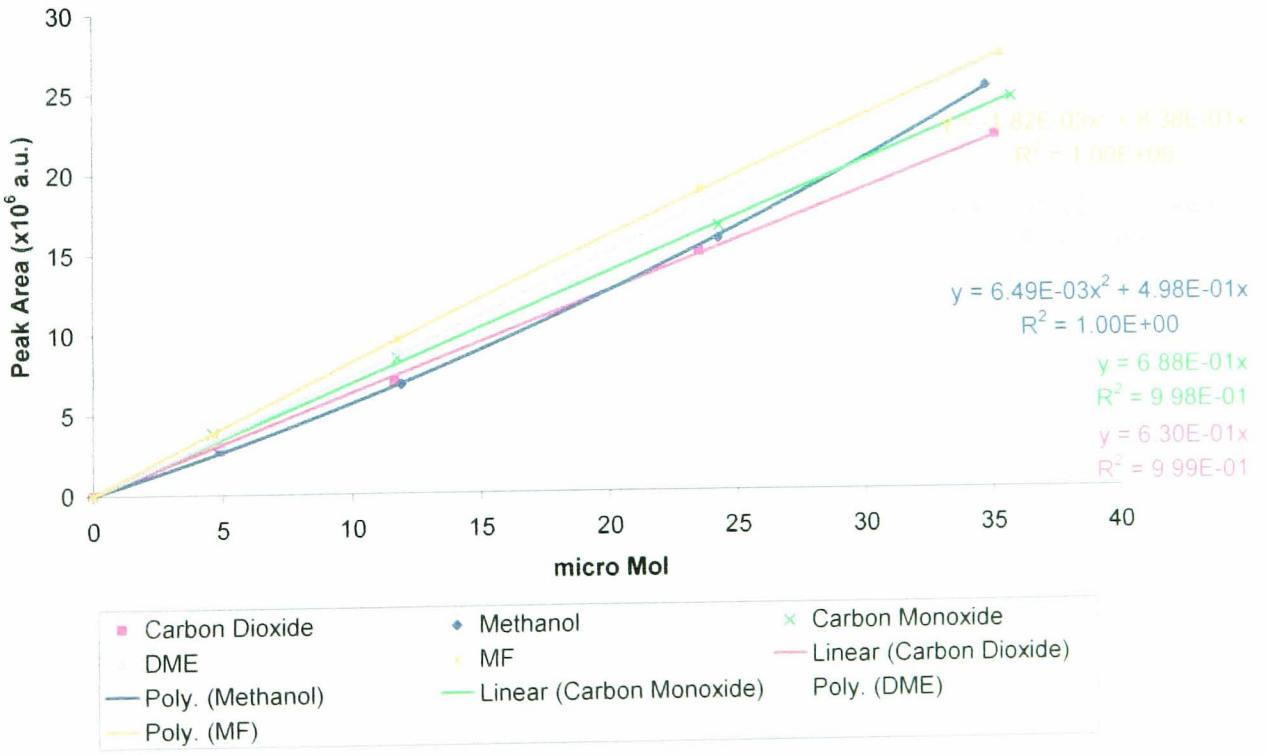

Water-Gas Shift Reaction

GC Settings: TCD Temp 423 K TCD Current 150 mA
Column Temp 333 K Carrier Gas (Flow) He (40 cm^3 min^{-1})

Figure 2.6. Water-gas-shift reaction - carbon dioxide calibrations.

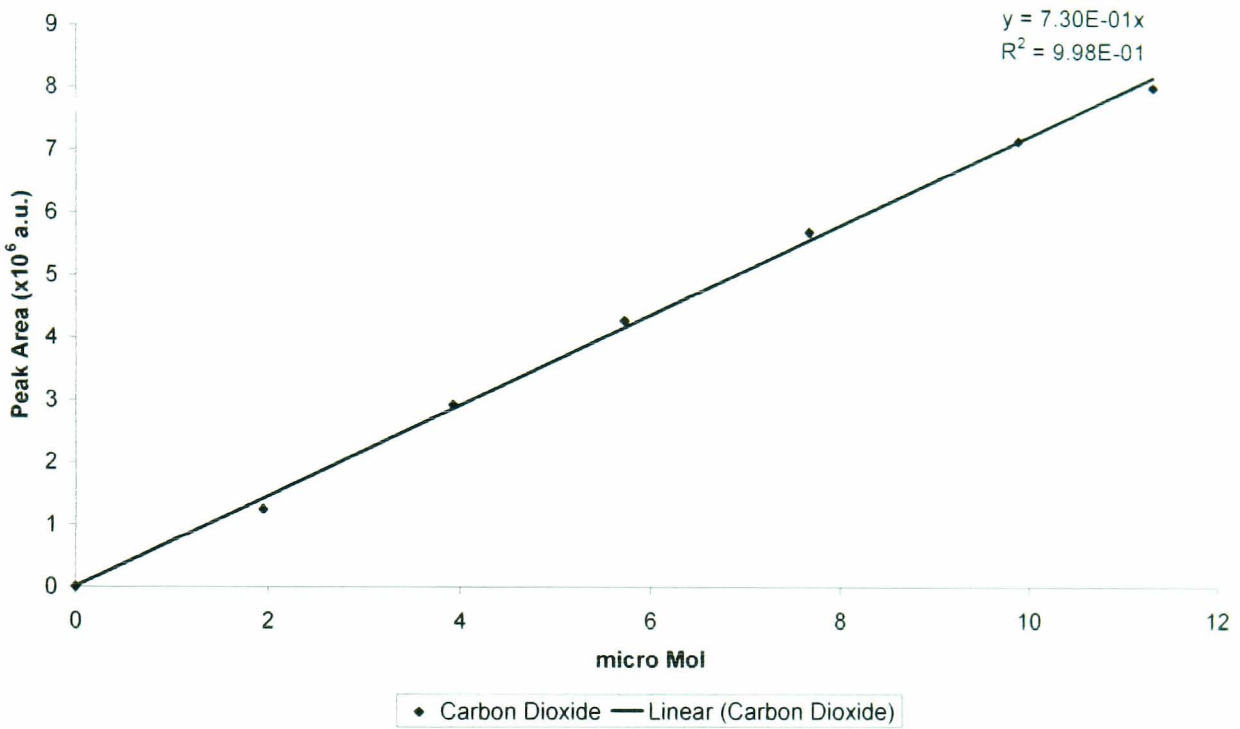

To improve the quantification technique mass spectrometry was used for the quantification of carbon monoxide and hydrogen during the water gas shift reaction (figure 2.7).

Figure 2.7. Water-gas-shift calibrations (MS) – carbon monoxide and hydrogen.

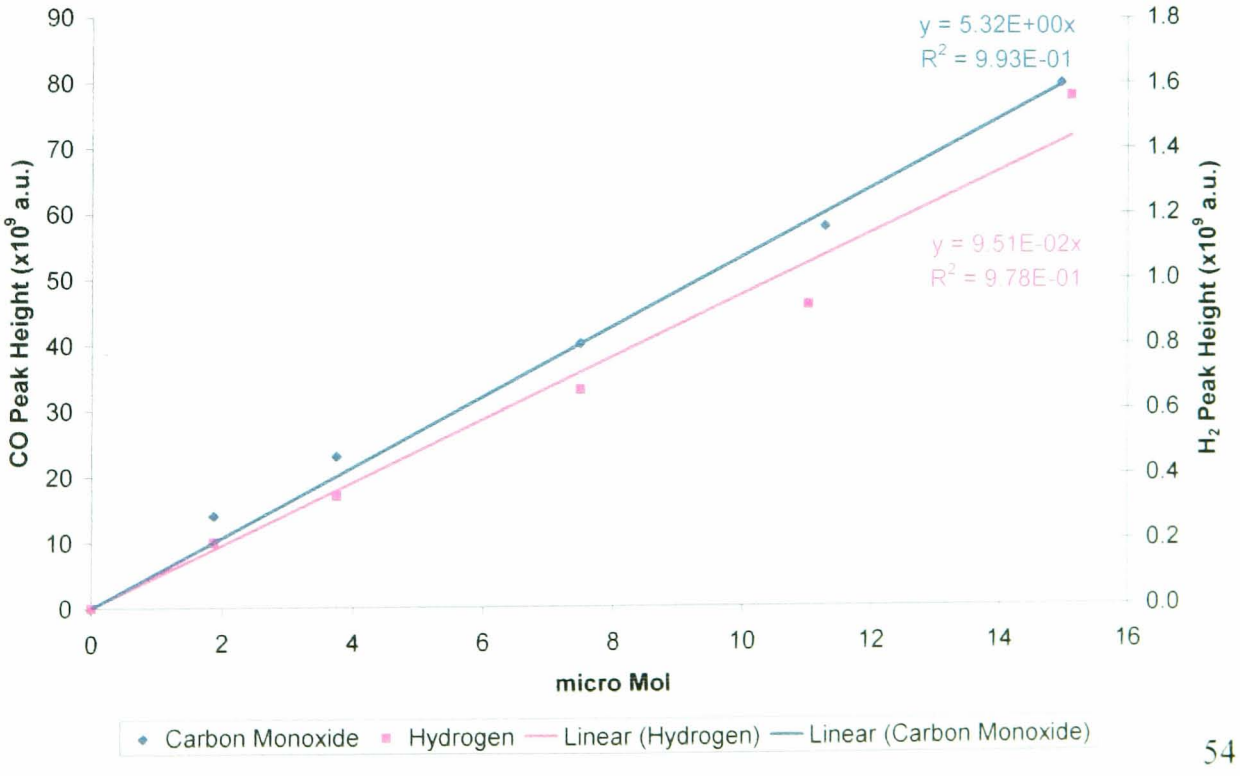

Due to variations in the mass spectrometer base line, a reference pulse was used to calibrate the carbon monoxide concentration for each of the shift reactions. Calibrations were repeated at regular intervals to improve the reproducibility of the results.

Propyne Hydrogenation

GC Settings: TCD Temp 423 K TCD Current 150 mA
Column Temp 333 K Carrier Gas (Flow) He (40 cm^3 min^{-1})

Figure 2.8. Propyne hydrogenation calibration graph.

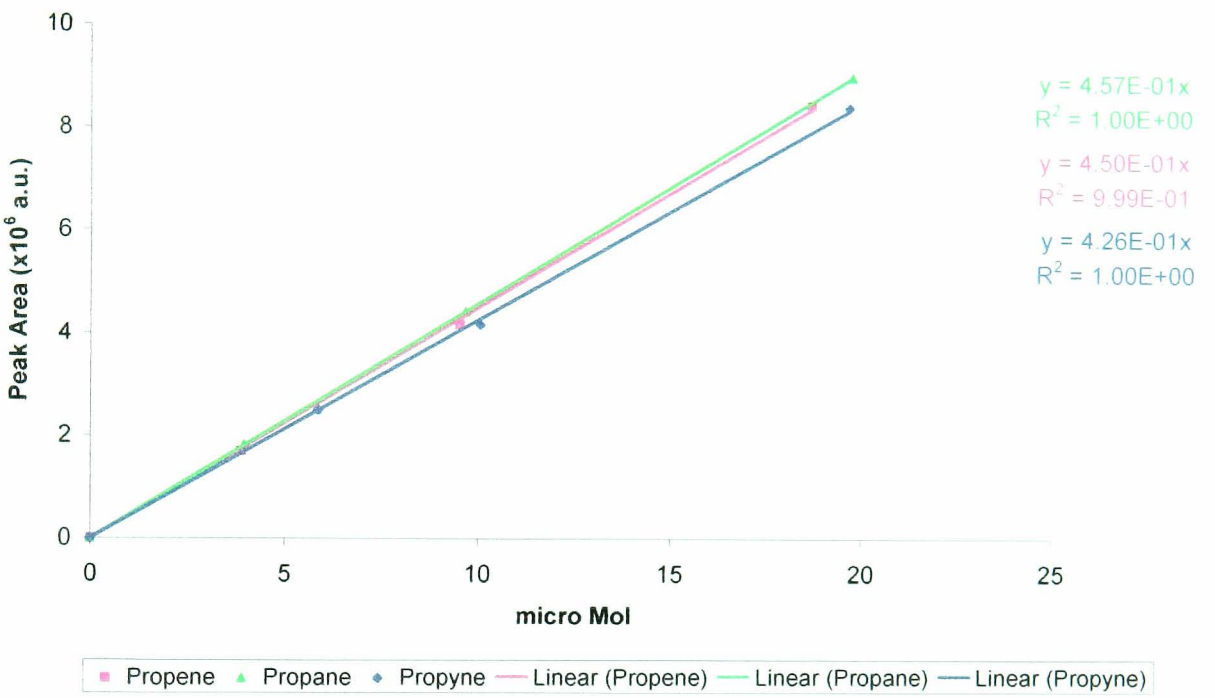

2.2.5 Continuous Flow Mode

A continuous flow of gas through the catalyst could also be achieved using the glass rig. Helium, 2% hydrogen/nitrogen or 5% oxygen/argon were passed through the catalyst bed to perform temperature-programmed reactions. For these reactions the sample loop was not required and was left in the bypass position, figure 2.4 (a). This mode was used mainly for catalyst characterisation such as temperature-programmed reduction (TPR) using the hydrogen/nitrogen mixture. Exit gases were analysed by mass spectroscopy. Continuous flow mode was used to produce qualitative rather than quantitative information from the exit reaction gases.

2.3 Hydrogenation Rig (Continuous Flow)

2.3.1 Apparatus

The mini-hydrogenation rig was used to investigate the hydrogenation of unsaturated hydrocarbons under continuous flow conditions. The system consisted of 4 Brooks Mass Flow Controllers (MFC's), a plug-flow reactor (0.4 cm inside diameter, 30 cm in length) within an oven (adapted Pye Unicam GC Oven) and a Hewlett Packard (HP 6890 series) Gas Chromatograph linked to a computer output (figure 2.9). Hydrogen and nitrogen gas were permanently connected to the line, however cylinders A and B could be interchanged for any of the C3 or C4 hydrocarbons used during reaction or calibrations. The GC had a flame ionisation detector (FID), a 50 μL automatic gas sample loop and a CP7568 capillary column (plot fused silica, 50 m x 0.53 mm), which separates C1 to 4 hydrocarbons. A Sper Scientific Datalogger (Model 800008) was used to record temperature changes of the reactor bed throughout the reactions.

The mass flow controllers were used to regulate the mixtures of gases, which flow through the system. The MFC's have been calibrated previously for hydrogen, nitrogen, propyne and carbon dioxide. The calibrated MFC's can be used to determine the flow of any subsequent gases using the following equation [112]:

$$\text{Actual Gas Flow Rate} = \text{Output Reading} \times \frac{\text{Factor of the new gas}}{\text{Factor of the calibrated gas}}$$

The plug-flow reactor was filled with enough fused alumina packing to cover the thermocouple before placing the catalyst on top of the thermocouple. More alumina packing was then added to fill the remaining space in the reactor. The end of the reactor was then plugged with quartz wool and the reactor was connected to the rig.

Table 2.3. Gas conversion factors for MFC.

Gas	*Gas Factor*	*Gas*	*Gas Factor*
1,3-Butadiene	0.354	*Propyne*	0.473
Butane	0.257	*Propene*	0.401
Trans-2-Butene	0.291	*Propane*	0.343
Carbon Dioxide	0.773		

Figure 2.9. Schematic diagram of mini-hydrogenation rig.

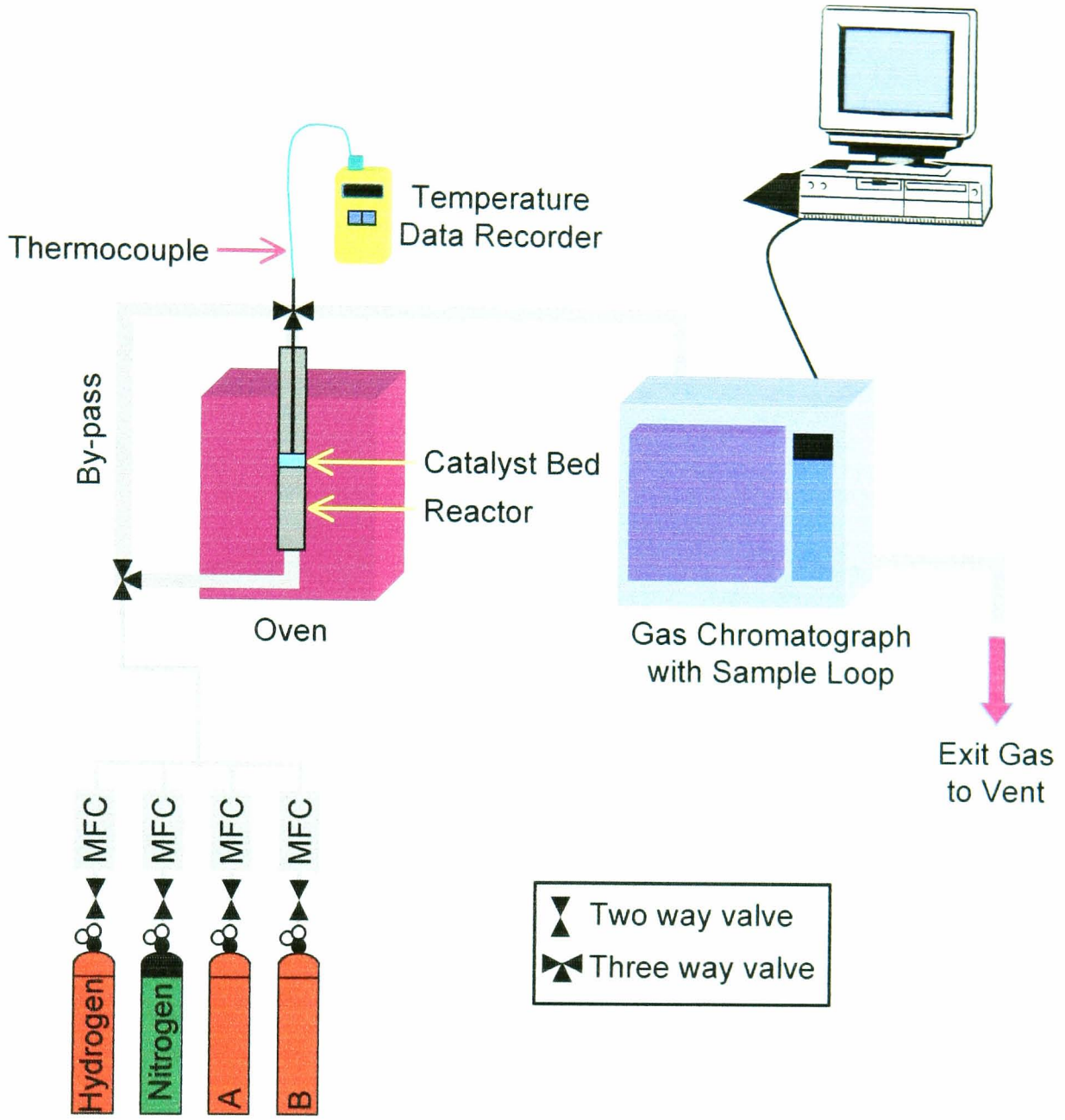

2.3.2 Calibrations

Calibrations were carried out for the reactant and all available hydrogenation products. Each gas was calibrated by taking samples from a hydrocarbon/nitrogen mixture, which had been passed through a blank reactor (filled with fused alumina packing only) at 373 K. Flows between 1 and 10 $cm^3 min^{-1}$ were selected for each hydrocarbon and nitrogen was used to make the flow up to 50 $cm^3 min^{-1}$. After setting the flow rates for the gases, they were allowed to equilibrate before sampling the gas mixture. For each flow rate, two samples were run through the GC and an average of the peak area was calculated.

The calibration lines for each compound are shown in figure 2.10. Peak areas for the trans-but-2-ene were used to calibrate for both the cis and trans isomers.

Figure 2.10. Calibration graph for the hydrogenation of 1,3-butadiene.

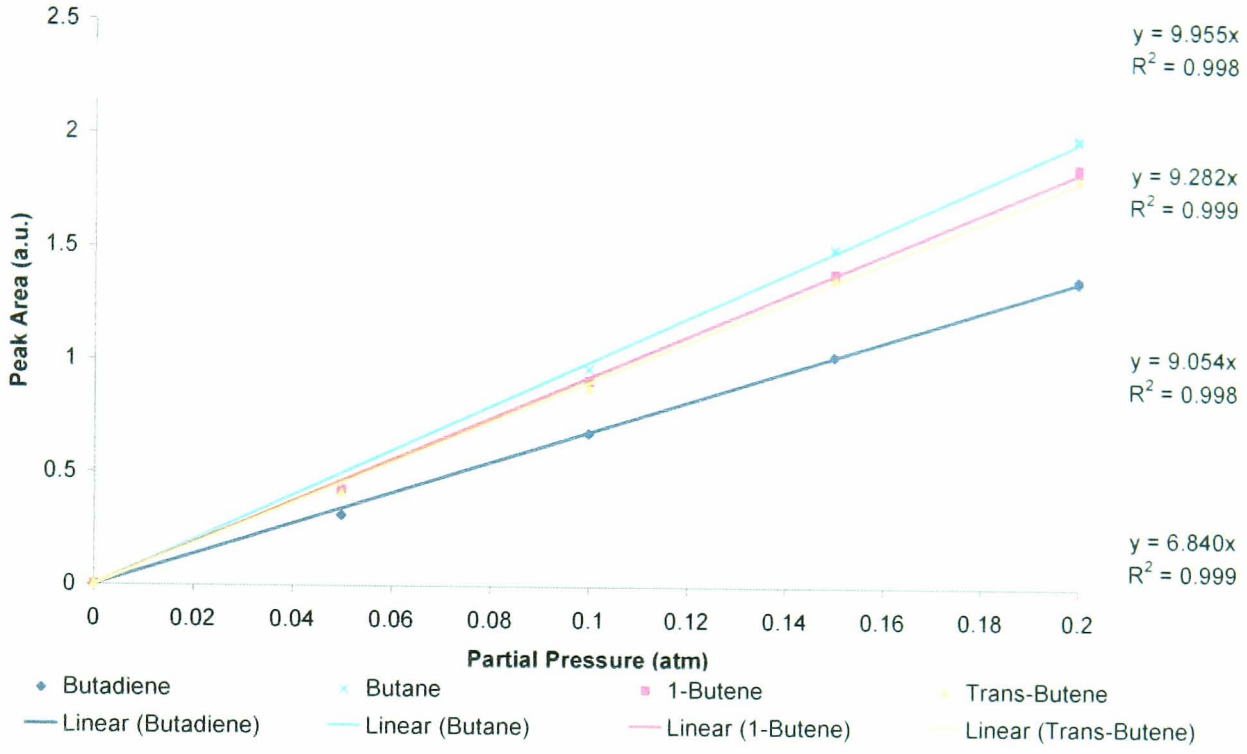

These calibrations were achieved using the following GC settings, which were also used while sampling from the reaction gases:

Oven Temperature: 388 K (Isothermal)

Front Inlet: 473 K, Pressure = 5.2×10^4 Pa (7.5 psi), Split ratio = 1:30

Column: Pressure = 5.2×10^4 Pa (7.5 psi), Flow = 4 $cm^3 min^{-1}$

FID: 523 K, H_2 flow = 20 $cm^3 min^{-1}$, Air flow = 200 $cm^3 min^{-1}$, He make-up = 30 $cm^3 min^{-1}$

2.4 Characterisation Techniques

As the condition of the catalyst surface plays an important role in heterogeneous catalysis, a number of techniques were used to investigate the materials and their surfaces. These techniques included chemisorptions, temperature-programmed reduction (TPR), solid-state UV-Vis-NIR spectroscopy, powder X-Ray Diffraction, Raman spectroscopy and BET surface area. The results of each of these techniques are detailed in section 3.

2.4.1 Oxygen Chemisorption

The chemisorptions were carried out on glass rig 2. Using a slow reduction method (see section 2.5.1). The catalyst (0.4 g) was reduced at 523 K in flowing hydrogen (30 cm^3 min^{-1}). Pulses of oxygen (~19.8 μmol) were introduced to the hydrogen carrier gas (40 cm^3 min^{-1}) from the sample loop. Aliquots of oxygen were continually passed through the catalyst bed until saturation occurred. Although not the conventional test for copper surface area, oxygen chemisorptions were used as a comparison with N_2O chemisorptions.

2.4.2 Temperature Programmed Reduction (TPR)

Temperature programmed reduction (TPR) is a "finger print" technique [113, 114] for the characterisation of catalysts. However, the results can be affected by a number of factors including: catalyst preparation, pre-treatment of catalyst and the conditions used to carry out the TPR.

Temperature programmed reductions were performed on glass rig 2. The rig was used in a continuous flow mode and the mass spectrometer was used to follow mass to charge ratios: 28 (nitrogen), 2 (hydrogen) and 18 (water). Hence, the hydrogen uptake could be plotted against reactor temperature and the peak maximum for the curves was determined. The catalyst sample (0.4 g) was purged with helium (35 cm^3 min^{-1}) for 20 mins. The gas flow was switched to 2% hydrogen/nitrogen (35 cm^3 min^{-1}) and the reactor was purged with gas until the mass spectrometer signals had equilibrated. The temperature was then ramped from 393 K to 873 K (at 3 K min^{-1}) and the temperature held for 10 mins.

The resulting temperature programmed reduction graphs were plotted as hydrogen uptake against temperature. The TPR traces provided information about the number of different species being reduced and also the minimum temperature required to reduce the catalyst prior to reaction. Hence, the temperatures at which peaks were observed (T_{max}), the temperature at which the peak started ($T_{Initial}$) and the temperature at which reduction had ceased (T_{final}) could be determined.

2.4.3 UV-Vis-NIR Spectroscopy

Solution UV-Vis-NIR spectroscopy was determined using a Varian Cary 500 (version 8.0). Air was used as the blank sample to measure the background spectrum. Then a 1 cm cuvette was filled with the solution to be examined and placed in the sample holder. A spectrum was taken over the range of 1900 to 200 nm. The settings used were a scan rate of 200 nm min^{-1}, data interval of 0.33 nm and average time between data points of 0.1 sec.

Solid-state UV-Visible-NIR spectroscopy was carried out using a Praying Mantis Diffuse Reflectance Accessory on the Varian Cary 500. Two hemispherical mirrors positioned above the sample collected the light reflected by the sample/reference. The light collected was then projected onto the instrument detectors. The advantage of using this attachment was that very small solid samples could be analysed, without reducing the wavelength that could be examined. Baselines were collected using barium sulphate as the reference. Samples were ground into a fine powder (<250 micron) before being added to the sample holder. The range of wavelengths scanned was from 1900 nm to 190 nm (at a scan rate of 200 nm min^{-1}, data interval of 0.33 nm and average time of 0.1 sec).

2.4.4 Raman Spectroscopy

A selection of the silica-supported catalysts were examined using Raman spectroscopy. The Raman spectra were performed at Johnson Matthey Catalysts in Billingham and Malcolm Kett provided training on the apparatus.

Apparatus

A LabRam Infinity Spectrometer was used to run spectra of eleven of the silica-supported catalysts, the silica and the main catalyst precursor (copper (II) nitrate hemipentahydrate). The spectrometer also had an environmental cell that could be used to study the surface of the catalyst under realistic reaction conditions e.g. reduction and oxidation. The temperature programmer (TMS 93 temp controller for the TS 1500 high temperature stage) controlled the temperature of the sample while gases (N_2, 2% O_2/He or 3% H_2/He) flowed through the reaction cell.

Settings

The settings were adjusted to achieve the best spectra for the copper and cerium-supported samples:

Excitation line	632.81 nm (red laser)
Grating	1800 gr/mm^2
Time	60 seconds
Accumulations	10
Confocal Hole	800 μm
Wavenumber Range	100 - 1652 cm^{-1}

Simple Raman Spectra

Beads of catalysts/support were loaded onto glass slides using blu-tak to hold them in place. For one sample, both beads and a pressed disc were examined. The pressed sample provided very little information, due to the fact that it shows mainly bulk interactions. The graph produced was noisy and showed one weak peak from the nitrate. Subsequently, the beads were examined as they provided greater surface detail of the sample. Once the glass slide was fitted into the sample holder, the laser was focused using visual imaging and the confocal microprobe. Samples of the catalysts, copper nitrate and silica support were analysed using this method.

Environmental Cell

The environmental cell consisted of a heater/sample holder with inlets for gas to flow through the reaction chamber. The cell also had a cooling system. By flowing water into the cooling stage of the reaction cell, the heat generated by the sample heater and laser was reduced (figure 2.11). Three catalysts were examined using this in situ technique, 5Ce/Silica, 5Cu/Silica (WetImpreg) and 5Cu5Ce/Silica.

Figure 2.11. Diagram of Raman environmental cell.

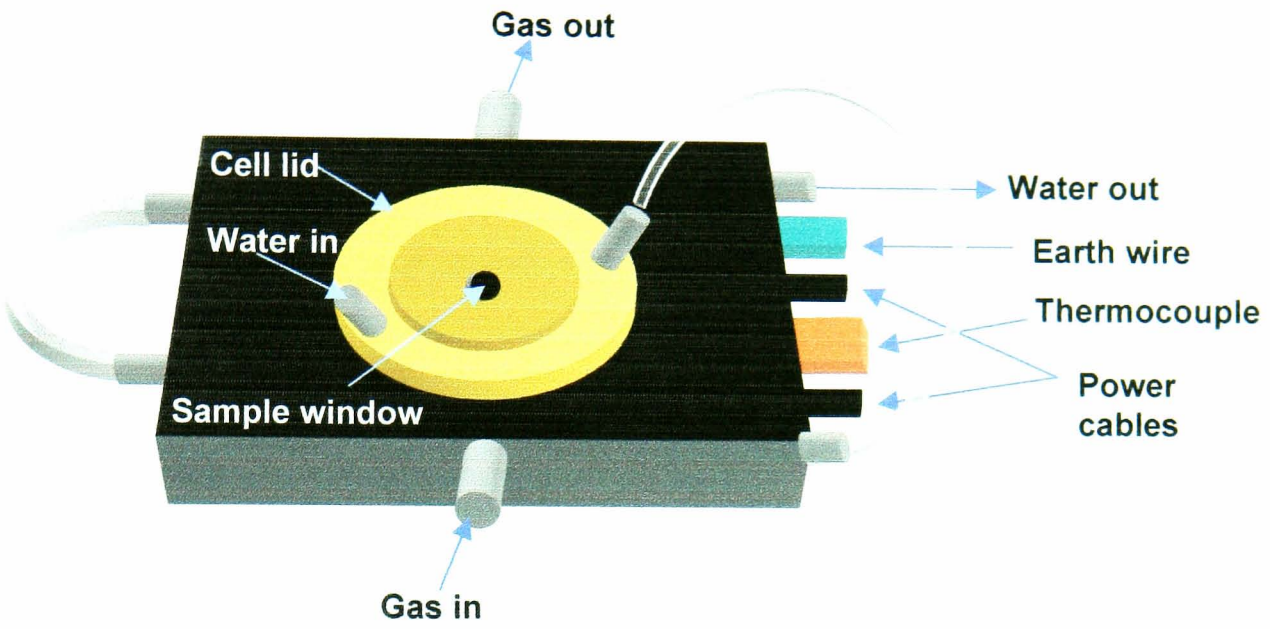

A bead of catalyst was placed on a sapphire window on the heater/sample holder and covered with a radiation shield. The lid of the cell was then screwed into place and the tubing for the gas and water was attached to the cell. Once the laser was focused on the sample, nitrogen (10 cm^3 min^{-1}) was used to purge the cell. The nitrogen was then turned off, the reaction gas turned on and the heater ramped at the required rate. Each of the three samples was reduced (3% hydrogen/helium, 8 cm^3 min^{-1}), then oxidised (2% oxygen/helium, 20 cm^3 min^{-1}) then reduced (3% hydrogen/helium, 8 cm^3 min^{-1}) in the environmental cell. The heating conditions were the same for each of the three procedures: the sample was heated from room temperature to 523 K at 5 K min^{-1} and the temperature was held for 30 mins. Spectra were taken at regular intervals during the reaction (approx. every 10 mins). At the end of the heating process the cell was cooled to room temperature and another spectrum collected. Hence, the presence of any temperature dependent peaks could be detected.

2.4.5 Surface Area Measurement (BET)

The BET (Braunauer, Emmett, Teller) process uses the physisorption of nitrogen to determine the surface area of solids. Surface area measurements for all of the catalysts prepared were carried out on a Micromeritics Gemini III 2375 Surface Area Analyser. Between 0.03 g and 0.04 g of each sample was added to a sample tube and dried over-night at 383 K in a nitrogen gas flow. The samples were granular (250-425 micron) and the evacuation rate used was 4.0×10^4 Pa min^{-1} (300 torr min^{-1}).

2.4.6 Copper Surface Area (N_2O)

Copper surface areas were determined by N_2O frontal chromatography by Colin Ranson at Johnson Matthey Catalysts in Billingham. Standard operating conditions were used and the measurements were made on samples with a particle size between 0.6-1 mm. Copper surface areas were all expressed on a discharged weight basis. Estimation of errors was calculated at approximately ±4%.

This technique works by measuring the amount of nitrogen produced from passing N_2O over the catalyst surface. From equation 1.3, the ratio of nitrogen to copper can be deduced and hence the number of moles of surface copper can be calculated.

$$2Cu\ (s) + N_2O\ (g) \longrightarrow Cu_2O\ (s) + N_2\ (g)$$

The copper surface area per gram of catalyst is then calculated from equation 1.4, where the surface density of a copper atom was taken as 1.0×10^{19} atoms m^{-2}.

$$\text{Area of Cu Surface } (m^2g^{-1}) = \frac{\text{Number of Atoms of Cu}}{\text{Catalyst Mass x Surface Density of Cu Atoms}}$$

Dispersion

The dispersion was calculated from the copper surface area determined by N_2O chemisorption.

$$\text{Metal Dispersion (\%)} = \frac{\text{Surface Metal (mol)}}{\text{Total Metal (mol)}} \times 100$$

Average Particle Size

From the oxygen chemisorption results, dispersions calculated were used to determine the average Cu particle size using the following formula [115]:

$$\text{\% Dispersion} = \frac{A \times 6}{\rho \times S_a \times N_a \times d} \times 100$$

Where: -

A	Atomic weight = 63.55 amu.
ρ	Density of metal = 8.92×10^{-21} g nm^{-3}.
S_a	Atomic cross section of copper [116] = 0.068 nm^2 $atom^{-1}$.
N_a	Avogadro constant = 6.022×10^{23} atoms mol^{-1}.
d	Average particle diameter (nm).
D	Dispersion (%).

By substituting the constant values, the equation was simplified to the following relationship for copper particles:

$$d\ (nm) = \frac{104}{D}$$

This formula was used to calculate the average particle diameter of each of the catalysts.

2.4.7 Powder X-Ray Diffraction (XRD)

Bill Higgison at the University of Glasgow's Earth Science Department carried out the powder XRD experiments. The samples were examined in the range of 5 to 80 °2θ using a step size of 0.02° and a counting rate of 1s/step. The patterns were obtained from a Philips PW 1050/35 X-ray diffractometer using Co-Kα radiation (λ = 0.178897 nm). All of the fresh samples were examined as well as a selection of post-reaction samples to determine any changes in catalyst morphology.

Where possible, the Scherrer equation [117] was used to determine the average crystallite size by using the line-width of the strong signals in each sample.

$$\Delta'(2\theta) = \frac{K\lambda}{L \cos\theta}$$

Where: $\Delta'(2\theta)$ = Full width at half peak height (2θ in radians)

K = Constant (0.9)

λ = Wavelength of Co source (0.178897 nm)

L = Average length of crystallite (nm)

θ = Angle of peak (°)

2.4.8 Atomic Absorption Spectroscopy (AAS)

A Perkin Elmer 1100B Atomic Absorption Spectrometer was used to determine the actual copper content of the catalysts prepared. The element used was copper (324.7 nm), slit 0.7 nm and lamp current of 10 mA. Solutions were prepared by adding 0.1 to 0.2 g of catalyst to 10 ml of Aqua Regia and the solution refluxed for 2 hours. The mixture was then filtered through hardened filter paper, before diluting the solution with distilled water to achieve concentrations of between 1 and 5 ppm of copper. Standards were prepared using a copper atomic absorption standard solution (Aldrich), which was again diluted with distilled water to prepare solutions with concentrations of between 1 and 5 ppm. The spectrometer was used to determine copper contents for all of the fresh copper-containing catalyst as well as the copper (II) ethylenediamine complex prepared in section 2.1.2.

2.4.9 ^{1}H Nuclear Magnetic Resonance (^{1}H NMR)

A few granules of copper (II) ethylenediamine (section 2.1.2) were dissolved in 4 ml of $CDCl_3$ and the resulting solution was analysed on a Brucker-spectrospin 400 Ultrashield NMR spectrometer. The supported copper (II) ethylenediamine catalyst (5Cu/silica (en)) was examined in a similar way, however the solution was filtered through alumina prior to analysis to improve the spectrum.

2.4.10 Solid-State Infrared Spectroscopy (Golden Gate)

Infrared spectroscopy was carried out on a JASCO-410 FTIR using a Golden Gate attachment for determination of IR solid-state samples. A few grains of sample were placed on the window of the attachment, before securing the lid. The wavenumber range examined was from 4000 to 750 cm^{-1} (at a resolution of 4 cm^{-1} and scan speed of 2mm sec^{-1}).

2.4.11 Carbon, Hydrogen and Nitrogen Microanalysis

Microanalysis was carried out on the copper (II) ethylenediamine complex prepared in section 2.1.2. Kim Wilson carried out the analysis at the University of Glasgow department of chemistry. The percentage of carbon, hydrogen and nitrogen in the sample was calculated and the results are shown in section 3.

2.5 Catalyst Testing

2.5.1 Standard Catalyst Reduction

Other than for temperature-programmed reductions all catalysts were reduced prior to testing. Two different reductions were attempted, a slow reduction to 523 K and a faster reduction to 948 K. The fast reduction was similar to that used by Toupance et al [118] for copper silica catalysts. The sample was heated to 948 K at 5 K min^{-1} in flowing hydrogen (30 cm^3 min^{-1}) then held for 1 hour and allowed to cool to room temperature in hydrogen.

The slow reduction heated the catalyst in stages in flowing hydrogen (30 cm^3 min^{-1}) to 523 K using a ramp rate of 1 K min^{-1}. The heating stages were as follows:

- 298 to 373 K then held for 1 h
- 373 to 423 K then held for 1 h
- 423 to 473 K then held for 1 h
- 473 to 523 K then held for 1 h

The reduction was carried out over-night and the catalyst was allowed to cool in hydrogen.

2.5.2 Methanol Decomposition

All of the catalysts prepared were examined for methanol decomposition. The decomposition reaction was studied using glass rig 2 (figure 2.1). The catalyst (0.4 g) was added to the reactor vessel and reduced *in situ* using the slow reduction method. During the reaction, the reactor temperature was maintained at 473 K in helium (40 cm^3 min^{-1}). Methanol was introduced to the carrier gas as described in section 2.2.3. Hence, pulses of known volume and pressure of methanol (typically 42.4 μmol) were incorporated into the carrier gas via the sample loop. Five pulses were passed over each catalyst and the effluent gases were examined by gas chromatography.

Both columns were used to analyse the exit gases. The molecular sieve column was used first to analyse for H_2, CO and CH_4. The liquid nitrogen trap was then removed from the spiral trap and the remaining compounds (CO_2, H_2O, methyl formate and methanol) were analysed through a Porapak Q column.

The resulting gas mixture was used to determine the conversion of methanol to products, the selectivity and yield of the catalyst towards each product and the carbon/oxygen count achieved for each pulse.

Calculations

By converting the peak area for each compound to the number of moles of each compound produced, the following equations can be used:

$$\% \text{ Conversion} = \frac{\text{in-out}}{\text{in}} \times 100$$

$$\% \text{ } CO_2 \text{ Selectivity} = \frac{CO_2 \times 100}{(CO_2 + CO)}$$

$$\% \text{ Yield} = \frac{\text{Product (moles)}}{\text{in}} \times 100$$

Where: **in** Reactant in (moles)

out Reactant out (moles)

CO_2 Carbon dioxide in exit gases (moles)

CO Carbon monoxide in exit gases (moles)

The carbon and oxygen balances were also to determine any loss/gain of material to the surface of the catalyst. An increase in carbon or oxygen due to the catalyst would result in value of over 100% carbon/oxygen. Whereas a loss of material would result in a value of less than 100%.

$$\% \text{ Carbon OUT} = \frac{\Sigma \text{ Carbon containing products (mol)}}{\Sigma \text{ Carbon containing reactants (mol)}} \times 100$$

$$\% \text{ Oxygen OUT} = \frac{\Sigma \text{ Oxygen containing products (mol)}}{\Sigma \text{ Oxygen containing reactants (mol)}} \times 100$$

2.5.3 Water-Gas-Shift Reaction

The water-gas shift reactions were carried out on glass rig 2 (figure 2.1). The catalyst (0.4g) was added to the reactor vessel and reduced *in situ* using the slow reduction method. After reduction the reactor was flushed with helium (40 cm^3 min^{-1}) and heated to 473 K at 6 K min^{-1}. The catalyst was then maintained under a helium gas flow (40 cm^3 min^{-1}) at 473 K throughout each reaction.

Reaction 1 – Water-Gas-Shift (WGS) Reaction. The reactant mixture was prepared by adding water vapour (~3.8 μmol) to the vacuum manifold before adding carbon monoxide gas (~7.6 μmol) to the vapour. The gas mixture was allowed to equilibrate for approx. 30 mins before use. Six aliquots of the carbon monoxide/water mixture (2:1 ratio) were pulsed through the catalyst bed. Exit gases were analysed by gas chromatography and mass spectroscopy.

Reaction 2 – CO pulses, WGS, O_2 pulse then WGS. The catalyst is initially treated with carbon monoxide pulses (~19 μmol, 4 pulses), then carbon monoxide/water pulses, a pulse of oxygen and finally the shift reaction is repeated. The mixture of water and carbon monoxide gases was prepared by adding water vapour (~3.8 μmol) to the vacuum manifold before adding carbon monoxide (~7.6 μmol). The ratio of reactant gases was 2:1 of carbon monoxide to water. The temperature change observed on reaction of the catalyst with the 38 μmol pulse of oxygen was also recorded.

The main products of the reaction such as carbon dioxide and water were analysed by gas chromatography, whereas hydrogen and carbon monoxide were analysed by mass spectroscopy. Similar calculations to those used in section 2.5.2 were used to determine the conversion of carbon monoxide to products as well as to determine the final carbon and oxygen mass balances for the reaction.

2.5.4 Hydrogenation of 1,3-Butadiene

The hydrogenation of 1,3-butadiene was carried out on the mini-hydrogenation rig (Section 2.3). The glass-lined reactor was filled with boiling chips to cover the thermocouple before adding 0.125 g (0.25 cm^3) of catalyst. Once attached to the rig, the reactor was purged with nitrogen (10 cm^3 min^{-1}) before switching to hydrogen gas (20 cm^3 min^{-1}). Heating in a hydrogen stream to 523 K at 1 K min^{-1} and holding the temperature over-night reduced the catalyst. Before reaction the catalyst was cooled in a nitrogen flow (20 cm^3 min^{-1}) to 373 K. The reactor was then by-passed before setting the reaction flow.

A sequence of reactions was then performed on each catalyst. The first reaction used a 1,3-butadiene to hydrogen ratio of 1:4. Hence, the feed was composed of 5 cm^3 min^{-1} 1,3-butadiene and 20 cm^3 min^{-1} of hydrogen. After allowing the gas mixture to flow

through the bypass for 10 mins, a reference gas sample was collected via the automatic sample valve. The gas flow was then switched to flow through the reactor and samples were collected during the reaction every 20 mins for 2 hours. After 2 hours the hydrocarbon was switched off and the hydrogen and nitrogen remained on. Samples were taken every 10 mins via the automatic sample valve for approximately one hour or until no more hydrocarbons were observed.

The same catalyst was then used at three further 1,3-butadiene to hydrogen ratios. After the 1:4 hydrogenation the ratios were 1:2, 1:1 then 1:4 again. For each ratio the hydrocarbon flow was held at 5 cm^3 min^{-1} and the hydrogen flow was varied.

This series of reactions was used to examine 5Cu/Silica (WetImpreg), 5Ce/Silica and 5Cu5Ce/Silica for the hydrogenation of 1,3-butadiene. The yield and selectivity towards the reaction products was calculated assuming that all of the products were detected in the exit gases and that there was no loss of reactant/product to the catalyst.

2.5.5 Cerium Metal Investigation

Due to the highly reactive nature of cerium metal, preparation of samples and loading of reactors was carried out under a nitrogen atmosphere (M Braun Unilab Glovebox, processing gas: nitrogen). Quartz reactors were loaded with 0.5 g of metal in a nitrogen atmosphere. Mixed metal samples were also prepared in the glove box by dry mixing 0.5 g of cerium metal with 0.27 g of copper metal (1:1 mole ratio). Similarly, 0.4g of 5Cu/silica was mixed with 0.5 g of cerium metal.

Once prepared, the samples were loaded into the reactor and the taps to the reactor were closed to allow the reactors to be transferred to glass rig 3 (figure 2.2 and table 2.2). The reactor was then black waxed to the rig. To ensure low levels of impurities such as air or water, the glass line was purged with carrier gas such as argon (40 cm^3 min^{-1}) for at least one hour before opening the reactor and sample to the system gases. Once opened, the metal samples were heated to 523 K (at 2 K min^{-1}) and maintained in argon. Pulsed reactions were then carried out at 523 K as described in section 2.2.3.

Hydride Formation and Deuterium Exchange

Pulses of hydrogen (~200 μmol) were passed through the cerium metal in an argon carrier gas (40 cm^3min^{-1}). Deuterium exchange was carried out using argon as the carrier gas with the same flow. Two deuterium pulses (between 27 and 41 μmol of D_2) were used to determine the exchange properties of the samples. For subsequent reaction pulses, the carrier gas was switched to helium.

Carbon Monoxide and Carbon Dioxide Pulses

Carbon monoxide (~20 μmol) and carbon dioxide (~20 μmol) were pulsed over the cerium hydride. Each reaction was attempted initially using a helium carrier gas (40 cm^3min^{-1}) before switching to a hydrogen flow (40 cm^3min^{-1}).

Propyne Reactions

Pulses of propyne (~20 μmol) were reacted over the cerium hydride in either an inert carrier gas (helium 40 cm^3min^{-1}) or a reducing carrier gas (hydrogen 40 cm^3min^{-1}).

Reactions with Oxygen

The carrier gas for the oxygen pulses was helium (40 cm^3min^{-1}). The pulse size was initially low, to gauge the effect of oxygen pulses on the temperature of the sample. Hence, pulse size was varied between 15.4 μmol and 170 μmol.

Methanol Decomposition

Several pulses of methanol (~15 μmol) were passed over the cerium hydride in a helium carrier gas (40 cm^3min^{-1}). The decomposition reaction was examined further by using fully deuterated methanol pulses (~ 20 μmol). Both reactions were carried out in a helium carrier gas (40 cm^3min^{-1}).

3 RESULTS AND DISCUSSION

The following chapter encompasses both experimental results and discussion of results and is divided into five sections. The first section describes the characterisation of the supported catalysts and a precursor that was prepared at the University of Glasgow. This section includes a discussion of the species present on the fresh and used catalysts, and the effect of cerium addition on the copper catalysts. The second section describes the results of the methanol decomposition reaction that was carried out on all of the characterised catalysts. This led to the need to investigate the reactivity of the cerium hydride (thought to play a major role in the synthesis of methanol from alloys) and to determine whether its properties could be applied industrially, which is discussed in section three. In the fourth section, the properties of the prepared catalysts were explored for use within the water gas shift reaction. Finally, two catalysts were chosen to examine the effect of catalyst ageing which had occurred after storing the catalyst for two years.

3.1 Precursor and Catalyst Characterisation

Characterisation of catalysts is crucial to understanding the active components of a catalyst. There are several books dedicated to describing the characterisation of catalysts [119-122]. Development of future generations of catalysts requires an in-depth knowledge of the surface species, which participate in a reaction. Hence, a variety of spectroscopic and reaction techniques are often combined to examine a catalyst's surface. By examining pre- and post- reaction samples some information can be gained about the species present in the active catalyst. The growing use of *in situ* spectroscopic techniques can provide information not only about the active surface species of the catalyst during reaction, but can identify intermediate adsorbate species present. By closely examining surface species and intermediates, this can lead to a greater understanding of the reaction mechanism and active species of the catalyst. Hence, future catalysts can be designed with the aim of achieving specific properties suitable for each reaction.

In this section, a number of techniques were combined to examine a copper amine complex prepared at the University of Glasgow. The precursor was characterised before preparing a copper (II) ethylenediamine catalyst, supported on silica. The

remainder of this section details the characterisation of all of the catalysts prepared. Pre-reaction samples were examined by XRD, BET, chemisorption, AAS, UV-Vis-NIR spectroscopy and TPR. Post-reaction samples were studied using XRD. To follow the effect of the reduction and oxidation processes on a selection of catalysts, in-situ Raman spectroscopy was used.

3.1.1 Characterisation of Copper (II) Ethylenediamine Precursor

An investigation into NiO_X/Al_2O_3 catalysts [123] found that the anions and ligands of the nickel precursor strongly influenced the nickel surface species of the catalyst. After thermal treatment in nitrogen $[NiL_2(H_2O)_2]X_2$ (where L=diamine and X=Cl^- or NO_3^-) produced either easily reducible nickel (II) ions or dispersed metal particles. The chelating diamines (ethylenediamine or trans-1,2-cyclohexanediamine) prevented the migration of Ni (II) into the alumina lattice and formation of $NiAl_2O_4$ [123]. The catalysts prepared were readily reduced at lower temperatures than expected for conventional Ni/alumina catalysts. Hence, an investigation was carried out to determine whether or not a similar effect could be observed with copper catalysts. Copper (II) ethylenediamine nitrate was prepared and characterised before being loaded onto a silica support for further testing. The aim was to prepare a highly dispersed copper catalyst through a novel route. Once prepared, additional metals such as cerium could then be added. The first step of this study was to prepare and characterise the copper (II) ethylenediamine complex.

Elemental Analysis

Microanalysis and atomic adsorption spectroscopy were used to determine the percentage of carbon, hydrogen, nitrogen and copper present in the copper (II) ethylenediamine complex prepared as in section 2.1.2. The results of the elemental analysis are shown in table 3.1.1.

Table 3.1.1. Results of elemental analysis for copper (II) ethylenediamine complex.

	Element (%)			
	Carbon	*Hydrogen*	*Nitrogen*	*Copper*
Theory	15.6	5.2	27.3	20.6
Found	15.6	5.2	26.5	20.3
Repeat	15.7	5.3	26.6	-

Elemental analysis was in good agreement with the theoretical values for $[Cu(en)_2(NO_3)_2]$ (where en = ethylenediamine). ^1H NMR was used to contrast the reactant ethylenediamine with the copper (II) ethylenediamine complex product which was prepared.

^1H NMR

The ^1H NMR spectra for the as-purchased ethylenediamine (not shown) revealed no impurities and compared well with literature values [124]. The spectrum had two features: a broad peak at 1.5 ppm (NH_2) and a sharp peak at 2.7 ppm (methylene protons R-CH_2-H). After formation of the copper complex, the spectrum altered slightly. The broad -NH_2 peak decreased in size and shifted to 1.2 ppm and a sharp peak at 1.5 ppm was now likely to be due to the R-CH_2-N protons. Several very weak features in the spectra were either satellite peaks due to the presence of copper in the sample, or due to minor impurities in the complex. The intensity of the peak for the NH_2 protons had decreased, suggesting that the ligand was co-ordinated to the copper through the nitrogen atoms. The position of the peak for the methylene protons was shifted due to the co-ordination of the ligand with the copper.

Infrared Spectroscopy (Golden Gate)

The IR spectrum for the copper ethylenediamine was in good agreement with a study by Fleming and Shepherd [125]. The spectra showed that there were still N-H bonds present, even though the broad N-H peak was very weak in the ^1H NMR spectrum. The IR results also confirmed the presence of nitrate ions in the complex [126], see table 3.1.2.

Table 3.1.2. Infrared peak assignments for copper (II) ethylenediamine complex.

Wavenumber (cm^{-1})		*Peak Assignments*
Actual	*Literature*	*[125, 126]*
3328 (s) 3247 (s) 3160 (s)	3300-2880 (s)	N-H Stretch
2944 (m) 2886 (m)	2540-2880 (s)	C-H Stretch
1602 (s)	1600 (s)	H-N-H Scissoring
1450 (w)	1450 (w)	H-C-H Scissoring
1340 (s)	1350-1400 (s)	Nitrate ion $(NO_3)^-$ NO Stretch
821 (s)	800-840 (s)	Nitrate ion $(NO_3)^-$ ONO Bend

Solution UV-Vis-NIR Spectroscopy

As difficulties occurred when trying to examine the copper (II) ethylenediamine aqueous solution across the full range of the spectrometer, the range was shortened to between 200 and 1400 nm. The literature values for $[Cu(en)_2]^{2+}$ and $[Cu(en)]^{2+}$ are ~548 nm [127, 128] and 673 nm [129] respectively. The spectrum (figure 3.1.1) showed one main feature in the visible region at 544 nm which was due to the presence of $[Cu(en)_2]^{2+}$. The weak band at 745 nm may be due to the presence of $[Cu(H_2O)_6]^{2+}$ which has a literature value of ~800 nm [129]. This may be due to the presence of unreacted copper (II) nitrate hydrate precursor from the preparation process. The UV-Vis results confirmed that the copper complex had two ethylenediamine ligands attached. If a mixture of species had been present, the band at 544 nm would have been expected to shift to slightly higher wavelength.

Figure 3.1.1. UV-Vis spectrum of copper (II) ethylenediamine precursor in aqueous solution.

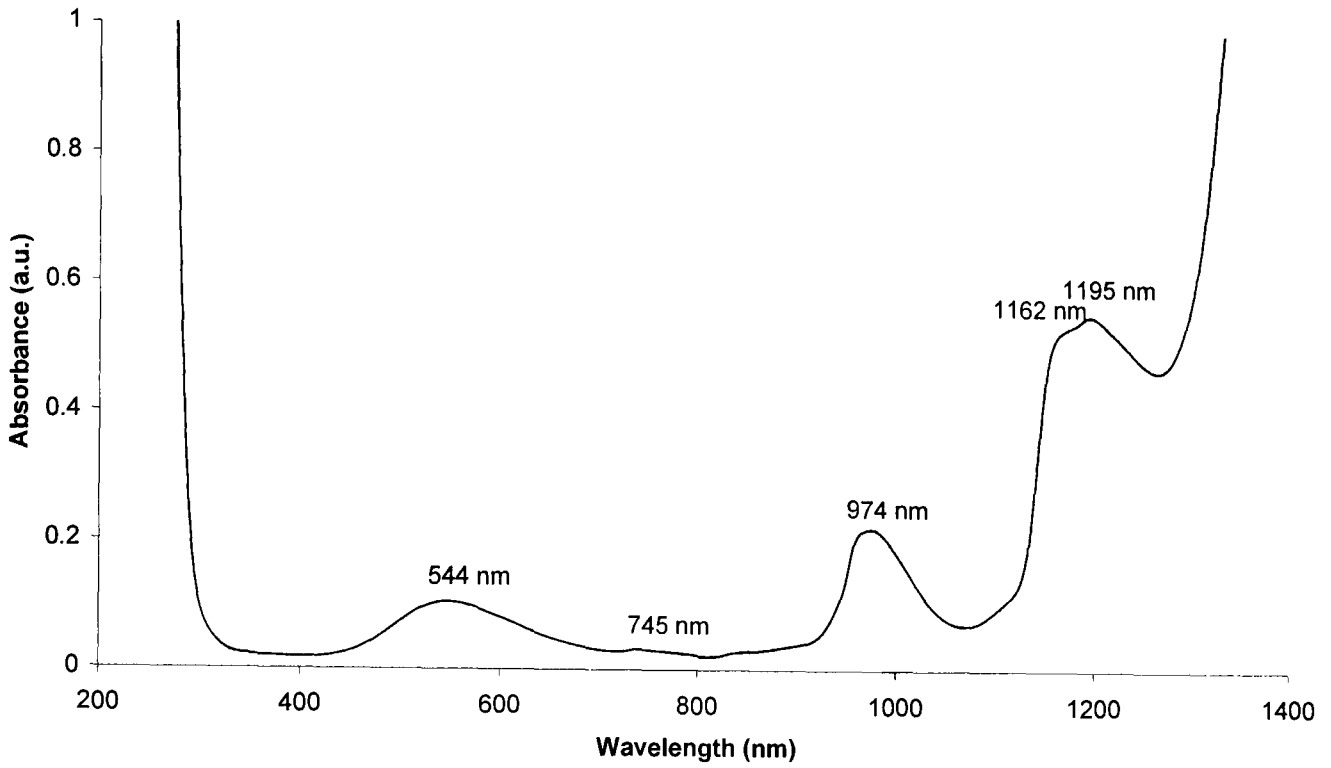

The peak at 544 nm was due to the Cu^{2+} d-d transition of the copper complex. It included the three spin allowed but symmetry forbidden transitions of the D_{4h} point group. The three transitions $^2B_{1g}$ to ^2E_g, $^2B_{1g}$ to $^2B_{2g}$ and $^2B_{1g}$ to $^2A_{1g}$ overlap to produce one broad band.

Three bands were observed in the near-IR region at 974, 1162 and 1195 nm. These features were out with the spectral range reported for copper (II) ethylenediamine solutions [110, 130]. The bands were also present for a copper (II) nitrate aqueous solution. Hence, the features in this region were probably due to the interaction of the Cu (II) species with water. It is likely that the bands were due to the solvation of the complex in water and not due to overtone and combination bands, which are normally sharp in this region.

From NMR and IR testing the ligand remained intact on complexation with the copper. The microanalysis results confirmed the elemental composition expected if two ligands were attached to the metal centre. These results were in good agreement with the UV-Vis spectrum which matched literature values for $[Cu(en)_2]^{2+}$. Characteristic bands in the infrared spectrum confirmed that nitrate species were retained by the complex.

The preferred geometry for σ-bonding ligands such as ethylenediamine is a distorted tetrahedral octahedron [131]. The ethylenediamine ligands occupy an equatorial position where as the NO_3^- ion occupies an axial position. Ligands in the axial position are more weakly co-ordinated to the copper (II) centre.

Therefore the complex formed is likely to be $Cu(en)_2(NO_3)_2$. Although it is also possible to produce a copper complex with either one [132, 133] or three [134] ethylenediamine ligands, the characterisation of the prepared complex ruled out the presence of either compound.

3.1.2 Characterisation and Testing of 5% Cu/Silica (en)

After preparing a 5% w/w loading of copper onto a silica support using the copper (II) ethylenediamine precursor, the resulting catalyst was characterised and tested for catalytic activity.

Solid-State UV-Vis-NIR Spectroscopy

On addition of the copper complex to the silica support the position of the d-d band remained unchanged. However, several broad bands from the near-IR region disappeared and were replaced by sharp peaks in the near-IR region ~1400 nm and above. The bands in the near-IR were due to vibrational overtone and combination bands of water, ethylenediamine and lattice hydroxyl groups, see figure 3.1.2. A shoulder at ~1400 nm indicated the presence of water or hydroxyl groups and the band at 1555 nm was due to the N-H stretch from the ethylenediamine ligand (Lit. value 1544 nm [128]). In the visible range there was a strong band at 545 nm (Lit. value 548 nm in aqueous solution [128]). This feature was due to the Cu^{2+} d-d transition of the complex, which has D_{4h} symmetry. The d-d band is composed of three peaks due to three spin-allowed but symmetry forbidden transitions, $^2B_{1g}$ to ^2E_g, $^2B_{1g}$ to $^2B_{2g}$ and $^2B_{1g}$ to $^2A_{1g}$. The shoulder at ~250 nm was due to ligand to metal charge transfers (LMCT) between Cu^{2+} and the ethylenediamine ligands of the complex (Lit. value 227 nm [128] in aqueous solution).

Figure 3.1.2. UV-Vis-NIR spectrum of 5% Cu/Silica (en) – using Praying Mantis attachment for solid samples.

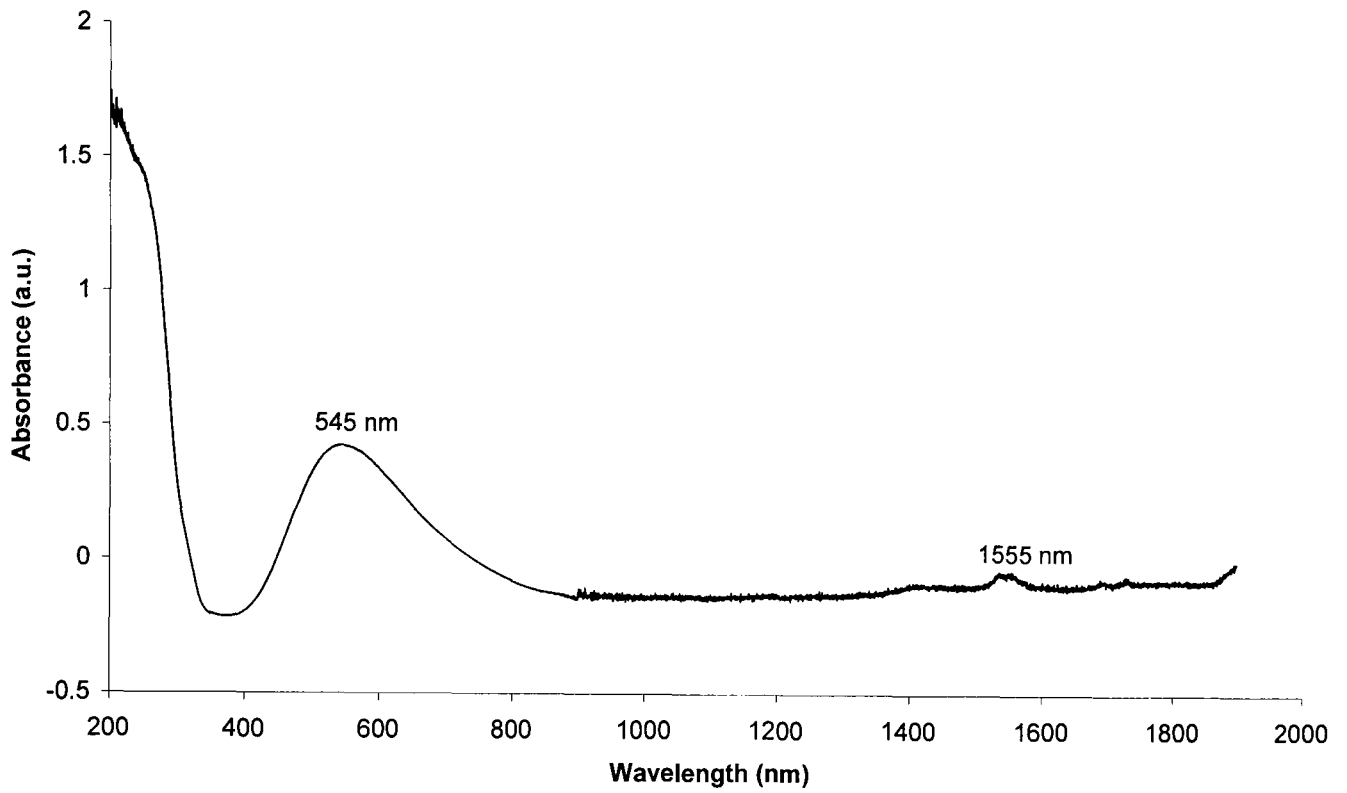

On addition of copper (II) ethylenediamine complexes to clays/zirconium molybdate a shift in the d-d band was observed [110, 127-129]. The change in position was ~20 nm lower in the case of the zirconium molybdate support [110] and ~27 nm less for the clay supports [128]. The difference was attributed to a slight change in the geometry of the complex, as it distorted on adsorption to the support material. Trouillet *et al* [133] found that after drying to 298 K or 373 K, the main species present on the silica surface was $[Cu(en)_2(H_2O)_2]^{2+}$ (figure 3.1.3). The group found that after drying (at 298 K) the d-d band had shifted from 550 nm (wet catalyst) to 570 nm [133]. However this did not occur with the catalyst prepared in this study. The position of the d-d peak remained unchanged after drying at 333 K. Hence Trouillet and co-workers [133] may have produced a small amount of $[Cu(en)(H_2O)_4]^{2+}$ on drying which caused a shift in the position of the UV-Vis band. UV-Vis results confirmed that the 5% Cu/silica (en) catalyst was composed predominantly of $[Cu(en)_2(H_2O)_2]^{2+}$. The adsorbed complex was in electrostatic interaction with the silica.

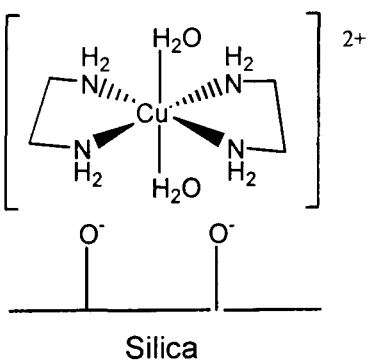

Figure 3.1.3. Representation of copper species present after catalyst drying.

Powder X-Ray Diffraction

Powder XRD analysis was used to examine the supported catalyst after drying (at 333 K) and after treatment in helium to 673 K. Although there was a broad feature due to the silica support, sharp peaks were observed in the XRD pattern of the dried sample, indicating that a crystalline material was present. The strongest peaks in the diffraction pattern for the dried sample were at 13.6, 20.8, 26.2, 36.6, 17.4 and 24.8 °2θ (figure 3.1.4 (b)). There was no diffraction pattern in the JCPDS database for copper (II) ethylenediamine or similar complexes. Attempts to use the strongest peaks to identify a matching compound were also unsuccessful. Hence, the as prepared copper (II) ethylenediamine nitrate complex was analysed by XRD. Figure 3.1.4 (a) shows the diffraction pattern for copper (II) ethylenediamine nitrate. The XRD pattern of the original compound had lines of greater intensity, as the complex was a crystalline material. The positions of the sharp peaks were in good agreement with those complex supported on silica (Fig. 3.1.4 (b)). The peaks did not match any files in the crystallographic database (including the file for copper (II) nitrate hydrate, the reactant used to produce the complex).

UV-Vis-NIR spectroscopy revealed that $[Cu(en)_2(H_2O)_2]^{2+}$ was present on the catalyst support, in agreement with the XRD results which showed that the crystalline species present on the amorphous silica was copper (II) ethylenediamine nitrate. As the UV and XRD results varied only slightly on addition of the complex to the support, this indicated that only electrostatic interactions were present between the complex and the catalyst.

The strongest peak at 13.6 °2θ was used to calculate the average crystallite size from the Scherrer equation (see section 2.4.7). The average copper (II) ethylenediamine crystallite size was calculated as ~31 nm for the complex and ~ 30 nm for the catalyst. Hence, addition of the complex to a support did not affect the crystallite size of the complex.

Figure 3.1.4. X-Ray Diffraction pattern of dried (a) Copper (II) ethylenediamine precursor (b) 5% Cu/Silica (en) catalyst and (c) 5% Cu/Silica (en) after TPD in helium to 673 K.

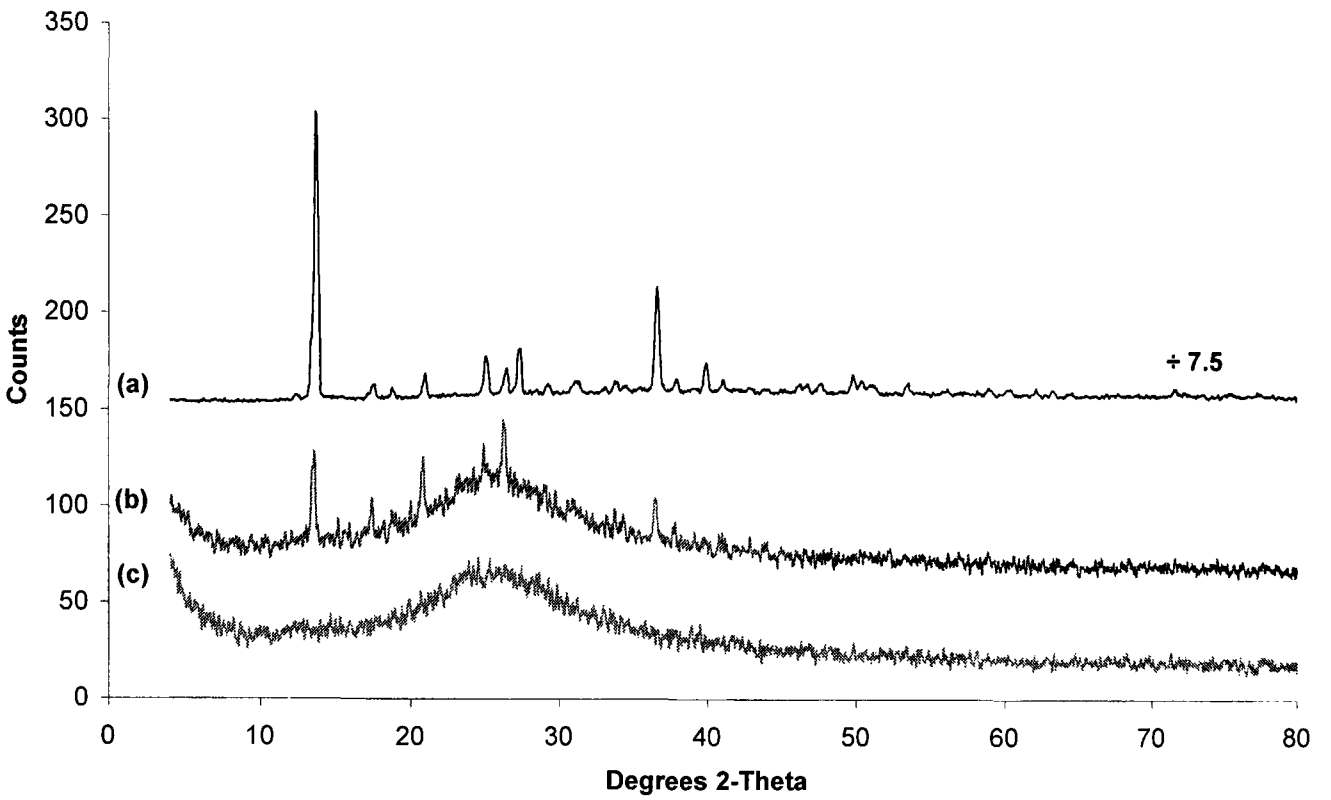

An XRD sample, which had been treated in helium to 673 K, was also examined in figure 3.1.4 (c). After treatment in helium, the catalyst was amorphous to x-rays. The original defined peaks were no-longer present. There were no peaks corresponding to CuO, Cu_2O or Cu metal, which may have been expected for the sample after treatment in helium. As the sample was also black in colour, it is possible that the ligand had decomposed into an amorphous carbonaceous layer.

Raman Spectroscopy

A Raman spectrum was taken of the fresh 5Cu/silica catalyst, which had been dried at 333 K (figure 3.1.5). As this catalyst (5Cu/silica (en)) was prepared from the $Cu(en)_2(NO_3)_2$ precursor there was a strong peak at 1044 cm^{-1} from the nitrate. There were a number of new bands due to the presence of the amine and some of the silica bands had disappeared or shifted. Peaks at 482 and 603 cm^{-1} were attributed to the presence of siloxane linkages. See table 3.1.3 for full peak assignment. The weak peak at 1117 cm^{-1} was not described in literature studies. However, it was present (although often very weak), in several of the silica-supported catalysts, which are described later in section 3.1.7.

Figure 3.1.5. Raman spectrum of dried 5% Cu/Silica (en).

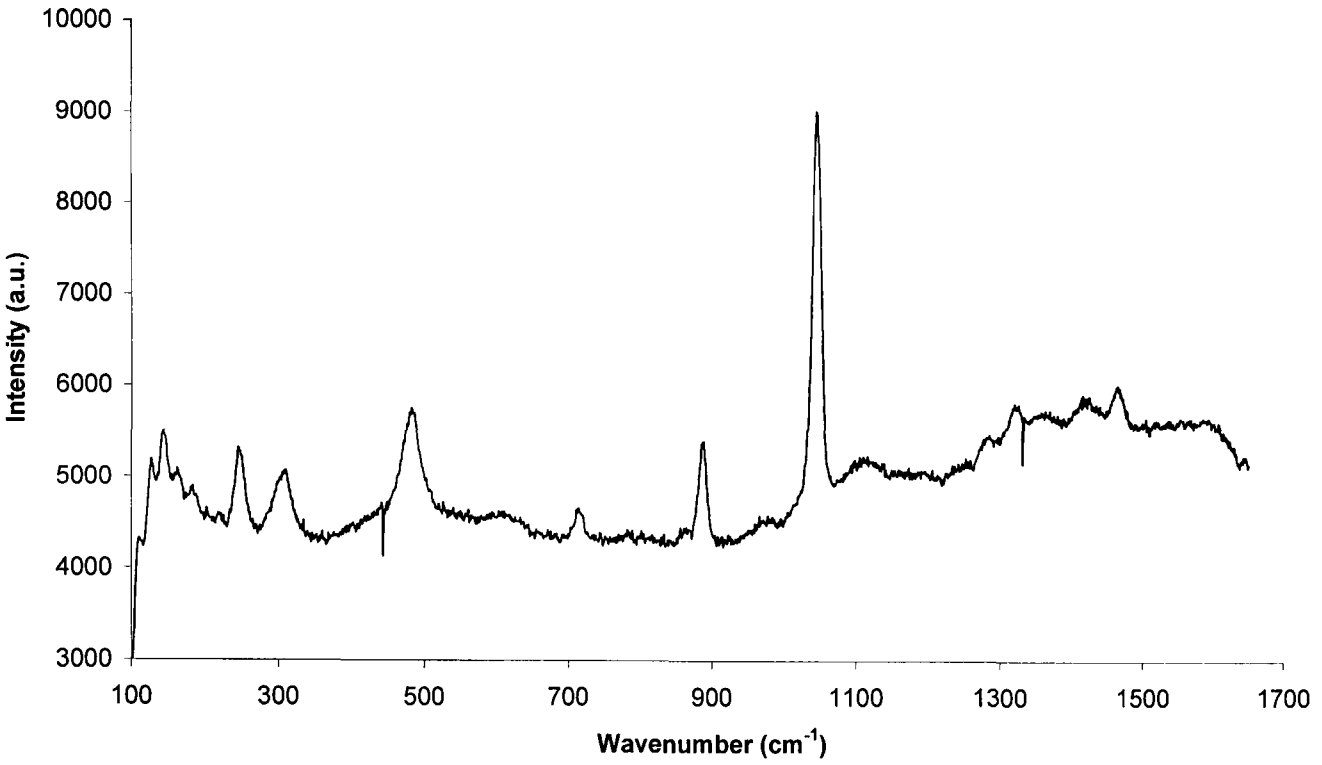

Table 3.1.3. Assignment of Raman spectrum peaks for 5% Cu/silica (en).

*Peak Wavenumber** (cm^{-1})	*Literature Value* (cm^{-1})	*Ref.*	*Assignment*
246	254	[135]	Totally symmetric vibrations of NCCN
310	310		
483	450-600	[126]	υ_4 M-N stretching
604 (w)	605 (+ 488)	[136]	3 and 4-fold siloxane rings
714	757	[137]	NO_2 symmetric bend
782 (w)	803	[136]	Siloxane linkages
888	850-950	[126]	CH_2 rocking (active in IR)
1045 (s)	1050	[137]	υ_1 NO_3^- symmetric stretch
1117 (b)	-	-	Silica
1320 (w)	1320	[137]	NO_2 symmetric stretch
1416 (w)	1407	[137]	υ_3 NO_3^- anti-symm. stretch
1465 (w)	1494	[137]	NO_2^- anti-symmetric stretch

*w-weak, s-strong and b-broad.

Although there were no Raman spectroscopy studies of copper (II) ethylenediamine nitrate available from literature, there was a study with a $Pt(en)_2Cl_2$ complex [138]. From this study, the vibrations from the ethylenediamine ligand were assigned. As the fundamental vibrations of NO_3^- were not split, this indicated that only one form of the nitrate was present.

Hence, a combination of UV-Vis, XRD and Raman spectroscopy confirmed that the species present on the silica after drying was $[Cu(en)_2(NO_3)_2]$. Furthermore, the techniques used suggested that the interactions between the complex and support were weak electrostatic interactions.

Reduction of 5% Cu/Silica (en)

A temperature programmed desorption (TPD) was carried out using the same procedure as for TPR reactions (section 2.4.2) with helium as the reaction gas instead of the hydrogen/nitrogen mix. The TPD of the 5Cu/silica (en) catalyst showed that decomposition of the ethylenediamine ligand occurred in two stages. Firstly, a small peak was observed at ~470 K (nitrogen (II) oxide) followed by a larger peak between 500 and 560 K (nitrogen (II) oxide, ammonia and water), figure 3.1.6. Decomposition of the ligand was complete by 580 K. After treatment in helium the catalyst was examined by microanalysis, table 3.1.4.

Figure 3.1.6. TPD of 5% Cu/Silica (en).

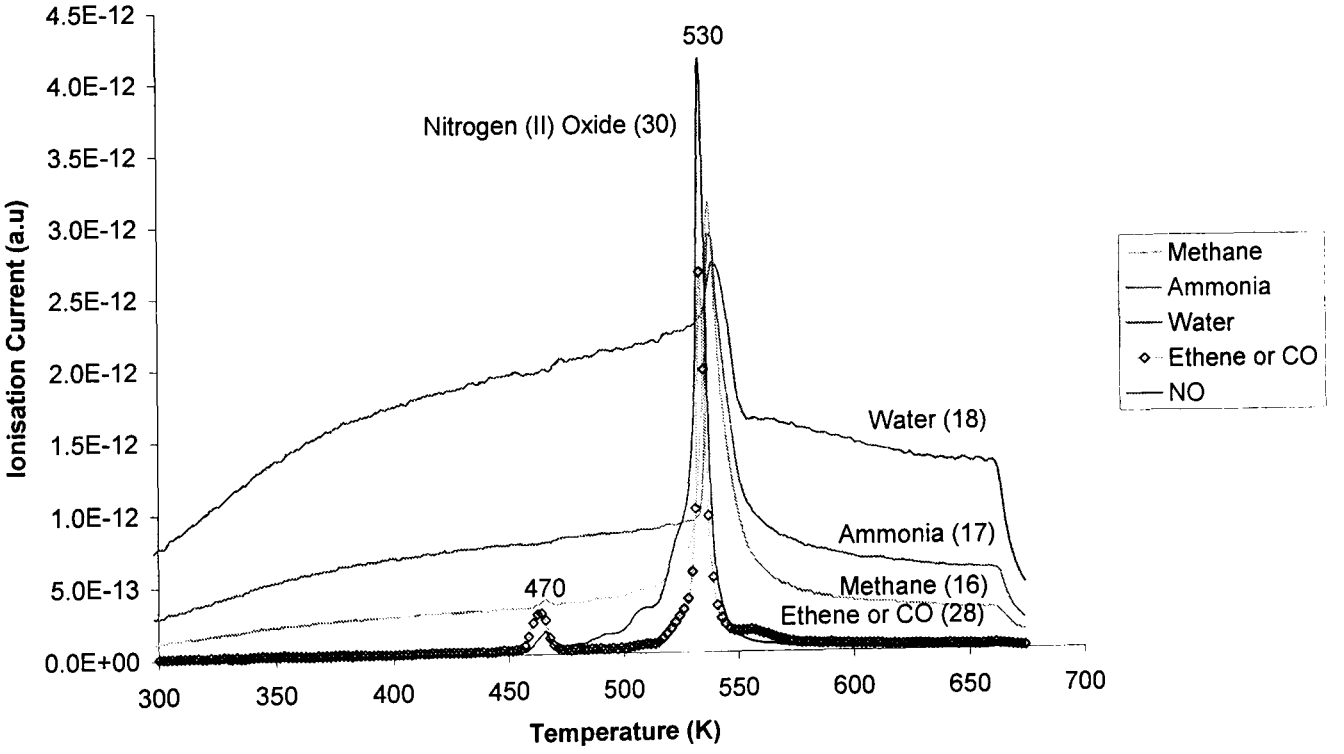

The microanalysis results revealed that the ligand had been partially removed from the catalyst. However, approximately 70% of the carbon from the ligand remained on the catalyst surface. The catalyst was black in colour after the TPD and there was no red colouring of the catalyst, which would have indicated the presence of large copper

crystallites. The XRD of this compound provided inconclusive evidence of the species present.

Table 3.1.4. Microanalysis of 5Cu/silica (en) after treatment in helium.

	Element (%)		
	Carbon	*Hydrogen*	*Nitrogen*
Fresh 5Cu/silica (en)	3.59	1.20	6.28
Found	2.54	0.26	1.76
Repeat	2.77	0.30	1.72

TPR of both the unsupported copper (II) ethylenediamine precursor and 5Cu/silica (en) was attempted. For the unsupported complex, two peaks were observed at 523 K (nitrogen (II) oxide) and 550 K (water and ammonia). The supported complex also decomposed at similar temperatures: 460 K (nitrogen (II) oxide), 525 K (nitrogen (II) oxide) and 530 K (water, ammonia and nitrogen (II) oxide). The position of the peaks was similar for both samples, with the supported catalyst producing more intense peaks. Hence, the amine ligand begins to decompose above 523 K whether or not it is supported on the silica. These results suggested that the interaction between silica support and complex was weak. After TPR, microanalysis was completed on the used sample, table 3.1.5. The results indicated that decomposition of the ligand occurred, leaving mainly carbon species.

Table 3.1.5. Microanalysis of copper (II) ethylene diamine complex after TPR.

	Element (%)		
	Carbon	*Hydrogen*	*Nitrogen*
Fresh $Cu(en)_2(NO_3)_2$	15.6	5.2	26.5
Found	12.3	0.9	8.3
Repeat	12.2	0.8	8.3

A further attempt was made to reduce the catalyst by treatment in helium (to 673 K) followed by treatment in hydrogen/nitrogen. The treatment in reducing gas produced a small peak at ~650 K due to formation of methane. This confirmed that after reduction or treatment in helium, carbon remained on the surface of the catalyst.

After treatment in either reducing or inert flow, the catalyst was tested for adsorption of oxygen and reaction with methanol. However, after several attempts at reduction and

testing, the catalyst remained inactive. Pulses of methanol were adsorbed without reaction and oxygen pulses neither reacted nor adsorbed. Unlike the nickel catalyst [123] no lowering of reduction temperature was observed. Also, work with the nickel complex showed that no decomposition of the ligand occurred below 500 K [123]. Ethylenediamine had behaved as a hydrogen source when activating the sample in a nitrogen flow. Copper/silica catalysts are normally reduced in the region of 430-570 K [139], this was also the temperature at which the ligand decomposed.

Unlike similar work with nickel catalysts [123] there was no decrease of the reduction temperature using a copper (II) ethylenediamine precursor. Interaction between the support and complex was weak as can be seen from the temperature-programmed reactions. It was probable that as the ligand decomposed it deposited a carbonaceous layer on the catalyst surface as opposed to providing a source of hydrogen to reduce the copper. The carbon residues blocked the active metal sites, rendering the catalyst inactive.

Although it was apparent that the catalyst was unlikely to be active, it was reduced using the standard catalyst reduction (section 2.5.1) and tested for methanol decomposition and metal surface area. The catalyst showed a negligible metal surface area when examined by N_2O or oxygen chemisorptions. The sample adsorbed a small amount of oxygen after reduction, which equated to a copper dispersion of less than 1%. The oxygen was pulsed at room temperature and no production of carbon monoxide or carbon dioxide was observed. A value of metal surface area from the N_2O chemisorption could not be determined. In addition, the methanol decomposition reaction was unsuccessful. The sample adsorbed ~20 % of each pulse reacted over the catalyst bed and the remaining methanol did not react.

Literature studies have been carried out on copper (II) ethylenediamine complexes supported on clays [128], zeolites [140], alumina [141], silica [133] and zirconium molybdate [110]. The studies characterised the samples and in most cases tested the catalyst prepared to examine its reactivity. There were no literature reports of copper (II) ethylenediamine/silica catalysts prepared via wet impregnation. However, the copper amine complex has been used to prepare silica-supported catalysts by cation exchange [133].

$[Cu(en)_2]^{2+}$ sorbed onto zirconium molybdate was catalytically active for the decomposition of hydrogen peroxide [110]. However, no reduction procedure was used. The aim of the study was to 'heterogenise' metal complexes to examine them as catalysts. After exchange, the copper (II) ethylenediamine adsorbed was violet in colour. During reaction the catalyst changed to greenish-yellow (formation of peroxo intermediate species) [110]. Hence, the active species for this reaction was an intermediate species, which required the presence of the ligand. After reaction, the catalyst returned to its original colour. This suggested that the ligand played an important role in the catalytic activity of the compound.

Encapsulation of copper (II) ethylenediamine in zeolites was also attempted by Ganesan *et al* [140] who found the neat complex inactive towards dimethyl sulphide oxidation. The encapsulated complex had conversions greater than 75%. The higher activity was attributed to a change in the redox potential of the complex on encapsulation within the zeolite.

A basic alumina support was used to support the copper (II) ethylenediamine complex for use as a catalyst for the oxidation of methylene blue by hydrogen peroxide [141]. The catalysts were very stable and could be re-used several times. Reaction of the catalyst was accompanied by a colour change. The catalyst returned to its original colour by producing oxygen. The catalyst formed a peroxo intermediate species during reaction [141]. The reaction was reversible, allowing the complex to return to its original form after removal from the reaction.

The clays used to support copper (II) ethylenediamine [128] were not examined for catalytic activity. However, the report suggested an increase in the stability of the complex on the support surface. It was reported that the clays behaved as a rigid, anionic solvent towards the copper complex [128].

On all of the supports examined, the copper complex was catalytically active for oxidation reactions. However, it was only tested at temperatures below 313 K. The ligand played an important role in the catalytic activity of the complexes. In all cases it remained intact after the reaction and the catalyst was re-used. Hence, it is possible that the silica-supported copper (II) ethylenediamine catalyst may have been more active at

low temperatures without an activation process. The copper/silica (en) catalyst prepared by Trouillet [133] was calcined after the drying stage to remove the ethylenediamine ligand. After calcination and exposure to air the copper (II) species was determined as $(\equiv SiO)_2Cu(H_2O)_4$, where λ_{max} was approximately 750 nm [133]. However, the catalyst produced was not tested for catalytic activity.

It is possible that oxidation of the 5Cu/silica (en) catalyst to remove the ligand may have allowed subsequent reduction of the copper metal. However, the aim of this study was to examine the improvements to dispersion and reduction produced by using a copper precursor with a chelating ligand. It was also hoped that this catalyst would be suitable for use as a catalysts for the methanol industry. As this process was unsuccessful, no further investigations were carried out on this catalyst.

3.1.3 Surface Area Measurement (BET)

The surface area of the catalysts as well as the average pore diameter and volume of the materials was determined as described in section 2.4.5 and the results are shown in table 3.1.6. Two general trends were observed for the silica and alumina supports. Firstly, an increase in metal loading led to reduction of the total surface area when compared with the support. Secondly, addition of more than one metal led to a further loss in surface area.

The catalysts that did not fit these trends were those dried at room temperature and prepared using wet impregnation. The preparation technique and in particular the drying temperature had a huge effect on the surface area of the catalysts. For the 5% copper/silica catalysts, the surface area increased in the order of 5Cu/Silica (wet impregnation, dried at 293 K), 187 m^2g^{-1} < 5Cu/Silica (wet impregnation), 247 m^2g^{-1} < 5Cu/Silica (spray impregnation), 280 m^2g^{-1}. Therefore the use of spray impregnation and a drying temperature of 333 K maintained the high surface area of the catalyst. The effect of drying temperature was similar for the 10% copper/silica catalysts. By increasing the drying temperature to 333 K from 293 K the surface area increased from 213 to 224 m^2g^{-1}.

The pore diameter does not change markedly on addition of metal salts to the silica. The pore volume on the other hand decreases on addition of one or more metal salts.

The maximum reduction in pore volume was approximately 40 %. This reduction occurred in the catalysts with multiple salts present and the 5Cu/silica (en) catalyst. The reduction in pore volume indicated that the pores of the support were blocked during catalyst preparation.

Table 3.1.6. Surface area measurements for catalysts and supports.

Sample	*BET*		*Single Point*
	Surface Area (m^2g^{-1})	*Average Pore Diameter (Å)*	*Pore Volume* (cm^3g^{-1})
Silica Support (S)	296	145	1.10
5Cu/Silica (293 K)	187	141	0.70
5Cu/Silica (WetImpreg.)	247	146	0.91
10Cu/Silica (293 K)	213	142	0.76
10Cu/Silica	224	144	0.81
5Ce/Silica	250	141	0.90
10Ce/Silica	208	153	0.80
5Cu/Silica	280	144	1.01
5Cu5Ce/Silica	220	147	0.80
5Cu/Silica (en)	165	157	0.64
5Cu/Silica (ac)	273	146	1.00
10Cu5Ce/Silica	172	154	0.66
10Cu5Ce0.05Pd/Silica	187	146	0.69
5Cu1Ce/Silica	239	144	0.87
Alumina Support (A)	104	199	0.52
5Ce/Alumina	90	194	0.44
5Cu/Alumina	82	207	0.43
5Cu5Ce/Alumina	66	201	0.33
Commercial	56	112	0.16
1% Pd/SiO_2	150	188	0.71

The commercial catalyst had the lowest surface area of all the catalysts examined. However, this was due to the catalyst preparation method. The commercial catalyst was prepared by co-precipitation rather than impregnation, which in general produces catalysts with lower surface areas.

3.1.4 Atomic Absorption Spectroscopy (AAS)

Each of the copper containing catalysts was analysed by atomic absorption spectroscopy to determine the actual copper loading, table 3.1.7.

Table 3.1.7. Copper content as determined by AAS.

Sample	*Copper (%)*	*Sample*	*Copper (%)*
5Cu/Silica (293 K)	4.0	5Cu/Alumina	4.1
5Cu/Silica (WetImpreg.)	4.8	5Cu5Ce/Alumina	4.0
10Cu/Silica (293 K)	6.5	Commercial	34.3
10Cu/Silica	6.8		
5Cu/Silica	4.8		
5Cu5Ce/Silica	3.9		
5Cu/Silica (en)	4.3		
5Cu/Silica (ac)	4.1		
10Cu5Ce/Silica	6.3		
10Cu5Ce0.05Pd/Silica	9.3		
5Cu1Ce/Silica	4.2		

Most of the catalysts showed a lower actual loading than their nominal loadings, which at first suggested that there might have been a loss of metal precursor solution during catalyst preparation. However subsequent X-ray fluorescence analysis (XRF) analysis of two sample catalysts showed that actual and nominal copper loadings were in good agreement. The catalysts analysed were 5Cu/silica (Wet Impreg.) and 10Cu/silica and the copper contents were determined as 5.4 and 9.0 % respectively. It was concluded that the analysis by AAS was not been suitable for metal/support catalysts prepared in this study. This was possibly due to strong interactions between the metal precursor and support hence changes to the extraction method may be required to improve the accuracy of the results. The copper content of the commercial methanol synthesis catalyst was as expected for a co-precipitated commercial catalyst, as copper oxide content can range from 40 to 80 % in industrial catalysts [42].

3.1.5 Solid-State UV-Vis-NIR Spectroscopy

UV-Vis-NIR spectroscopy was used to investigate the nature of the copper present in the catalysts. The copper (II) ion has a $3d^9$ outer electron configuration. As the outer electron configuration lacks cubic symmetry, the basic forms of stereochemistry are

distorted. The electronic properties of Cu(II) complexes are relatively sensitive to changes in stereochemistry. There are four main types of transition, which can occur in the electronic spectra range. These are: pure d-d transitions (> 500 nm), combination and overtone vibrations of the ligands (> 500 nm), charge-transfer transitions (< 500 nm) and internal ligand transitions (< 500nm) [131]. The results of UV-Vis-NIR spectroscopy are shown in table 3.1.8.

Table 3.1.8. Assignment of UV-Vis-NIR bands for each catalyst.

Sample	*Wavelength Assignment (nm)*	
	LMCT	*d-d Transition*
Silica Support (S)	-	-
5Cu/Silica (293 K)	265	789
5Cu/Silica (WetImpreg.)	265	783
10Cu/Silica (293 K)	265	800
10Cu/Silica	265	800
5Ce/Silica	260	-
10Ce/Silica	258	-
5Cu/Silica	266	785
5Cu5Ce/Silica	261	784
5Cu/Silica (ac)	247	729
10Cu5Ce/Silica	263	807
10Cu5Ce0.05Pd/Silica	265	803
5Cu1Ce/Silica	266	801
Alumina Support (A)	-	-
5Ce/Alumina	270	-
5Cu/Alumina	~270	750
5Cu5Ce/Alumina	~260	743
Commercial	234	447, 576, 723

Initially, a copper (II) nitrate solution was investigated and had features at 301 and 809 nm. These figures were compared with those for the supported metal catalysts, table 3.1.8. The strong absorptions between 200 and 300 nm are due to ligand to metal charge transfers (LMCT) from the ligands $(NO_3)^-$ to Cu^{2+} [118]. The main band at approximately 780 nm was due to the d-d transitions of the Cu^{2+} ion (d^9). This is due to the presence of a distorted octahedral Cu^{2+} species with D_{4h} symmetry.

The cerium samples examined provided little information; only showing bands that corresponded to the presence of nitrate (270 nm) see table 3.1.8. Bulk cerium oxide and cerium oxide supported on silica have been examined using diffuse reflectance spectroscopy [142]. Peaks were observed in the range of 250 to 425 nm. The bands were mainly due to cerium to oxygen transfer. According to the literature, $Ce^{III}(H_2O)$ has a band at 253 nm [142]. However, this band was obscured due to the strong band at 270 nm, which was due to the presence of the nitrate.

When added to either the silica or alumina supports the d-d band for the copper nitrate shifted by 10 to 20 nm. This indicated that the co-ordination of the copper metal was altered by adsorption onto a support. Table 3.1.8 shows that with increasing copper loading this band shifted to a higher wavelength. The UV-Visible spectroscopic data for catalysts 1 to 4 compared well with literature values for similar uncalcined copper/silica catalysts [118]. The copper/silica catalysts examined had peaks at approx. 1430 nm, which were in the near IR region, the intensity of this peak increased for those samples dried at room temperature. These peaks were attributed to overtones of the hydroxyl stretching vibrations of adsorbed water and lattice hydroxyl groups (literature value 1428 nm [129]).

The copper/alumina catalysts showed a greater shift of the d-d transition band (table 3.1.8). It has been suggested that this shift occurs on conversion of copper (II) nitrate hydrate to copper (II) nitrate hydroxide [118]. The literature showed that for copper/silica catalysts the band shifted towards 730 nm.

The UV spectrum of the commercial catalyst showed one broad band with very weak features near 450, 575 and 720 nm. The shape of the band for the commercial catalyst was asymmetric towards the shorter end of the spectrum. Marion and co-workers [143] suggested that a maximum at 730 nm corresponded to the presence of octahedrally co-ordinated copper ions of a copper oxide supported on a zinc spinel. A sharp increase in absorption was observed at 550 nm for the literature sample and was attributed to charge transfer similar to that for copper aluminate [143]. Hence, the UV-Vis results indicate that copper oxide was present in close association with the support materials of the commercial catalyst.

3.1.6 Powder X-Ray Diffraction (XRD)

X-ray diffraction can provide information regarding a material's crystal structure, degree of crystallinity and crystallite size. Although unable to determine the complete active phase of a catalyst, XRD can be used to gain information about materials with long-range order. This technique is used extensively in the characterisation of well-ordered structures such as zeolites [120, 144]. However, amorphous solids (such as silica) can still be examined by XRD to gain useful information about active species present on the support if it exists as a crystalline phase. Powder XRD was used to examine fresh and used catalysts to determine any changes to the active species that occurred during reaction. As well as using XRD to identify the active species, it was used to determine average crystallite size for samples with well-defined peaks (see Scherrer equation, section 2.4.7). The Scherrer equation is based on the fact that smaller crystallites show a greater deviation from Bragg's law, hence the peaks become broader.

Identification of the species present was made by comparison of the XRD data with the Powder Diffraction Database [145]. Attempts were made to relate the strongest lines of the sample with standard compounds that were available from the database.

Silica Catalysts

The XRD results for the dried silica catalysts produced very little information. Most of the catalysts examined showed a broad band due to the amorphous nature of the silica support, higher loadings of copper also failed to produce peaks. A representative sample of spectra from the copper/silica catalysts is shown in figure 3.1.7.

Figure 3.1.7. XRD spectrum of dried samples (a) 10Cu/Silica, (b) 5Cu/Silica (Wet Impreg.) and (c) silica support.

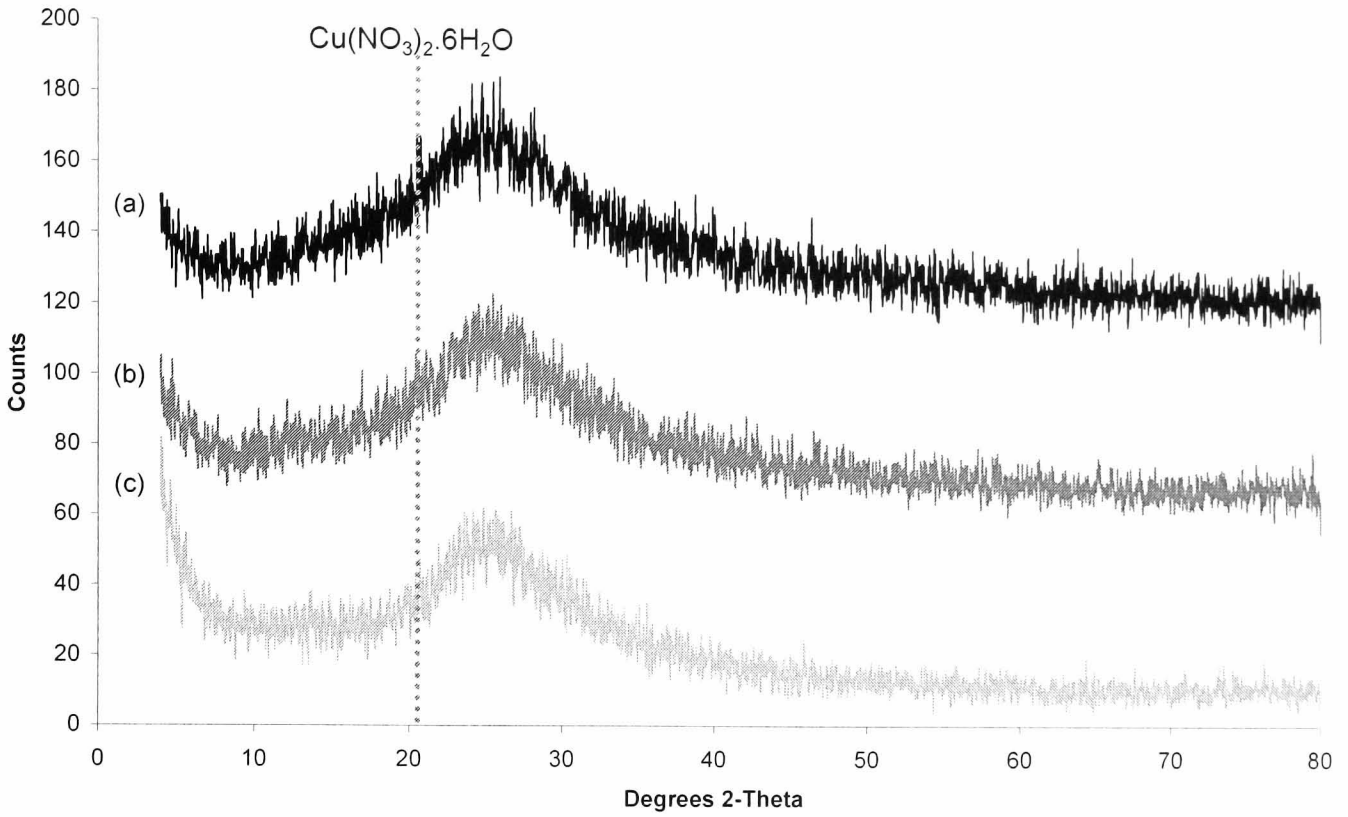

As a crystalline species such as copper (II) nitrate hydrate (or hydroxide) would have been expected on the catalyst surface, it was surprising that no lines were present in the diffraction pattern (figure 3.1.7). As the UV-Vis spectrum for the catalysts shows the presence of a copper (II) species, peaks corresponding to the copper nitrate precursor or a similar compound would be expected. However, the samples were mainly amorphous to X-rays.

The catalyst with the highest loading (10% Cu/silica, figure 3.1.7 (a)) showed only one peak in the diffraction pattern. This peak matched the strongest line for a copper (II) nitrate hydrate complex (19-0410). The presence of this phase agreed with the UV-Vis-NIR results, which showed only a slight shift of the d-d band on impregnation of the support with the precursor. Hence, the copper/silica catalysts were composed of copper (II) nitrate hydrate prior to reduction/reaction.

Post-reaction samples were also examined by XRD. After reduction to 523 K, reaction with methanol pulses and exposure to air, the spectra of the used catalysts were collected see figure 3.1.8.

Figure 3.1.8. XRD spectrum of post-reaction samples (a) 10Cu/Silica, (b) 5Cu/Silica (Wet Impreg.) and (c) silica support.

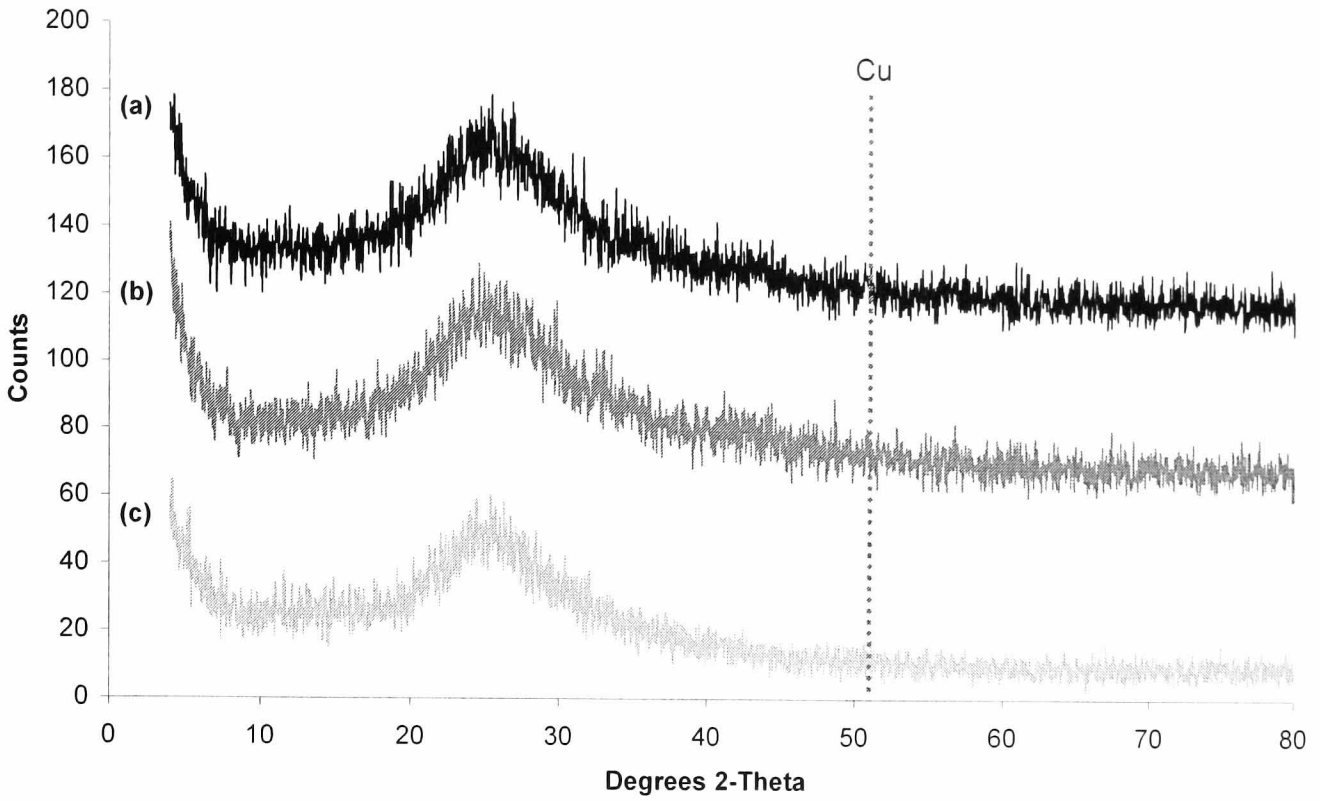

The diffraction pattern shows that after reaction there was still no crystalline material detected on the catalyst surface. In addition, there was no longer a peak due to the initial copper (II) nitrate hydrate. After reaction and exposure to air the products expected would have been copper (II) oxide or possibly copper metal. As red particles were present it is likely that copper metal was present in the post-reaction sample although the sample remained amorphous to x-rays. However, after exposure to air it is likely that the major species was a copper oxide.

Cerium/Silica Catalysts

The pre-reaction cerium/silica catalysts did not show any features in their diffraction patterns other than for silica. However, both the 10% and 5% cerium/silica catalysts had several broad peaks after reduction to 523 K, reaction and air exposure. The lines were more pronounced in the 10 % sample, figure 3.1.9 (a). The diffraction pattern was due to CeO_2 (04-0593); no other phases were identified. Due to the level of noise in the diffraction pattern, line width was difficult to calculate; hence the average crystallite size of CeO_2 was not determined.

Figure 3.1.9. XRD spectrum of 10Ce/Silica (a) post-reaction and (b) fresh sample.

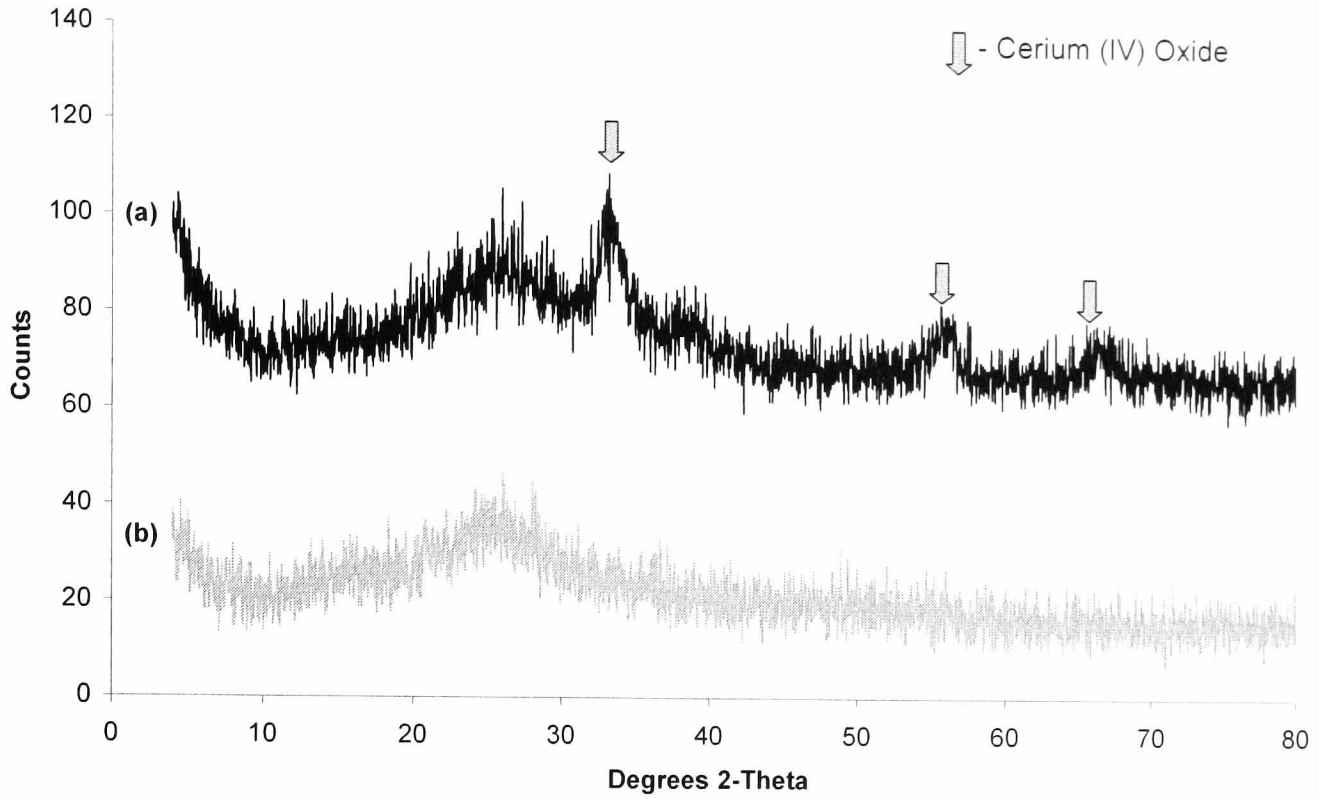

No peaks were observed which would correspond to the formation of cerium (III) oxide. However this was as expected, after reduction to 523 K and reaction with methanol it would be unlikely that any of the cerium oxide would be present in a reduced form.

Copper and Cerium/Silica Catalysts

Of the pre-reaction mixed copper and cerium/silica catalysts, only the 10Cu5Ce0.05Pd/silica catalyst (figure 3.1.10) had lines in its diffraction pattern. The spectrum showed the presence of copper (II) nitrate hydroxide (15-0014) with peaks at 15.06 and 30.1 °2θ. Using the <001> line at 15.06 °2θ, the average crystallite size was calculated as 59 nm. Hence inclusion of a small amount of palladium improved the crystallinity of the species adsorbed onto the support.

Figure 3.1.10. XRD spectrum of (a) pre and (b) post-reaction 10Cu5Ce0.05Pd/silica catalyst.

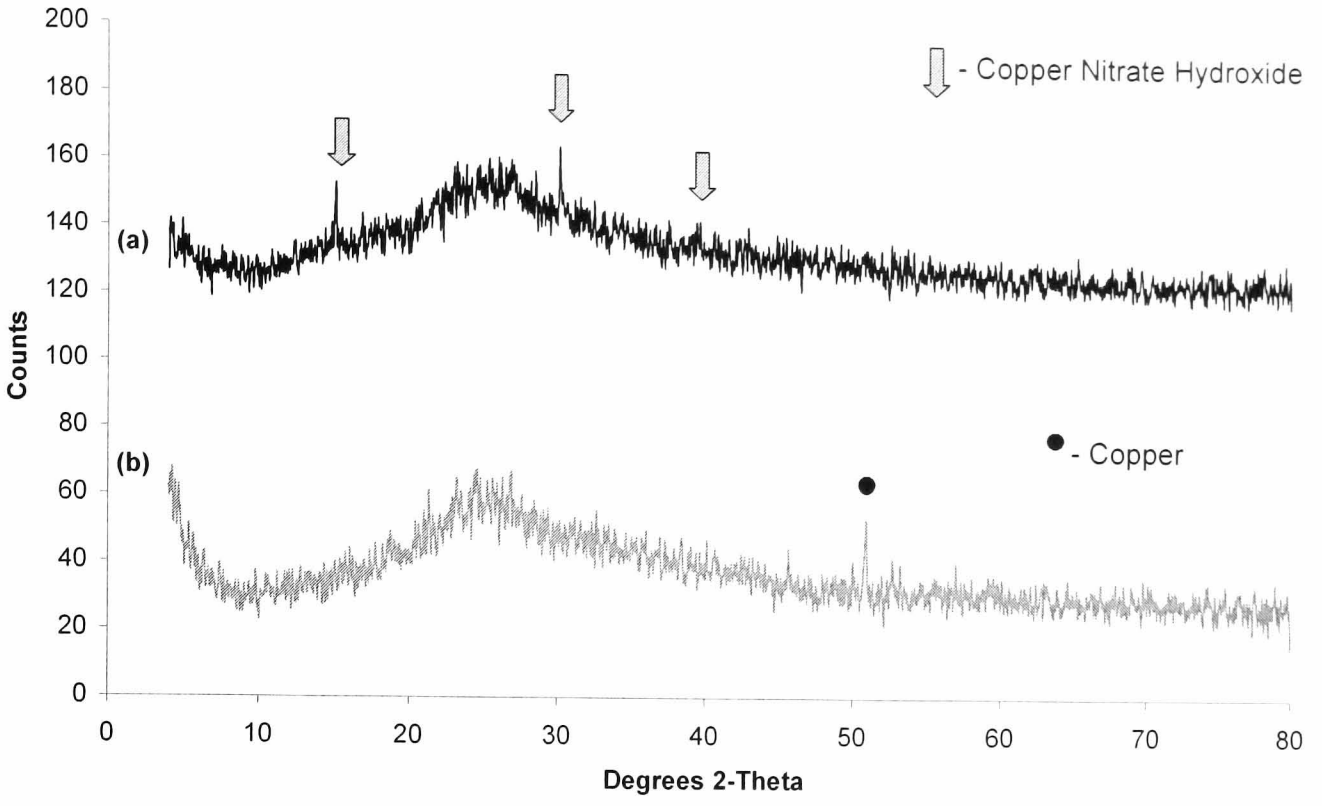

The post-reaction samples showed that all of the mixed catalysts contained a crystalline copper phase after reaction. The catalyst with the most pronounced peak for copper was the palladium containing catalyst. This indicated that addition of a low concentration of palladium to the catalyst increased the crystallinity of the material on the surface of the catalyst both pre- and post-reaction. On examination of the used catalyst, a peak was observed at 50.9 °2θ. This corresponded with the strongest peak from the diffraction pattern of copper at 50.75 °2θ (85-1326). The average copper crystallite size for 10Cu5Ce0.05Pd/silica was calculated as 35 nm. For the remaining copper and cerium/silica samples, the crystallite size could not be calculated. The copper peak for the copper and cerium mixtures was very weak and obscured by background noise.

The amorphous nature of the copper/silica catalysts was not completely unexpected as several other groups had reported similar results on freshly prepared copper/silica catalysts [118, 139, 146]. Toupance *et al* [118] found that diffraction lines were not observed for catalysts dried at room temperature, but were present for an impregnated catalyst dried at 373 K for more than 3 hours. The lines of the pattern increased in intensity with increasing drying time. The group found that the species present was copper (II) nitrate hydroxide [118], not copper (II) nitrate hydrate as expected. This change in the copper nitrate was accompanied by a change in the d-d transition band in the solid state UV-Vis-NIR spectrum, towards 730 nm [118]. UV-Vis-NIR spectra of

5% and 10% copper/silica catalysts showed that the d-d transition occurred between 780 and 800 nm (section 3.1.5, table 3.1.8). Hence it was probable that the predominant species on the catalyst surface was copper (II) nitrate. This was in agreement with the XRD of the 10% Cu/silica catalyst, which indicated the presence of the copper (II) nitrate hydrate.

A study by Selim and co-workers [146] suggested that the preparation conditions for copper/silica catalysts resulted in them being amorphous to x-rays. The study investigated the preparation of impregnated copper/silica catalysts at pH values of ~10 and 4.5. Those prepared at pH = 4.5 were amorphous to x-rays and it was proposed that this was due to the presence of small crystallites [146]. Kohler *et al* [147] found that copper/silica catalysts were amorphous to x-rays and attributed this to the small crystallite size. The group suggested that crystallite sizes below 5 nm (assuming spherical geometry) or below 10 nm (for raft-like crystals) were amorphous to x-rays [147].

Therefore, the copper catalysts prepared in this study had small crystallites, which were below the detection limit of the XRD technique. The copper particle size will be examined further in section 3.1.9.

Alumina Catalysts

The alumina catalysts were examined after preparation and several peaks were observed for these catalysts. As can be seen from figure 3.1.11, the peaks between 35 and 55 °2θ were from the alumina support (fig. 3.1.11 (d)) and were similar to those from the XRD database [145] for δ-alumina (46-1215).

Figure 3.1.11. XRD of alumina catalysts (a) 5Cu/alumina, (b) 5Cu5Ce/alumina, (c) 5Ce/alumina and (d) alumina support.

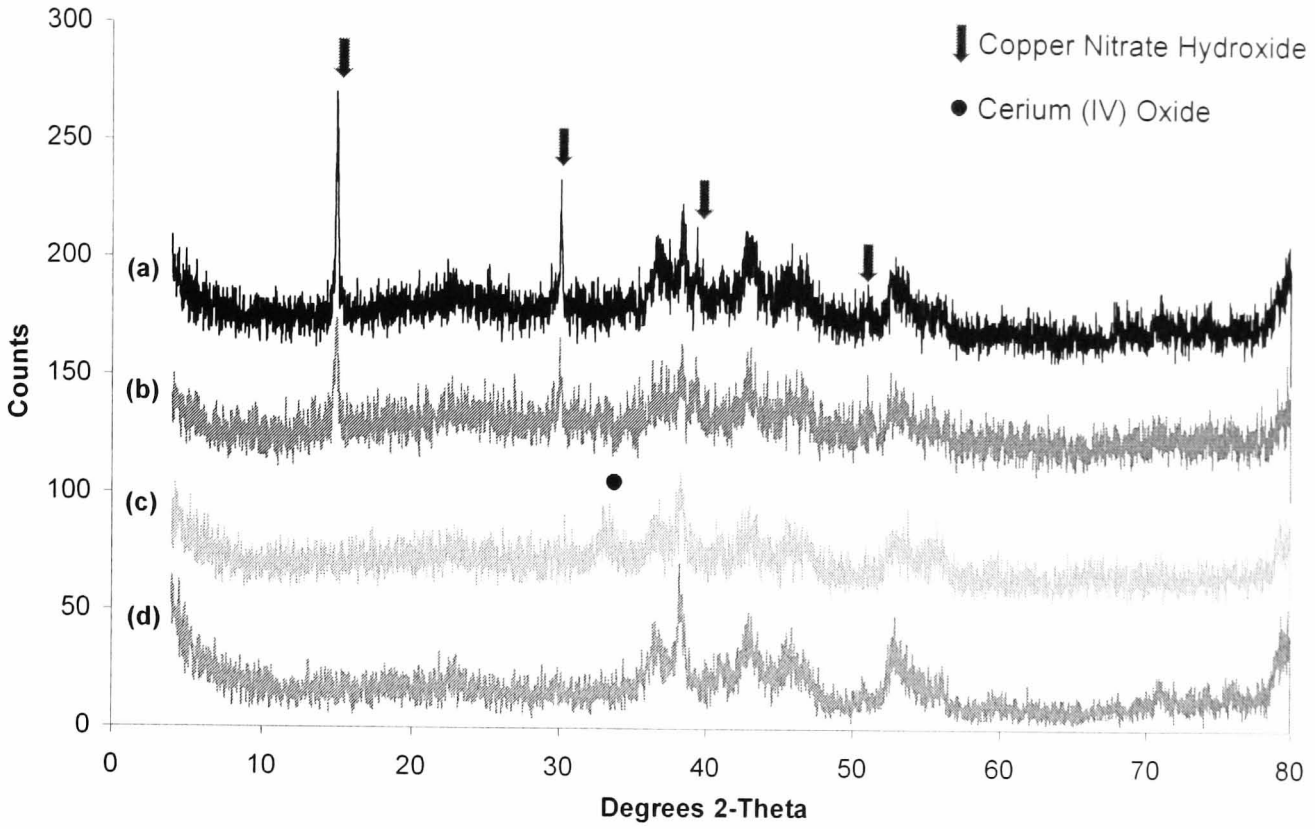

From the powder XRD database [145], it was found that the species present on the fresh 5Cu/alumina and 5Cu5Ce/alumina catalysts was copper (II) nitrate hydroxide (Card no. 15-0014). Toupance and co-workers [118] observed the formation of copper nitrate hydroxide on similarly prepared copper/silica catalysts. The most intense peaks of the reference spectrum were found at 15, 30, 39 and 51 °2θ. This matched well with the actual spectra of 5Cu/alumina and 5Cu5Ce/alumina, which showed sharp peaks at 15 and 30 °2θ. The formation of the nitrate hydroxide was confirmed by the UV-Vis spectrum (table 3.1.8) of the metal/alumina catalysts. The d-d transition for copper (II) nitrate solution was ~809 nm. A shift to ~750 nm was observed after supporting the metal salt onto the alumina and drying the catalyst. As copper (II) nitrate hydroxide had a peak maximum near 730 nm, this confirmed that the main Cu(II) species was copper (II) nitrate hydroxide.

Using the Scherrer equation (See section 2.4.7), the line broadening of the <100> peak at approximately 15 °2θ was used to calculate the average crystallite size for both the 5Cu/alumina and 5Cu5Ce/alumina catalysts. These were determined as 38 nm for 5Cu/alumina and 23 nm for 5Cu5Ce/alumina. Hence, the smaller crystallite size of the copper and cerium catalyst suggested that dispersion of active species improved on addition of the cerium component, leading to reduced crystallite size. The effect of

cerium addition on copper crystallite size and dispersion will be investigated further in section 3.1.9.

The 5Ce/alumina sample (figure 3.1.11 (c)) showed one peak in addition to those for the alumina support, which occurred at 33 °2θ. This agreed well with the strongest peak from the reference XRD spectrum of cerium (IV) oxide. The most intense peak for the reference spectrum was at 33 °2θ. This peak did not occur in the XRD pattern of the mixed metal catalyst (5Cu5Ce/alumina). Hence, cerium oxide was only present in the 5Ce/alumina catalyst. The presence of copper in the catalyst prevented the formation of crystalline cerium oxide after drying the catalyst (i.e. prior to heat treatment or reaction). An investigation by Park and co-workers [148] of cerium/alumina catalysts after calcination, found that low cerium loading and higher surface area alumina increased the amount of crystalline CeO_2, which was detected. Park *et al* [148] also suggested that it was possible to form $CeAlO_3$ dispersed surface phases and/or small CeO_2 crystallites undetectable by XRD. It was probable in the case of the catalyst prepared in this study that cerium nitrate hydrate (or hydroxide) was still present on the dried catalyst. The UV-Vis spectrum of the fresh catalyst contained a band at ~270 nm from charge transfer of the nitrate to cerium. Therefore the dried 5Ce/alumina catalyst contained both cerium (IV) oxide and cerium nitrate hydrate (or hydroxide).

Post-reaction samples were also analysed by XRD (fig. 3.1.12). All three catalysts exhibited peaks corresponding to δ-alumina (04-0877). 5Cu/alumina and 5Cu5Ce/alumina contained a sharp peak, which corresponded to that of copper metal (04-0836). However, the 5Cu/alumina catalyst exhibited additional peaks. The peaks were at positions similar to those for corundum. Corundum is similar to α-alumina, as both materials are forms of completely dehydrated alumina. Loss of surface area would have been expected to accompany the transition to α-alumina. However, the BET surface area of the 5Cu/alumina catalyst did not decrease. The BET surface area results are shown in table 3.1.9 for the fresh alumina-supported catalysts and the corresponding post-reaction catalysts.

Figure 3.1.12. XRD of post-reaction alumina catalysts (a) 5Cu/alumina, (b) 5Cu5Ce/alumina, (c) 5Ce/alumnia and (d) alumina support.

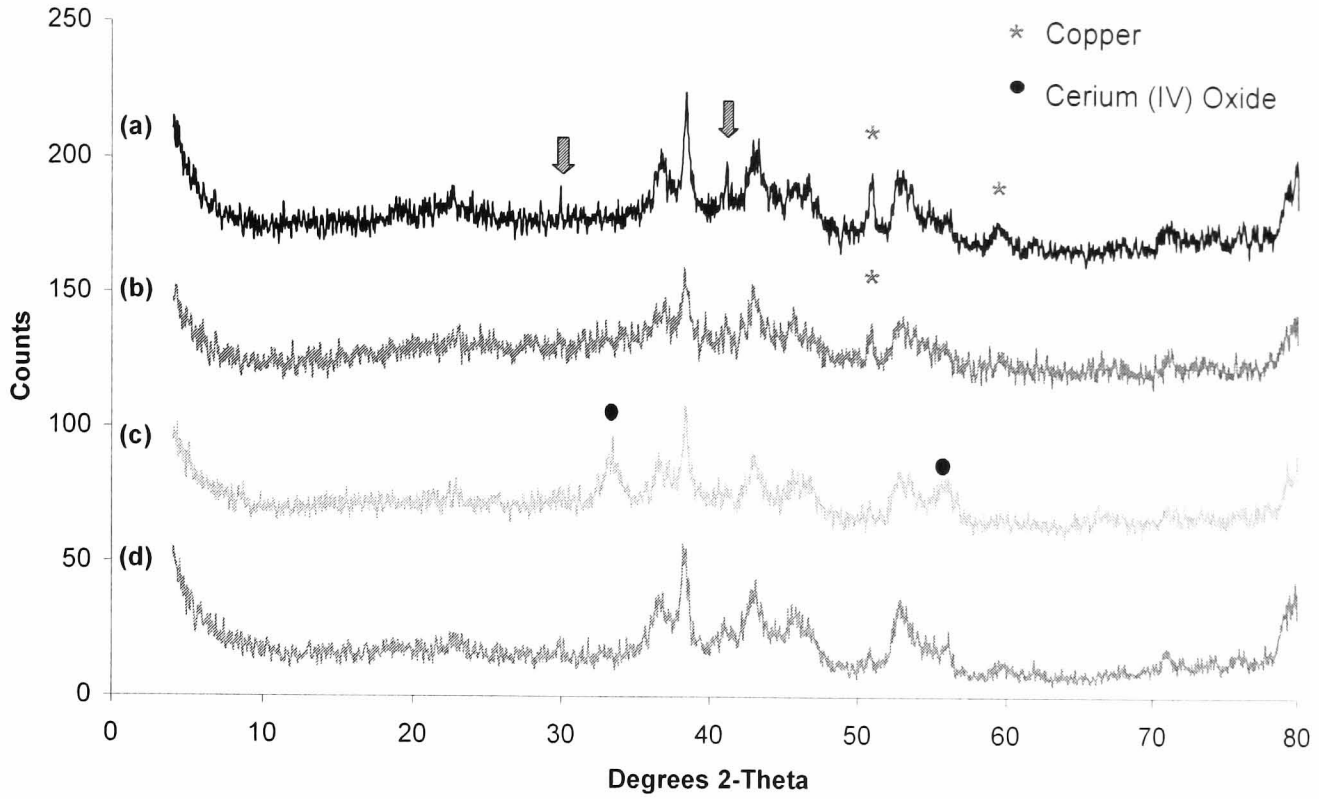

Table 3.1.9. BET surface areas of fresh and post-reaction alumina catalysts.

Catalyst	*BET Surface Area (m^2g^{-1})*	
	Fresh Sample	*Post-Reaction*
Alumina	104	-
5Cu/alumina	82	90
5Ce/alumina	90	87
5Cu5Ce/alumina	66	90

Although there were differences in the surface areas of the fresh catalysts, the post-reaction samples all had surface areas of ~90 m^2g^{-1}. Instead of a loss of surface area, the surface area of the 5Cu/alumina and 5Cu5Ce/alumina improved after the reaction process.

Normally transformation from transition aluminas to α-alumina only occurs at high temperature (~ 1473 K), see figure 3.1.13 [13]. However, the precursor used to form the alumina, the presence of impurities and changes to the reaction atmosphere can effect the transformation of transition aluminas. A chlorine atmosphere during heating was found to enhance the transformation of transition aluminas to α-alumina [149]. Heating in oxygen and water vapour also accelerated transformation of aluminas [150]. However the 5Cu/alumina catalyst was not exposed to temperatures greater than 523 K

(during reduction process). Even in the presence of impurities and a reducing gas atmosphere, it was unlikely that α-alumina would be formed below 1173 K. Therefore, it was improbable that the additional peaks in the diffraction pattern of 5Cu/alumina were due to the formation of α-alumina.

Figure 3.1.13. Transitional stages of alumina created on heating in air (from ref [13]).

(The values above the arrows are temperatures in K).

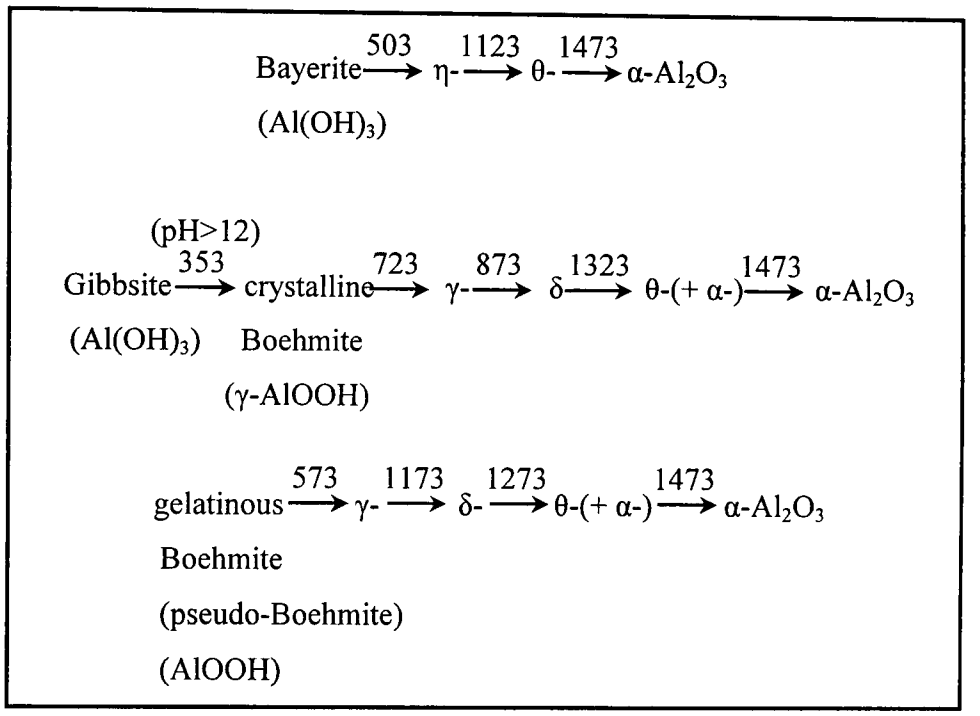

The additional peaks, which were present in the 5Cu/alumina catalyst, were not replicated in the 5Cu5Ce/alumina catalyst. Both samples had red/brown particles after reaction, confirming the presence of copper. Corundum and copper exhibited strong peaks at 50.81 and 50.75 °2θ respectively [145]. However, as it was unlikely that corundum was present in the catalysts, it was assumed that the peak at ~50 °2θ was from the copper crystallites. The average crystallite size was calculated as ~36 nm for 5Cu/alumina and 5Cu5Ce/alumina. Although the average crystallite size in the initial catalyst was different both 5Cu/alumina and 5Cu5Ce/alumina appeared to have the same crystallite size post reaction. The presence of copper crystallites suggested that the crystallites were large, as they had not re-oxidised to form copper oxide. The results indicated that there was no change to the final crystallite size of the copper on addition of cerium to the copper/alumina catalyst.

The 5Ce/alumina catalyst showed the presence of a δ-alumina phase with additional peaks from CeO_2 (04-0593). The CeO_2 features were more intense than those present in

the fresh catalyst. This confirmed that after reduction, reaction and air exposure there was an increase in the formation of CeO_2 crystallites.

3.1.7 Raman Spectroscopy

With the advancing design of lasers suitable for Raman spectroscopic techniques, the use of Raman spectroscopy in catalysis has increased exponentially. It has become increasingly popular for the investigation of structures of bulk metal oxides, surfaces and interfaces [59, 151-153]. Another advantage of this technique is its ability to be used '*in situ*'. In this way, the surface/bulk metal oxide material can be studied under realistic reaction conditions. One particular area of interest in catalysis is the investigation of transition metal oxides. Metal oxygen bonds (M=O and M-O) are difficult to examine using IR. This is due to strong IR adsorption of oxide supports in this region (<1000 cm^{-1}). Hence, Raman spectroscopy is complementary to IR in that peaks hidden in IR may be detected using Raman spectroscopy. In contrast to XRD, which is used to study crystalline material, Raman spectroscopy is a useful technique for the investigation of both crystalline and amorphous materials.

3.1.7.1 Raman Spectra

All of the fresh silica catalysts were examined by Raman spectroscopy after drying at 333 K for one week. The spectra were used to confirm the information gathered from the XRD and UV-Vis-NIR spectroscopy.

Silica Support

Silica and alumina supports exhibit only very weak bands in the 100-1100 cm^{-1} region. This is due to the low polarizability of light atoms and the ionic nature of the Al-O and Si-O bonds [154]. Hence, the simple spectra from the C10 silica provide very little information. All of the peaks detected were very weak and broad, however they were in agreement with spectra from Jehng *et al* [136], see table 3.1.10.

Table 3.1.10. Assignment of peaks for silica spectrum.

Wavenumber (cm^{-1})		*Assignment*
Experimental	*Jehng et al*	
497	488	4-fold siloxane rings
601	605	3-fold siloxane rings
782	803 (and 452)	Siloxane linkages
973	979	Surface silanol groups (Si-OH)
1079	1050	Asymmetric mode of Si-O-Si linkages

Spectra from the transparent silica samples suffered form fluorescence. Attempts to change the wavelength of the laser from 632.8 nm to 532.0 nm did not improve the spectrum. The increased noise in the spectra obscured many of the peaks. However, the positions of the peaks observed agreed well with the literature values. The absence of a peak near 880 cm^{-1}, indicated that 2-fold siloxane rings were not present [25]. Hence the initial silica support contained mainly 3- and 4-fold rings (with the possibility that higher member rings were also present).

Copper/Silica Catalysts

Uncalcined samples of copper/silica were examined and compared with the spectra from the copper nitrate hydrated salt (crystalline form). The copper/silica catalysts examined were 5Cu/silica (293 K), 5Cu/silica (WetImpreg), 10Cu/silica (293 K), 10Cu/silica and 5Cu/silica. The Raman spectrum for the copper (II) nitrate hydrate crystals was in good agreement with similar data for copper (II) nitrate solutions [137, 155] and crystals [156]. The spectrum and table of band assignments are shown in figure 3.1.14 (b) and table 3.1.11.

Figure 3.1.14. Comparison of Raman spectra for (a) 5Cu/silica and (b) the copper nitrate precursor.

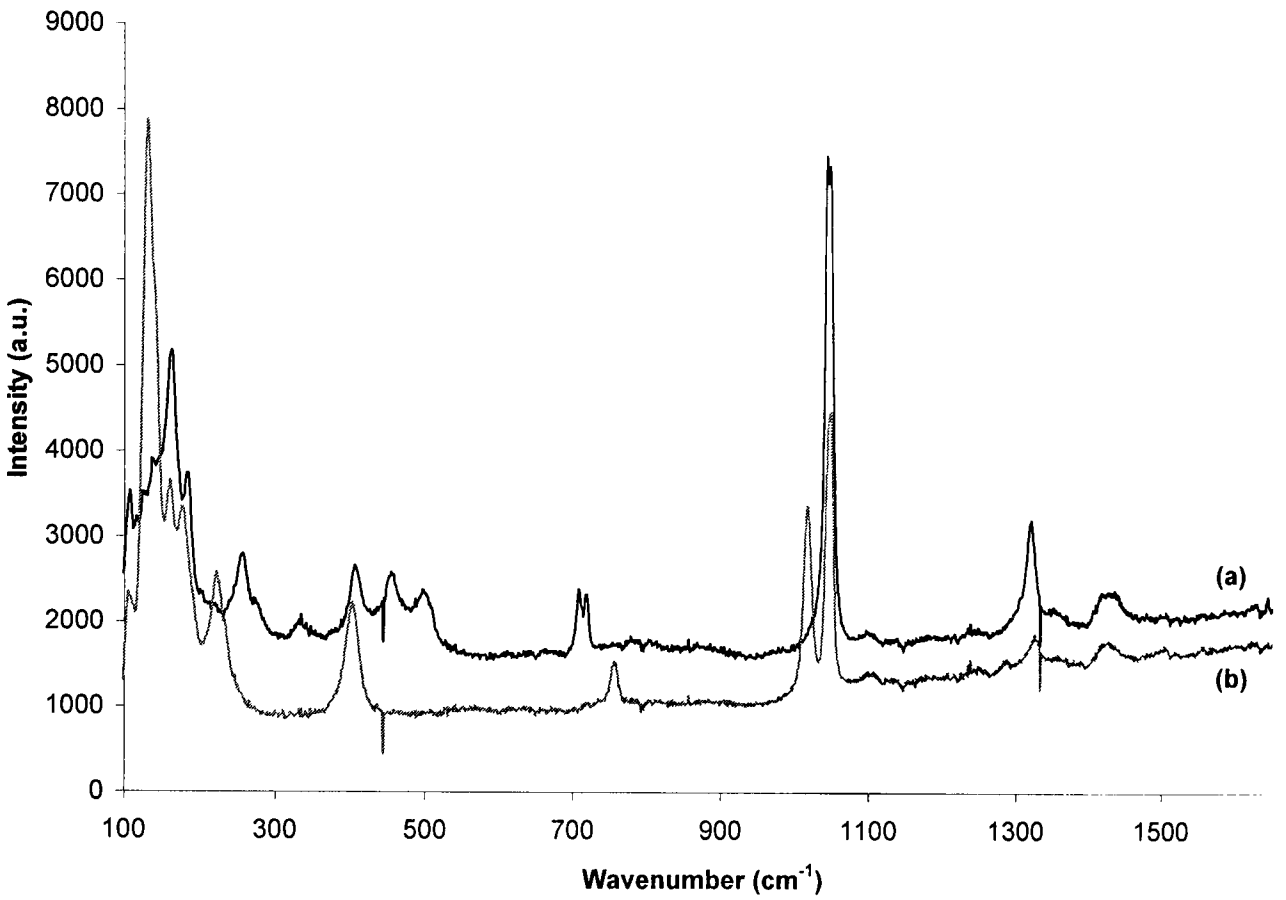

Table 3.1.11. Peak assignment for copper (II) nitrate hydrate crystals.

Experimental Wavenumber (cm^{-1})	*Literature Wavenumber (cm^{-1})*		*Assignment*
	Solution [137]	*Powder [156]*	
401 (b)	~450 (b)		υ_s (symm. stretch) of the $Cu(H_2O)_6^{2+}$ complex
755	757	756	υ_4 NO_2 symmetric bend
1017 (s)	} 1050(s)	1020	} υ_1 NO_3^- symmetric stretch
1047 (s)		1048	
1325 (w)	1320	1325	NO_2 symmetric stretch
1427 (w)	1407	1430	υ_3 NO_3^- anti-symmetric stretch
1503	1494	1500	NO_2^- anti-symmetric stretch

The literature values shown in table 3.1.11 for a copper nitrate solution are consistent with low concentration solutions of nitrate. However, as the concentration of the solution increased the three fundamental vibrations at 72, 1050 and 1360 cm^{-1} split into two peaks [155, 156]. Splitting of these peaks suggested that two states of the nitrate ion existed [155]. The splitting reveals a lowering of the symmetry of the nitrate ion, suggesting that the point group of the species in the crystals (or highly concentrated solution) was C_{2v} or lower. The peaks between 40 and 200 cm^{-1} were due to oscillations

of the lattice, in the course of which the ions/molecules executed translational or rotational vibrations. Hydrated nitrates are rich in this type of vibration; hence the spectrum showed several peaks below 200 cm^{-1}.

On addition of the salt to the silica support, the degree of splitting of the 1050 cm^{-1} peak was reduced and showed only slight splitting at the top of the peak (figure 3.1.14 (a)). The band near 720 cm^{-1} had split into a doublet and shifted to a lower wavelength. As the stretching band of the $Cu(H_2O)_6^{2+}$ complex shifted only slightly (~5 cm^{-1}), a change in the nitrate species occurred after supporting the complex on silica.

The increase in the number and strength of bands at ~1350 cm^{-1} was due to either complexation or solvation of the nitrate. When complexation occurs, the degenerate υ_3 band of the NO_3^- ion is transformed into its A_1 and B_2 components. This change may have occurred when supporting of the precursor on silica, and subsequent drying in air at 333 K.

Table 3.1.12. Peak assignment for copper/silica catalysts.

Wavenumber (cm^{-1})	*Assignment*
406	v_s of $Cu(H_2O)_6^{2+}$ complex
454	Siloxane linkage
496	3 and 4-fold siloxane rings
610 (w)	
707 (doublet)	υ_4 NO_2 symmetric bend
778 (w)	} Siloxane linkages
802 (w)	
1043	υ_1 NO_3^- symmetric stretch
1320	NO_2 symmetric stretch
1427	υ_3 NO_3^- anti-symm. stretch

As splitting of the bands was attributed to degenerate vibrations of the free nitrate ion [137], complexation of the ion would result in reduced splitting of the nitrate peaks. The reduction in splitting of the ~1050 cm^{-1} peak indicated that although co-ordination of the water around the copper ion had not changed, the role of the nitrate ion had. The change in the nature of the nitrate group was also recognised in the UV-Visible spectrum of the copper/silica catalysts. The band for the LMCT from $(NO_3)^-$ to Cu^{2+},

shifted from 301 nm for the copper (II) nitrate solution to ~260 nm for the silica supported catalyst.

Additional features were observed for the silica-supported complex. These were attributed to the silica support and the band assignments are given in table 3.1.12. The silica bands were stronger than for silica alone as the copper/silica beads did not suffer from fluorescence. However, the bands for silica remained weak in comparison with the nitrate peaks.

It is possible that condensation of the silanol groups occurred after drying the catalysts, for example:

$$\equiv Si\text{-}OH + \equiv Si\text{-}OH \longrightarrow \equiv Si\text{-}O\text{-}Si\equiv + H_2O$$

This would have resulted in the formation of siloxane linkages resulting in a reduction of the presence of surface silanol groups. However it was unlikely that this reaction would have taken place, as the drying temperature of the catalyst was only 333 K. Literature reported that the dehydroxylation of surface hydroxyl groups was initiated at approximately 453 K [157]. Although there was no peak near 980 cm^{-1} due to the presence of surface silanol groups in the copper/silica samples, the corresponding band for the silica support was very weak. Hence silanol groups may still have been present in the copper/silica catalysts, even though the band was too weak to be observed in the Raman spectrum.

Cerium/Silica Catalysts

The catalysts examined were 5Ce/silica and 10Ce/silica and the results are shown in table 3.1.13. The cerium/silica catalysts were transparent hence there was some fluorescence present in the spectra. Both spectra were almost identical, although the catalyst with the higher cerium loading had more intense peaks and less fluorescence. The main peak observed at 1045 cm^{-1} was from the nitrate precursor. No splitting of this peak was observed, however the other nitrate peak at ~740 cm^{-1} (NO_2 symmetric bend) appeared to have split. Other weaker peaks were observed as can be seen from table 3.1.13 and figure 3.1.15. The peaks for a similar cerium nitrate powder [156] were in good agreement with those of the catalyst.

Table 3.1.13. Raman peak assignments for cerium/silica catalysts.

Wavenumber (cm^{-1})	*Literature Value [156] (cm^{-1})*	*Assignment*
435		Siloxane linkages
485		} 3 and 4-fold siloxane rings
612		
740 (doublet)	736	υ_4 NO_2 symmetric bend
802		Siloxane linkages
978		Surface silanol groups (Si-OH)
1045	1043 and 1053	υ_1 NO_3^- symmetric stretch
1455 (w)	1464 (w)	υ_3 NO_3^- anti-symmetric stretch

The Raman spectra of the cerium/silica catalysts contained a very weak peak at around 977 cm^{-1}. This was due to silanol peaks remaining on the surface of the catalyst. Splitting of the peaks was similar to that for the copper (II) nitrate/silica catalysts. The supported cerium catalyst showed only one peak at ~1050 cm^{-1}, which did not appear to have split. The powder spectrum of cerium (III) nitrate has two peaks in this region [156]. However, the band remained broad which suggested that there were two bands present, which were over lapping. The band at ~740 cm^{-1} was split into two peaks; however unlike the copper/silica spectrum the peaks were not equal in intensity. The change in splitting of the fundamental nitrate vibrations suggested an increase in symmetry of the nitrate species after supporting the compound on silica.

Figure 3.1.15. Raman spectrum of 10Ce/silica.

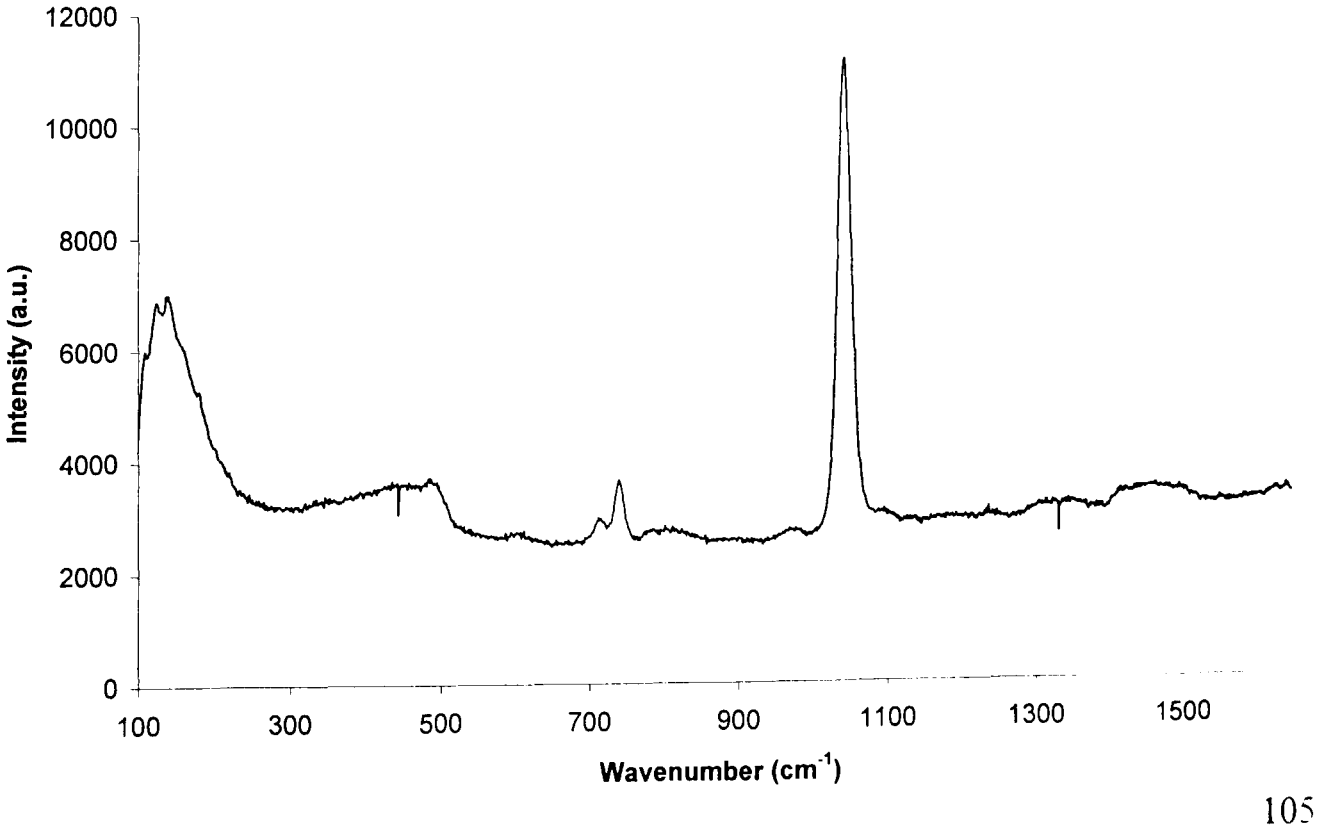

The peaks in the region of ~450 and 1400 cm^{-1} were poorly defined. This was as a result of fluorescence, which caused the bands for silica to be broad and weak. As the bands at ~450 cm^{-1} were in the region where bands for metal to oxygen bonds occur, it was possible that ceria was present on the catalyst surface. Although ceria was not identified in the XRD patterns of fresh samples of cerium/silica, it was observed for the cerium/alumina catalyst. A peak corresponding to cerium oxide would be expected near 450 cm^{-1} for CeO_2. Hence, it was likely that the broad peak was due to several species including peaks for siloxane linkages and 3/4-fold siloxane rings merging.

Copper and Cerium/Silica Catalysts

Both copper and cerium-supported catalysts (5Cu5Ce/silica and 10Cu5Ce/silica) produced very similar Raman spectra to the copper/silica spectra. The catalysts with different metal loadings had different peak intensities.

As can be seen from figure 3.1.16, the catalysts that contained copper and cerium were almost identical to the copper/silica catalyst. There was only a very slight deviation at ~740 cm^{-1} which was either due to the addition of cerium or the nature of the nitrate in the material. It appeared that the peaks at ~740 and ~1050 cm^{-1} both increased simultaneously. Possibly as a result of more nitrate species present on the catalyst surface. In solution Raman spectroscopy, the peak at 740 cm^{-1} becomes better defined as the concentration of the solution increases [137]. From the spectrum in figure 3.1.16, the 10Cu5Ce/silica catalyst had the highest copper content, although the spectrum of 5Cu5Ce/silica had the most intense peaks. Hence, peak intensity was possibly related to the dispersion of the copper (II) nitrate on the support.

Figure 3.1.16. Raman spectrum of copper and cerium/silica catalysts: (a) 10Cu5Ce/silica, (b) 5Cu5Ce/silica and (c) 5Cu/silica.

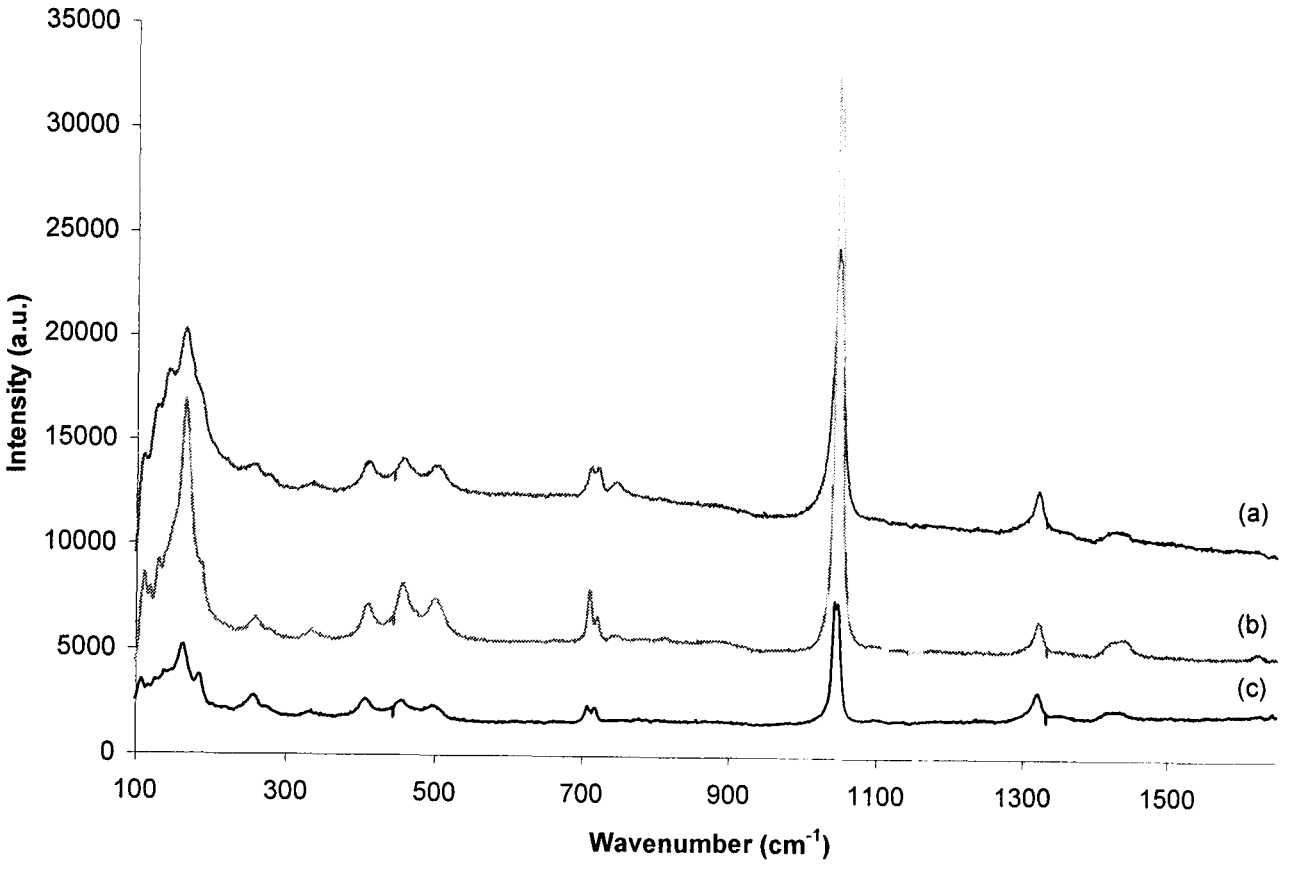

This study confirmed the presence of copper nitrate on the surface of the prepared catalysts. Although only the 10% Cu/silica catalyst showed a copper (II) nitrate hydrate phase in the XRD pattern, the UV-Vis and Raman spectroscopy confirmed the presence of copper (II) nitrate on the fresh silica-supported catalyst.

Copper Acetate/Silica Catalyst

As the catalyst prepared using copper (II) acetate as the precursor (5 % Cu/silica (ac)) was transparent, it was subject to higher levels of fluorescence than the nitrate catalysts. The spectrum collected showed mainly weak bands, many of which were broad (see figure 3.1.17). The bands between 300 and 620 cm^{-1} were due to siloxane linkages and rings and the peak near 800 cm^{-1} was due to siloxane linkages (see silica peak assignments in table 3.1.10). As well as the peaks already attributed to the silica support, there was a feature at 947 cm^{-1} band due to the acetate precursor. The peak (near 940 cm^{-1} from literature) has been attributed to the presence of acetate anions (CH_3COO^-) [158]. However, literature suggests that a higher frequency spectral range is required to determine further information about the nature of the acetate ligand.

Figure 3.1.17. Raman spectrum of 5% Cu/silica (acetate).

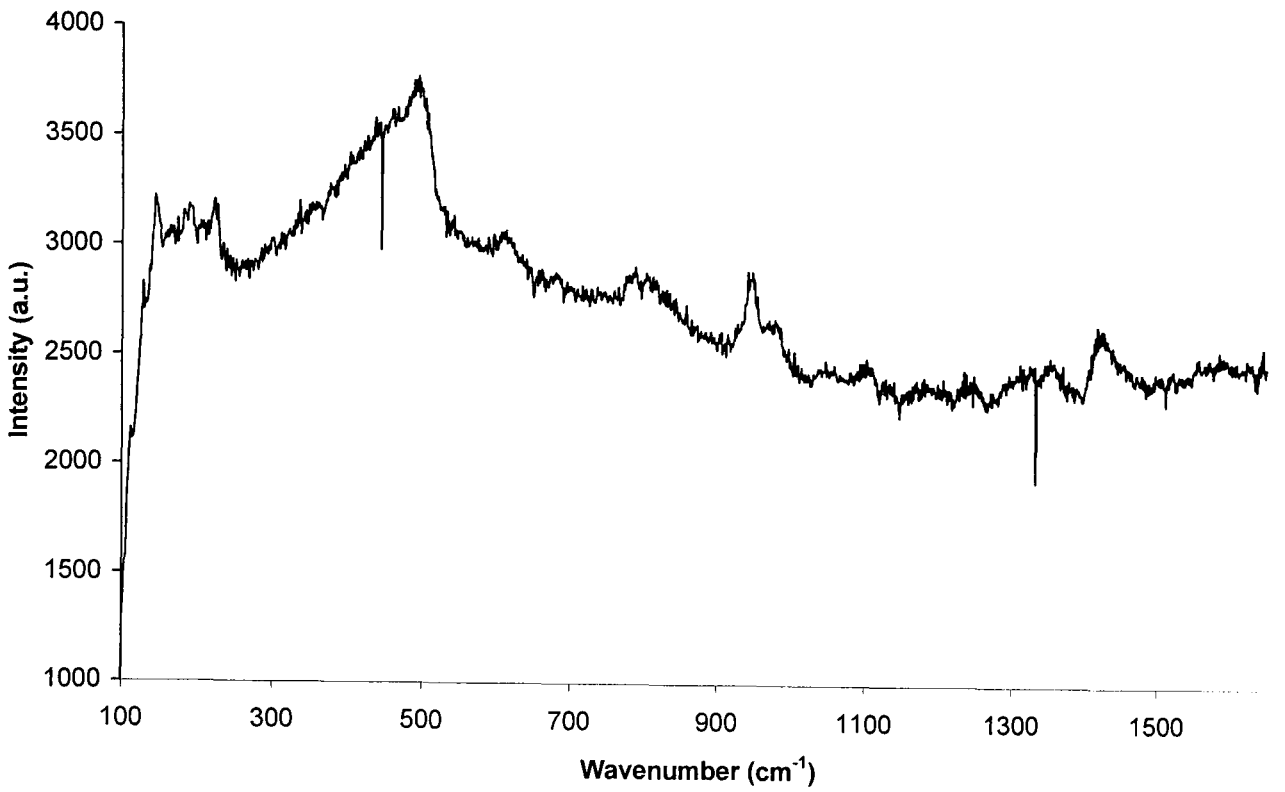

3.1.7.2 Environmental Cell

Three samples were examined in the environmental cell 5Cu/silica, 5Ce/silica and 5Cu5Ce/silica. They were examined under reduction and oxidation conditions, up to a maximum temperature of 523 K. The experiments were designed to investigate the nature of the metal species under different reductive and oxidative conditions.

Copper on Silica

As described in section 2.4.4, the catalyst was heated to 523 K and a Raman spectrum recorded periodically. Initially, the spectrum of the catalyst was the same using the environmental cell as it had been for the initial Raman spectrum of the catalyst. On heating under hydrogen, bands for the nitrate ion decreased in intensity until they were no longer visible. As the temperature increased, fluorescence increased until no peaks were visible. Hence, at the end of each heating step, the sample was cooled to room temperature in the reaction gas before a Raman spectrum was collected (fig. 3.1.18).

Figure 3.1.18. Raman spectra of copper/silica catalyst after each stage of the reaction.

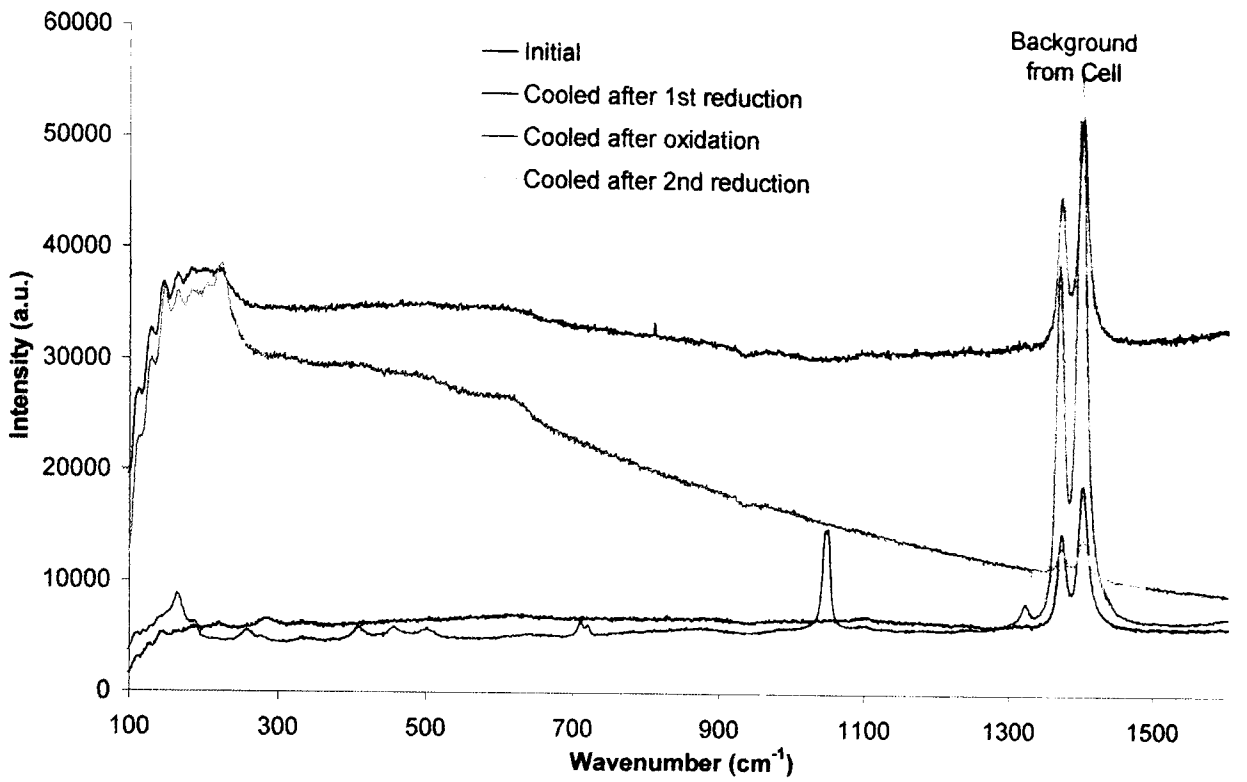

After reduction in hydrogen, there were no well-defined bands other than those that were attributed to background from the cell, figure 3.1.18. There was a very weak peak near 630 cm^{-1}, indicating the presence of copper (I) oxide. There were few peaks in the M-O bond region, indicating that the majority of the copper was present as metal. The appearance of copper (I) oxide indicated that the catalyst was only partially reduced under the conditions used (heating to 523 K in hydrogen/nitrogen at 5 $Kmin^{-1}$ for 1 hour). Peaks that were previously assigned to the silica support of the fresh copper/silica samples were no longer observed. Hence a change in the nature of the support had occurred during reduction of the catalyst.

On oxidation of the same sample a weak peak occurred at 288 cm^{-1}. This was due to the formation of copper (II) oxide [159, 160]. A second reduction procedure was then carried out. As expected, the oxide peak disappeared during heating in the hydrogen/helium mixture. After cooling the sample, the peak at ~630 cm^{-1} became more pronounced indicating that a greater proportion of copper (I) oxide was present. The post-reaction XRD samples did not show the presence of any crystalline copper oxide phases after reaction and exposure to air. However, as the samples were slightly brown in colour, it was possible that there were copper oxides present on the used sample, which were amorphous to x-rays.

The peaks between 1300 and 1500 cm^{-1} (highlighted on figure 3.1.18) were due to the environmental cell. Although the peaks varied slightly under the reaction conditions they did not appear to affect analysis of bands in the metal-oxygen bond region.

The initial stages of the Raman experiment under environmental conditions indicated that changes occurred to both the nature of the copper and the silica support. Selim *et al* [146] proposed that copper nitrate/silica catalysts prepared at low pH values (~4.5) produced copper (II) ions, which were adsorbed on to the weakly polarized surface hydroxyl groups by simple electrostatic attraction forces. As the zero point charge (or isoelectric point) of silica is close to 1 and the catalysts from Glasgow were also prepared at a pH of ~4.5, a similar interaction would have been expected. At a pH of ~4.5, the silica surface was weakly polarized. Due to the absence of strong interactions between the support and copper nitrate the initial Raman spectrum closely resembled that of the individual components.

During the reduction procedure, heating of the catalyst may have caused condensation of the silanol groups. This can lead to formation of rings. The dehydroxylation of the surface can begin at ~473 K [10, 157]. The Raman spectrum of the reduced 5Cu/silica indicated that 3- and 4-fold siloxane rings were no-longer present on the catalyst surface. The relationship between the siloxane ring size and energetic stability can be arranged as [25]:

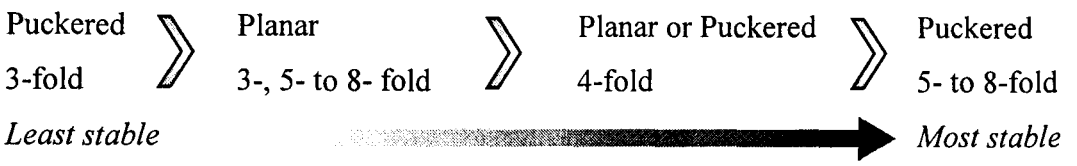

In general, the stability of the ring increases with increasing ring size. The increased stability corresponds to a reduction in ring strain on forming larger arrangements. The energy or strain of the silica is reduced by 2- and 3-fold rings breaking bonds and re-arranging into rings of higher order, puckered 3-fold rings relaxing to planar 3-fold rings and planar 5- to 8-fold rings relaxing to puckered 5- to 8- fold rings [25]. It has been suggested that porous silicas have a high content of 3-membered rings [26].

Loss of bands for the 3- and 4-membered siloxane rings indicated that larger rings had formed during the catalyst reduction. This may have occurred due to ring expansion to

encapsulate the copper species, forming more energetically favourable rings. The low energy region of the Raman spectrum also changed after catalyst reduction. This was possibly due to changes in ring structure, however there was limited information available in the literature regarding the region below 200 cm^{-1}, therefore it was not possible to assign the bands. The proposed structures and changes on reduction are shown in figure 3.1.19.

Figure 3.1.19. Schematic of reactions occurring during reduction process.

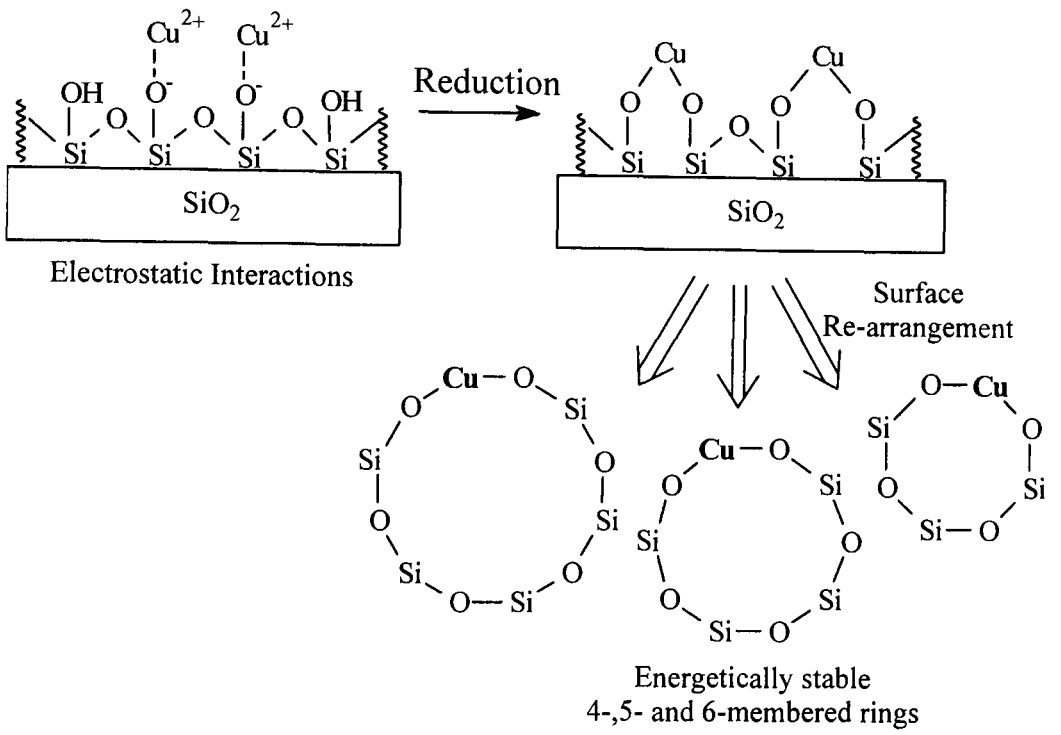

The copper incorporated within the silica rings may have been present as copper particles of varying size. Gladden and co-workers [161] suggested that the structure of the initial silica support strongly influenced the activity of Ni/silica catalysts.

Cerium on Silica

The cerium/silica sample could not be investigated in the environmental cell, as the strongest peaks that appeared were due to the cell itself. This was due to the transparency of the cerium/silica beads, which enhanced fluorescence in the Raman spectrum.

Copper and Cerium on Silica

The copper and cerium/silica catalyst was heated to 523 K in flowing hydrogen/nitrogen. Spectra were recorded throughout the reduction process. The initial spectrum of 5Cu5Ce/silica in the environmental cell was the same as the spectrum for the 5Cu/silica catalyst in the environmental cell. For both the 5Cu/silica and

5Cu5Ce/silica as the reduction progressed, the nitrate peak became smaller then disappeared. The peak did not reappear after oxidation or re-reduction, confirming that the nitrate had been completely removed on reduction to 523 K.

Figure 3.1.20 shows the changes in the surface during the reduction, oxidation then reduction cycle. Unlike the copper/silica catalyst, after the first reduction three broad bands were observed at 415, 530 and 630 cm^{-1}. The 630 cm^{-1} band was due to the presence of copper (I) oxide. Only a weak band for Cu_2O was observed for the copper/silica catalyst exposed to the same reaction conditions, indicating that addition of cerium oxide enhanced stability of Cu_2O. Cu^{+1} species have been observed in CuO/CeO_2 catalysts [162]. They were formed by the interaction of copper clusters with cerium oxide. This effect was also observed on $Cu/CeO_x/Al_2O_3$ catalysts, where the copper species tended to associate with the surface ceria (rather than surface alumina sites) and become stabilised in the Cu^+ state [163]. This extra stabilisation of the Cu_2O phase by ceria explained why the Cu_2O peak was of greater intensity for 5Cu5Ce/silica than the peak for the copper/silica catalyst.

There were no Raman spectroscopy literature values available for of Ce_2O_3 however; it was likely that the 415 and 530 cm^{-1} peaks were due to a CeO_{2-X} phase. Several authors have assigned peaks or shoulders in the 500 to 600 cm^{-1} region to oxygen vacancies in the cerium (IV) oxide fluorite lattice [164-166]. Indeed, Wang *et al* [167] found that CeO_2 was partially reduced at 523 K in a $CuO/CeO_2/Al_2O_3$ catalyst. This was thought to be aided by the formation of a Cu-O-Ce shared oxygen ion linkage [167]. Results indicated that the cerium oxide had been reduced to a non-stoichiometric oxide (CeO_{2-x}) and synergy between the copper oxide and surface oxygen vacancies of ceria was present [167]. Hence, it is possible that interfacial active centres, $Cu\text{-}Ce^{3+}$ had formed and resulted in a change in activity of the catalyst.

Figure 3.1.20. Raman spectra of copper and cerium catalyst after each stage of the reaction.

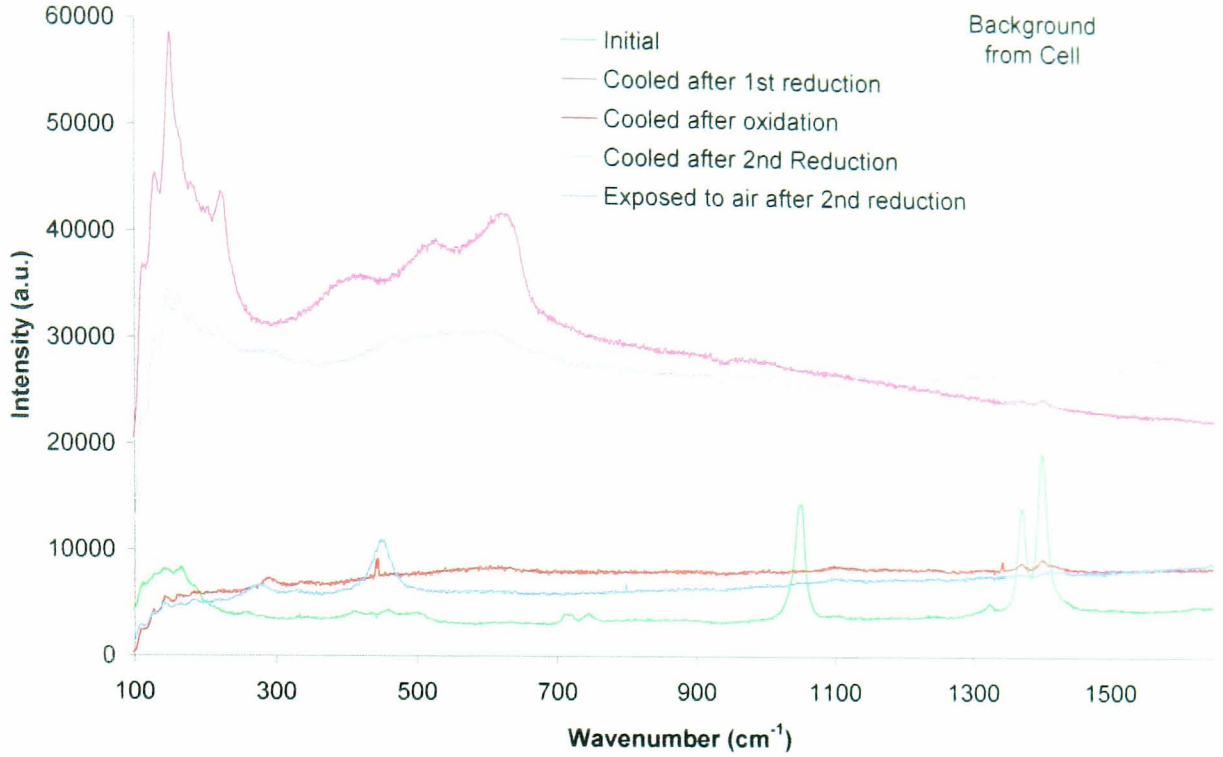

Table 3.1.14. Raman bands of pure oxides [168].

Metal Oxide	*Raman Peak Positions (cm^{-1})*
CuO	123 (s), 158 (m), 294 (m), 462 (w), 632 (w)
Cu_2O	122 (m), 154 (m), 219 (s), 633 (s)
CeO_2	450 (s)

Although greatly shifted, the 415 cm^{-1} band was probably due to the presence of cerium (IV) oxide, as reduction to 523 K in hydrogen was unlikely to fully reduce the cerium oxide present. Shan *et al* [166] found a similar shift of approximately 20 cm^{-1} (to 443 cm^{-1}) for a cerium (IV) oxide peak. They attributed the shift to either an increase in CeO_2 particle size or the presence of oxygen vacancies. It was also thought that this latter property might be enhanced by the presence of copper in the solid solution [166].

After oxidation, the catalyst showed smaller peaks at 290 and 444 cm^{-1}. The peaks were due to the formation of copper and cerium oxides (CuO and CeO_2, see table 3.13). The second reduction did not have the same effect as the first. The three bands were no longer distinct as they had merged into one broad band. This may have been due to increased reduction of the catalyst surface or due to stronger interactions between the cerium and copper species after the oxidation and reduction treatments.

Finally, the sample was exposed to air and large peaks were observed due to the cerium and copper oxides. No features corresponding to the silica support were evident from the spectrum. As the support bands were weak, the metal oxygen bands from the cerium and copper oxide might have overlapped with the support peaks. However it was possible that a similar mechanism during reduction could be proposed for the 5Cu5Ce/silica catalyst as for the 5Cu/silica catalyst. As a result, the absence of peaks corresponding to 3 and 4-membered siloxane rings might be associated with an increase in ring size and encapsulation of the copper and/or cerium species into the rings. The enhanced formation of Cu_2O for the 5Cu5Ce/silica catalyst suggested that there was a synergetic interaction between the copper and cerium species in the catalyst.

The results showed that reduction of the copper/silica catalyst to 523 K resulted in the complete removal of the nitrate and that a small amount of copper (I) oxide was produced during reduction. As the nitrate bands disappeared completely, the cerium was present as cerium oxide after the reduction procedure. In the 5Cu5Ce/silica catalyst, the copper species was in close contact with the cerium oxide. The results showed that the cerium (IV) oxide surface was partially reduced during the reduction procedure. This could be as a result of spillover from the copper to the ceria or as a result of the formation of copper-ceria interfacial sites. The effect of adding cerium to copper/support catalysts will be investigated further using temperature programmed reduction.

3.1.8 Temperature Programmed Reduction (TPR)

Temperature programmed reduction (TPR) is a popular technique used to investigate the nature of catalyst surface species during reduction [169]. In this section, the effect of combining copper and cerium on the catalysts and the effect this has on the reduction temperature was examined. The advantage of using a technique such as TPR is that it follows the reduction of the catalyst *'in-situ'*. It can be used to identify intermediate metal species, metal support interactions and changes to the reduction process, which occur on addition of a second metal (e.g. alloying).

Copper/Silica Catalysts

XRD, UV-Vis and Raman spectroscopy showed that copper species on the silica-supported catalysts was mainly copper (II) nitrate hydrate. The precursor on the silica

catalysts was either amorphous or composed of small crystallites according to the XRD results. Hence, TPR was used to identify whether or not more than one species of copper was present on the catalyst surface.

Reduction of pure copper oxide supported on silica usually occurs in one step at ~563 K. However, supported copper oxide aggregates can be reduced at temperatures as low as ~473 K [170]. In copper/support catalysts copper can be present as isolated ions, clusters and bulk CuO particles. Depending on catalyst preparation/calcination conditions and TPR reaction conditions, the temperature of the reduction peak (T_{max}) can vary widely. When more than one peak is produced in the TPR profile, this can either be due to the single stage reduction (Cu^{2+} to Cu^0) of more than one type of copper (II) species, or the two-stage reduction (Cu^{2+} to Cu^{1+} to Cu^0) of a single copper (II) phase. Hence, more than two peaks imply that there are several types of copper (II) species present. The overall reaction for copper oxide reduction is:

$$CuO + H_2 \longrightarrow Cu^0 + H_2O$$

However, in the case of the copper/silica catalysts the copper species on the surface of the catalyst was copper (II) nitrate hydrate. During the in-situ Raman spectroscopic investigation, Cu_2O was identified after reduction of 5Cu/silica in a hydrogen/nitrogen mix to 523 K. Hence, reduction of the catalysts could occur in several steps, with intermediates such as CuO, Cu_2O and copper (II) nitrate hydroxide. Not only can the reduction profile be complicated by the formation of intermediates, but dispersion and interaction with the support can also increase the number of peaks observed in the profile. However, on examination of the TPR profiles for the copper/silica catalysts only one peak was produced. A typical reduction profile for the copper/silica catalyst is shown in figure 3.1.21. The temperature for the peak maximum (T_{max}), initial reduction temperature (T_I) and final reduction temperature (T_F) for all of the silica catalysts are shown in table 3.1.15.

Figure 3.1.21. Typical TPR profile for a copper/silica catalyst.

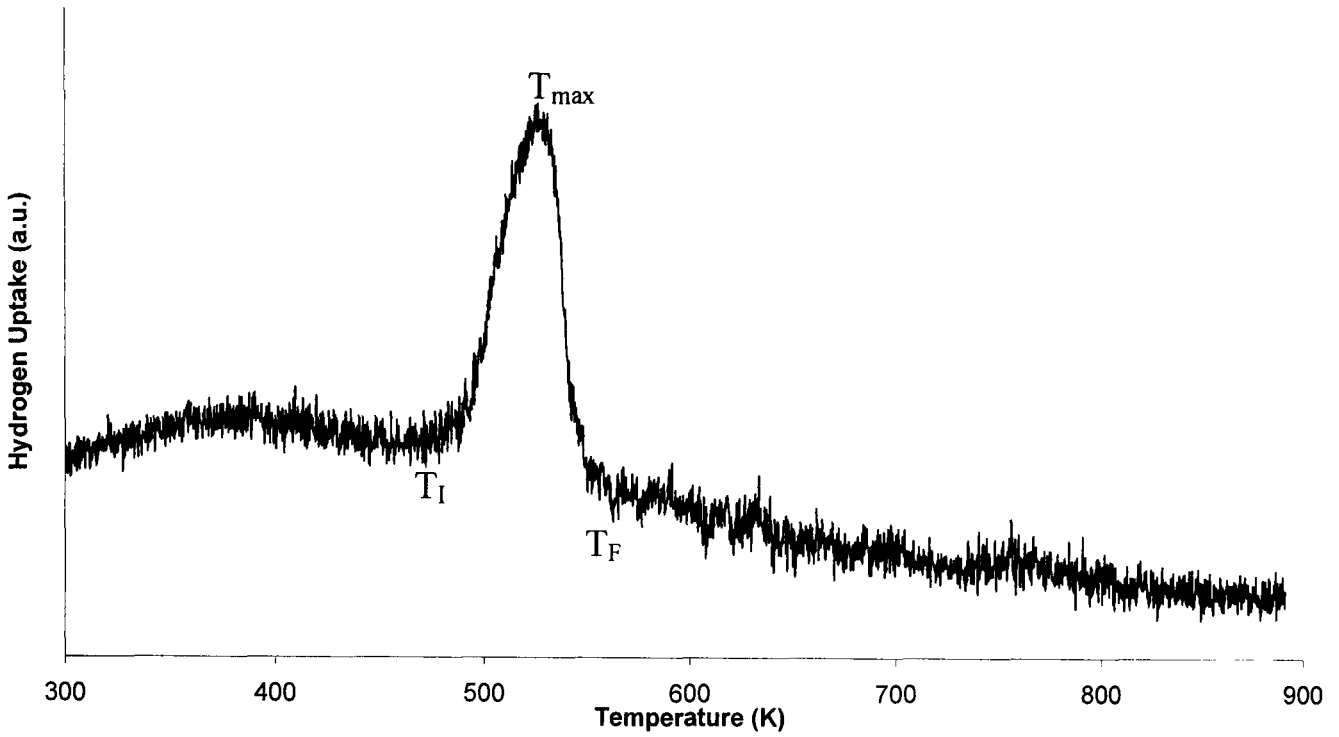

Table 3.1.15. Comparison of reduction profiles – silica catalysts.

Sample	T_I	T_{max}	T_F
5Cu/Silica (293 K)	460	503	521
5Cu/Silica (Wet Impreg.)	478	515	532
10Cu/Silica (293 K)	480	521	546
10Cu/Silica	487	526	556
5Ce/Silica*	-	661, 1084	-
10Ce/Silica	-	669	-
5Cu/Silica	465	512	529
5Cu5Ce/Silica	487	490(sh), 517, 528, 580	620
5Cu/Silica (ac)	491	513	544
10Cu5Ce/Silica	454	480(sh), 520, 540	558
10Cu5Ce0.05Pd/Silica	449	480(sh), 520, 544	561
5Cu1Ce/Silica	465	515, 524	580

* 5Ce/silica TPR maximum temperature was increased to 1173 K.

(sh) denotes shoulder peak.

For the copper/silica catalysts, as the copper loading increased, the T_{max} value increased. The T_{max} value ranged from 503 to 515 K for the 5% copper loaded catalysts and from 521-526 K for the 10% copper/silica catalysts. This indicated that at lower copper loadings the copper (II) species was well dispersed, providing a large surface area for reaction to occur [114] and also producing smaller, more easily reducible copper nitrate

clusters. It was suggested that the T_{max} increased for CuO/silica catalysts with increased loading, as reduction is controlled by the rate of diffusion of hydrogen through the CuO particles [171].

Several groups have investigated the reduction of uncalcined catalysts, which were prepared by impregnation of copper nitrate onto silica [113, 114, 139]. It was reported that direct reduction of the impregnated catalyst led to smaller copper particles dispersed on the catalyst support [114]. Calcination before reduction led to the presence of larger copper crystallites. Although removing the calcination step improved the dispersion of the copper species, reports suggested that nitrogen was retained on the catalyst surface during reduction in hydrogen [114, 172]. Formation of a copper nitride species affected subsequent chemisorptions and activity testing [172]. Hence, in most cases calcination is used to remove the nitrate completely prior to reduction.

Jackson and co-workers [139] studied the reduction of a selection of copper nitrate/silica catalysts which were not calcined prior to reduction. They found that on heating the catalyst in a nitrogen atmosphere water was lost below 373 K and between 373 and 423 K copper nitrate decomposed to form $Cu(NO_3)_2.2Cu(OH)_2$. Thermogravimetric analysis showed that weight loss between 573 and 673 K was due to decomposition of any copper nitride present, desorption of NO and decomposition of $Cu(NO_3)_2.2Cu(OH)_2$ [139]. In hydrogen, there was an additional weight loss between 473 and 523 K, due to reduction of $Cu(NO_3).2Cu(OH)_2$ to copper metal. Above 673 K, no further weight loss was observed other than that for the dehydroxylation of the silica support [139]. Hence, there were two routes through which reduction of copper could occur [139]:

$$Cu(NO_3)_2.2Cu(OH)_2 + 11H_2 \longrightarrow 3Cu + 2NH_3 + 10H_2O$$

$$Cu(NO_3)_2 + 9H_2 \longrightarrow Cu + 2NH_3 + 6H_2O$$

Although the TPR profiles for copper/silica showed only one peak, this was in agreement with the TPR profile for the copper nitrate precursor under the same reaction conditions. The TPR for the precursor contained one peak at 574 K. Decomposition of the copper nitrate was observed between ~420 and 580 K. According to literature, copper nitrate decomposes at 443 K to lose nitrate species [173]. Two peaks were

observed due to the production of NO_x's at ~450 and 550 K and were in a 1:2 ratio. The first peak was due to the decomposition of the precursor to form copper nitrate hydroxide. The second peak was due to the decomposition of $Cu(NO_3)_2.2Cu(OH)_2$ and remaining copper nitrate. Additional hydrogen consumption was due to the reduction of copper nitrate hydroxide and remaining copper nitrate to copper metal.

Hence, the main feature of the reduction profile for the copper/silica catalysts was from the reduction of copper nitrate hydroxide to copper. During reduction a brown gas was observed in the exit gases at ~450 K. The gas was due to the production of NO_2 during decomposition of the precursor. After reduction to 523 K, a weak band due to Cu_2O formation was observed by *in-situ* Raman spectroscopy. Although reduction of copper/silica catalysts occurred in one step, it was possible that a small amount of Cu_2O was produced during the reduction. The Cu_2O may have reduced to copper metal if the reduction conditions had been more intense, i.e. prolonged exposure to hydrogen gas.

The reactions proposed by Jackson *et al* [139] during the reduction process formed ammonia, however this product was not detected during the reduction of the copper/silica catalyst. Ammonia would have been difficult to detect by mass spectrometry as water was produced during the reduction. An alternate route for the decomposition of the copper nitrate is:

$$Cu(NO_3)_2.2Cu(OH)_2 + 3H_2 \longrightarrow Cu + Cu_2O + 2NO_2 + 5H_2O$$

Hence, the production of copper and copper oxide would be possible during catalyst reduction. It was possible that the copper nitrate decomposed to copper (II) oxide during reaction, before being reduced to copper (I) oxide and copper metal. Van der Grift *et al* [114] reported that copper (II) nitrate melted at 387 K and decomposed to copper (II) oxide at 447 K. However, peaks corresponding to copper (II) oxide were not detected by Raman spectroscopy, during the reduction process.

The 5Cu/silica (acetate) catalyst was reduced in one step, with a T_{max} of 523 K. The T_{max} value was similar to that of the 5% Cu/silica (nitrate) catalysts. The acetate precursor was examined to explore its benefits when compared with a nitrate precursor. However, due to problems with solubility the spray impregnation technique could not

be used and wet impregnation was used to prepare the catalyst. TPR showed that reduction occurred in one step as for copper/nitrate catalysts.

Cerium/Silica Catalysts

Ceria is a partially reducible oxide (only at high temperatures), with reduction features typically observed at ~770 K and 1100 K [30]. The first peak is attributed to easily removable surface capping oxygen and the latter peak to bulk ceria reduction to Ce_2O_3 [30]. To investigate these peaks, the TPR temperature was extended to 1173 K for 5Ce/silica. When examined the catalyst produced two peaks at 660 and 1085 K. The profile showed that the peaks were broad and of low intensity. Hence, the remaining catalysts were examined to a maximum of 873 K to focus on the copper oxide reduction peaks and any effect observed on addition of ceria.

The data handbook [173] showed that cerium nitrate decomposed at 473 K. Although no hydrogen consumption peak was observed in this region, this indicated that the nitrate decomposed without adsorption of hydrogen. During reduction of the catalyst, colour changes were observed as shown in figure 3.1.22.

Figure 3.1.22. Cerium species observed during reduction of cerium nitrate/silica catalyst.

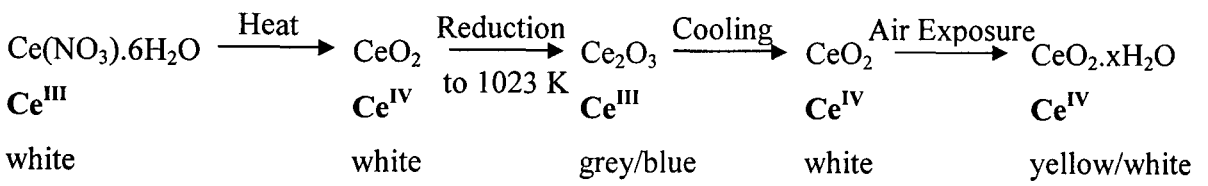

On heating, the copper nitrate decomposed to form cerium oxide on the surface of the catalyst. After temperature-programmed reduction to 873 K, the samples were grey/blue in colour. This showed that the ceria was partially reduced to Ce_2O_3. However, after cooling and exposure to air the sample was yellow/white in colour. The results were in agreement with the XRD pattern of the used reaction samples that contained a cerium oxide phase (CeO_2).

The reduction temperature of the cerium oxide decreased when dispersed on a support. This was in agreement with literature, which showed that the reductive behaviour of ceria changed on addition of a support [30, 34]. The change in behaviour was dependent upon the extent and nature of the interaction between the two oxides.

Trovarelli *et al* [34], found that the degree of reducibility of ceria was strongly enhanced by deposition on silica. The low temperature reduction peak for the ceria/silica catalyst was ~800 K [34]. This was still higher than the reduction temperature for the cerium/silica catalyst prepared in this study. However, small crystallite size and low loading of CeO_2 were found to improve reduction of CeO_2 on silica [34]. Therefore on heating cerium nitrate/silica, a dispersed cerium oxide species was formed on the silica support. This would explain the low reduction temperature at ~660 K for 5Ce/silica. Larsson *et al* [174] reported that the high temperature peak (~1163 K) was due to bulk CeO_2 crystallites and low temperature peak (673 to 773 K) due to a dispersed CeO_2 phase, for CeO_2/Al_2O_3 catalysts. Although not present in the fresh Ce/silica samples, the XRD pattern of the post-reaction samples confirmed the formation of CeO_2 crystallites (section 3.1.6). Therefore, it is possible that two forms of ceria were present on the support, a dispersed CeO_2 phase and bulk CeO_2 crystallites.

During the standard reduction used before testing the catalysts, cerium oxide was formed. The oxide was in the form of CeO_2 after reduction, as 523 K was a high enough temperature to decompose the nitrate to cerium oxide, but not to reduce the cerium oxide.

Copper and Cerium/Silica Catalysts

On combining copper and cerium on a catalyst, T_{max} for copper increased from that found for Cu/silica. From literature, it was expected that T_{max} would decrease as association of copper and ceria resulted in enhanced reducibility of both oxides in a study by Liu *et al* [162] on Cu-CeO_2 catalysts.

Figure 3.1.23. TPR profile for 5Cu5Ce/silica.

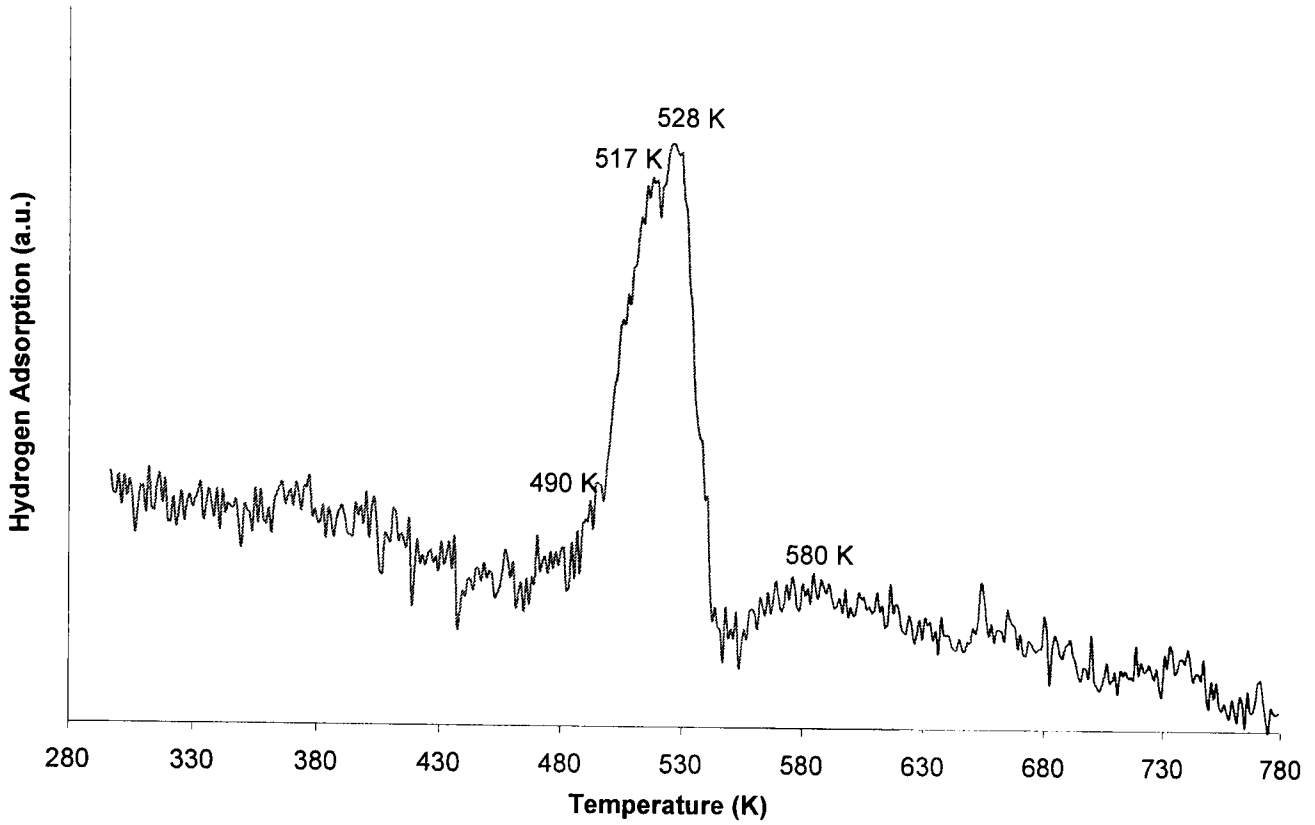

As can be seen from table 3.1.15, the position of T_{max} increased on addition of cerium to a copper/silica catalyst. There were also a number of new features evident for the 5Cu5Ce/silica catalyst. The peak at 580 K was only observed for the 5Cu5Ce/silica catalyst. It is most likely as a result of the decomposition of copper nitride (Cu_3N), which occurs at ~573 K [139]. Formation of copper nitride can be caused by retention of nitrogen atoms during reduction of the catalyst [114]. Retention of nitrogen can affect chemisorption and catalytic activity tests [172]. However, this could be avoided by calcination to remove the nitrate. Formation of copper nitride was not observed over the copper/silica catalysts or any of the other mixed copper and cerium catalysts. If the 580 K peak had been due to the reduction of surface capping oxygen of the cerium oxide, this would have required that the interaction between the copper and cerium was strong enough to induce a shift of almost 100 K (from the temperature observed for 5Ce/silica) for surface cerium oxide reduction. As the position of the peak was in good agreement with that of the decomposition temperature for copper nitride, it was more likely that the peak was due to either decomposition of the nitride or desorption of NO as described by Jackson *et al* [139]. Hence, it was possible that the preparation conditions used for the 5Cu5Ce/silica catalyst favoured the formation of copper nitride during reduction.

The main reduction peak for 5Cu5Ce/silica was split, with a shoulder at 490 K and two peaks at 517 and 528 K. The splitting of the main reduction peak on addition of cerium oxide to the catalyst was probably due to the formation of a Cu_2O phase which was observed by Raman spectroscopy of the 5Cu5Ce/silica catalyst reduced to 523 K. The nitrate had fully decomposed by this temperature. Although the reduction peaks of the copper/silica catalysts did not appear to split, the peak was broad which suggested the possibility that there were several over-lapping bands present. The addition of cerium oxide stabilised the copper (I) species allowing the reduction to occur in two steps. Liu *et al* [38] proposed that addition of cerium oxide stabilised Cu^+ species, therefore reduction was observed in two stages Cu^{2+} to Cu^+ then Cu^+ to Cu^0.

During calcination, copper (II) nitrate trihydrate melts at 387 K and decomposes to copper (II) oxide at 447 K [114]. As cerium oxide was present in the post reaction 5Cu5Ce/silica (Raman and XRD), it was possible that CeO_2 provided a source of oxygen for the formation or stabilisation of copper oxide. The formation of Cu_2O and splitting of the main hydrogen adsorption peak was only observed for catalysts containing CeO_2. The absence of a peak in the 660 K region indicated that the CeO_2 was (partially) reduced at the same time as reduction of the copper species occurred. Hence, the surface oxygen was utilised in the formation or stabilisation of Cu_2O. T_{max} for unsupported CuO was ~580 K and Cu_2O ~750 K [175]. Shifting of the second reduction peak to higher temperature (~530 K) may indicate the presence of copper oxide species. For higher loadings of copper (10Cu5Ce/silica and 0.05Pd10Cu5Ce/silica) the T_{max} value increased again to ~540 K. This may have been due to increased CuO formation at higher copper loadings. Involvement of ceria in the reduction process was confirmed by the results of the Raman spectroscopy. The Raman spectroscopy confirmed that after reduction Cu_2O, CeO_2 and CeO_{2-X} was present on the catalyst. Therefore supporting a mechanism where the oxygen from CeO_2 was able to stabilise a Cu_2O phase during reduction.

The shoulder at ~480 K for the 5Cu5Ce/silica catalyst was due to the reduction or decomposition of cerium nitrate. Cerium nitrate decomposes at 473 K [173] and loses nitrate species. A peak in this region was not observed for the cerium/silica catalysts. The intensity of this peak increased for the 10Cu5Ce/silica and the 0.05Pd10Cu5Ce/silica catalysts. The 5Cu1Ce/silica catalyst did not have a peak in this

area of its TPR profile. The low loadings of cerium would be highly dispersed on the silica support. As the cerium loading increases, cerium oxide could form agglomerates on the surface of the silica. Over copper oxide/ceria/alumina catalysts, preferred nucleation of the copper oxide species on ceria regions was observed [163]. This led to a decrease in formation of $CuAl_2O_4$ spinel and smaller particle size of copper species when compared with copper oxide/alumina catalysts [163]. The increasing intensity of the band at 480 K may be due to increased reduction of the cerium species at this temperature as a result of spill over effects or the formation of Cu-O-Ce species [163].

Both the 10Cu5Ce/silica and the 10Cu5Ce0.05Pd/silica catalysts had very similar TPR profiles to the 5Cu5Ce/silica catalyst. The addition of only 0.05 w/w % of palladium did not affect the reduction of the metals. Both catalysts had broad peaks, the maximum of which was at ~540 K.

The 5Cu1Ce/silica catalyst was different from the other mixed catalysts, in that it did not show the broad shoulder at ~480 K. The T_{max} value was closer to that of the 5% copper/silica catalysts, although the peak remained split. The low loadings of copper and cerium would suggest that the particles should be well dispersed. Copper was more likely associated with the ceria phase than with the silica phase. Hence reduction of both the cerium and copper occurred within one peak. The results of the TPR indicated that the ceria was in close contact with the copper species as reduction of both species was occurring simultaneously (i.e. there was no peak corresponding to the reduction of dispersed CeO_2).

From the XRD, TPR and Raman spectroscopy results, it was clear that several species were present on the reduced CuCe/silica catalysts. The forms of copper and cerium present were copper metal, copper (I) oxide, ceria and a non-stoichiometric CeO_{2-x}. The different types of copper and cerium are represented in figure 3.1.24. Most of the Cu_2O produced would be in close contact with the cerium oxide. However, from the Raman spectra of 5Cu/silica under reduction conditions it was also possible that copper and a small amount of Cu_2O were present on the surface of the copper/silica catalysts.

Figure 3.1.24. Proposed species present on reduced copper and cerium/silica catalysts.

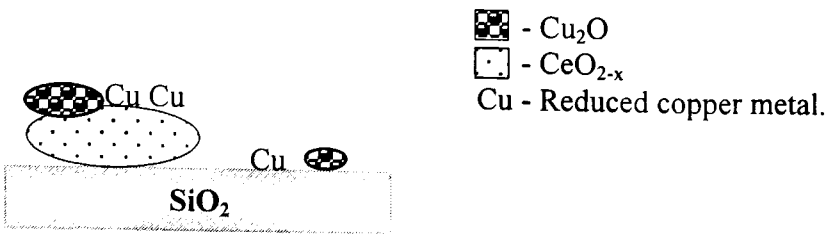

Alumina Catalysts

Crystalline copper nitrate hydroxide was observed from the XRD of the alumina-supported catalysts. Hence, the starting point of the reduction process was slightly different to that of the silica catalysts. The profiles of the catalysts supported on alumina were more complex than their silica counterparts, figure 3.1.25. After treatment in hydrogen up to 873 K, the alumina support was resistant to reduction.

The 5Ce/alumina catalyst produced a broad peak at 655 K, due to the removal of surface capping oxygen from ceria. The T_{max} value was slightly lower than reported in literature (Lit. T_{max} = 770 K [30]). However this might have been due to the enhanced dispersion of the ceria on the alumina support. Improved dispersion, reduced crystallite size and increased surface area are factors which contribute to a decrease in the reduction temperature for ceria [170]. The figure was slightly lower than figure given by Decarne *et al* [170] of between 696 and 727 K depending on the cerium to aluminium ratio of the catalyst. A similar colour change was observed for the cerium/alumina catalyst as for the cerium/silica catalyst. After the TPR and exposure to air the catalyst became paler in colour. The change in colour confirmed that cerium oxide was present and that it was in a partially reduced state (Ce_2O_3) after TPR to 873 K. After exposure to air the XRD pattern (section 3.1.6) confirmed the presence of CeO_2 crystallites.

Figure 3.1.25. TPR profiles of catalysts supported on alumina. (a) 5Cu/alumina, (b) 5Cu5Ce/alumina, (c) 5Ce/alumina and (d) alumina support.

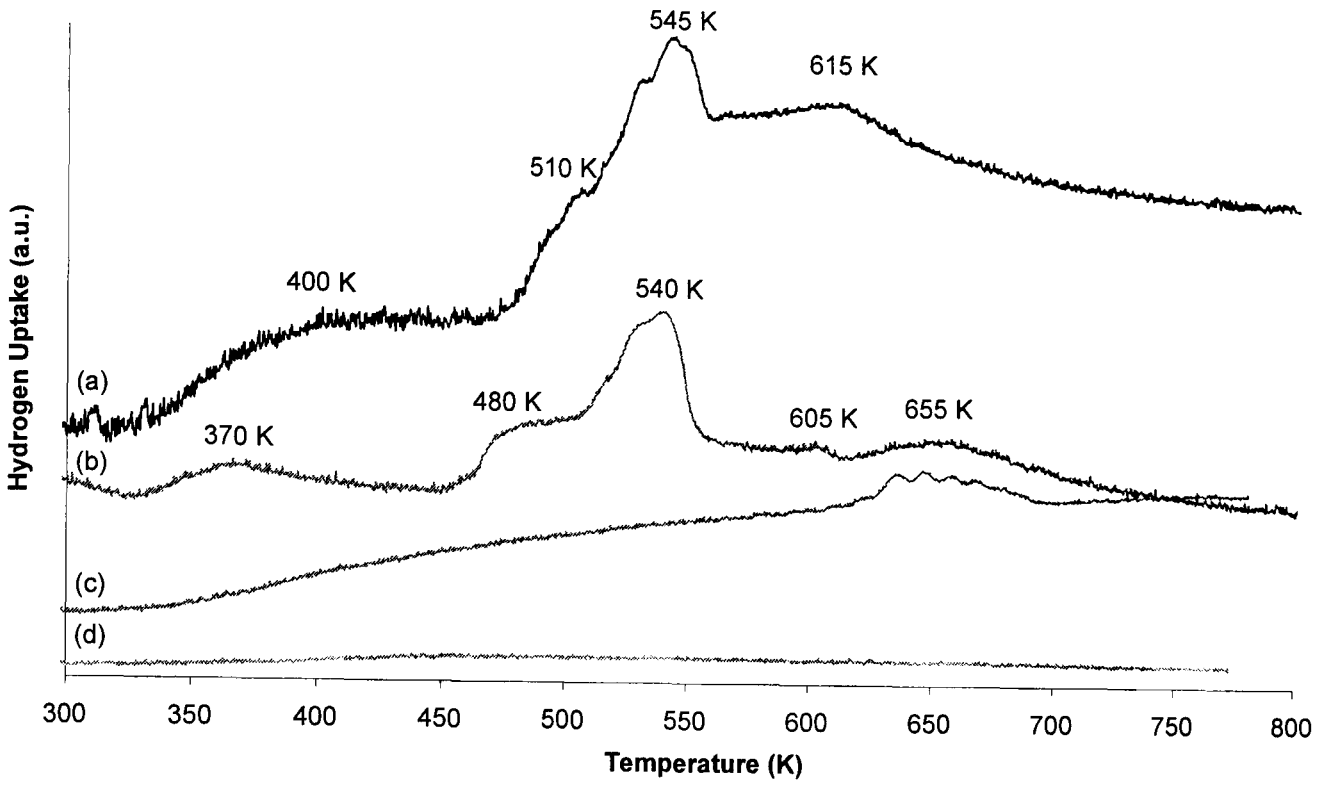

Table 3.1.16. Comparison of reduction profiles – alumina catalysts.

Sample	T_{max} *(K)*
5Cu/alumina	400, 510, 545, 615
5Cu5Ce/alumina	370, 480, 540, 605, 655
5Ce/alumina	~655 (5 peaks)
Alumina (A)	-

The profile for 5Cu/alumina (figure 3.1.25 (a)) had several reduction peaks, indicating that several copper species were present on the catalyst. Repeating the TPR produced a graph with the same number of features in identical positions (figure not shown). When compared with 5Cu/silica the alumina catalyst had two extra peaks. The first broad peak at 350-450 K was possibly due to the removal of surface hydroxyls, as the catalysts were only dried to 333 K prior to reduction. At temperatures below 450 K the reduction peak is unlikely to be as a result of the copper constituent. The higher temperature peak at 615 K was due to the reduction of bulk copper (II) oxide. Copper oxide was not detected by XRD of the post reaction samples. Therefore it must have been present as very small crystallites or an amorphous phase, following the reaction stage.

The main peak for the 5Cu/alumina catalyst was a broad band with several shoulders. On closer examination of the decomposition products observed during the TPR reaction, it was found that NO_x's were produced in one broad peak from ~450 to 600 K with a hydrogen consumption temperature maximum at ~570 K. This may be due to the fact that the first stage of decomposition had been initiated during the drying process. After drying to 333 K, the UV-Vis and XRD results showed that copper (II) nitrate hydroxide was the main copper species on the catalyst. Hence, the broad band is due to the reduction of the copper nitrate hydroxide to copper. The asymmetry of the band and the appearance of shoulders suggested that the interaction of the copper nitrate hydroxide with the alumina varies. It is possible that a copper oxide species is produced during decomposition of the nitrate precursor.

The 5Cu5Ce/alumina catalyst produced similar peaks to the 5Cu/alumina catalyst, figure 3.1.25 and table 3.1.16. The peak at 655 K showed that dispersed ceria was present on the alumina support. This reduction peak had not shifted when compared with the 5Ce/alumina catalyst, suggesting that copper addition did not affect the reducibility of the surface oxygen of cerium oxide on the alumina support. Hence, not all of the ceria was in close contact with the copper species. The copper peaks had shifted and changed intensity when compared with the 5Cu/alumina catalyst. The feature due to bulk copper (II) oxide at 605 K decreased in intensity and reduction temperature. The copper peaks at 480 and 540 K also decreased in temperature, suggesting that there was an increase in dispersion of the copper species. Decarne and co-workers [170] found that low cerium loading on Cu-Ce-Al oxides led to two copper species being identified, small copper clusters and highly dispersed copper oxides [170]. The shoulder at ~480 K was due to the decomposition of cerium nitrate hydrate, as observed for the CuCe/silica catalysts. When following the reduction of the 5Cu5Ce/alumina catalyst, two peaks were observed at 485 and 552 K, probably corresponding to the formation of NO_2 as the nitrate decomposes. Production of NO_x gases was complete by 600 K. The first peak was due to cerium nitrate decomposition and the second due to the decomposition of the copper nitrate hydroxide.

It was concluded that by varying the support, the nature of the active species of the catalyst was altered. The species present were similar to those for the CuCe/silica catalyst, with the addition of dispersed ceria on alumina (see figure 3.1.26).

Figure 3.1.26. Proposed species present on reduced copper and cerium/silica catalysts.

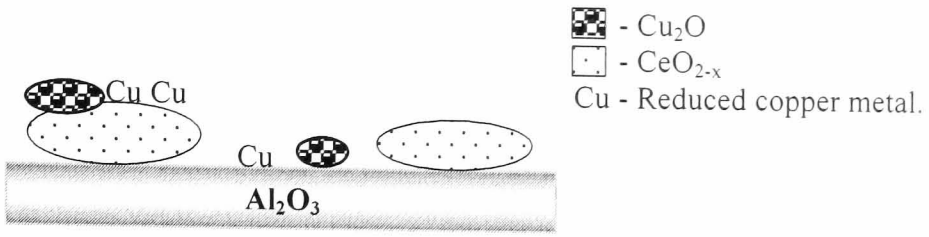

3.1.9 Metal Surface Area Determination

A variety of techniques can be used to determine the free copper surface area and particle size of individual copper crystallites. The techniques include: XRD, TEM, XPS and chemisorption of suitable gases. Chemisorption is a useful technique as it provides a direct assessment of the free metal surface area. Over the past 40 years, a number of adsorbate gases have been investigated for the purposes of copper surface area determination. Although hydrogen [176], carbon monoxide [177], oxygen [178, 179] and N_2O [178, 180-182] have all been investigated, N_2O chemisorption is widely accepted as the most reliable method of copper surface area determination.

Although N_2O chemisorptions were carried out at Johnson Matthey Catalysts, oxygen chemisorptions were used at Glasgow as a further test of the metal surface area. The reactions of oxygen or N_2O with surface copper are temperature dependent reactions. At ideal temperature, the adsorbate gases react with surface copper to form Cu_2O. N_2O chemisorptions are normally carried out in the range of 293 to 363 K, whereas the ideal temperature for oxygen chemisorption is 137 K.

$2Cu_s + ½O_2 \longrightarrow (Cu\text{-}O\text{-}Cu)_s$ **or** $Cu + ½O_2 \longrightarrow CuO$

$2Cu_s + N_2O \longrightarrow (Cu\text{-}O\text{-}Cu)_s + N_2$ Where s denotes surface atoms.

Although only surface oxidation of the copper occurs at room temperature using N_2O, oxidation of bulk and surface material is observed using oxygen chemisorption. This is due to the fact that the surface is readily oxidised by oxygen, which is followed by slow migration of oxygen into the bulk of the material [178].

As table 3.1.17 shows, the metal surface area calculated from the oxygen chemisorption was consistently higher than that for N_2O chemisorptions. The ratio of oxygen surface area to N_2O surface area showed that for copper/support catalysts the ratio was ~1.1 to

1.8 times higher for oxygen chemisorption. Hence, there was some migration of oxygen into the bulk of the copper catalyst. One group which carried out oxygen chemisorptions at 195 K for copper/silica catalysts used a copper: oxygen ratio of 1:1 [179]. They suggested that copper (II) oxide had formed during the chemisorption process as distinct from copper (I) oxide. The copper/support catalysts had oxygen to N_2O surface area ratios of less than two. On combining copper and cerium together on the support, the ratio increased above two. The higher ratios suggested that bulk oxidation increased for the CuCe/support catalysts; however surface oxidation by N_2O decreased.

Table 3.1.17. Results of oxygen and N_2O chemisorptions.

Sample	*O_2 Metal Surface Area (m^2g^{-1})*	*N_2O Metal Surface Area (m^2g^{-1})*	*Ratio O_2/N_2O*	*N_2O*	
				Metal Disperision (%)	*Average Particle Size (nm)*
5Cu/Silica (293 K)	11.7	9.5	1.2	20.0	5.2
5Cu/Silica (WetImpreg)	17.2	15.3	1.1	32.3	3.2
10Cu/Silica (293 K)	24.4	21.9	1.1	23.1	4.5
10Cu/Silica	32.3	20.0	1.6	21.1	4.9
5Ce/Silica	2.5	0.2	12.5	-	-
10Ce/Silica	2.7	0.2	13.5	-	-
5Cu/Silica	20.6	11.3	1.8	23.9	4.4
5Cu5Ce/Silica	17.0	6.9	2.5	14.6	7.1
5Cu/Silica (ac)	13.3	1.9	7.0	4.0	25.9
10Cu5Ce/Silica	23.9	6.9	3.5	7.3	14.3
10Cu5Ce0.05Pd/Silica	36.9	8.0	4.6	16.9	6.2
5Cu1Ce/Silica	15.6	6.0	2.6	12.7	8.2
5Ce/Alumina	0.0	<1.0	-	-	-
5Cu/Alumina	11.4	7.2	1.6	15.2	6.8
5Cu5Ce/Alumina	21.1	8.3	2.5	17.5	6.0
Commercial	43.2	-	-	13.0*	8.0*

* Calculated from O_2 metal surface area.

There are a number of factors, which can affect the adsorption of gases by the reduced copper species. Reduction treatment affects oxygen uptake during N_2O decomposition. Increasing the duration of the reduction results in larger uptake of oxygen during passivation [180]. The reduction process used for the oxygen chemisorptions was

longer than the standard reduction used by Johnson Matthey prior to the N_2O chemisorptions. It was expected that by carrying out the oxygen chemisorption experiment at room temperature that oxidation of surface and bulk copper species would occur, resulting in a much higher adsorption of oxygen form the O_2 compared with N_2O chemisorptions.

The cerium/support catalysts were inactive for N_2O chemisorption. However, the cerium/silica catalysts did adsorb a small amount of oxygen even though the cerium/alumina catalyst did not. Hence, the different supports had varying degrees of interaction with the cerium species. Adsorption of oxygen on a CeO_2/SiO_2 catalyst may be due either to re-oxidation of reduced ceria or formation of superoxide or peroxide species on the catalyst surface. Yao *et al* [33] observed a number of surface oxygen species during oxygen storage on ceria. These included surface peroxide and superoxides. Formation of these species would lead to additional oxygen adsorption by the catalysts. As oxygen mobility is reportedly higher on Al_2O_3 than SiO_2 [183], the opposite trend in oxygen adsorption might have been expected. Superoxide intermediates have been observed on CeO_2, CeO_2/SiO_2 and CeO_2/Al_2O_3 as well as transition metal and ceria containing catalysts [30]. On metal-free samples a reductive pre-treatment was required to induce O_2^- formation. The extent of formation of superoxide or peroxide species is dependent upon the electron donor ability of the surface. Hence the varying interactions between the cerium oxide and support strongly influence the reactivity of the cerium oxide/support catalysts. The silica support appeared to produce a surface upon which the reduction of the cerium oxide was slight and hence able to adsorb oxygen. However TPR results suggested that reduction of the dispersed ceria did not occur until approximately 660 K. It was therefore unlikely that reduction of cerium oxide had occurred under the reduction procedure utilised (up to 523 K).

By combining both cerium and copper on the support, the N_2O surface area decreased. This might have been due to the stabilisation effect of the ceria. As described in section 3.1.8, it is likely that the cerium oxide was able to stabilise the formation of copper (I) oxide. Therefore, full reduction to copper metal would have been more difficult, leading to a lower metal surface area as detected by N_2O. The oxygen surface area did not decrease, indicating that bulk oxidation and formation of copper (II) oxide was still

possible. The increase in oxygen adsorption might also have been due to re-oxidation of the partially reduced cerium oxide, which was detected by *in-situ* Raman spectroscopy (3.1.7.2).

A second possibility was that there might have been encapsulation of the copper species by cerium oxide during reduction. Lamonier *et al* [184] found that after high temperature treatment during catalyst preparation, copper remained partly inserted in the CeO_2 lattice. As a result, this could reduce the free copper surface area. The slight increase in surface area calculated from oxygen chemisorption was due to either re-oxidation of the partially reduced ceria or bulk oxidation of copper. TPR (section 3.1.8) and Raman spectroscopy (section 3.1.7.1) have already shown that the combination of copper and cerium on silica allowed partial reduction of the ceria on the support to occur. Hence either oxidation of the partially reduced cerium oxide or formation of superoxide and/or peroxide surface species may have occurred [30]. This may occur via spillover from oxygen adsorbed onto copper, although from table 3.1.17 it is clear that the 5Ce/silica catalysts adsorbed oxygen in the absence of copper.

An examination was carried out to examine the effect of drying temperature on copper/silica catalysts. Toupance *et al* [118] found that drying catalysts at room temperature improved the metal dispersion when compared with higher temperatures. However, the N_2O chemisorption results revealed that for 5Cu/silica (293 K) and 5Cu/silica (333 K), the catalyst dried at 333 K had the highest dispersion (N_2O and O_2 results). The 10% Cu/silica catalysts showed conflicting results when the drying temperature was varied. N_2O surface area decreased slightly after drying the 10Cu/silica at higher temperature, whereas the O_2 metal surface area was almost 50% higher for the catalyst dried at room temperature (see table 3.1.17). Comparison of the N_2O metal surface area for both catalysts at 293 and 333 K are shown in figure 3.1.27. As no benefits were gained from drying the catalysts at room temperature, the remaining catalysts were dried at 333 K.

Figure 3.1.27. Effect of drying temperature on metal dispersion.

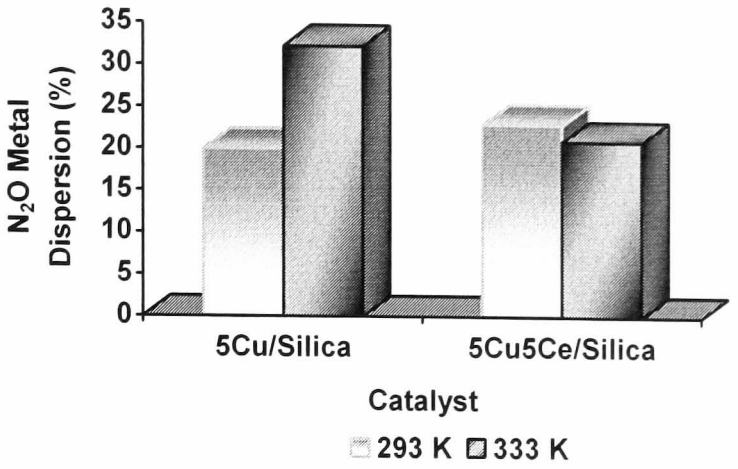

The 5% copper/silica (acetate) catalyst was the only catalyst examined which was not prepared from a nitrate precursor. N_2O surface area was very low when compared with 5% copper/silica (nitrate) catalysts. It was hoped that the acetate precursor would produce highly dispersed copper species. However after reduction, the catalyst formed large particles (~26 nm), which were poorly dispersed (~4 %). The use of the acetate precursor was not pursued further as nitrates produced catalysts with better dispersion of copper species. Nitrate precursors were also more soluble, whereas the acetate precursors were sparingly soluble in water. In addition, direct reduction of the copper acetate/silica catalyst might not have completely removed the carbon species from the catalyst. Similarly to the direct reduction of copper nitrate/support catalysts [114, 172], any remaining carbon residue would have affected the reactivity of the catalyst. Hence to maintain a simple catalyst preparation and remove the possibility of carbon species being deposited on freshly reduced catalysts, nitrate precursors were chosen to prepare the catalysts examined in this study.

Although the commercial catalyst had the lowest copper dispersion, it had the highest value of copper surface area (calculated by O_2 chemisorption). This was due to the high copper loading (~35 w/w %) of the catalyst. Catalysts prepared by co-precipitation (as for the commercial catalyst) usually have low total surface areas, but high metal loadings.

The effect of changing to an alumina support was examined by comparison of the 5Cu/silica and 5Cu5Ce/silica catalysts with the 5Cu/alumina and 5Cu5Ce/alumina catalysts. All of the catalysts were prepared using identical preparation conditions, i.e. spray impregnation followed by drying at 333 K. Figure 3.1.28 shows the values of N_2O metal dispersion for the four catalysts.

Figure 3.1.28. Comparison of N_2O dispersion for copper and cerium/support catalysts.

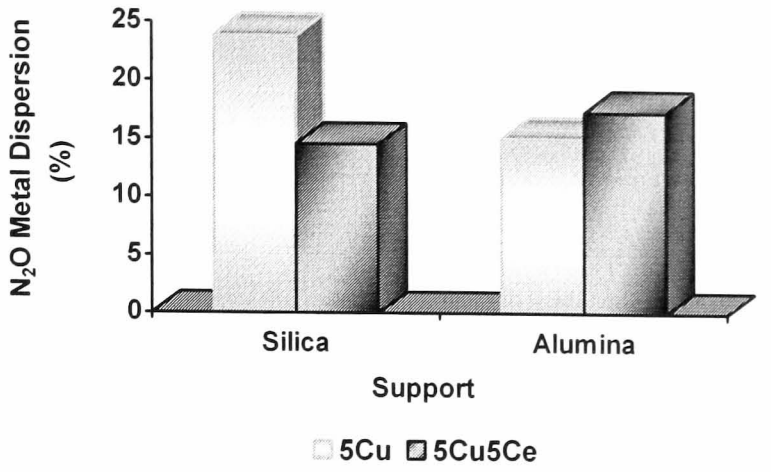

The 5Cu/silica catalyst appeared to have the highest metal dispersion from N_2O chemisorption. Addition of cerium to create the 5Cu5Ce/silica catalyst appeared to have a detrimental effect on the metal dispersion. However this trend was reversed for the alumina supported catalyst. Combining both metals on the alumina support had a slight improvement on the metal dispersion. The oxygen chemisorptions were not in agreement with the N_2O chemisorptions. Both techniques confirmed that the lowest metal surface area was achieved on the 5Cu/alumina catalyst. The oxygen chemisorption showed the metal surface area to increase in the order of 5Cu/alumina < 5Cu5Ce/silica < 5Cu/silica ≤ 5Cu5Ce/alumina. The average particle sizes calculated for the four catalysts were between 4.4 and 7.1 nm. This was in agreement with XRD analysis, which suggested that small crystallites were present (less than ~5 nm).

Average metal particle sizes calculated from the chemisorption values were in agreement with XRD results, many of the particles produced would be close to the lower detection limit for XRD analysis (<5 nm average crystallite size). However the catalysts, which crystallite size could be calculated for (after reduction and air exposure) were in the region of 30 nm. As chemisorption is an *in-situ* technique, it is most likely to provide the more accurate value for copper particle size. XRD particle sizes are often higher than expected due to the fact that XRD does not detect highly dispersed species. Copper surface phase/small copper oxide particles are also below detection limits of the technique. Therefore the estimate of average crystallite size would be much greater than expected. Hence the low values of average particle size indicated that the particles were well dispersed prior to reaction.

3.2 Methanol Decomposition over Copper/Cerium Catalysts

The methanol decomposition reaction was used to examine the reactivity of the catalysts. This enabled the use of pulse flow reactions under mild reaction conditions. As the copper/cerium alloy catalysts produced methanol from carbon monoxide and hydrogen [71-73, 75, 185] it was hoped that similar copper/cerium catalysts would decompose methanol to produce solely carbon monoxide and hydrogen. The production of carbon dioxide during decomposition would suggest that the catalysts followed a different mechanism from that of the alloy catalysts. All of the catalysts prepared, the commercial methanol synthesis catalyst and the palladium/silica catalyst were examined as catalysts for the decomposition of methanol.

There are a number of routes by which methanol can decompose. The main products of methanol decomposition (between 423 and 523 K) are carbon dioxide, carbon monoxide, methyl formate and hydrogen. Additional by-products such as methane, formaldehyde and dimethyl ether are formed during the methanol decomposition reaction.

$CH_3OH \longrightarrow CO + 2H_2$ } Methanol Decomposition

$2CH_3OH \longrightarrow CO_2 + H_2 + C$

$CH_3OH + H_2O \longrightarrow CO_2 + 3H_2$ - Methanol Steam Reforming

$CH_3OH \longrightarrow (CH_3)_2O + H_2O$ - Dimethyl ether

$2CH_3OH \longrightarrow HCO_2CH_3 + 2H_2$ - Methyl formate

$CH_3OH \longrightarrow HCHO + H_2$ - Formaldehyde

$CO + 3H_2 \longrightarrow CH_4 + H_2O$ - Methane

$CO + H_2O \longrightarrow CO_2 + H_2$ - Water-gas shift

$2CO \longrightarrow CO_2 + C$ - Boudouard reaction

The production of dimethyl ether (DME) is normally only observed in the presence of acidic sites of the catalysts. It is prepared industrially by the dehydration of methanol using γ-alumina or another dehydration catalyst [54]. Methyl formate (MF) can form by intermolecular dehydrogenation of methanol and is a possible intermediate of the decomposition process [54]. Although it is readily formed on copper-based catalysts, reaction conditions and catalyst additives can control its yield. Methane is unlikely to be produced in large quantities over copper-based catalysts as copper has poor

methanation ability [47]. In general methane is only observed as a methanol decomposition product when the catalyst contains nickel [186]. The build up of carbon deposits is a possible cause of deactivation of methanol decomposition catalysts [4]. Carbon deposition (or coking) can occur either via the Boudouard reaction or formation of polymeric species on the catalyst surface [4]. A study of copper/silica catalysts for methanol decomposition also reported that carbon species were lost to the catalyst surface during the reaction [187].

3.2.1 Commercial and Palladium/Silica Catalysts

Examining two commercially available catalysts, a commercial methanol synthesis catalyst and a 1% palladium/silica catalyst, tested the validity of using methanol decomposition to investigate the reactivity of the catalysts. Figures 3.2.1 and table 3.2.1 show the results of the methanol decomposition reaction over the commercial catalyst.

Figure 3.2.1. Conversion of methanol and yield of carbon monoxide, carbon dioxide and methyl formate over commercial methanol synthesis catalyst at 473K.

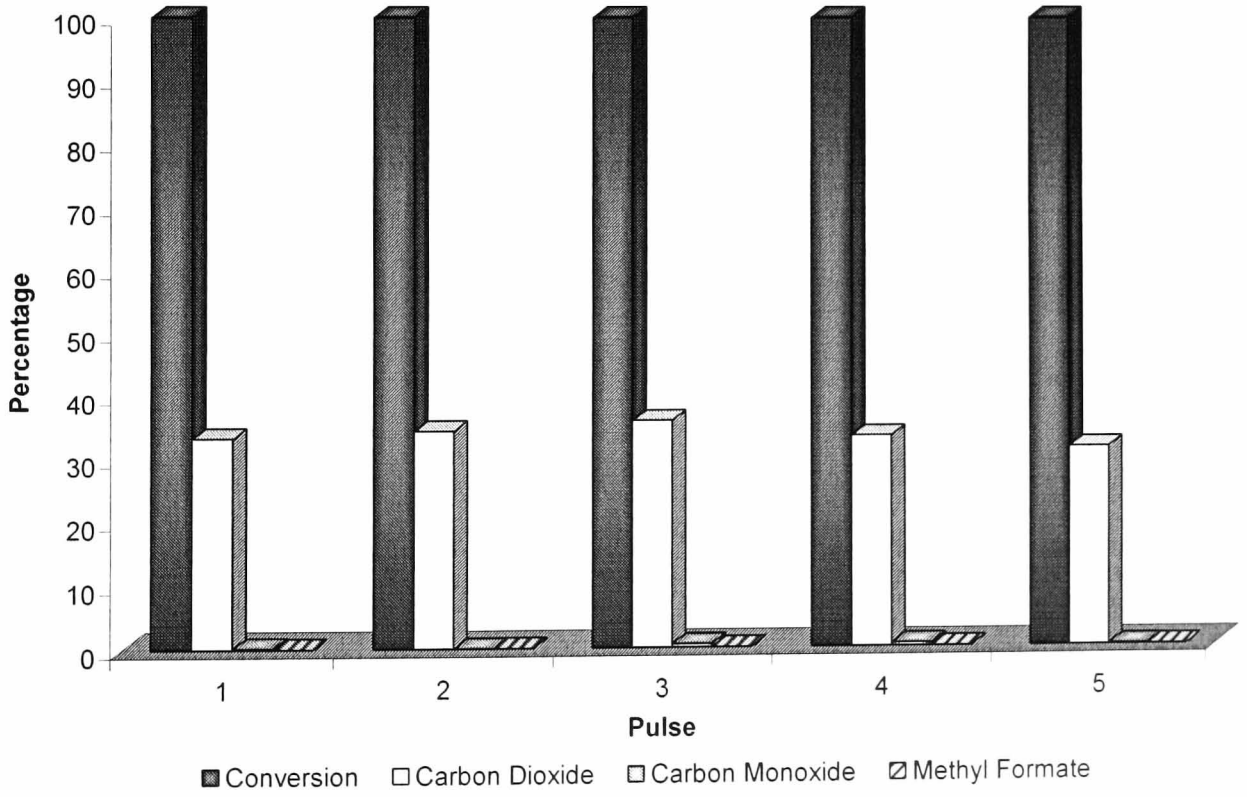

Table 3.2.1. Mass balance and yield of products during methanol decomposition, commercial methanol synthesis catalyst.

Pulse	Mass Balance (%)		Yield of Products (%)			Selectivity (%)
	Carbon	Oxygen	CO_2	CO	MF	$CO_2/(CO+CO_2)$
1	33.4	66.7	33.2	0.2	0.0	99.4
2	34.4	68.7	34.3	0.0	0.0	99.9
3	36.4	72.3	35.9	0.6	0.0	98.5
4	33.7	67.0	33.3	0.5	0.0	98.7
5	31.6	63.0	31.4	0.1	0.0	99.6

As expected, the commercial catalyst produced mainly carbon dioxide. This was in agreement with results from the methanol synthesis reaction, which produces methanol predominantly from carbon dioxide [2, 46]. No methyl formate and only a small quantity of carbon monoxide were produced during the decomposition reaction. The yield of carbon-containing products was much lower than the percentage conversion of methanol. This showed that carbon species were adsorbed on to the surface of the catalyst. Conventional methanol synthesis catalysts were examined, but were among some of the least successful decomposition catalysts tested [188]. The deactivation of the commercial catalyst was due mainly to thermal sintering in the methanol synthesis process [4]. However, in the methanol decomposition and steam reforming reactions poisoning and coking of the catalyst were observed [4]. Although the main products were CO and H_2, side-products such as methyl formate, methane, formaldehyde, dimethyl ether, carbon dioxide and water were formed. The catalysts were rapidly deactivated, due to the formation of carbonaceous deposits [188].

Choi and Stenger [189] reported deactivation over a commercial copper/zinc oxide/alumina catalyst during methanol decomposition. Deactivation was faster during methanol decomposition than the methanol reforming reaction at temperatures between 523 and 573 K. They found that Cu^{2+} favoured methanol decomposition and that deactivation was as a result of the state of copper changing form Cu^{2+} to Cu^{0} [189]. Contrary to this, Cheng *et al* [188] found no evidence for the presence of Cu^{2+} and attributed the activity of copper-containing catalysts to metallic copper or Cu^{+}. The group suggested that loss of activity of Cu/ZnO catalysts was due to reduction of the ZnO phase, allowing dissolution of Zn into the copper phase under methanol decomposition conditions. They revealed that improved activity of copper-containing catalysts for methanol decomposition was observed in the absence of ZnO [188].

Both groups were in agreement that the presence of water improved the activity and stability of the catalysts in the methanol decomposition process [188, 189]. The presence of water may have decreased the reduction of the ZnO support. Although conversion of methanol was low, the product composition was in agreement with literature, as the catalyst was more than 98% selective towards carbon dioxide (table 3.2.1). The higher oxygen than carbon mass balance indicated that either reduction of ZnO support or deposition of oxygen deficient species on the catalyst surface was occurring, table 3.2.1. In addition, it is possible that unreduced copper may also have been a source of excess oxygen.

Although zinc oxide is an important component of synthesis catalysts, it was found to have a detrimental effect within decomposition catalysts [188]. Hence, catalysts were developed using promoters such as Si, Ba, or Mn oxides to increase the stability of the catalysts in the absence of ZnO [188]. Once stable catalysts were developed, group I elements (Li, Na or K) were also added. They were an improvement on the previous catalysts as the dispersion of the active copper increased, hence increasing catalytic activity [190]. However, addition of cerium to copper/zinc oxide catalysts was found to have a detrimental effect on catalytic activity [47]. Addition of carbon dioxide to the methanol feed reduced the deactivation observed over Cu/ZnO catalysts [191]. The enhanced stability of the catalyst was due to carbon dioxide providing a source of surface oxygen. This reduced the formation of coke deposits on the catalyst and reduced the sintering of the copper species, without changing the product distribution of the reaction.

Methanol decomposition mechanisms by Rozovskii and Lin [54] suggested that carbon dioxide could only form in the presence of water, i.e. via the reverse water gas shift reaction or steam reforming of methanol. Carbon dioxide was not expected to be the main product of methanol decomposition, however this would be the product expected from the theory of microreversibility. The high selectivity of the commercial catalyst towards carbon dioxide in the absence of water suggested that the study of the reverse reaction would provide information as to the suitability of the catalysts for the forward reaction.

Contrary to the commercial synthesis catalyst, the palladium/silica catalyst produced predominantly carbon monoxide from the decomposition of methanol, fig. 3.2.2. The selectivity towards carbon dioxide was low, less than 17 % (c.f. approx. 98% selectivity of the commercial catalyst). This was in agreement with literature that reported carbon monoxide and hydrogen to be the main products of methanol decomposition across palladium based catalysts [192]. In particular, palladium/silica catalysts did not produce carbon dioxide or methane while the reaction temperature was varied from 423 to 723 K [192]. This was attributed to the inability of the catalyst to activate carbon monoxide to form methane via C-O bond rupture. The results were supported by the methanol synthesis process, which produced methanol solely from carbon monoxide and hydrogen using palladium/support catalysts [76, 77]. Therefore, the results supported the theory that the reverse reaction can be used to examine the reactivity of the forward methanol synthesis reaction.

Figure 3.2.2. Conversion of methanol and yield of carbon monoxide, carbon dioxide and methyl formate over 1% Pd/Silica at 473K.

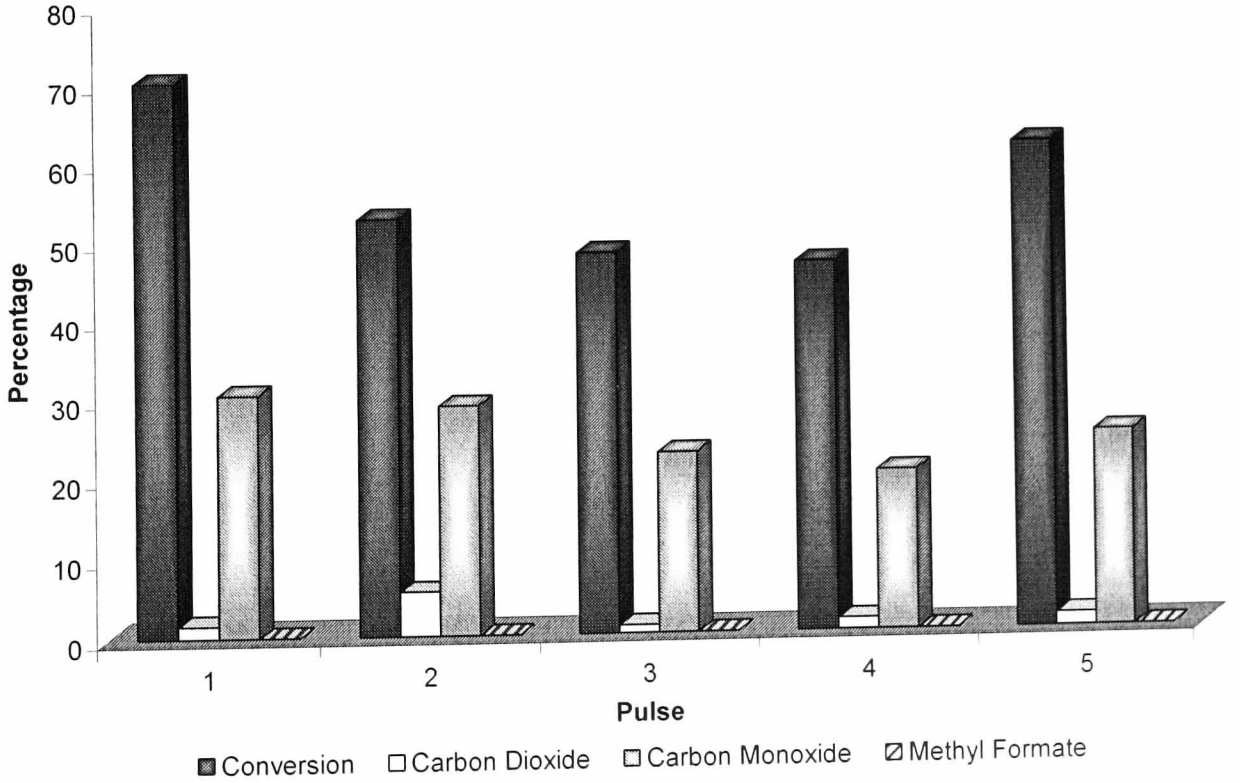

The values of methanol conversion for the reaction were approximately 50-70%. This was similar to a literature report which suggested that the maximum conversion of methanol to products was observed at a temperature of ~673 K for palladium/silica catalysts [192]. The mass balance for the reaction pulses is shown in table 3.2.2. Unlike the values for the commercial catalyst, the oxygen and carbon mass balance for

the methanol pulses were similar. The values showed that the palladium/silica catalyst retained less carbon and oxygen species than the commercial catalyst. The second pulse produced more carbon and oxygen species than was present in the reactants. This may either have been due to removal of carbon and oxygen deposition in the first pulse, or due to an accumulation of errors in the analysis method.

Table 3.2.2. Mass balance and yield of products during methanol decomposition, commercial palladium/silica catalyst.

Pulse	*Mass Balance (%)*		*Yield of Products (%)*			*Selectivity (%)*
	Carbon	*Oxygen*	*CO_2*	*CO*	*MF*	*$CO_2/(CO+CO_2)$*
1	81.5	83.6	1.6	30.4	0.0	4.9
2	104.9	112.0	5.6	28.8	0.0	16.2
3	94.4	95.6	1.0	22.6	0.0	4.2
4	91.0	92.7	1.4	20.0	0.0	6.6
5	76.1	78.0	1.6	24.6	0.0	6.1

Recent studies have proposed the following mechanism for the decomposition of methanol to form carbon monoxide over palladium catalysts [79, 193]:

$$CH_3OH + 2Pd \rightleftharpoons CH_3O\text{-}Pd + H\text{-}Pd$$

$$CH_3O\text{-}Pd + H\text{-}Pd \longrightarrow CH_2O\text{-}Pd + H_2$$

$$CH_2O\text{-}Pd + 2Pd \rightleftharpoons CO\text{-}Pd + 2H\text{-}Pd$$

$$2H\text{-}Pd \rightleftharpoons H_2 + 2Pd$$

$$CO\text{-}Pd \rightleftharpoons CO + Pd$$

The initial step is the formation of adsorbed methoxy groups onto palladium. This is followed by decomposition to formaldehyde, which then decomposes further to form carbon monoxide and hydrogen. The final steps are desorption of the products from the surface. As the Pd/silica catalyst in this study produced mainly carbon monoxide, it is likely that a similar mechanism occurred.

Methanol decomposition was then used to examine the reactivity of the copper and cerium catalysts.

3.2.2 Copper/Support Catalysts

All of the silica and alumina-supported catalysts prepared in this study were examined as methanol decomposition catalysts. A number of variables were changed to determine the effect of different preparation conditions and different metal composition of the catalysts. Cheng and co-workers [188] showed that the predominant products observed during methanol decomposition using copper-containing catalysts were hydrogen and carbon monoxide, with methyl formate produced at low methanol conversions. Formation of mainly carbon monoxide and hydrogen over copper/silica catalysts was supported by pulse studies carried out by Jackson *et al* [187]. However, Bell and co-workers [194] found carbon dioxide and hydrogen to be the major products during methanol.TPD studies.

Three 5% copper/silica catalysts, which were prepared using slightly different techniques, were tested. The first two catalysts were prepared by wet impregnation and then dried at 293 or 333 K, and the third was prepared using spray impregnation and dried at 333 K. Although spectroscopic analysis was similar for the three catalysts, oxygen and N_2O chemisorption showed differences between the catalysts. Both chemisorption methods showed that the catalyst dried at room temperature had the lowest copper surface area. The catalyst with the highest surface area depended on the method used to analyse the catalyst. For N_2O chemisorption the catalyst prepared by wet impregnation of the metal salt and drying at 333 K had the highest copper surface area. Although the species identified on the catalysts were similar, the preparation technique had clearly affected the dispersion of the active species. Hence, it was not unexpected when the 5% copper/silica catalysts did not behave identically. Figures 3.2.3 to 3.2.5 show that conversion of methanol was 100% over each catalyst, however the product distribution varied slightly. As expected a mixture of carbon monoxide, carbon dioxide and methyl formate was produced during the reaction. Although observed by mass spectrometry, the hydrogen produced was not quantified during the decomposition reactions.

Figure 3.2.3 and table 3.2.4 show that the first methanol pulse over 5Cu/silica (293K) produced mainly methyl formate. However, the yield decreased on subsequent pulses and remained steady at approximately 13% yield. After the first pulse, the main product was carbon monoxide, followed by methyl formate then carbon dioxide. The selectivity

towards carbon dioxide varied between 28 and 42 % across the pulses, i.e. carbon monoxide was the favoured product. During the reaction, the mass balance revealed that carbon species were retained by the catalyst surface. The oxygen mass balance was slightly higher than the carbon value for all of the pulses examined. This indicated either that an oxygen deficient species was adsorbed onto the surface or that there was removal of oxygen from the catalyst surface.

Figure 3.2.3. Conversion of methanol and yield of carbon monoxide, carbon dioxide and methyl formate over 5% Cu/Silica (293 K), reaction at 473K.

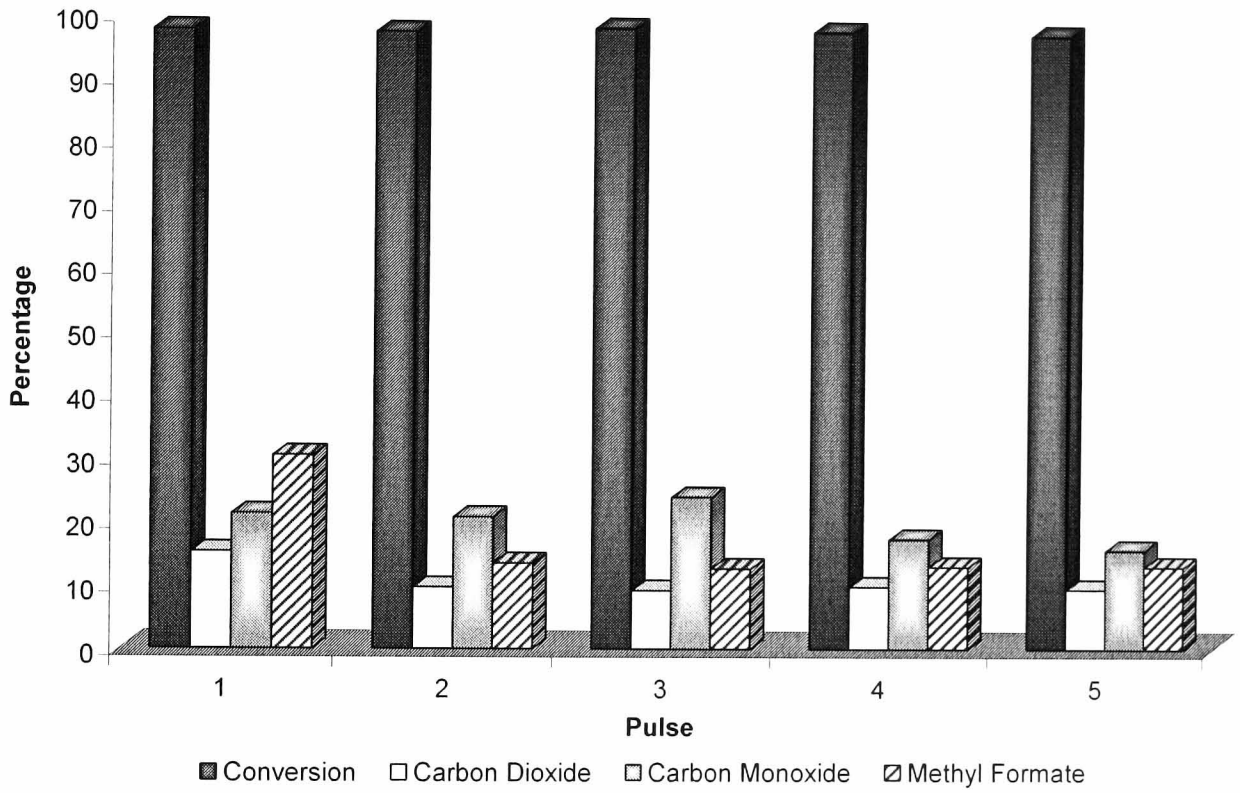

Table 3.2.3. Mass balance and yield of products during methanol decomposition, 5% Cu/Silica (293 K).

Pulse	*Mass Balance (%)*		*Yield of Products (%)*			*Selectivity (%)*
	Carbon	*Oxygen*	CO_2	*CO*	*MF*	$CO_2/(CO+CO_2)$
1	100.0	115.2	15.3	21.4	30.6	41.7
2	60.1	69.8	9.8	20.9	13.6	31.9
3	60.3	69.6	9.3	24.1	12.8	27.8
4	55.3	65.2	9.9	17.6	13.1	36.1
5	53.5	63.0	9.6	15.8	13.2	37.6

Adsorbed oxygen species on the catalyst surface was thought to play a major role in the methanol synthesis process using commercial Cu/ZnO based catalysts [195]. Although oxygen coverage was observed on Cu/silica catalysts, it was to a lesser extent. It was possible that the increased oxygen mass balance was due to either the species deposited

on the catalyst surface or removal of surface oxygen. As *'in-situ'* Raman studies (section 3.1.7.2) detected Cu_2O on the surface of a reduced 5% copper/silica catalyst it is likely that the partially reduced Cu_2O behaved as a source of excess oxygen.

By using the same preparation technique but changing the drying temperature a slight difference was observed in the product ratios (figure 3.2.4 and table 3.2.4). This was due to the improved dispersion observed on drying the catalyst at a higher temperature. Although there was little change in the production of carbon dioxide, carbon monoxide formation increased and methyl formate yield decreased on changing the drying temperature of the catalyst. In addition, there was a decrease in selectivity towards carbon dioxide.

Retention of carbon species decreased on improving the copper dispersion of the catalyst from 9.5 % for 5Cu/silica (293 K) to 15.3 % 5Cu/silica (Wet Impreg.) as determined by N_2O chemisorption in section 3.1.9. The improvement in metal surface area was attributed to the increase in catalyst drying temperature. When compared with the similarly prepared 5Cu/silica (293 K), the oxygen mass balance for both catalysts was higher than the carbon mass balance, indicating that carbon species were retained by the catalyst surface during reaction. Eventually this adsorption of carbon species may lead to deactivation of the catalyst, however the five pulses examined did not detect a decrease in conversion. Prolonged testing would be required to investigate any effects of carbon deposition.

Table 3.2.4. Mass balance and yield of products during methanol decomposition, 5% Cu/Silica (Wet impregnation and dried at 333 K).

Pulse	*Mass Balance (%)*		*Yield of Products (%)*			*Selectivity (%)*
	Carbon	*Oxygen*	*CO_2*	*CO*	*MF*	*$CO_2/(CO+CO_2)$*
1	68.7	81.6	12.9	25.6	14.5	33.5
2	49.5	61.0	11.6	32.5	2.2	26.3
3	61.1	72.8	11.7	36.5	5.8	24.3
4	63.4	75.4	12.0	28.9	10.7	29.3
5	60.7	71.7	11.0	30.7	9.0	26.3

Figure 3.2.4. Conversion of methanol and yield of carbon monoxide, carbon dioxide and methyl formate over 5% Cu/Silica (WetImpreg), reaction at 473K.

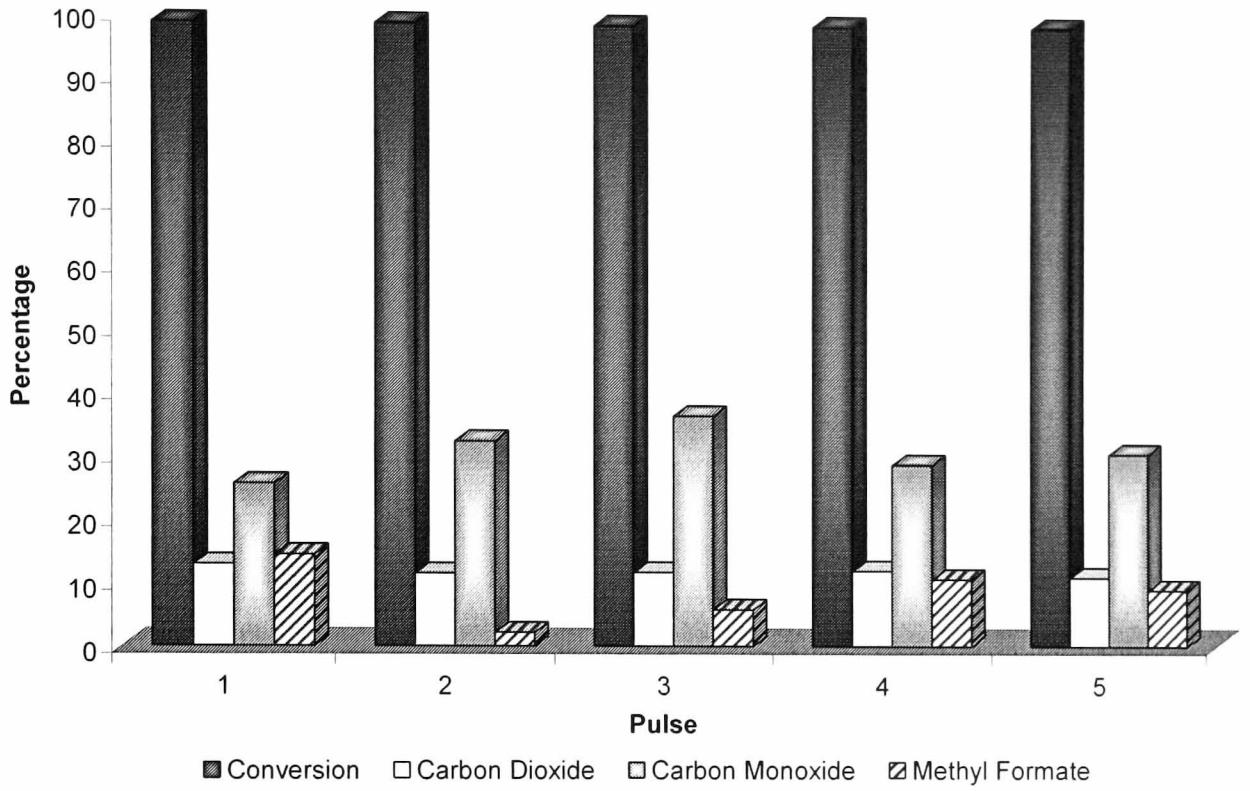

The final variable changed for the 5% copper catalyst was the preparation method. The catalyst was prepared by spray impregnation and then dried at 333 K. It was hoped that this technique would improve the dispersion of the active copper species. However, N_2O chemisorption (section 3.1.9) suggested that dispersion was slightly less than for the catalyst prepared by wet impregnation and dried at the same temperature.

Figure 3.2.5 and table 3.2.5 revealed that initially the reactivity was similar to the previously examined 5% copper/silica catalyst. However, during the course of the reaction, the yield of carbon monoxide increased while the other products remained at steady values. Hence, the selectivity towards the formation of carbon monoxide decreased. The values of carbon monoxide selectivity were similar to those of the catalysts prepared by wet impregnation (5Cu/silica (293 K) and 5Cu/silica (WetImpreg)).

Figure 3.2.5. Conversion of methanol and yield of carbon monoxide, carbon dioxide and methyl formate over 5% Cu/Silica (Spray Impreg), reaction at 473K.

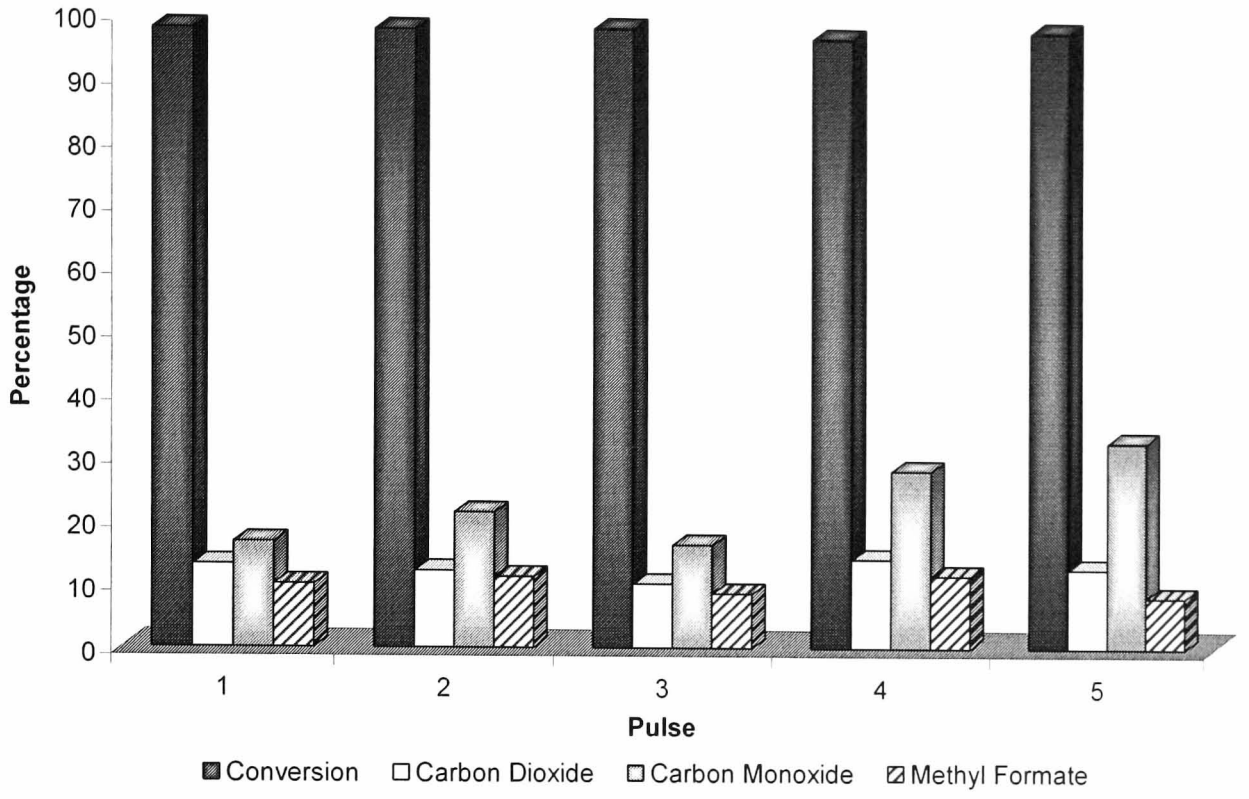

Table 3.2.5. Mass balance and yield of products during methanol decomposition, 5% Cu/Silica (Spray impregnation, 333 K).

Pulse	*Mass Balance (%)*		*Yield of Products (%)*			*Selectivity (%)*
	Carbon	*Oxygen*	CO_2	*CO*	*MF*	$CO_2/(CO+CO_2)$
1	51.9	65.0	13.1	16.7	10.0	43.9
2	58.0	70.2	12.2	21.5	11.2	36.2
3	45.3	55.5	10.2	16.4	8.7	38.3
4	68.1	82.2	14.1	28.3	11.5	33.3
5	63.1	75.8	12.6	33.0	8.2	27.6

On comparing the three 5% copper/silica catalysts there were only slight variations in the yield and selectivity during methanol decomposition. As TPR (section 3.1.8) and Raman spectroscopy (section 3.1.7.1) indicated that the 5% copper/silica catalysts contained similar active species, the differences in reactivity might have been due to the differences in dispersion of the active species.

Two catalysts with 10% copper loading were examined for the decomposition process. Catalyst preparation was identical with the exception of the drying temperature; either 293 or 333 K was used. The increase in copper metal loading led to an increase in the carbon mass balance of the catalysts. Both catalysts had conversions of approximately

100% and produced predominantly carbon monoxide, as did the 5% copper catalysts (figures 3.2.6 and 3.2.7). The increase in copper loading from 5 to 10 % shifted the product selectivity in favour of carbon monoxide formation. Table 3.2.6 and 3.2.7 show that selectivity towards carbon monoxide increased with increasing pulse number. This might have been due to a reduction in the availability of excess surface oxygen.

Figure 3.2.6. Conversion of methanol and yield of carbon monoxide, carbon dioxide and methyl formate over 10% Cu/Silica (293 K), reaction at 473K.

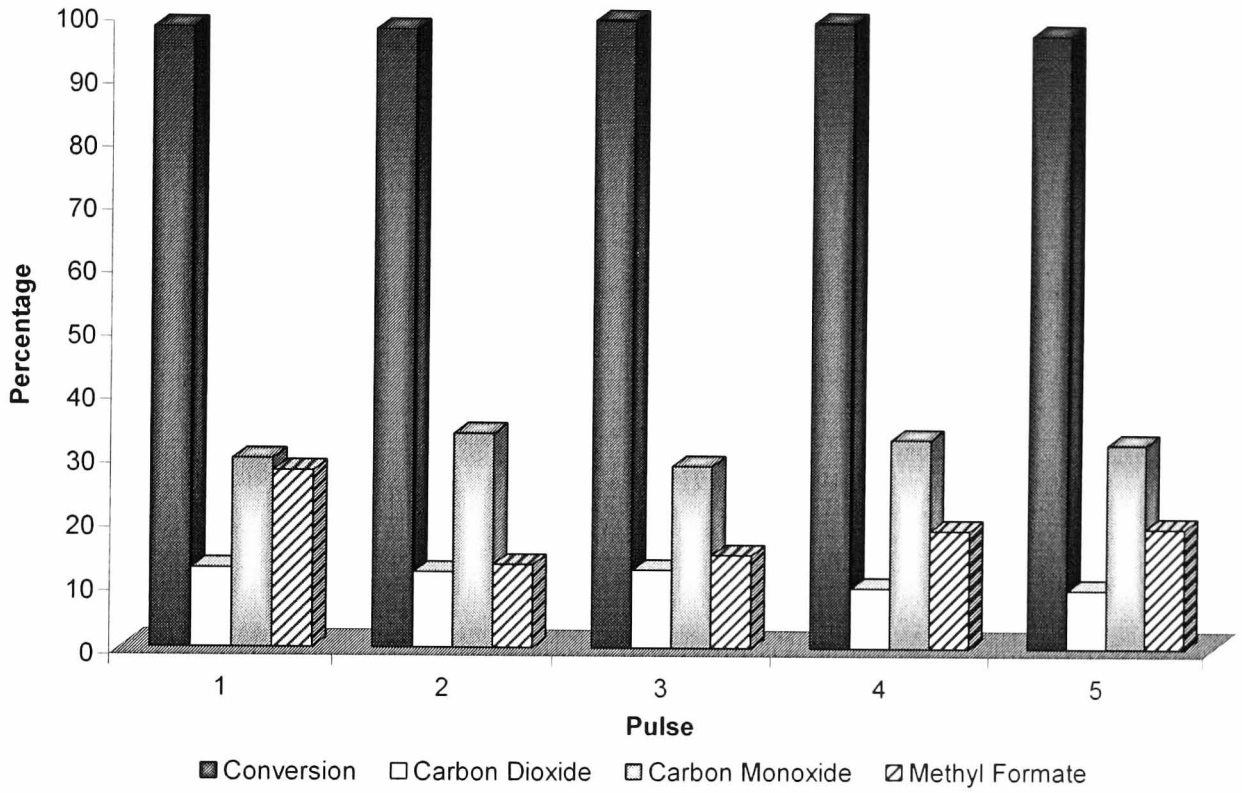

Table 3.2.6. Mass balance and yield of products during methanol decomposition, 10% Cu/Silica (Wet impregnation, 293 K).

Pulse	*Mass Balance (%)*		*Yield of Products (%)*			*Selectivity (%)*
	Carbon	*Oxygen*	CO_2	*CO*	*MF*	$CO_2/(CO+CO_2)$
1	100.0	112.6	12.6	29.7	27.9	29.7
2	74.1	86.0	12.0	33.8	13.2	26.2
3	71.1	83.5	12.4	28.8	14.8	30.1
4	80.6	90.3	9.6	33.1	18.8	22.5
5	82.2	91.7	9.4	32.6	19.2	22.4

Increasing the drying temperature to 333 K greatly increased the yield of both carbon dioxide and carbon monoxide while reducing the methyl formate yield by a factor of ~10, figure 3.2.7 and table 3.2.7. The increase in drying temperature resulted in an increase in both carbon and oxygen mass balances. Almost all of the carbon species

were recovered across the pulses, however an excess of oxygen species was detected (table 3.2.7). As more oxygen was present in the products than the reactants the excess oxygen was from the catalyst surface.

Figure 3.2.7. Conversion of methanol and yield of carbon monoxide, carbon dioxide and methyl formate over 10% Cu/Silica (333 K), reaction at 473K.

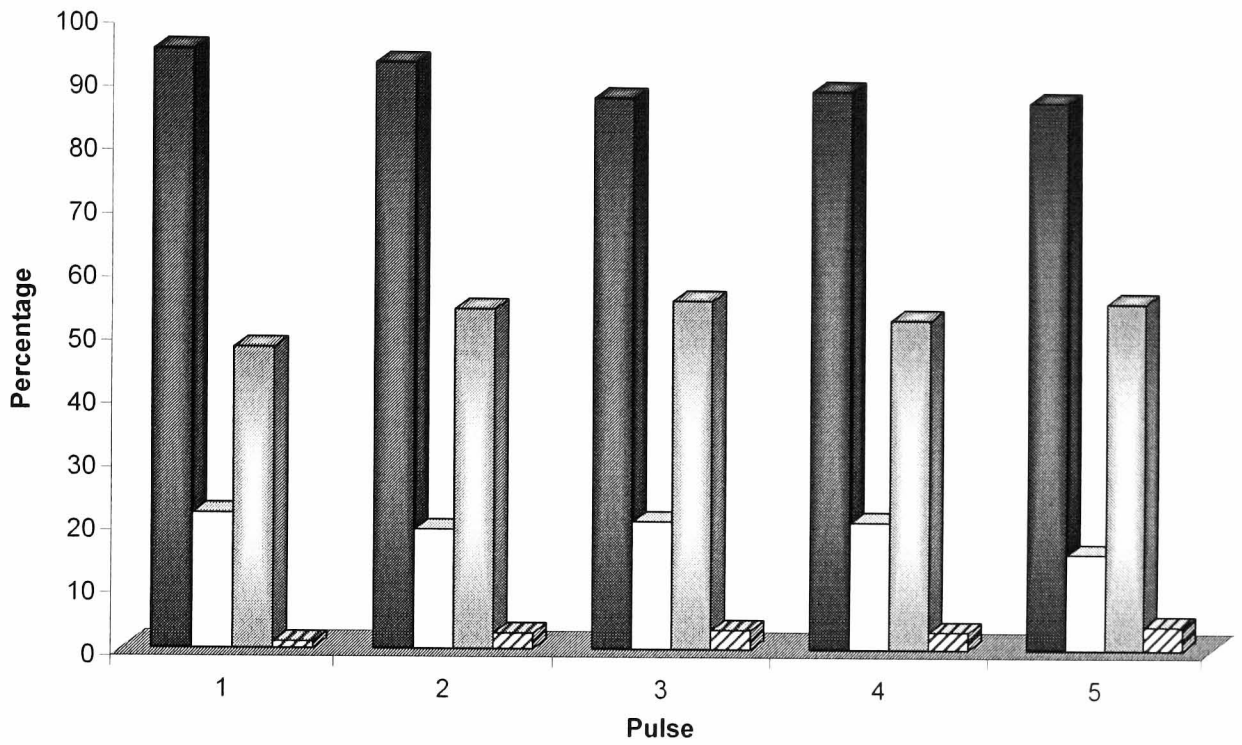

Table 3.2.7. Mass balance and yield of products during methanol decomposition, 10% Cu/Silica (Wet impregnation, 333 K).

Pulse	*Mass Balance (%)*		*Yield of Products (%)*			*Selectivity (%)*
	Carbon	*Oxygen*	CO_2	*CO*	*MF*	$CO_2/(CO+CO_2)$
1	76.8	98.4	21.6	47.9	1.1	31.1
2	85.2	104.3	19.1	54.2	2.5	26.1
3	94.5	115.0	20.5	55.8	3.1	26.9
4	89.8	110.3	20.5	53.0	2.8	27.9
5	91.1	106.6	15.5	55.9	3.8	21.7

Both the 5 and 10% loaded catalysts showed a decrease in the formation of methyl formate after drying at 333 K as opposed to 293 K. This effect was more pronounced for the 10% copper catalysts. From N_2O and oxygen chemisorptions, the 10% copper catalysts had a higher copper surface area than the 5% copper/silica catalysts (section 3.1.9). In particular, the 10% loaded catalyst dried at 333 K had the highest metal surface area. Therefore, there appeared to be a link between product selectivity and

copper metal surface area within this group of catalysts. Higher metal surface area led to reduced methyl formate yield and increased yield of carbon monoxide.

Fisher and Bell examined the mechanism of methanol decomposition over copper/support catalysts [196]. They found that decomposition occurred via an adsorbed methyl formate intermediate on copper/silica catalysts, fig. 3.2.8.

Figure 3.2.8. Mechanism for methanol decomposition over copper/silica catalysts as proposed by Fisher and Bell [196].

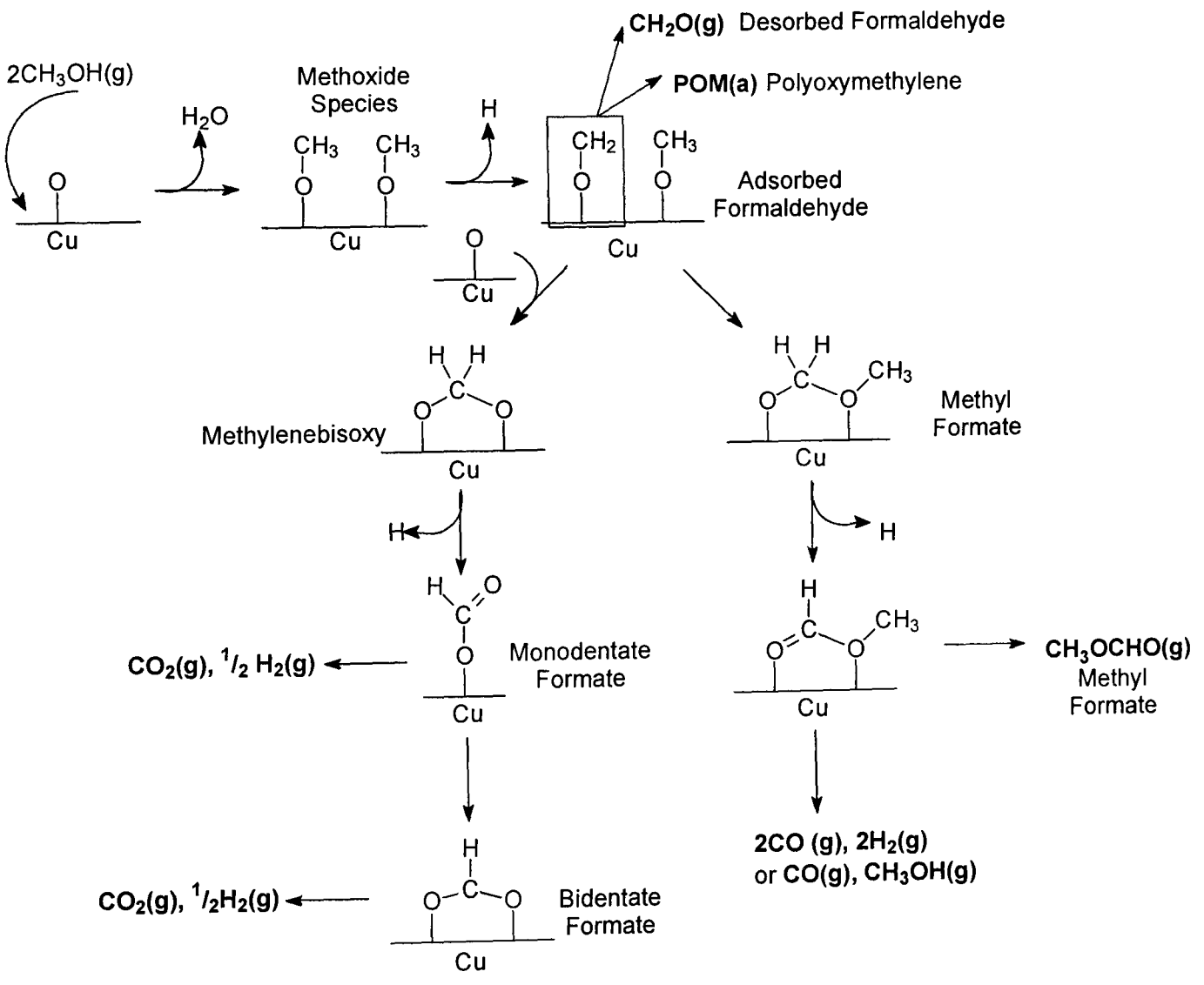

The reactions carried out show that the main route for methanol decomposition over silica catalyst was the formation of adsorbed methyl formate species rather than the methylenebisoxy route [196]. Hence, the formation of methyl formate and carbon monoxide was favoured. It is possible that the methyl formate was fully decomposed to carbon monoxide and hydrogen over the higher surface area catalyst.

The formation of carbon dioxide requires either the presence of an excess of copper oxide species as shown in fig. 3.2.8 to form methylenebisoxy species or one of the following reactions to occur:

(1) $2CH_3OH \longrightarrow CO_2 + 8H_2 + C$

(2) $CH_3OH + H_2O \longrightarrow CO_2 + 3H_2$

(3) $CO + H_2O \longrightarrow CO_2 + H_2$

Reaction (1) is the decomposition of methanol, which produces carbon species. The carbon and oxygen mass balance would support this reaction, where more of the oxygen species was recovered than the carbon species. Reaction (2) would require the presence of water in the system. Although unlikely that water remained on the catalyst surface after reduction to 523 K, water could be formed by the reverse water gas shift reaction (3). The third reaction is the water gas shift reaction, which could also have formed carbon dioxide in the presence of water. Peña *et al* [197] suggested that carbon dioxide was most likely formed from the water-gas shift, Boudouard or the steam reforming of methanol during the decomposition reaction. However, this route was not likely in the current methanol decomposition study due to the absence of water as a reactant.

Copper/Alumina

A second support was used to determine the differences in catalytic activity on switching from silica to alumina support. It was expected that dimethyl ether might be observed due to acidic sites of the alumina support. However, as figure 3.2.9 and table 3.2.8 show, the sole product of methanol decomposition was carbon dioxide. Unlike 5Cu/silica (Spray), an excess of oxygen was removed from the 5Cu/alumina surface. This highlighted the importance of the support as it had a strong effect on the reactivity of the catalyst.

Figure 3.2.9. Conversion of methanol and yield of carbon monoxide, carbon dioxide and methyl formate over 5Cu/Alumina at 473K.

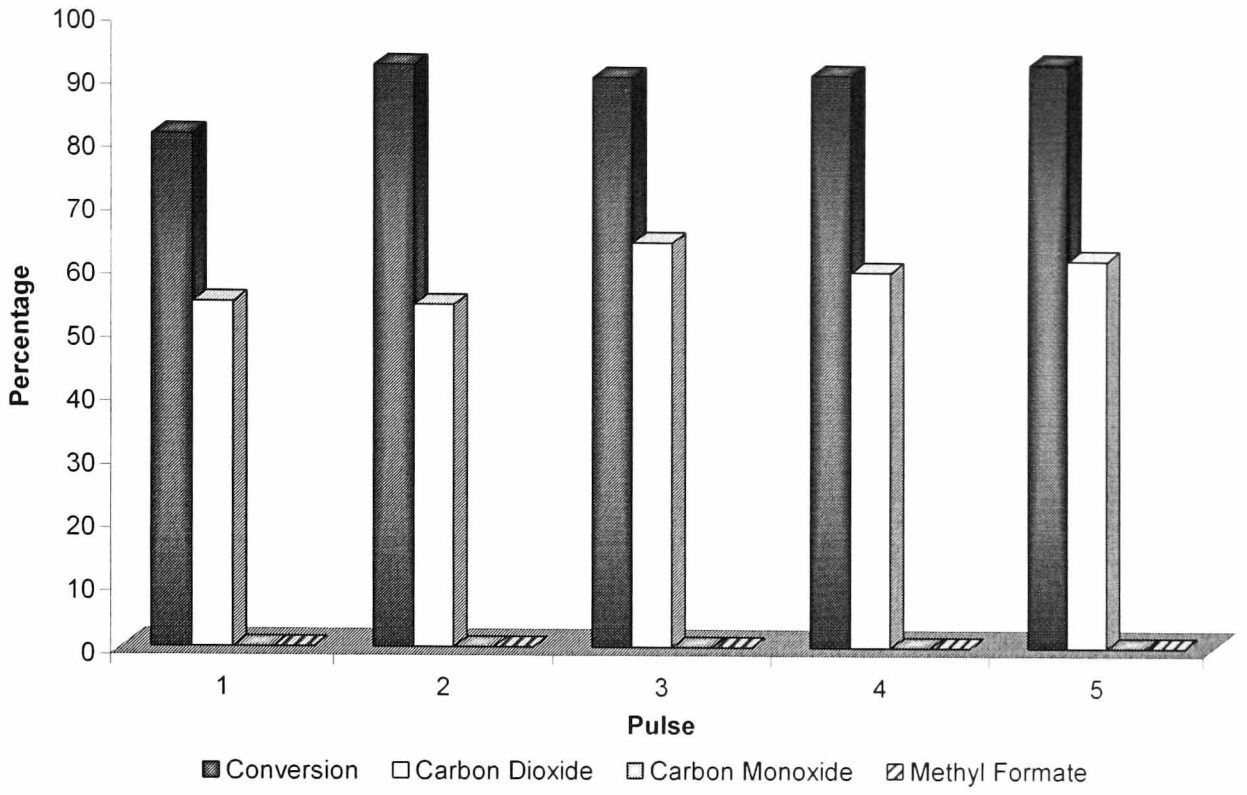

Table 3.2.8. Mass balance and yield of products during methanol decomposition, 5Cu/Alumina.

Pulse	*Mass Balance (%)*		*Yield of Products (%)*			*Selectivity (%)*
	Carbon	*Oxygen*	CO_2	*CO*	*MF*	$CO_2/(CO+CO_2)$
1	73.5	128.2	54.7	0.0	0.0	100.0
2	62.0	116.4	54.5	0.0	0.0	100.0
3	73.8	138.3	64.5	0.0	0.0	100.0
4	68.6	128.8	60.1	0.0	0.0	100.0
5	68.7	131.0	62.3	0.0	0.0	100.0

Due to the acidic sites present on an alumina support the formation of dimethyl ether (DME) was a viable methanol decomposition route. Methanol can be dehydrated over acidic sites to produce DME in large quantities over Cu/alumina catalysts, as reported by Robinson and Mol [198]. However, DME was not detected during the reaction with methanol.

A change in decomposition products to form only carbon dioxide, highlighted that a different decomposition mechanism was followed, compared with the products of the copper/silica reaction. It was probable that the copper/alumina reaction followed a mechanism similar to that on the left hand side of figure 3.2.8. Hence the reaction followed a route, which utilised excess surface oxygen and resulted in the formation of

carbon dioxide and hydrogen. Unfortunately, literature for the decomposition of methanol over alumina catalysts was not available. However, data for the methanol synthesis reaction using copper/alumina showed that methanol could be produced from carbon dioxide and hydrogen [167] or carbon monoxide and hydrogen [198]. Gotti and Prins [199] reported that copper/alumina catalysts were almost three times more active than copper/silica catalysts for methanol synthesis. However, the high activity was partly attributed to the promotion of the reverse water gas shift reaction by the copper/alumina catalyst [199].

The commercial catalyst showed a similarly high selectivity towards the formation of carbon dioxide. Both catalysts contained copper and alumina, hence the similarities in decomposition products were expected. The results suggested that the copper/alumina and commercial catalysts follow a similar mechanism to decompose methanol.

A methanol TPD study of CuO/Al_2O_3 catalysts showed that methanol dehydrogenated to form carbon monoxide and hydrogen, and that carbon dioxide and water formed as a result of oxidation by lattice oxygen of CuO [200]. In addition, they did not detect the formation of DME. At lower concentrations of methanol coverage carbon dioxide and water were favoured due to the increased availability of lattice oxygen [200]. The group detected a greater oxygen/carbon ratio in the products than reactants and this was attributed to oxygen extracted from CuO [200]. This study suggested that the 5Cu/alumina catalyst might have contained excess copper oxide species, which may have encouraged formation of carbon dioxide during methanol decomposition. If copper oxide was present on the copper/alumina catalyst it was no longer present in the post-reaction sample. XRD analysis (section 3.1.6) did not detect the presence of crystalline copper oxide in the post reaction samples; however it might have been present as small particles below the detection limits of the XRD technique. It is possible that Cu_2O was present on the catalyst similar to the 5Cu/silica catalyst, which contained Cu_2O after reduction (section 3.1.7.2).

3.2.3 Cerium/Support Catalysts

Two cerium/silica catalysts were examined for methanol decomposition, a 5% cerium/silica and 10% cerium/silica. Figures 3.2.10 and 3.2.11 show that although copper/silica catalysts were active for methanol decomposition, cerium/silica catalysts

were relatively inactive. No reaction products were detected for the 5% cerium/silica catalyst. A small yield of carbon dioxide (<1.5 %) was observed for the higher loaded catalyst (10Ce/silica) however this value decreased on subsequent pulses.

Figure 3.2.10. Conversion of methanol and yield of carbon monoxide, carbon dioxide and methyl formate over 5% Ce/Silica at 473K.

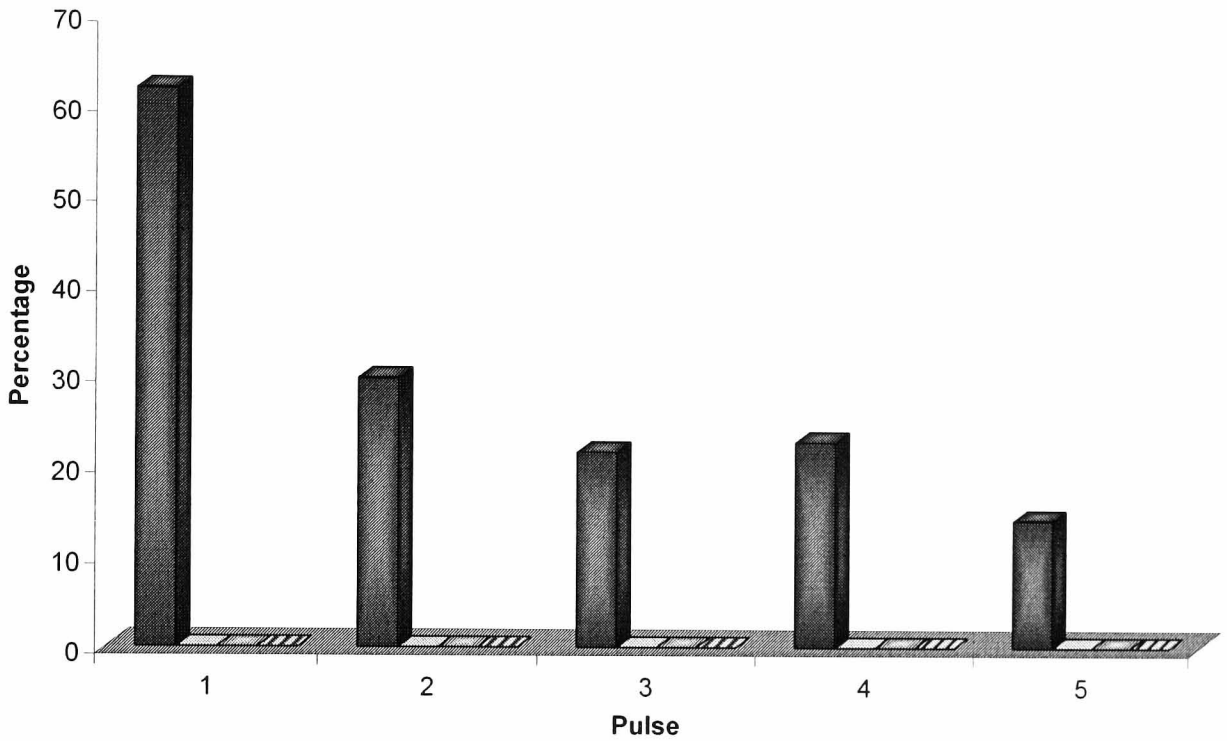

Table 3.2.9. Mass balance and yield of products during methanol decomposition, 5% Ce/Silica.

Pulse	*Mass Balance (%)*		*Yield of Products (%)*			*Selectivity (%)*
	Carbon	*Oxygen*	CO_2	*CO*	*MF*	$CO_2/(CO+CO_2)$
1	38.1	38.1	0.0	0.0	0.0	-
2	70.2	70.2	0.0	0.0	0.0	-
3	78.3	78.3	0.0	0.0	0.0	-
4	77.1	77.1	0.0	0.0	0.0	-
5	85.7	85.7	0.0	0.0	0.0	-

The carbon and oxygen mass balance values for the 5Ce/silica catalyst were very similar, confirming that no reaction occurred at 523 K. The conversion of methanol decreased as the catalyst surface became saturated with methanol.

Figure 3.2.11. Conversion of methanol and yield of carbon monoxide, carbon dioxide and methyl formate over 10% Ce/Silica at 473K.

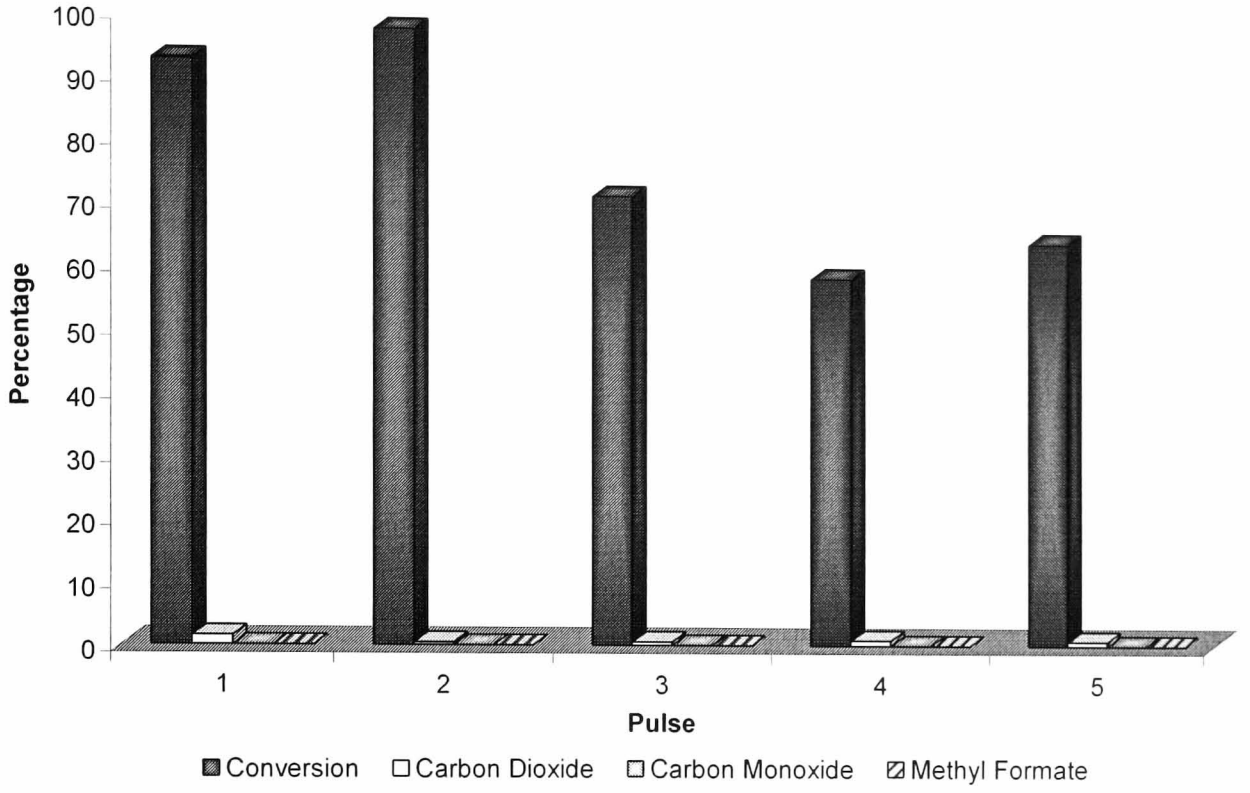

Table 3.2.10. Mass balance and yield of products during methanol decomposition, 10% Ce/Silica.

Pulse	*Mass Balance (%)*		*Yield of Products (%)*			*Selectivity (%)*
	Carbon	*Oxygen*	CO_2	*CO*	*MF*	$CO_2/(CO+CO_2)$
1	8.7	10.2	1.5	0.0	0.0	100.0
2	2.7	3.1	0.4	0.0	0.0	100.0
3	29.2	29.8	0.6	0.0	0.0	100.0
4	42.2	43.1	0.8	0.0	0.0	100.0
5	36.3	37.1	0.7	0.0	0.0	100.0

As reported in the XRD characterisation results (see section 3.1.6), cerium (IV) oxide was present on the 10Ce/silica catalyst after treatment at 523 K in hydrogen. As the temperature was below the reduction temperature for cerium oxide, cerium would only be present in its unreduced +4 oxidation state. As ceria is well known for its ability to store and release oxygen it is probably this property, which was involved in the production of carbon dioxide during methanol decomposition. The higher oxygen mass balance than carbon mass balance, table 3.2.10, supported the theory that the surface was behaving as a source of oxygen. Ceria is known to dissociate methanol into methoxy species at room temperature [201]. This process was as a result of O-H bond cleavage rather than C-O bond breaking. Hence it is possible that the adsorbed methoxy could react with surface oxygen species to produce carbon dioxide. Ferriz *et al* [202]

carried out studies on model CeO_2 surfaces and found that a fully oxidised CeO_2 (111) surface was almost inactive towards dissociative adsorption and oxidation of methanol. They concluded that adsorption and reaction of methanol occurred at surface defect sites. Increasing the surface defects and creation of oxygen vacancies improved the activity of the surfaces towards methanol [202]. This suggested that there were a greater number of defect sites on 10Ce/silica as it was not only able to adsorb methanol but also to form a small amount of carbon dioxide.

Craciun [203] examined a cerium/silica catalyst for carbon monoxide oxidation. The source of oxygen used to oxidise carbon monoxide over the ceria-supported catalysts was ceria lattice oxygen. The group found that high CeO_2 dispersion improved the contact between the reactant CO and the ceria, favouring production of carbon dioxide [203]. Hence it is likely that the extra oxygen used to form carbon dioxide from methanol was extracted from the ceria lattice.

On highly reduced ceria surfaces with exposed Ce^{3+} cations, the primary reaction pathway for adsorbed methoxide intermediates is complete dehydrogenation to CO and H_2 [202]. The results for the 5Ce/silica and 10Ce/silica catalysts confirm that the cerium of the catalyst was not reduced to Ce^{3+} during reduction, as no carbon monoxide or hydrogen were formed. This was in agreement with the characterisation result, which showed that reduction to Ce_2O_3 occurred only at high temperatures (surface reduction began at ~660 K and full reduction to Ce_2O_3 required temperatures around 1100 K).

Adsorption of methanol occurred over both catalysts. As an increase in cerium loading led to an increase in methanol adsorption, the cerium oxide species on the reduced catalyst was able to adsorb methanol. When the silica support was examined for methanol decomposition without additional metals, the adsorption of methanol increased across the pulses unlike the cerium containing catalysts (fig. 3.2.12).

Figure 3.2.12. Conversion of methanol and yield of carbon monoxide, carbon dioxide and methyl formate over silica support at 473K.

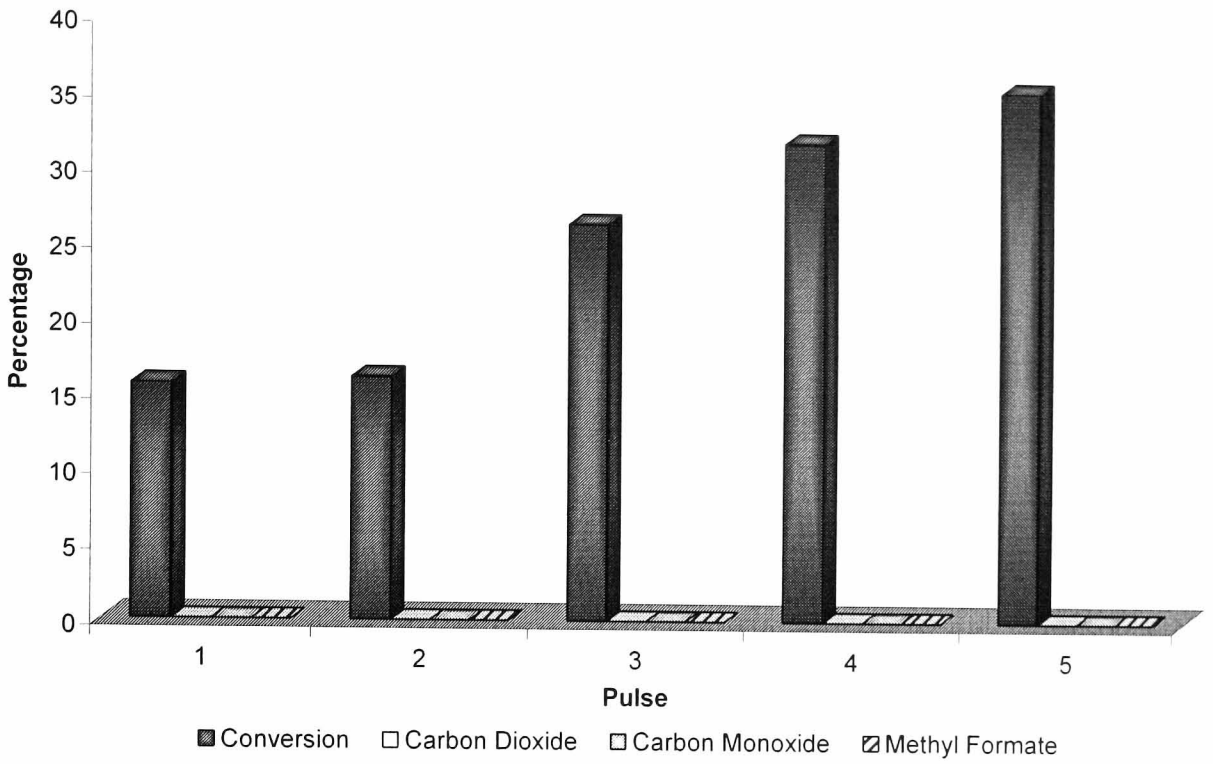

No decomposition products were observed when pulsing methanol over the silica support. Adsorption of methanol by the silica was contrary to findings by Jackson and co-workers [187]. The group [187] found that when pulsing methanol over copper/silica and silica samples at 523 K, methanol species were only retained in the presence of copper. Further studies would be required to determine the nature of the adsorbed species on the support.

Table 3.2.11. Mass balance and yield of products during methanol decomposition, silica support.

Pulse	*Mass Balance (%)*		*Yield of Products (%)*			*Selectivity (%)*
	Carbon	*Oxygen*	CO_2	*CO*	*MF*	$CO_2/(CO+CO_2)$
1	84.4	84.4	0.0	0.0	0.0	0.0
2	83.8	83.8	0.0	0.0	0.0	0.0
3	73.5	73.5	0.0	0.0	0.0	0.0
4	67.9	67.9	0.0	0.0	0.0	0.0
5	64.3	64.3	0.0	0.0	0.0	0.0

The 5% cerium/alumina catalyst behaved similarly to the 5% cerium/silica catalyst. Only adsorption of methanol occurred and no reaction products were observed, figure 3.2.13. Hence, at 473 K mainly associative adsorption of methanol occurred, as described for the cerium/silica catalysts. The conversion of methanol decreased during the pulses due to increased saturation of the catalyst surface with methanol.

Figure 3.2.13. Conversion of methanol and yield of carbon monoxide, carbon dioxide and methyl formate over 5Ce/Alumina at 473K.

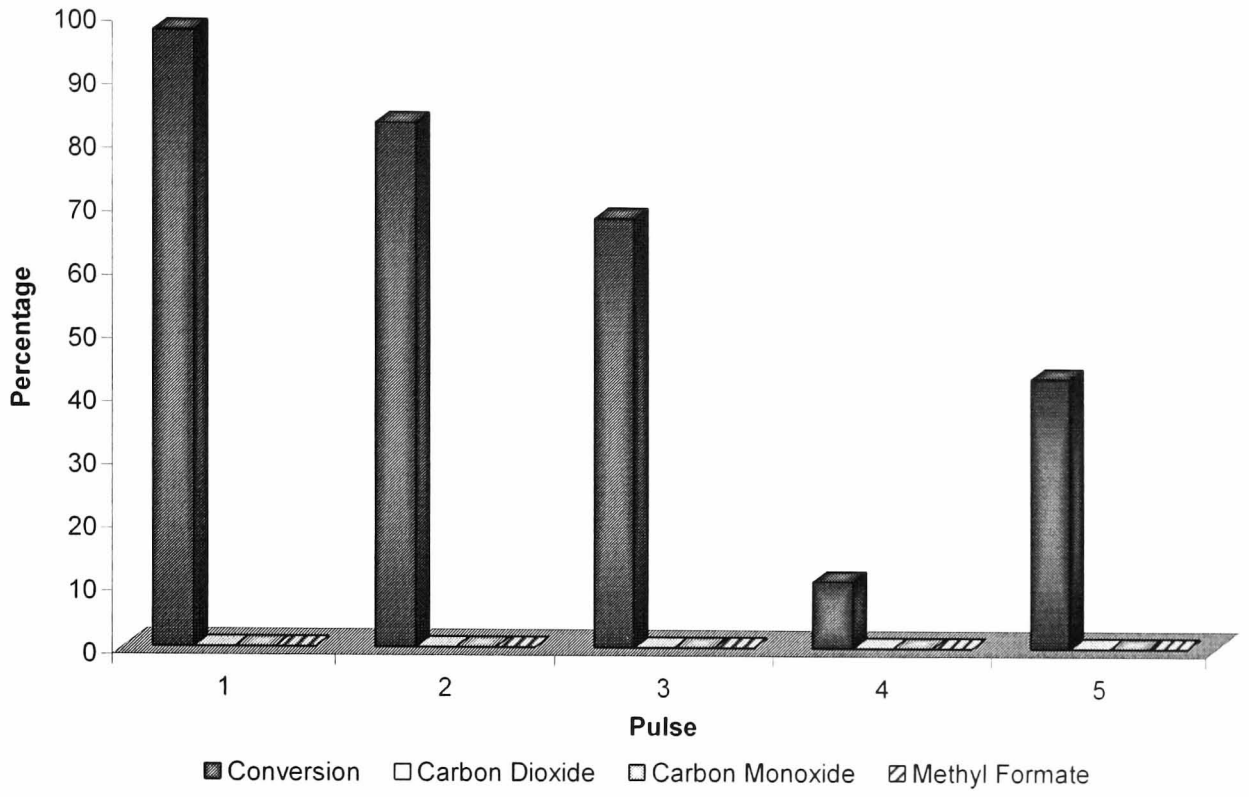

Table 3.2.12. Mass balance and yield of products during methanol decomposition, 5Ce/Alumina.

Pulse	*Mass Balance (%)*		*Yield of Products (%)*			*Selectivity (%)*
	Carbon	*Oxygen*	CO_2	*CO*	*MF*	$CO_2/(CO+CO_2)$
1	2.4	2.4	0.0	0.0	0.0	0.0
2	16.6	16.6	0.0	0.0	0.0	0.0
3	31.5	31.5	0.0	0.0	0.0	0.0
4	89.3	89.3	0.0	0.0	0.0	0.0
5	56.5	56.5	0.0	0.0	0.0	0.0

Hence, the catalyst support and the support modified with cerium oxide proved relatively unreactive for the decomposition of methanol under mild conditions. The results confirmed that cerium oxide provides an adsorption site for methanol, however dissociative adsorption and reaction occurred only in the presence of defect sites of cerium oxide or a partially reduced cerium oxide.

Adsorption of methanol has been combined with IR techniques to investigate the surface of polycrystalline ceria [32, 201]. Highly reduced cerium oxide contains Ce^{3+} cations, which can decompose methanol to carbon monoxide and hydrogen at temperatures near 670 K [202]. In the absence of reduced cerium oxide, methanol is dissociatively adsorbed on Ce^{4+} O^{2-} sites [201, 202]. Hence, it is possible that the

adsorption of methanol could provide an indication as to the dispersion of cerium oxide on the support. The cerium/support catalysts examined were not completely saturated by methanol after five pulses. 5Ce/silca, 10Ce/silica and 5Ce/alumina adsorbed 178, 464 and 265 $\mu molg^{-1}$ of methanol respectively. From these values it was possible to calculate the dispersion of cerium oxide on the support, assuming that one molecule of methanol would be adsorbed onto each Ce^{4+} site. The dispersions were determined as: 50 % (5Ce/silica), 65 % (10 Ce/silica) and 74 % (5Ce/alumina). This would suggest that the highest dispersion of ceria was achieved using an alumina support. However, to confirm these values further investigation would be required to determine any support effect and the effect of completely saturating the catalyst surface with methanol.

3.2.4 Copper and Cerium/Support Catalysts

After looking at the individual copper and cerium components supported on silica, the catalytic activity of the combined catalysts was examined. Literature reports suggested that strong metal to support interactions would be found when combining copper and ceria on a catalyst [162, 204]. In this study, the copper to cerium ratio was varied to examine the differences if any observed by changing the ratio of the components.

The first mixed catalyst examined was the 5Cu5Ce/silica catalyst. Characterisation of the catalyst suggested that after catalyst reduction a mixture of Cu^0, Cu_2O and partially reduced cerium oxide were present. The cerium oxide was partially reduced in the presence of the copper species, creating oxygen vacancies. 5Cu5Ce/silica was initially highly selective towards carbon dioxide. However successive pulses saw a decrease in selectivity as the carbon monoxide yield increased. Unlike the 5% copper/silica catalysts methyl formate was not produced. The increase in carbon monoxide indicated that formation of carbon dioxide might have been due to excess oxygen on the catalyst surface. The yield of carbon dioxide did not appear to decrease with increasing pulses as might have been expected if surface oxygen was being removed. The quantity and source of excess oxygen removed from the catalyst will be discussed in section 3.2.7.

Figure 3.2.14. Conversion of methanol and yield of carbon monoxide, carbon dioxide and methyl formate over 5Cu5Ce/Silica at 473K.

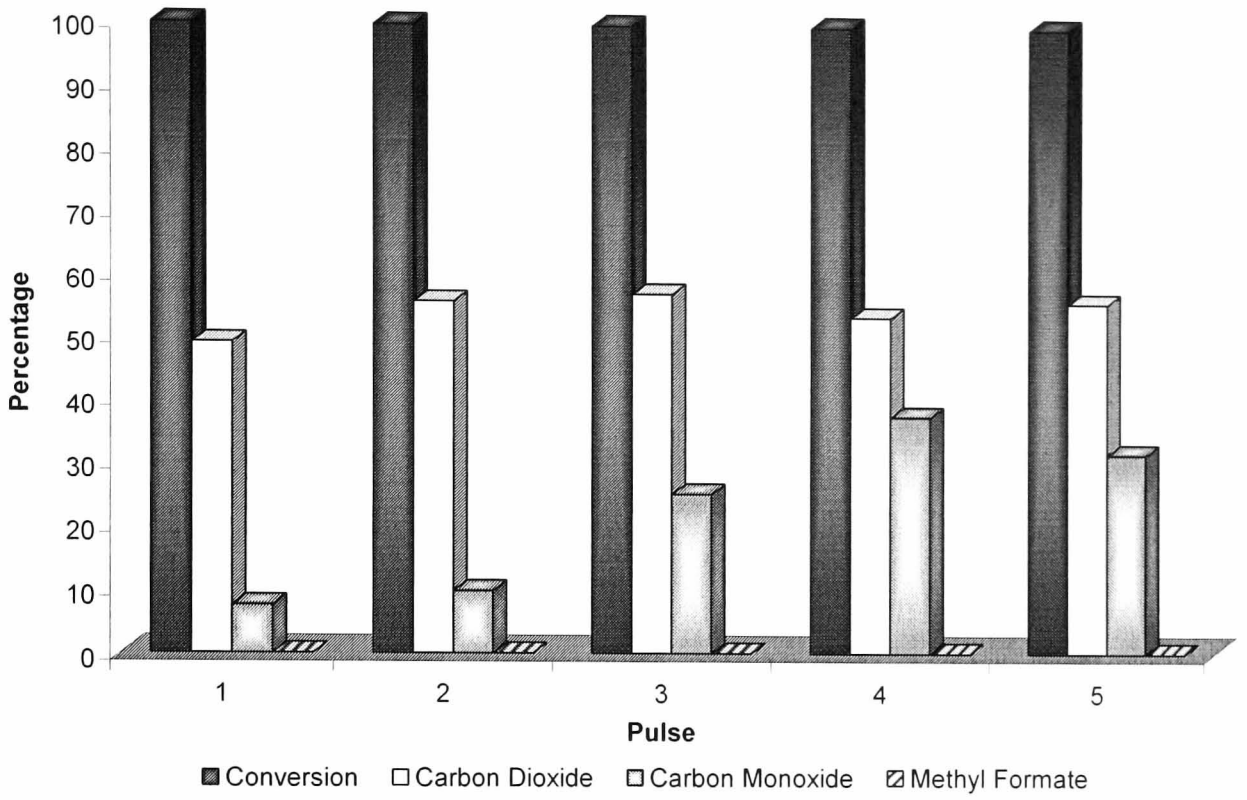

Table 3.2.13. Mass balance and yield of products during methanol decomposition, 5Cu5Ce/Silica.

Pulse	*Mass Balance (%)*		*Yield of Products (%)*			*Selectivity (%)*
	Carbon	*Oxygen*	CO_2	*CO*	*MF*	$CO_2/(CO+CO_2)$
1	56.7	105.9	49.2	7.6	0.0	86.7
2	65.8	121.8	56.0	9.8	0.0	85.1
3	82.5	139.8	57.3	25.2	0.0	69.4
4	91.3	145.0	53.7	37.6	0.0	58.8
5	87.9	144.0	56.1	31.8	0.0	63.9

As the reaction progressed, carbon deposition to the surface decreased (table 3.2.13). The oxygen mass balance was approximately 50 to 60% higher than the carbon mass balance during the pulsed reaction. This was most likely due to the presence of cerium oxide, which is able to behave as an oxygen store [30]. Instead of decreasing, the amount of oxygen removed from the surface appeared to increase as the reaction progressed.

By increasing the copper loading to 10%, a change was observed in the catalytic activity. 10Cu5Ce/silica did not convert 100% of the methanol reactant, figure 3.2.15. The ratio of products changed and an increase in selectivity towards carbon dioxide was observed. The yield of carbon monoxide remained below 12% during the reaction and

decreased slightly in latter pulses. When compared with 10Cu/silica (333 K), addition of cerium oxide greatly increased the selectivity towards carbon dioxide formation. The oxygen mass balance was too high to be solely a result of oxygen from the reactant methanol. Hence the surface was supplying extra oxygen required for product formation in a manner similar to that found with the 5Cu5Ce/silica sample.

Figure 3.2.15. Conversion of methanol and yield of carbon monoxide, carbon dioxide and methyl formate over 10Cu5Ce/Silica at 473K.

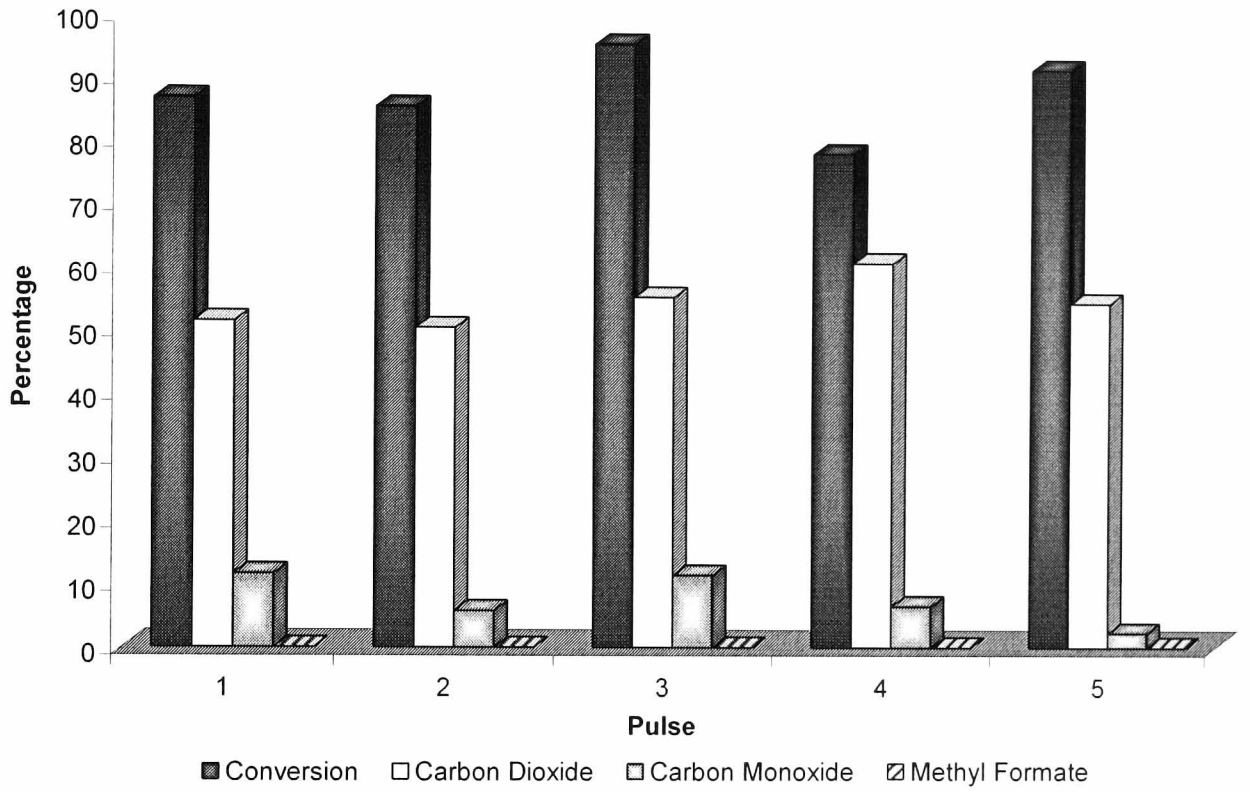

Table 3.2.14. Mass balance and yield of products during methanol decomposition, 10Cu5Ce/Silica.

Pulse	*Mass Balance (%)*		*Yield of Products (%)*			*Selectivity (%)*
	Carbon	*Oxygen*	CO_2	*CO*	*MF*	$CO_2/(CO+CO_2)$
1	76.3	127.8	51.5	11.7	0.0	81.5
2	70.6	121.2	50.6	5.9	0.0	89.6
3	71.1	126.6	55.5	11.5	0.0	82.8
4	89.2	150.5	61.2	6.6	0.0	90.3
5	64.9	119.8	54.9	2.4	0.0	95.8

The addition of only 1% cerium to a 5% copper/silica catalyst had an unexpected effect. Although the catalyst contained cerium, the initial carbon dioxide selectivity fell from 49 to 13 % across the pulses. 5Cu1Ce/silica produced a high yield of carbon monoxide, produced less methyl formate and less carbon species were retained by the catalyst (figure 3.2.16). As the reaction proceeded, the yield of carbon dioxide decreased,

indicating that the removal of excess oxygen from the catalyst surface was a transient process. The 5Cu5Ce/silica and 10Cu5Ce/silica catalysts continued to produce predominantly carbon dioxide throughout the decomposition reaction. However, it is possible that this was due to the increased loading of cerium, which increased the availability of oxygen stored within the cerium oxide.

Figure 3.2.16. Conversion of methanol and yield of carbon monoxide, carbon dioxide and methyl formate over 5Cu1Ce/Silica at 473K.

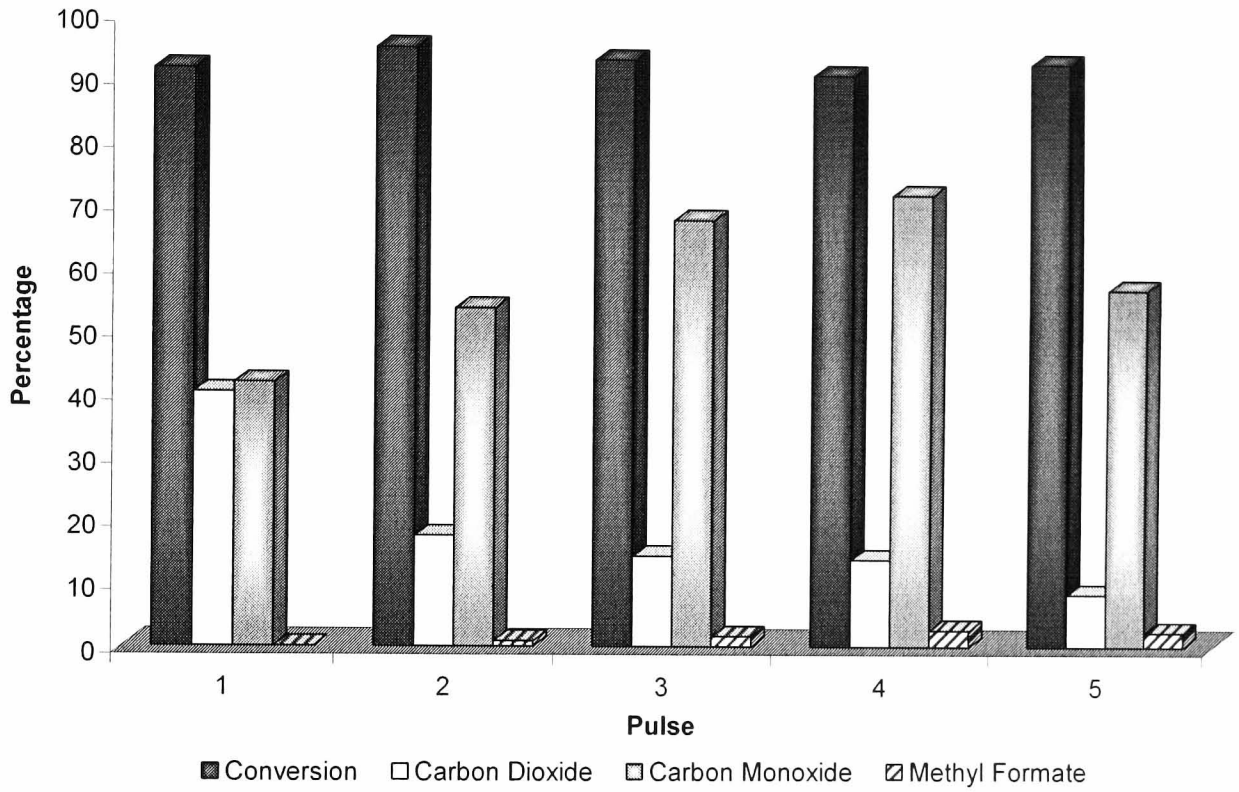

Table 3.2.15. Mass balance and yield of products during methanol decomposition, 5Cu1Ce/Silica.

Pulse	*Mass Balance (%)*		*Yield of Products (%)*			*Selectivity (%)*
	Carbon	*Oxygen*	CO_2	*CO*	*MF*	$CO_2/(CO+CO_2)$
1	90.5	130.8	40.3	41.9	0.0	49.0
2	77.8	95.3	17.5	53.9	0.9	24.6
3	92.1	106.5	14.4	68.1	1.6	17.4
4	100.0	113.8	13.9	72.3	2.6	16.1
5	76.6	84.9	8.3	57.3	2.3	12.7

The last of the mixed metal/silica catalysts investigated included 0.05% palladium with 10% copper and 5% cerium. It was hoped that the high loading of copper with the addition of palladium would encourage the formation of carbon monoxide from methanol decomposition. It was thought that the beneficial effect of synergy between palladium and cerium oxide would have a positive effect on the catalytic activity.

However, the results in figure 3.2.17 show that addition of such a low percentage of palladium made little difference to the performance of the catalyst. Methanol conversion was similar to the 10Cu5Ce/silica catalyst and the main product was carbon dioxide. Although initial selectivity towards carbon dioxide was high at approximately 98%, this value decreased on subsequent pulses (table 3.2.16).

Addition of palladium did not improve the carbon or oxygen mass balances. Similarly to 10Cu5Ce/silica, the oxygen mass balance was continually higher than the carbon mass balance. Table 3.2.16 shows that more oxygen was present in the reaction products than the reactants. Therefore, the catalyst was behaving as an oxygen reservoir.

Figure 3.2.17. Conversion of methanol and yield of carbon monoxide, carbon dioxide and methyl formate over 10Cu5Ce0.05Pd/Silica at 473K.

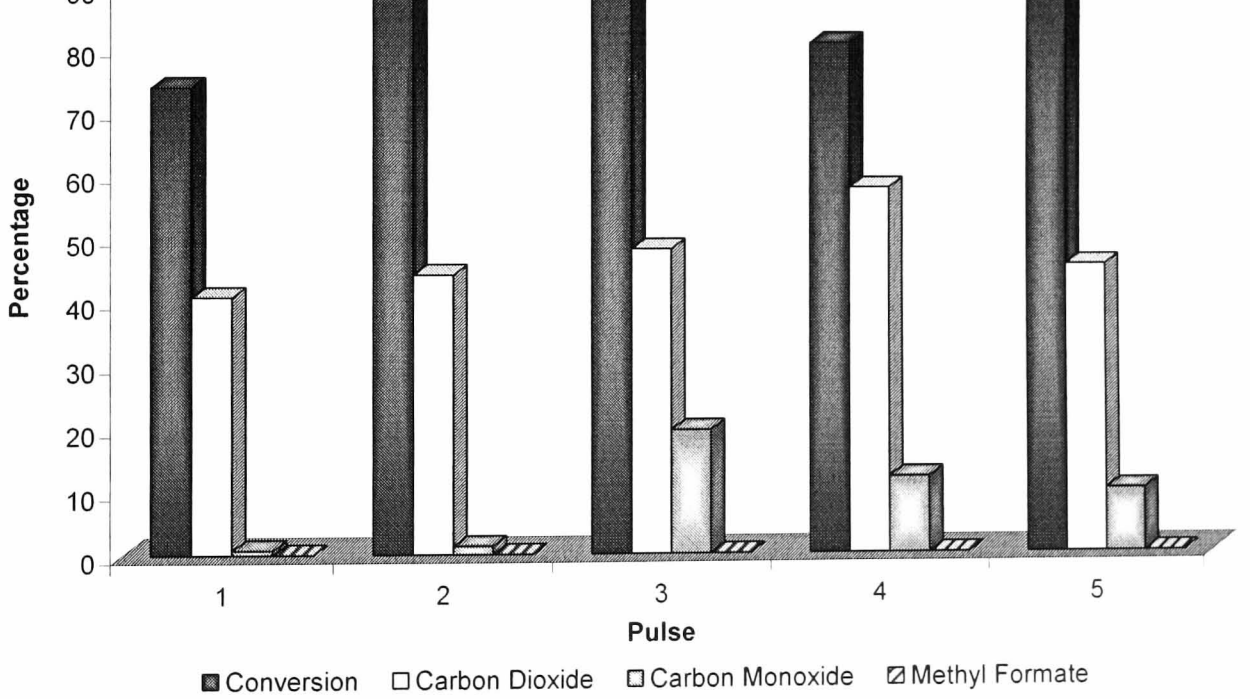

Table 3.2.16. Mass balance and yield of products during methanol decomposition, 10Cu5Ce0.05Pd/Silica.

Pulse	Mass Balance (%)		Yield of Products (%)			Selectivity (%)
	Carbon	Oxygen	CO_2	CO	MF	$CO_2/(CO+CO_2)$
1	67.5	108.1	40.6	0.8	0.0	98.2
2	50.7	94.8	44.1	1.3	0.0	97.1
3	68.9	117.2	48.3	19.6	0.0	71.1
4	88.9	146.9	58.0	12.0	0.0	82.8
5	59.5	105.2	45.7	10.1	0.0	82.0

The 5Cu5Ce/alumina catalyst produced both carbon monoxide and carbon dioxide on reaction with methanol (figure 3.2.18). The conversion of methanol to products was ~100% for each pulse. No methyl formate was produced and the production of carbon monoxide appeared to reach a maximum after the third pulse. Although the catalyst adsorbed the majority of the first pulse, as the number of pulses increased the carbon mass balance improved, again reaching a maximum on the third pulse, table 3.2.17.

Unlike the silica-supported catalysts, the addition of cerium to a 5% copper/alumina catalyst increased the yield of carbon monoxide, while decreasing the carbon dioxide yield (figure 3.2.18). The first three pulses showed that the yield of carbon dioxide and carbon monoxide were almost equal. The final two pulses showed a decrease in yield of carbon monoxide. Hence, as the reaction progressed the composition of the reactants switched to favour carbon dioxide formation. This may suggest that the effect of adding cerium oxide was temporary as carbon dioxide was the major product of 5Cu/alumina during the decomposition reaction.

Figure 3.2.18. Conversion of methanol and yield of carbon monoxide, carbon dioxide and methyl formate over 5Cu5Ce/Alumina at 473K.

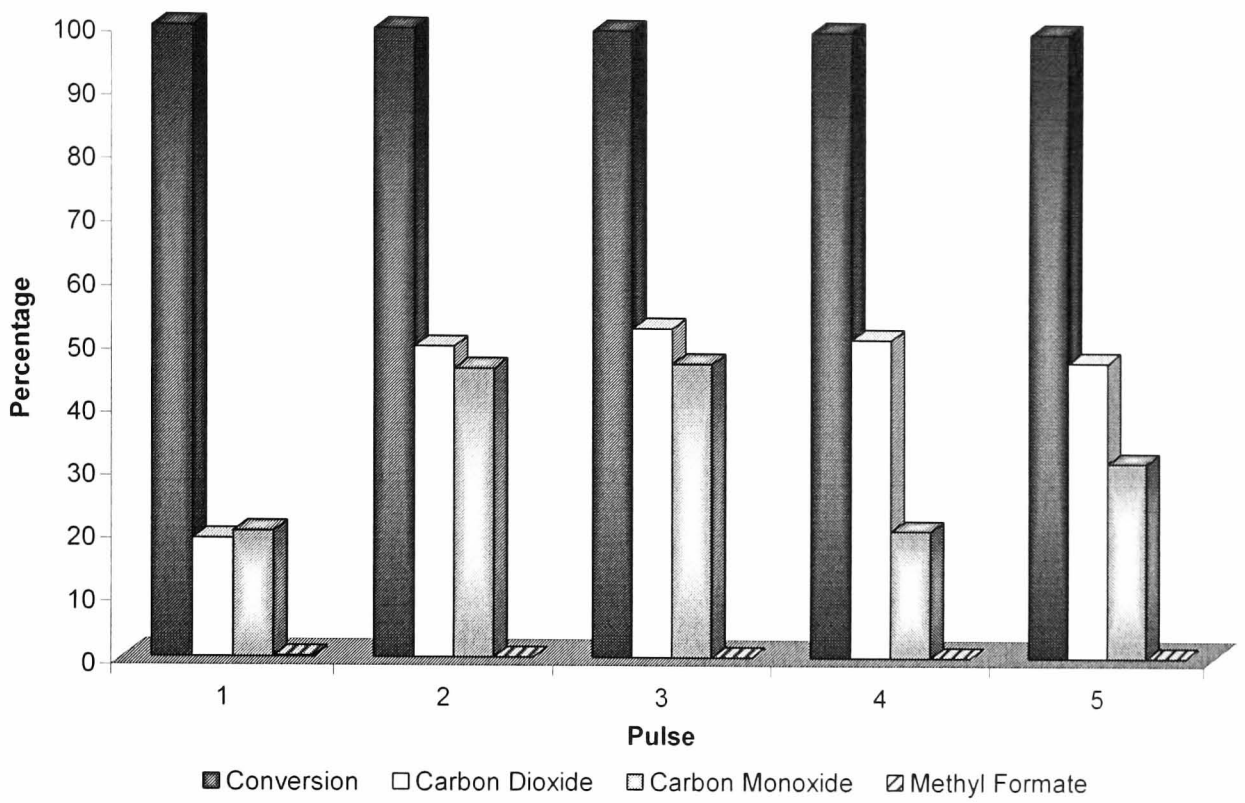

Table 3.2.17. Mass balance and yield of products during methanol decomposition, 5Cu5Ce/Alumina.

Pulse	*Mass Balance (%)*		*Yield of Products (%)*			*Selectivity (%)*
	Carbon	*Oxygen*	CO_2	*CO*	*MF*	$CO_2/(CO+CO_2)$
1	39.3	58.2	18.9	20.0	0.2	48.5
2	96.0	145.7	49.7	46.3	0.0	51.8
3	100.0	152.8	52.8	47.2	0.0	52.8
4	71.6	122.8	51.2	20.4	0.0	71.5
5	79.3	127.1	47.8	31.5	0.0	60.2

The following redox mechanism was thought to be responsible for the high activity of Cu/CeO_2 catalysts for the steam reforming of methanol [204]: $Ce^{4+} + Cu \longrightarrow Ce^{3+} + Cu^{+}$. Hence the cerium oxide, which can readily change oxidation state, had a stabilizing effect on the Cu^{+} species. The catalysts, which Liu *et al* [204] examined, were deactivated after time on stream. This was attributed to formation of carbonaceous deposits on the catalyst surface. This would explain the loss of carbon material during the methanol decomposition reaction over the copper/cerium catalysts. In the present study, addition of cerium to copper/silica catalysts did not have a major effect on the retention of carbon species, as the copper/silica catalysts lost similar amounts of carbon species to the catalyst surface.

The reaction mechanism of the multi-component copper/cerium oxide/support catalysts was complicated by the role of cerium oxide in the decomposition reaction. Cerium oxide is not likely to take part in the decomposition of methanol at temperatures below 670 K [202]. By combining the copper and cerium together on a support different decomposition products were observed than from either of the individual metals on a support. It has been proposed that Pd/CeO_2 and Cu/CeO_2 produce methanol via a formate intermediate [205]. In the case of Pd/CeO_2, Pd-O-Ce was detected, which highlighted the strength of interaction between the two metals during the reaction [85, 206]. This was in agreement with the mechanism for the synthesis of methanol from carbon monoxide and hydrogen using alloy catalysts [74]. Fakley and co-workers [74], described the mechanism as utilising a formate intermediate at the periphery between copper and ceria. Shen *et al* [84] discussed a similar mechanism for methanol synthesis using copper/ceria catalysts prepared by co-precipitation. Therefore, it is possible that a similar formate mechanism could be proposed for the reverse reaction using the copper/cerium oxide/support catalysts.

3.2.5 Summary of Catalyst Reactivity

By taking an average value for the five pulses examined, several trends were observed between the different catalysts shown in table 3.2.18.

The selectivity of the commercial and palladium/silica catalysts towards carbon dioxide was as expected from literature. The commercial and palladium catalysts were used to compare the remaining catalysts prepared. It was expected that catalysts with a high selectivity towards carbon dioxide would follow a similar mechanism to the commercial methanol synthesis catalyst.

Table 3.2.18. Comparison of copper containing catalysts for the methanol decomposition reaction.

Catalyst	*Av. Mass Balance (%)*			*Average Yield (%)*			*Av. Selectivity (%)*
	Carbon	*Oxygen*	*(Oxygen-Carbon)*	*CO_2*	*CO*	*MF*	$CO_2/(CO+CO_2)$
5Cu/Silica (293 K)	65.8	76.6	10.8	10.8	20.0	16.7	35.0
5Cu/Silica (WetImpreg.)	60.7	72.5	11.8	11.8	30.8	8.4	28.0
10Cu/Silica (293 K)	81.6	92.8	11.2	11.2	31.6	18.8	26.2
10Cu/Silica (393 K)	87.5	106.9	19.5	19.5	53.4	2.7	26.7
5Cu/Silica (SprayImpreg.)	57.3	69.7	12.4	12.4	23.2	9.9	35.9
5Cu5Ce/Silica	76.9	131.3	54.5	54.5	22.4	0.0	72.8
5Cu/Silica (ac)	73.4	84.9	11.5	11.5	24.8	10.8	31.7
10Cu5Ce/Silica	74.4	129.2	54.8	54.8	7.6	0.0	88.0
10Cu5Ce0.05Pd/Silica	67.1	114.4	47.3	47.3	8.8	0.0	86.2
5Cu1Ce/Silica	96.6	117.4	20.9	20.9	64.9	1.6	24.0
5Cu/Alumina	69.3	128.5	59.2	59.2	0.0	0.0	100.0
5Cu5Ce/Alumina	77.2	121.3	44.1	44.1	33.1	0.0	57.0
Commercial	33.9	67.5	33.6	33.6	0.3	0.0	99.2
1Pd/Silica	89.6	92.4	2.8	2.2	25.3	0.0	7.6

The table shows that the copper and cerium catalysts produced did not follow the same mechanism as the copper-cerium intermetallic alloy catalysts. The alloy catalysts were thought to produce methanol solely from carbon monoxide and hydrogen [72], similar to palladium based catalysts [192]. As all of the copper and cerium catalysts produced carbon dioxide they did not follow the same mechanism. The silica-supported catalysts produced a mixture of products, although in general were more selective towards carbon monoxide. It appeared that to achieve the highest selectivity for carbon monoxide production only small amounts of cerium oxide (<1 wt % of Ce on catalyst) were required. Addition of a small percentage of cerium did not appear to improve the copper dispersion (from N_2O chemisorptions). However, addition of a large amount of cerium oxide favoured the production of carbon dioxide as reflected in the high selectivity towards carbon dioxide in the decomposition products. This process was probably due to removal of excess oxygen from the cerium oxide lattice.

Source of Excess Oxygen/Transient Process?

Only two catalysts, which did not contain cerium oxide, removed oxygen from the catalyst surface, 10Cu/silica and 5Cu/alumina. At 673 K, alumina has higher oxygen mobility than silica [31]. However even if a similar phenomenon occurred at 473 K, it would not explain the extreme change in selectivity of the catalyst. It is likely from the TPR study (section 3.1.8) that 5Cu/alumina was not completely reduced by 523 K, whereas reduction of the silica catalyst was almost complete. Therefore unreduced copper oxide may have provided a source of oxygen for the formation of carbon dioxide.

Table 3.2.19. Excess oxygen removed from catalysts.

Catalyst	*Excess O_2 Removed from Catalyst ($\mu molg^{-1}$)*	
	*Theory**	*Actual*
5Cu5Cu/Silica	89.0	97.8
10Cu5Ce/Silica	89.0	97.8
10Cu5Ce0.05Pd/Silica	89.0	53.5
5Cu1Ce/Silica	17.8	16.5
5Cu5Ce/Alumina	89.0	43.8
10Cu/Silica	-	21.5
5Cu/Alumina	-	77.3

* Theoretical value was the maximum amount of oxygen, which could be removed to reduce all CeO_2 present to Ce_2O_3.

An increase in the oxygen content of the products was observed over all the cerium containing catalysts, 5Cu1Ce/silica catalyst was the most interesting as it appeared that the formation of carbon dioxide decreased as the excess oxygen was removed. For 5Cu1Ce/silica, the total number of moles of excess oxygen removed from the surface while decomposing methanol was 16.5 $\mu molg^{-1}$ (of O_2). If all of the cerium species on the catalyst was present as CeO_2 after reduction to 523 K, then 17.9 $\mu molg^{-1}$ (of O_2) could be removed to form Ce_2O_3. Therefore the cerium oxide appeared to be the main source of excess oxygen. As carbon monoxide was a better reducing agent for cerium oxide than hydrogen, it was likely that the surface was further reduced by the carbon monoxide formed during methanol decomposition. In-situ tests would be required to confirm the formation of Ce_2O_3 during the reaction.

The production of high yields of carbon dioxide was accompanied by a greater difference between the oxygen and carbon mass balance. This suggested that the cerium oxide behaved as an oxygen source and it is possible that this was a transient reaction. Once removal of excess surface oxygen is complete, the yield of products may change to favour carbon monoxide production as for copper/silica catalysts. Continuous flow testing would be required to investigate further the activity of the catalysts for long-term stability.

3.3 Properties and Reactivity of Cerium Hydride

Cerium-copper alloys were investigated, and when activated were highly active for the production of methanol from carbon monoxide and hydrogen [71-73, 185]. The alloys were composed mainly of lanthanide and copper metals. Further investigation of the active catalyst suggested that the active species involved an intermetallic hydride or small copper particles in close contact with a lanthanide oxide [72]. It was also suggested that the presence of a rare-earth component in the ternary alloys increased the ability of the material to form a hydride [185]. However, the properties of the cerium metal itself were never fully investigated. Hence, the aim of this study was to further examine cerium hydride formation and its reactivity with other gases.

Most lanthanide metals react readily with hydrogen to produce di- or tri-hydrides. The level of hydriding that occurs is strongly dependent upon the pre-treatment temperature and the pressure of hydrogen gas during the reaction [207]. Lanthanide and actinide metals can take up hydrogen at room temperature or slightly elevated temperatures to form a dihydride [208]. Even the massive hydrides of the early lanthanides are pyrophoric, although thermal stability and resistance to pyrophoricity increase with increasing atomic number. Lanthanide hydrides are relatively stable towards water and although hydrolysis occurs, it is very slow. Direct combination of the metal and hydrogen is the usual preparation route, however lanthanide hydrides can also be prepared by using catalytic amounts of $TiCl_4$ in a solvent (such as THF) [209].

Once prepared the lanthanide hydrides generally have high hydrogen retention as well as high melting points. These properties are beneficial for applications such as hydrogen storage and catalysis. Early work on cerium metal was carried out using misch-metal, which was composed mainly of cerium (40-60 wt%) but contained large amounts of lanthanum as well as other lanthanide metals. Due to the impurities present in both the reaction metal and reaction gases, results from different groups were not in complete agreement [210]. Indeed, the presence of trace oxygen in the reaction gas was enough to severely decrease the rate of reaction of cerium with hydrogen, when compared with pure gas [211].

As all of the rare-earth hydrides are pyrophoric, they react easily with oxygen (and in some cases water) to produce hydrogen gas. However, it is not clear whether an oxide

layer forms on the surface or if hydroxyl groups are also present [212]. Thermodynamically, cerium oxide formation is more favourable than cerium hydride formation.

$Ce + O_2 \longrightarrow CeO_2$ $\quad \Delta H^o_f = -1083$ kJ mol^{-1}, $\Delta G^o_f = -1020$ kJ mol^{-1}

$2Ce + {}^3/_2O_2 \longrightarrow Ce_2O_3$ $\quad \Delta H^o_f = -1797$ kJ mol^{-1}, $\Delta G^o_f = -1707$ kJ mol^{-1}

$Ce + H_2 \longrightarrow CeH_2$ $\quad \Delta H^o_f = -205$ kJ mol^{-1}, $\Delta G^o_f = -163$ kJ mol^{-1}

Once formed, ceria is a stable material, which is able to store spilt over atoms, form intermetallic compounds, promote noble metal oxidation and reduction and form surface and bulk vacancies [30]. Ceria is often used as a support for oxidative catalysts. Although hydrogen and oxygen spillover are possible on ceria, a recent study has suggested that spilled over hydrogen onto ceria may not be recoverable [213].

Although there is still limited interest in cerium metal, several recent studies have investigated the formation of cerium hydride under ultra high vacuum (UHV) conditions [212, 214] or by using *in-situ* experimental techniques [215, 216]. From these experiments the kinetics of hydride formation were examined. Cerium metal has been examined recently with C_{60} for its possible superconducting and ferromagnetic properties [217].

The current study investigated the reaction of cerium metal with small molecules, under atmospheric pressure and relatively mild temperature (523 K). A series of pulse-flow reactions was used to examine the reactivity of the cerium hydride produced. As well as selectively reacting with alkynes rather than carbon to oxygen bonds, the cerium hydride was highly reactive with oxygen and methanol.

3.3.1 Hydride Formation

Hydrogen was pulsed across both samples until saturation of hydrogen occurred. The hydrogen uptake showed that both the cerium and cerium/copper samples formed a metal hydride (table 3.3.1).

Table 3.3.1. Hydrogen absorbed by cerium metal and cerium/copper metal sample.

Sample	*Hydrogen Adsorbed (μmol)*	*Hydride Formed*
Ce	495	$CeH_{0.3}$
Ce and Cu	464	$CuCeH_{0.3}$

Although the ratio of cerium to hydrogen of 1 to 0.3 was lower than the values reported in literature [210], this was due to the major differences in experimental conditions. Previous work investigated hydride formation at high hydrogen pressures and a variety of temperatures [207, 211, 218]. Reactions were also left for several days, whereas the pulse reaction in this study had a residence time of only ~0.75 seconds at atmospheric pressure (gas flow of 40 cm^3min^{-1} and sample volume ~0.5 cm^3). Hence formation of bulk cerium hydride would require more severe conditions and prolonged exposure to hydrogen gas.

Korst and Warf [208] prepared a hydrogen poor rare earth hydride with approximately $RH_{0.4}$ (where R = rare earth metal). This restricted absorption of hydrogen gas was attributed to the formation of grain boundaries, which prevented all of the lanthanide metal from being exposed to hydrogen. This was in agreement with Holley *et al* [219], who described samples with less hydrogen than required to form CeH_2 as being composed of metal hydride and unreacted lanthanide metal. Surface to subsurface hydrogen penetration has been suggested to control the massive hydriding step in hydride formation [215]. However surface chemisorption (possibly linked to surface migration) seems to be involved in the initial surface growth process of the hydride nuclei.

Several authors suggested that on formation of cerium dihydride a brown/red colour would be observed [173, 214]. No colour change was observed during the reaction and the sample remained black in colour. However this was in agreement with literature reports that did not observe a colour change even on formation of the trihydride, which remained black in colour [208]. In addition, Gayer and Bos [211] observed dark grey spots during formation of a hydride. Hence, the colour change did not provide conclusive evidence of the level of hydriding which had occurred. It is likely that the $CeH_{0.3}$ was composed mainly of a sub-stoichiometric cerium hydride and possibly some unreacted cerium metal.

Addition of copper metal to the cerium powder had no beneficial effect on the hydrogen absorption of the sample. Copper metal was not expected to form copper hydride as copper hydride has only been prepared under wet [210] or high pressure conditions [220]. Copper hydride is unusual in that it is prepared in aqueous solution [221-223]. Although it decomposes at room temperature several attempts have been made to support the hydride for use in catalysis [223, 224]. Fitzsimons *et al* [224] found that CuH was stable on non-basic supports but decomposed on strongly basic surfaces, producing large copper particles. Copper hydride prepared under high pressure conditions was strongly thermodynamically unstable [220]. Pressure higher than 14.4 GPa was required to prepare the hydride and it decomposed at pressures below ~12.5 GPa. Hence, the formation of copper hydride was not expected. The addition of copper was to investigate any beneficial effects on the reactivity of the cerium metal.

3.3.2 Hydride Reactivity

A number of reactions were used to determine specific properties of the cerium hydride and copper and cerium hydride. Of particular interest was the reactivity of the hydrogen in the hydride, i.e. whether or not it was suitable for catalytic applications.

Reaction of Cerium Hydride with Deuterium

Deuterium pulses were used to investigate the exchange properties of the cerium hydride. The pulses of deuterium exchanged to form DH and H_2 gas. Table 3.3.2 shows that the percentage of deuterium converted to products for both the cerium hydride and copper/cerium hydride was greater than 90%.

Table 3.3.2. Deuterium conversion over cerium hydride and copper and cerium hydride at 523K.

Sample	*Total H_2 Absorbed (μmol)*	*D_2 Pulse (μmol)*	*Ratio of H_2 to D_2*	*Pulse*	*Deuterium Conversion (%)*	*Ratio of Products*		
						D_2	*DH*	*H_2*
$CeH_{0.3}$	495	41.3	12:1	1	92.6	1	5	7.5
				2	94.4	1	4.5	7.5
$CuCeH_{0.3}$	464	27.0	17:1	1	96.6	1	4.5	12
				2	95.5	1	5.5	13

The pulse of deuterium gas was approximately 10% of the hydrogen content of the sample and only two pulses were used to examine whether or not exchange had

occurred. The ratio of products was calculated from the mass spectrometer and showed that the main product was hydrogen. However, statistically the yield of hydrogen would be expected to be far greater, as it is by far in excess when compared with the deuterium available. The results confirmed that deuterium readily exchanged with the lattice hydrogen. The lower ratio of hydrogen in the products would suggest that removal of hydrogen is not completely facile. It may be possible that sub-surface hydrogen is more difficult to remove and that exchange occurs first with readily accessible surface hydrogen.

Reaction of Hydride with Carbon Monoxide and Carbon Dioxide

The cerium hydride and copper/cerium hydride samples were tested with pulses of carbon monoxide and carbon dioxide at 523 K. Under both helium and hydrogen gas flow no reaction products were observed. There was no evidence of adsorption of either gas by the sample. The cerium/copper mixture was similarly unreactive under these conditions.

Although intermetallic alloy catalysts were deactivated by less than 2% carbon dioxide [71-73, 185], the cerium hydride did not react with either gas. Reaction of the hydride with carbon monoxide/dioxide was thermodynamically favourable however, no reaction products were observed.

$$2CeH_2 + 3CO \longrightarrow Ce_2O_3 + CH_4 + 2C \qquad \Delta G^o_r = -1024 \text{ kJ mol}^{-1}$$

$$2CeH_2 + 3CO_2 \longrightarrow Ce_2O_3 + 3CO + 2H_2 \qquad \Delta G^o_r = -749 \text{ kJ mol}^{-1}$$

Owen and co-workers [72] proposed that although the oxide phase was not solely responsible for the alloy catalysts' high activity, it was possible that carbon dioxide formed strongly bound carbonates with lanthanide oxides, which were detrimental to the catalytic activity. As the high activity of the catalysts was not entirely due to the lanthanide oxide [72], it was possible that the cerium hydride reacted with the carbon oxides to form more stable compounds. However, even after exposure to oxygen, the $CeH_{0.3}$ samples remained inactive towards CO and CO_2. As the bulk cerium metal (powder >40 mesh) had a very low surface area this may explain the apparent lack of reactivity towards the gases. The reactions at Glasgow were carried out at 1 bar pressure and 523 K, whereas the conditions used to test the alloy catalysts were 50 bar

pressure and 513 K [72]. Hence the conditions used to examine the alloy catalysts would have favoured the formation of carbonate species on the lanthanide oxide.

Reaction with Oxygen

The cerium hydride reacted with oxygen to produce hydrogen in an exothermic reaction. At higher concentrations of oxygen, water was also formed by both samples. All of the oxygen pulses either reacted or were adsorbed by the hydride; hence oxygen was never detected in the exit gas. The exotherm of the reaction continued to rise with increasing concentration of the oxygen pulse. However at higher concentrations the temperature increase began to level out for the cerium hydride sample. Figures 3.3.1 and 3.3.2 show the temperature increase and hydrogen production for a range of oxygen pulses over the cerium hydride and copper and cerium hydride respectively.

Figure 3.3.1. Reaction of cerium hydride with oxygen pulses.

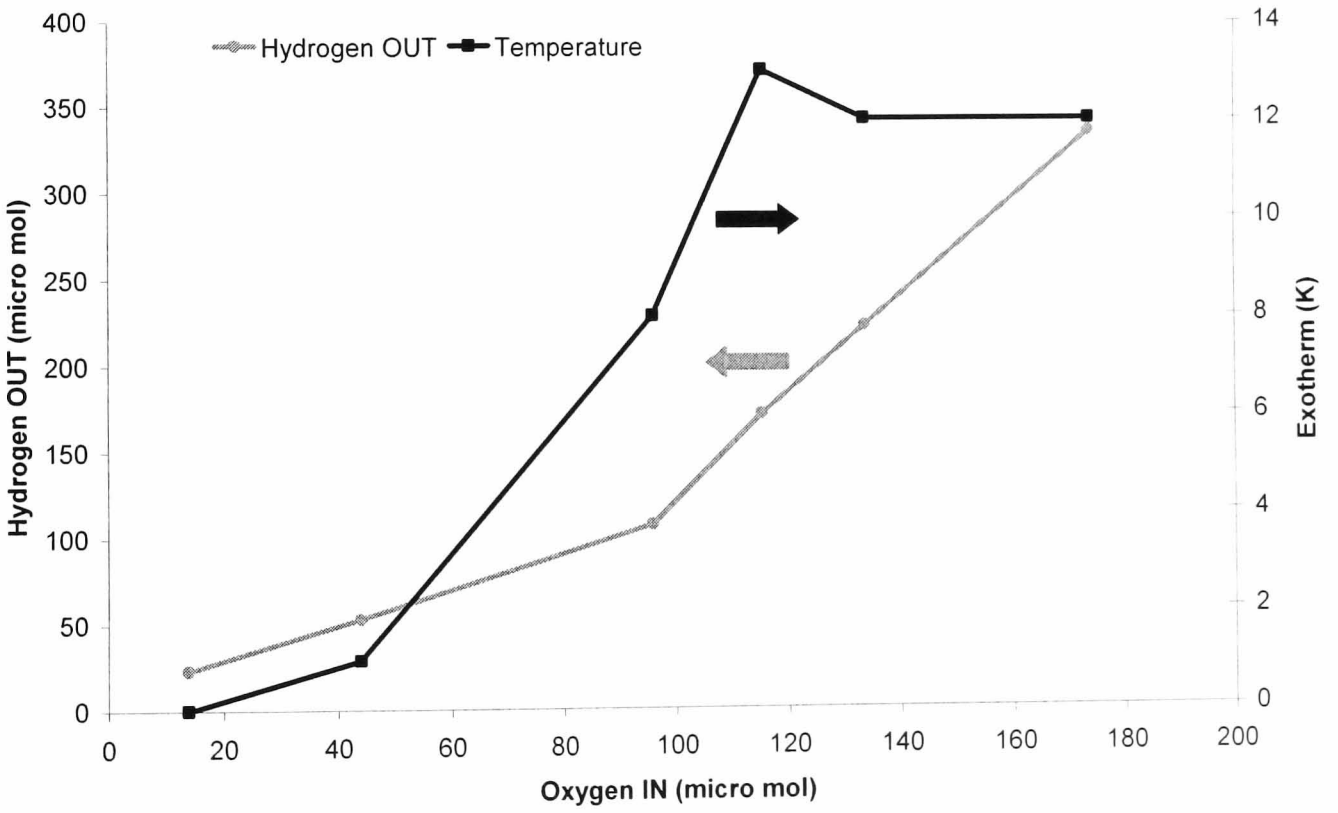

Table 3.3.3. Reaction of oxygen with cerium hydride.

Oxygen IN (μmol)	*Hydrogen OUT (μmol)*	*Exotherm (K)*
13.9	23.1	0
44.0	52.7	1
95.8	107.0	8
115.3	171.2	13
133.6	222.6	12
173.7	335.2	12

The addition of copper to the cerium metal increased the exotherm and decreased the hydrogen produced during the reaction, even though its presence had little effect on previous reactions, including the absorption of hydrogen.

Figure 3.3.2. Reaction of copper and cerium hydride with oxygen.

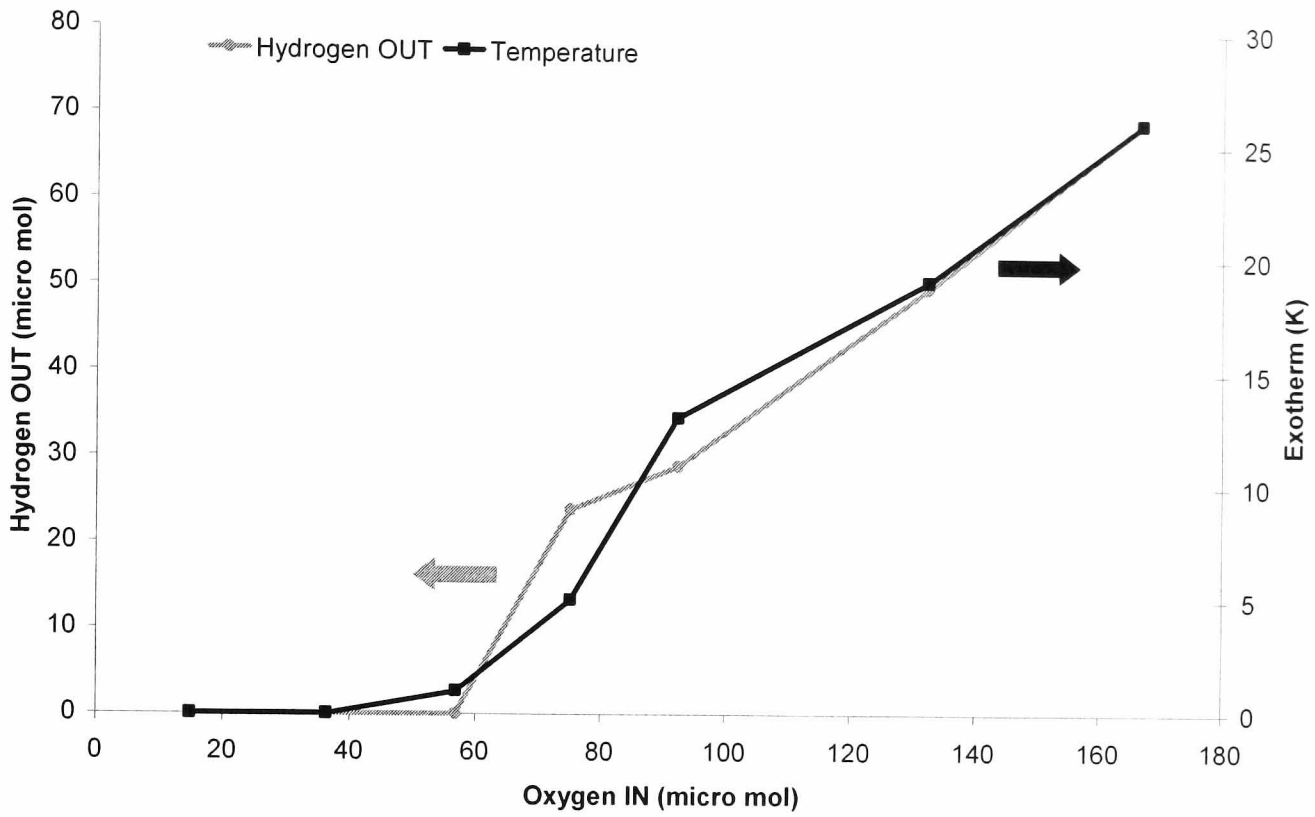

Table 3.3.4. Reaction of oxygen with copper and cerium hydride.

Oxygen IN (μmol)	*Hydrogen OUT (μmol)*	*Exotherm (K)*
14.8	0	0
36.3	0	0
56.9	0	1
75.2	23.9	5
92.4	29.0	13
132.4	49.9	19
166.8	69.4	26

The copper/cerium hydride appeared to produce a greater exotherm than the cerium hydride. However, this may have been due to a number of reasons including the difference in bed depth between the two catalysts. As the copper/cerium mixture had a greater bed depth, the thermocouple was closer to the sample, hence a greater exotherm was observed. Both samples were maintained in flowing carrier gas, which would have aided heat dissipation from the sample. After oxidation of the sample, the cerium hydride changed colour from black to grey/white. This was due to the formation of ceria. The grey/white colour indicated the formation of Ce_2O_3. Due to the low

concentrations of oxygen used, the majority of the sample remained black below the white/grey layer on the top of the sample. As more pulses of oxygen reacted with the hydride, the white/grey layer stretched further down the catalyst bed. Hence subsequent reactions were occurring further down the catalyst bed away from the thermocouple.

The reaction of cerium hydride with oxygen produced an increase in temperature, as expected from the thermodynamic values for the reaction (at 298 K):

$2CeH_2 + {}^3/_2O_2 \longrightarrow Ce_2O_3 + 2H_2$ $\quad \Delta G^o_r = -1349 \text{ kJ mol}^{-1}$

$\Delta H^o_r = -1387 \text{ kJ mol}^{-1}$

$2CeH_2 + {}^5/_2O_2 \longrightarrow Ce_2O_3 + 2H_2O$ $\quad \Delta G^o_r = -1860 \text{ kJ mol}^{-1}$

$\Delta H^o_r = -1959 \text{ kJ mol}^{-1}$

Or

$2CeH_2 + {}^5/_2O_2 \longrightarrow 2CeO_2 + H_2 + 2H_2O$ $\quad \Delta G^o_r = -2774 \text{ kJ mol}^{-1}$

$\Delta H^o_r = -2863 \text{ kJ mol}^{-1}$

The temperature increase calculated if the entire sample (0.5 g) had been converted to cerium (IV) oxide was 3570 K.

Hay et al [73] found cerium metal to be highly reactive towards oxygen. During a TPO, the group found that oxidation did not begin until 423 K with thermal runaway occurring above 548 K. They also found that after oxidation of the sample it could not be re-reduced up to 623 K [73]. These results would suggest that ceria was formed, which normally has two reduction features at approximately 770 K and 1100 K [225]. These bands are due to the removal of surface and bulk oxygen from CeO_2 to form Ce_2O_3.

Two mechanisms have been postulated for the reaction of cerium hydride with oxygen [212]:

i) Oxidation of the hydride by adsorption of oxygen atoms on the surface.

ii) Formation of water vapour by combination of dissociated oxygen atoms with hydrogen atoms of the hydride.

According to the literature, most oxygen molecules react with the hydride surface to form surface hydroxides [212]. Therefore, it is possible that both hydroxide and oxide species existed on the surface of the cerium hydride after reaction with oxygen.

Reaction with Methanol

Adsorption of methanol occurred on reaction with cerium hydride and expected decomposition products such as CO, CO_2 and MF were not observed. The mass spectrometer showed that initial pulses of methanol produced methane and hydrogen. As can be seen from table 3.3.5, approximately 1.5% of the methanol that reacted was converted to methane. Over the four pulses the total number of moles of methanol adsorbed was 89.1 μmol.

Table 3.3.5. Reaction of methanol with cerium hydride.

Pulse	*Methanol IN (μmol)*	*Methane Produced (μmol)*	*Methanol Adsorbed (μmol)*
1	14.9	0.2	14.7
2	14.3	0.2	14.1
3	13.7	0.2	13.5
4	13.2	0.2	13.0

On a fresh $CeH_{0.3}$ sample, methanol continued being adsorbed, however if the sample had been previously exposed to other gases, it adsorbed fewer methanol pulses. This is possibly due to the slow deactivation of the sample as an oxide layer formed on the surface of the cerium hydride.

The formation of methane and hydrogen from the decomposition of methanol over cerium hydride suggested that the cerium hydride was able to strip the oxygen from the methanol to form ceria. The reaction was thermodynamically feasible:

$$2CeH_2 + 3CH_3OH \longrightarrow Ce_2O_3 + 3CH_4 + 2H_2 \qquad \Delta G^o_r = -1100 \text{ kJ mol}^{-1}$$

The ability of cerium hydride to scavenge oxygen was similar to that of cerium/copper alloys, which produced methane during activation of the alloy to form the catalyst [72]. Hence, they were similarly able to cleave the C-O bond. The alloys were activated in synthesis gas composed of CO and H_2. The following scheme was proposed:

$$Ce_xCu_y + 2xCO + 4xH_2 \longrightarrow xCeO_2 + 2xCH_4 + yCu$$

Methanol was found to dissociate into methoxy groups on the surface of ceria samples [201]. It was determined that this species was formed by the O-H (and not C-O) breaking. This confirmed that the reactivity of the hydride varied considerably from that of the cerium oxide.

Fully deuterated methanol was used to determine the source of hydrogen in the methane produced. From the first pulse of d_4-methanol, CD_4, CD_3H and hydrogen were formed. The ratio of CD_4 to CD_3H in the first pulse was 1:1. Deuterium gas may also have been produced, however as the carrier gas was helium it would not have been detected by mass spectroscopy. Subsequent pulses showed an increase in unreacted deuterated methanol. Table 3.3.6 shows the rapid deactivation of the sample. As the surface became saturated with methanol, the conversion of methanol to products decreased. Although initial conversion appeared high, this was mainly due to adsorption of the methanol by the cerium hydride. The production of CD_3H revealed that surface hydrogen was utilised.

Table 3.3.6. Conversion of deuterated methanol over cerium hydride.

Pulse	*Methanol Conversion (%)*
1	98.4
2	64.6
3	45.4

The formation of deuterated products was similar to a study by Nix and co-workers [70]. After treatment of the alloy in deuterium before switching to the reaction gas (CO/H_2), all $CH_{4-x}D_x$ isotopic combinations were evident in the exit gases. Isotopic variants of methanol containing up to three deuterium atoms were also detected by the group [70].

The results of the methanol study suggested that the cerium hydride was not only poisoned by water and carbon dioxide as for the alloy catalysts [70-72], but that it was also poisoned by methanol. Although not previously described as a poison and the conditions used by Owen *et al* [72] were different from those used in this study, there

was evidence in their study to support this theory. When the flow of the reaction gas was increased from 36000 h^{-1} to 86000 h^{-1} over a $NdCu_2$ alloy catalyst, it was found that the rate of deactivation of the catalysts decreased while the steady state production of methanol increased [72]. It was thought that increasing the flow reduced the concentration of product molecules in contact with the catalyst [72]. Hence, impurities in the product stream such as carbon dioxide or water were less likely to poison the catalyst. However, the poisoning effect of the product methanol was never considered in great detail. From the study of the properties of cerium hydride, it is clear that methanol contributed to the deactivation of the alloy catalysts.

Although cerium hydride is unsuitable for catalysis of methanol reactions, research continues into the area of cerium and copper containing catalysts for methanol synthesis. Sakata *et al* [86] produced copper/lanthanide mixed oxide catalysts which were able to produce methanol from carbon monoxide and hydrogen. The catalytic activity was attributed to the fine lanthanide oxide particles homogeneously dispersed in copper metal [86]. During the initial stages of reaction in a hydrogen/carbon monoxide mixture, carbon dioxide and methane were produced. The promotion effect of the lanthanide was dependent upon a number of factors including: preparation conditions, precursor, loading, catalyst pre-treatment and reaction conditions. Although catalysts containing cerium hydride are unlikely to become industrially viable for methanol catalysis, research continues into the use of copper and lanthanide mixed oxides. This includes the use of co-precipitated ceria-supported copper catalysts as methanol synthesis catalysts [84].

Reaction with Propyne

From fresh samples of cerium metal and the copper/cerium metal mixture the hydride was prepared and deuterium exchanged with the hydride hydrogen. However, less hydrogen was adsorbed than previous reactions. Table 3.3.7 shows that the hydrides had the formula $CeH_{0.01}$ and $CuCeH_{0.05}$. No difference was observed between the hydrogen adsorption values for the initial cerium and copper/cerium samples. The fresh samples revealed that cerium absorbed most of the hydrogen and was unaffected by addition of copper. Under the conditions used it is likely that the species formed was cerium hydride in both samples, even though the concentration of absorbed hydrogen was reduced. Literature has shown that the formation of copper hydride [220] requires

high-pressure synthesis and a high pressure of hydrogen to maintain the hydride as it is strongly thermodynamically unstable.

Table 3.3.7. Reaction of hydrogen and deuterium with cerium and copper-cerium metal mixtures.

Sample	*H_2 Absorbed (μmol)*	*Pulse*	*Deuterium Conversion (%)*	*Ratio*		
				D_2	*DH*	*H_2*
$CeH_{0.01}$	20.4	1	97.0	1	23	24
	-	2	96.9	1	21	17
$CuCeH_{0.05}$	83.5	1	65.9	1	2.2	1
	-	2	65.9	1	2	0.6

The percentage of deuterium exchanged had also fallen from previous experiments. This was most likely due to the cerium metal aging over time. Another possible reason for the deterioration in the absorption of hydrogen by the sample was that the glove box required regeneration; hence it would have contained higher concentrations of water and oxygen vapour than when the initial study was carried out. Although the samples had adsorbed less hydrogen they were still able to exchange hydrogen hence, they were used to examine the reaction of propyne with the cerium hydride.

When an inert carrier gas was used no reaction or adsorption was observed. However by changing to a reducing flow, hydrogenation products were observed. Figures 3.3.3 and 3.3.4 show the production of propane and propene from a series of propyne pulses. The cerium hydride reaction (fig. 3.3.3) shows a rapid decrease in alkane production with a slight increase in propene yield. Table 3.3.8 reveals that as the reaction progresses the hydrogenated products favour alkene formation.

Figure 3.3.3. Conversion and yield of products during propyne hydrogenation with cerium hydride.

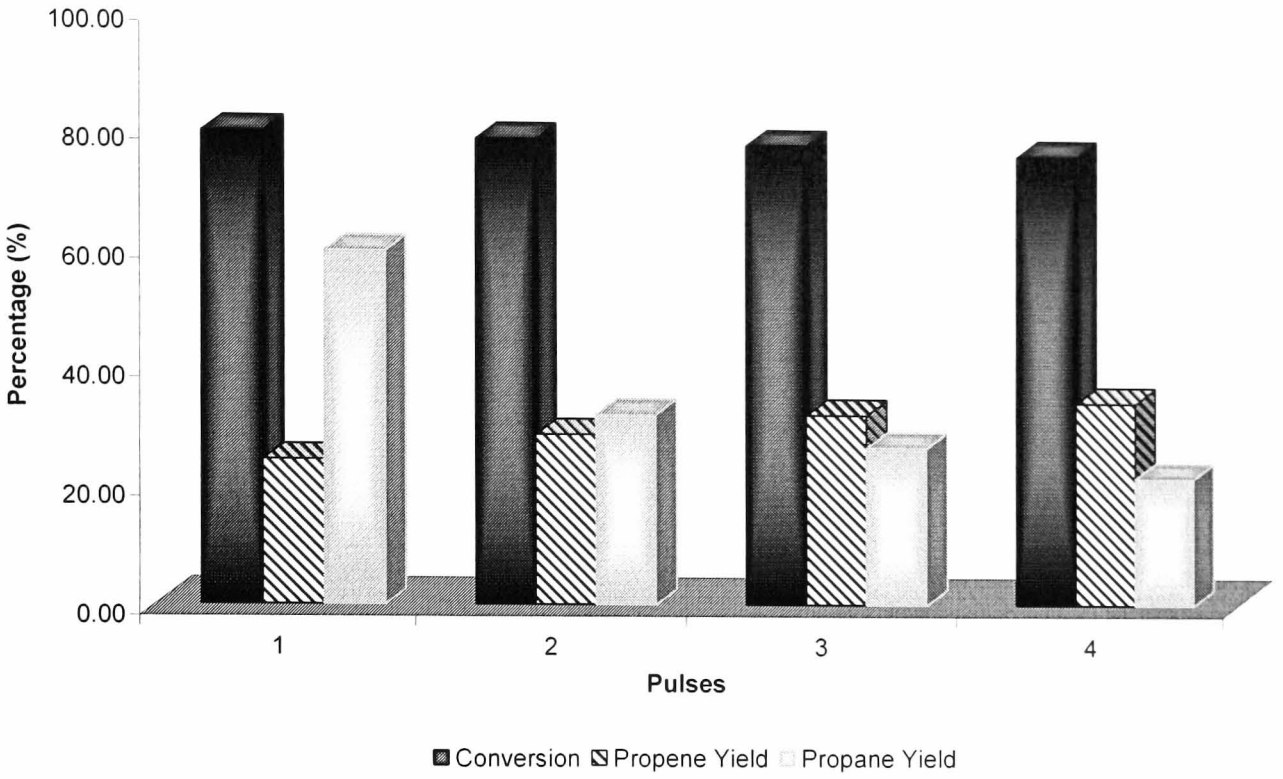

Table 3.3.8. Yield and selectivity of the reaction of propyne and hydrogen with cerium hydride.

Pulse	*Conversion (%)*	*Yield (%)*		*Selectivity (%)*		*Ratio* $C_3H_6/(C_3H_8+C_3H_6)$
		Propene	*Propane*	*Propene*	*Propane*	
1	80.8	23.0	56.3	28.5	69.7	0.3
2	80.0	27.2	30.4	33.9	37.9	0.5
3	79.2	30.4	25.2	38.4	31.8	0.5
4	77.7	32.4	20.5	41.7	26.4	0.6

On addition of copper to the cerium hydride, the propyne conversion increased to 100%. The yield of propene and propane altered, forming less propene while the yield of propane decreased less rapidly than for the cerium hydride catalyst.

Figure 3.3.4. Conversion and yield of products during propyne hydrogenation with copper and cerium hydride.

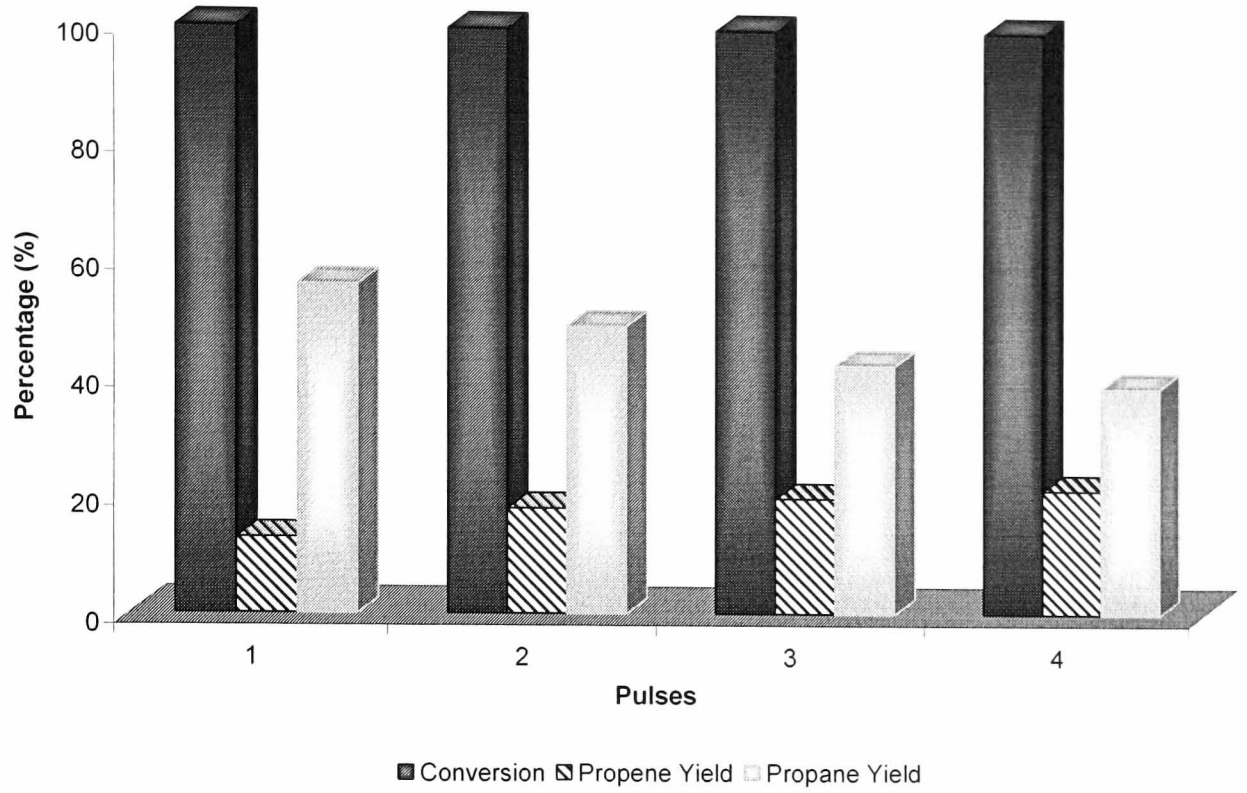

Table 3.3.9. Yield and selectivity of the reaction of propyne and hydrogen with copper and cerium hydride.

Pulse	*Conversion (%)*	*Yield (%)*		*Selectivity (%)*		*Ratio*
		Propene	*Propane*	*Propene*	*Propane*	$C_3H_6/(C_3H_8+C_3H_6)$
1	100.0	12.8	56.2	12.8	56.2	0.2
2	100.0	17.9	49.2	17.9	49.2	0.3
3	100.0	19.6	42.6	19.6	42.6	0.3
4	100.0	21.2	39.0	21.2	39.0	0.4

The carbon mass balance was calculated for both samples during the first four pulses of propyne in hydrogen, table 3.3.10. During the propyne hydrogenation reaction, carbon was deposited onto the $CeH_{0.01}$ and $CuCeH_{0.05}$. The loss of carbon would eventually cause a decrease in hydrogenation activity, which was reflected in the decreasing yield of propane.

Table 3.3.10. Carbon mass balance for each pulse during reaction with cerium hydride or copper and cerium hydride.

Carbon Mass Balance (%)	
Cerium Hydride	*Copper and Cerium Hydride*
100.5	67.3
82.4	68.2
84.6	65.8
86.5	66.4

The formation of hydrogenation products from the propyne reactions confirmed that cerium hydride could be utilised as a hydrogenation catalyst. However, the surface hydrogen was insufficient to carry out the reaction. Thermodynamically the reaction of propyne with cerium hydride to form propene or propane was not favoured:

$CeH_2 + CH_3CCH \longrightarrow Ce + CH_3CHCH_2$ $\Delta G^\circ = 75.1\ kJmol^{-1}$ $\Delta H^\circ = 80.8\ kJmol^{-1}$

$2CeH_2 + CH_3CCH \longrightarrow 2Ce + CH_3CH_2CH_3$ $\Delta G^\circ = 104.6\ kJmol^{-1}$ $\Delta H^\circ = 120.8\ kJmol^{-1}$

On addition of hydrogen to the reaction, the hydrogenation of propyne was thermodynamically favoured:

$H_2 + CH_3CCH \longrightarrow CH_3CHCH_2$ $\Delta G^\circ = -131.8\ kJmol^{-1}$ $\Delta H^\circ = -165.2\ kJmol^{-1}$

$2H_2 + CH_3CCH \longrightarrow CH_3CH_2CH_3$ $\Delta G^\circ = -218.1\ kJmol^{-1}$ $\Delta H^\circ = -289.5\ kJmol^{-1}$

As reference pulses did not contain alkene or alkane products, it was clear that although thermodynamically favourable the reaction did not proceed in the absence of a catalyst. This confirmed that unlike the reaction with methanol, which reacted stoichiometrically with the hydride, the cerium hydride behaved catalytically during propyne hydrogenation.

3.3.3 Supported Cerium Hydride

Attempts were made to improve the stability of the hydride by adding it to a silica support. The cerium metal was mechanically mixed with 5Cu/silica (wet

impregnation). The aim was to produce a more robust cerium hydride, which would be in close contact with small highly dispersed copper particles.

Hydride Formation

The temperature of the cerium metal and 5Cu/silica mixture was continually 15 to 25 K higher than the programmed temperature while heating in an argon flow. This would indicate that an exothermic reaction such as that of cerium with oxygen/water had occurred resulting in a net temperature gain. After heating, the cerium metal had changed colour and a yellow residue was present, which was attributed to the formation of ceria. Pulses of hydrogen were passed across the sample and only 2.6 μmol of hydrogen were adsorbed. Hence, it is unlikely that cerium hydride was formed.

By adding 5Cu/silica to the cerium metal the adsorption of hydrogen was greatly reduced. The results suggest that during heating in argon the sample was able to self-reduce. As the copper/silica catalyst was only dried to 333 K it would still have contained water, which may have initiated the following reaction during heating:

$$2Ce + 3H_2O \longrightarrow Ce_2O_3 + 6H_2 \qquad \Delta G^o_r = -1112 \text{ kJ mol}^{-1}$$
$$\Delta H^o_r = -939 \text{ kJ mol}^{-1}$$

The hydrogen produced then reduced the supported copper particles. Hence, the final compound contained reduced copper, supported on silica, doped with cerium oxide.

Reaction with Methanol

After attempting to form a hydride using hydrogen pulses, the sample was reacted with pulses of methanol in a helium carrier gas. Although very little hydrogen appeared to have been adsorbed by the sample, the resulting compound proved relatively active for methanol decomposition. Figures 3.3.5 and 3.3.6 show the yield of products formed by the 5Cu/silica and the Ce metal and 5Cu/silica mixture at 523 K.

Figure 3.3.5. Yield of products from methanol decomposition with 5Cu/Silica catalyst.

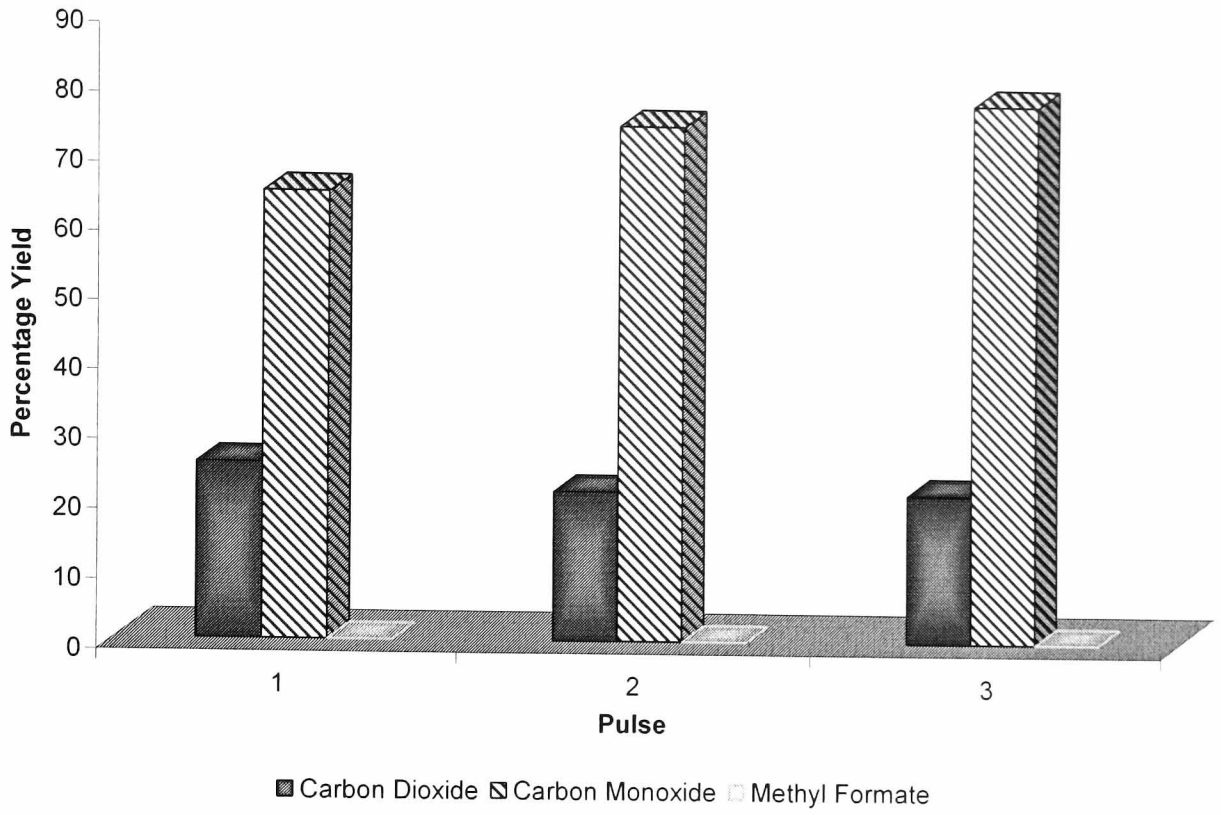

Table 3.3.11. Conversion and yield of products from methanol decomposition reaction with 5Cu/silica catalyst.

Pulse	*Conversion (%)*	*Yield (%)*	
		CO_2	CO
1	100.0	25.2	64.5
2	100.0	21.5	74.7
3	100.0	21.5	78.5

Fig. 3.3.5 shows that the predominant product of methanol decomposition at 523 K was carbon monoxide from 5Cu/silica. The decomposition products of both catalysts were similar, however the catalyst, which initially contained cerium metal, was less active than 5Cu/silica. More of the carbon species was retained by the sample containing the cerium metal. Initially, the activity of the cerium and 5Cu/silica catalyst was low, but increased over successive pulses.

Figure 3.3.6. Yield of products from methanol decomposition with 5Cu/silica and cerium metal mixture.

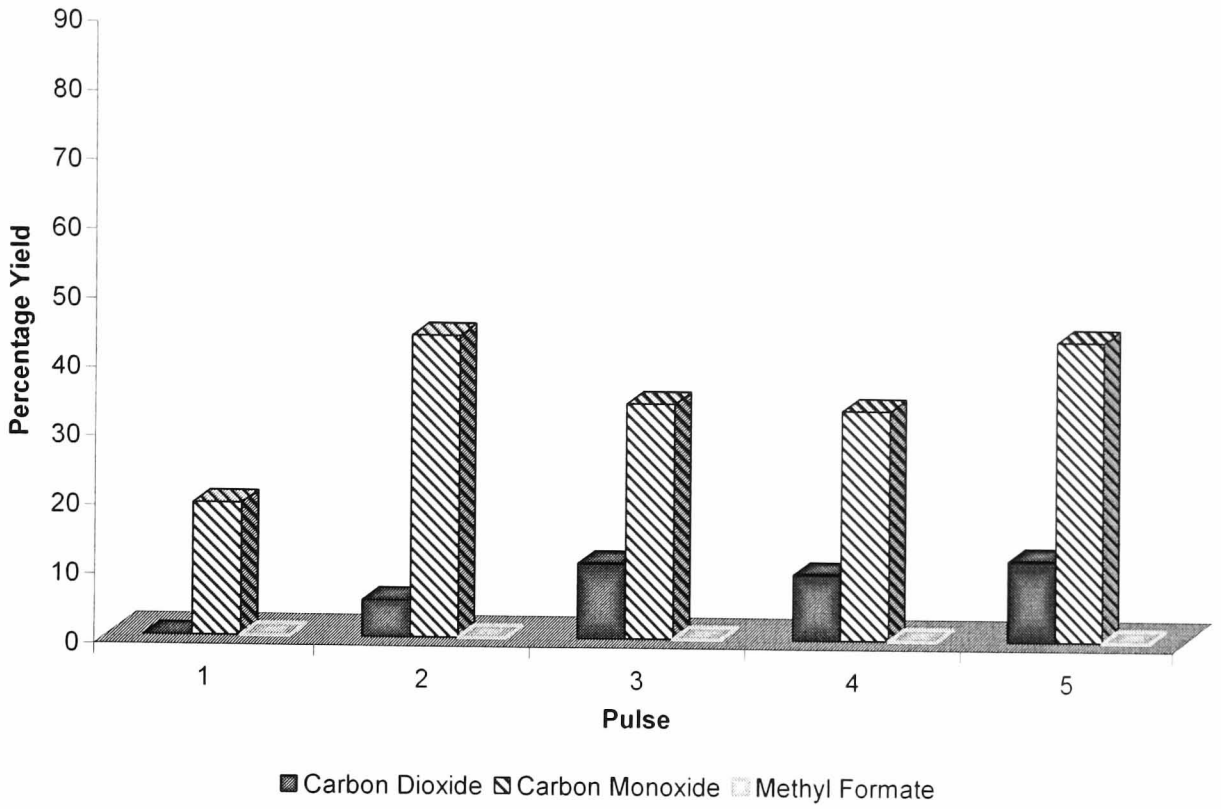

Table 3.3.12. Conversion and yield of products from methanol decomposition reaction with 5Cu/silica and cerium metal mixture.

Pulse	*Conversion (%)*	*Yield (%)*	
		CO_2	CO
1	100.0	0.0	19.2
2	100.0	5.3	44.1
3	100.0	10.9	34.3
4	100.0	9.6	33.6
5	100.0	11.8	44.2

The carbon mass balance for the reaction containing cerium metal was lower than that for 5Cu/silica. This may have been due to the presence of ceria, which is able to adsorb carbon oxides to form carbonate like species [201].

Although this attempt was unsuccessful, it may be possible to use supports free from hydroxyl groups to support cerium hydride. Treatment of silica at high temperatures (>1000 K) dehydroxylates the silica surface [27]. However, as cerium hydride has proven itself highly reactive with oxygen containing compounds, this method may also prove unsuccessful.

However, there are several reports of attempts to support metal hydrides on silica through novel routes. A metal hydride has been successfully supported in a silica matrix [226]. Advantages of this were that metal hydride fines were trapped in the silica pores and small pores prevented impurities reaching the hydride. The hydride/silica was able to withstand many adsorption/desorption cycles. Hence, the material was suitable for use in hydrogen separation columns.

A novel preparation was used to investigate Ln/SiO_2 [227, 228] and Ln/Pd/support [229, 230] catalysts prepared using Eu or Yb metals dissolved in liquid ammonia. The catalysts were sensitive to air once prepared and showed surprising hydrogen uptake during reaction. The prepared catalysts were active as hydrogenation catalysts [230]. Although a similar preparation could have been utilised in an attempt to support the cerium hydride, in the long term the method would still create problems with catalyst handling.

3.4 Effect of Copper and Cerium on Water Gas Shift Reaction

A representative selection of the catalysts examined for methanol decomposition was studied for use in the water gas shift reaction. The nine catalysts chosen for testing were: 5Cu/silica, 5Cu5Ce/silica, 10Cu5Ce0.05Pd/silica, 5Cu1Ce/silica, 5Ce/silica, 5Cu/alumina, 5Cu5Ce/alumina, 5Ce/alumina and a commercial methanol synthesis catalyst.

3.4.1 Water Gas Shift Reaction

Carbon monoxide and water (2:1 ratio) pulses were passed over the catalysts to examine their activity. Figure 3.4.1 shows the carbon monoxide conversion over the silica-supported catalysts. The graph shows that conversion was highest for catalysts containing a mixture of copper and cerium. Although carbon monoxide was converted by 5Cu/silica its conversion was greatly enhanced by the presence of cerium in the catalysts.

Figure 3.4.1. Carbon monoxide conversion during shift reaction – silica catalysts.

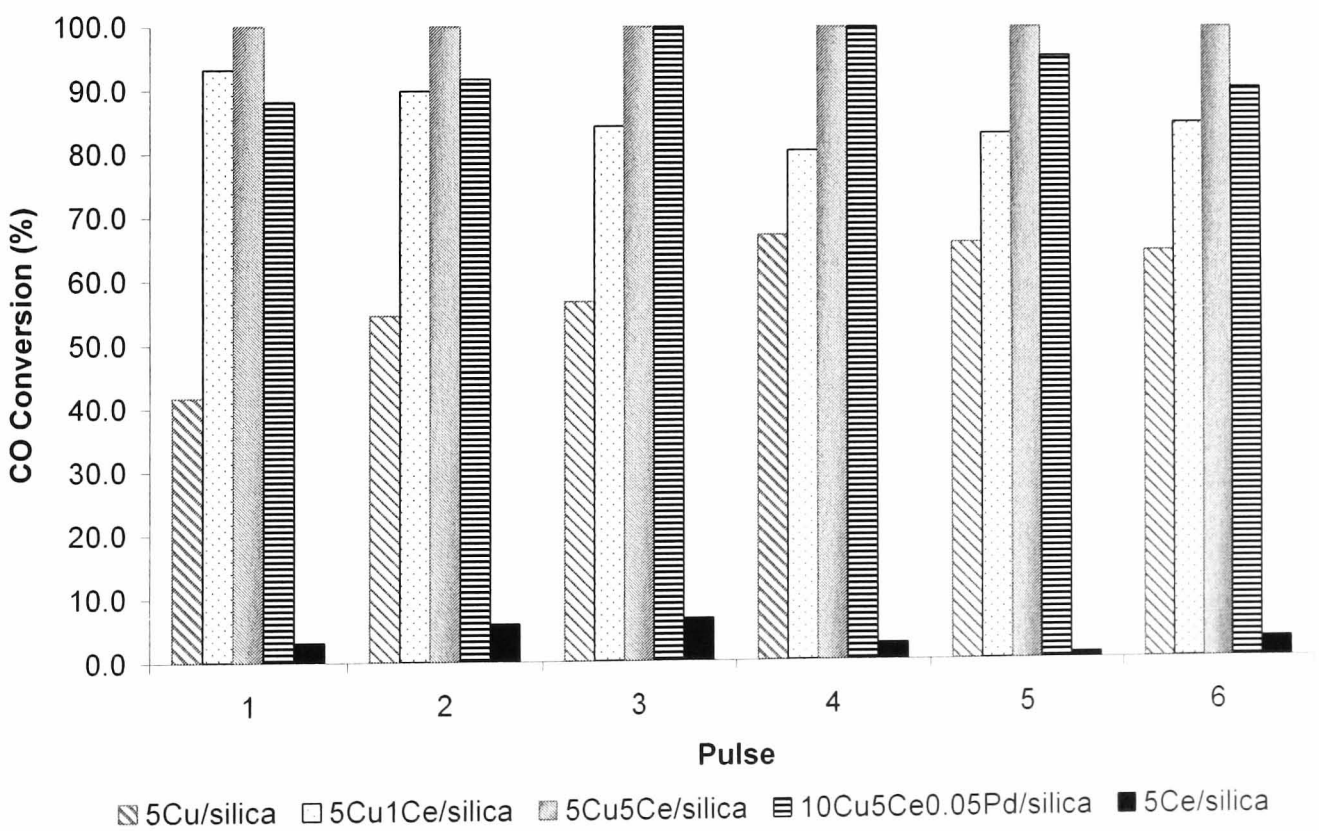

Carbon monoxide conversion by 5Ce/alumina was low, figure 3.4.2. The commercial and mixed metal catalysts gave the highest conversion. For both the 5% copper

catalysts (5Cu/silica and 5Cu/alumina) conversion was less than 60%. The difference in support had little effect on the catalysts ability to convert carbon monoxide and neither 5Ce/silica nor 5Ce/alumina reached an average conversion greater than 10%.

Figure 3.4.2. Carbon monoxide conversion during shift reaction – alumina and commercial catalysts.

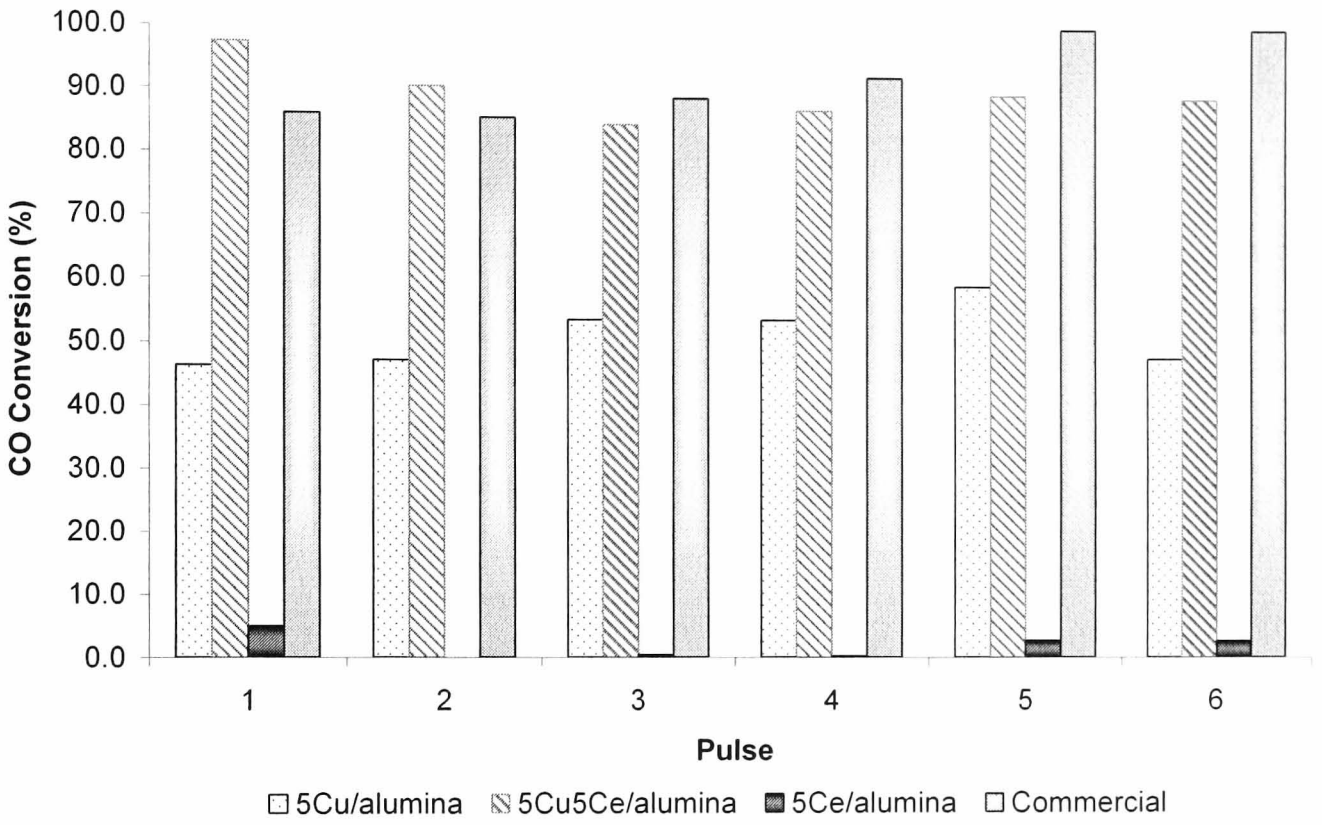

The reactants of the water gas shift reaction are a 1:1 mixture of carbon monoxide to water:

$$CO + H_2O \longrightarrow CO_2 + H_2$$

As the reaction mixture in this study contained a 2 to 1 ratio of carbon monoxide to water, the highest conversion of carbon monoxide should be 50%. For carbon monoxide conversions above 50% there must be alternative reactions taking place. There are two possible reasons for the high carbon monoxide conversion, either carbon monoxide was adsorbed onto the catalyst surface or surface oxygen was removed from the catalyst to form carbon dioxide.

During the shift reaction, hydrogen would have been produced from the reaction mixture; however difficulties were encountered on trying to verify the quantity of hydrogen produced. Gas chromatography could not be used, as the carrier gas (helium)

and the hydrogen produced had similar thermal conductivities. Mass spectrometry was explored as an alternative method for quantifying the hydrogen produced, however the values obtained were unreliable. Table 3.4.1 shows the catalysts, which produced hydrogen during reaction with the carbon monoxide and water pulses. The results showed that only the cerium/support catalysts did not produce hydrogen. Therefore, the shift reaction only occurred over catalysts, which contained copper.

Table 3.4.1. Hydrogen produced during reaction with shift mixture.

Catalyst	*Hydrogen Produced (✓/✗)*
5Cu/silica	✓
5Cu5Ce/silica	✓
5Cu1Ce/silica	✓
10Cu5Ce0.05Pd/silica	✓
5Ce/silica	✗
5Cu/alumina	✓
5Cu5Ce/alumina	✓
5Ce/alumina	✗
Commercial	✓

By making some basic assumptions, it is possible to deconvolute the carbon monoxide conversion into its component parts. The possible reactions from a water gas shift mixture are as follows (s – denotes surface species):

$CO\ (g) + H_2O\ (g) \longrightarrow CO_2\ (g) + H_2\ (g)$ - Water gas shift reaction

$CO\ (g) + O_S \longrightarrow CO_2\ (g)$ - Carbon monoxide oxidation

$CO\ (g) \longrightarrow (CO)_S$ - Adsorption of carbon monoxide

$H_2O\ (g) \longrightarrow (H_2O)_S$ - Adsorption of water

The component of carbon monoxide used in the shift reaction was calculated by assuming that if the catalyst produced hydrogen then all of the water that reacted was utilised in the shift reaction. It was deduced that the carbon dioxide not formed as a result of the shift reaction was due to removal of surface oxygen (i.e. carbon monoxide oxidation). In the case where hydrogen was not produced, it was assumed that the carbon monoxide which was reacted was either adsorbed onto the surface, or reacted

with surface oxygen to form carbon dioxide. The average values for the six pulses over each catalyst are shown in figure 3.4.3 and table 3.4.2.

Figure 3.4.3. Uses of carbon monoxide during reaction of catalyst with shift mixture.

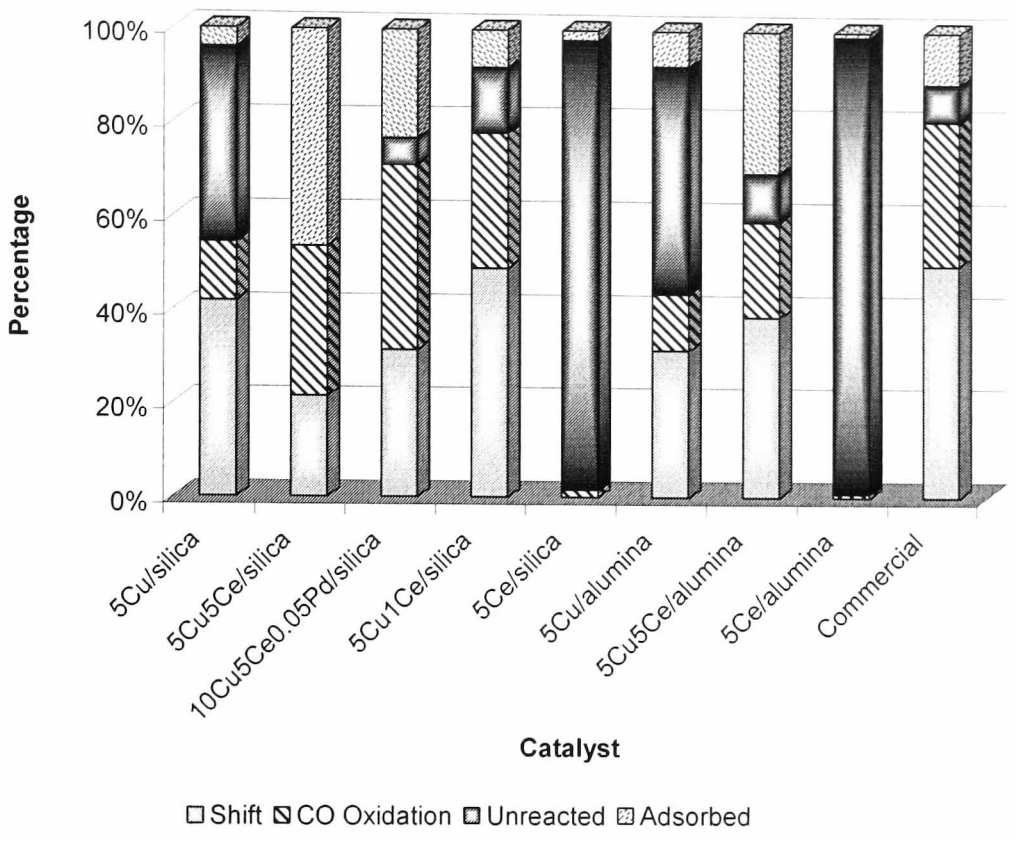

Table 3.4.2. Uses of carbon monoxide during reaction of catalyst with shift mixture.

Catalyst	*Uses of Carbon Monoxide (%)*			
	Shift	*Oxidised*	*Unreacted*	*Adsorbed*
5Cu/silica	41.8	12.5	41.6	4.0
5Cu5Ce/silica	21.5	32.1	0.0	46.4
10Cu5Ce0.05Pd/silica	31.4	39.5	5.7	23.3
5Cu1Ce/silica	49.0	28.8	14.1	8.1
5Ce/silica	0.0	1.6	96.4	2.1
5Cu/alumina	31.5	12.1	48.8	7.6
5Cu5Ce/alumina	38.7	20.4	10.4	30.4
5Ce/alumina	0.0	0.8	98.2	1.0
Commercial	50.0	30.9	7.9	11.1

Table 3.4.2 and figure 3.4.3 show that the catalysts, which utilised the greatest percentage of carbon monoxide in the shift reaction, were 5Cu/silica, 5Cu1Ce/silica, 5Cu5Ce/alumina and the commercial methanol synthesis catalyst. Addition of cerium to copper/support catalysts increased both the adsorption and oxidation of carbon monoxide. By decreasing the loading of cerium from 5 to 1 % there was less carbon

monoxide adsorption and more shift reaction. When the carbon monoxide and water mixture was pulsed over the Ce/support catalysts, they were relatively inactive.

3.4.1.1 Cerium/Support Catalysts

The products of the water gas shift reaction for 5Ce/silica are shown in figure 3.4.4. The figure shows that production of carbon dioxide was minimal and that only a small quantity of carbon monoxide actually reacted. Conversion of carbon monoxide was close to zero over each pulse (table 3.4.3), whereas the conversion of water increased to more than 90% during the reaction. From the carbon mass balance, adsorption of carbon species did not occur, however a consistent loss of oxygen was observed over the pulses due to adsorption of water.

Figure 3.4.4. Shift reaction products for 5Ce/silica.

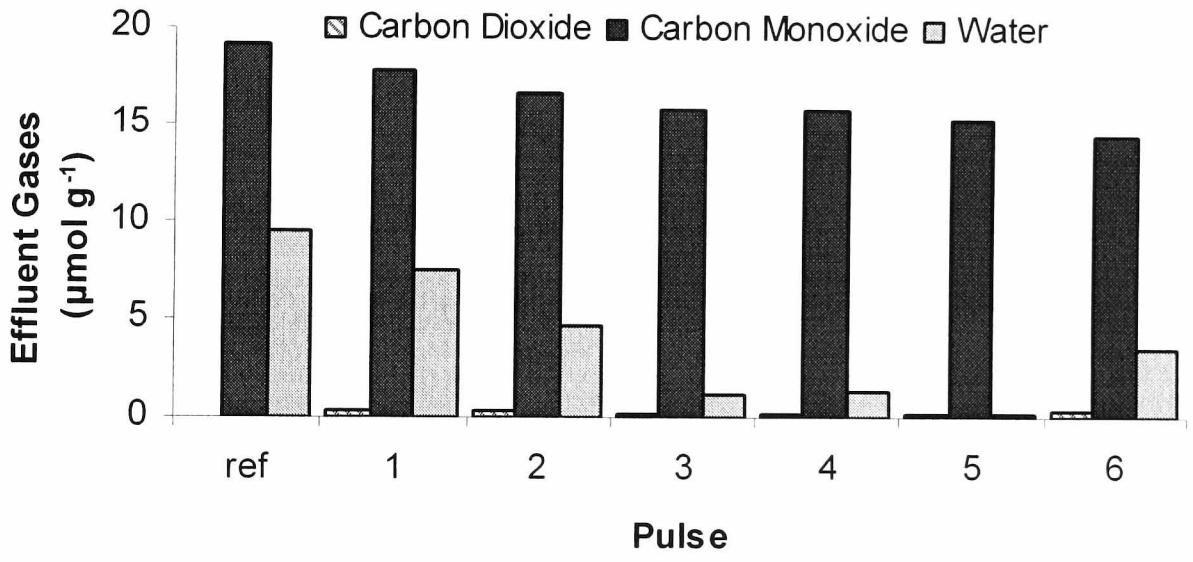

Table 3.4.3. Percentage of carbon and oxygen recovered across each pulse and conversion of reactants – 5Ce/silica.

Pulse	Conversion (%)		Mass Balance (%)		Effluent Gases (µmol $g_{catalyst}^{-1}$)		
	Carbon Monoxide	Water	Carbon	Oxygen	Carbon Dioxide	Carbon Monoxide	Water
1	3.0	18.8	98.9	94.3	0.4	17.9	7.5
2	5.9	47.1	95.8	82.7	0.3	16.6	4.7
3	6.6	86.6	94.7	68.4	0.2	15.8	1.1
4	2.5	82.9	98.8	72.4	0.2	15.8	1.4
5	0.8	98.2	100.0	67.8	0.1	15.4	0.1
6	3.0	54.3	99.2	82.9	0.3	14.6	3.4

By looking at the separate uses of carbon monoxide from the mixture, more information was determined regarding the reactivity of the catalysts. As hydrogen was not produced from the pulses of water and carbon monoxide (table 3.4.1) the reactions that took place were carbon monoxide oxidation/adsorption and adsorption of water (figure 3.4.5). Formation of carbon dioxide was due to the reaction of carbon monoxide with surface oxygen. The majority of carbon monoxide was unreactive, with only 4 μmol $g_{catalyst}^{-1}$ of oxygen removed from the catalyst surface to produce carbon dioxide.

Figure 3.4.5. Separation of carbon monoxide uses for 5Ce/silica.

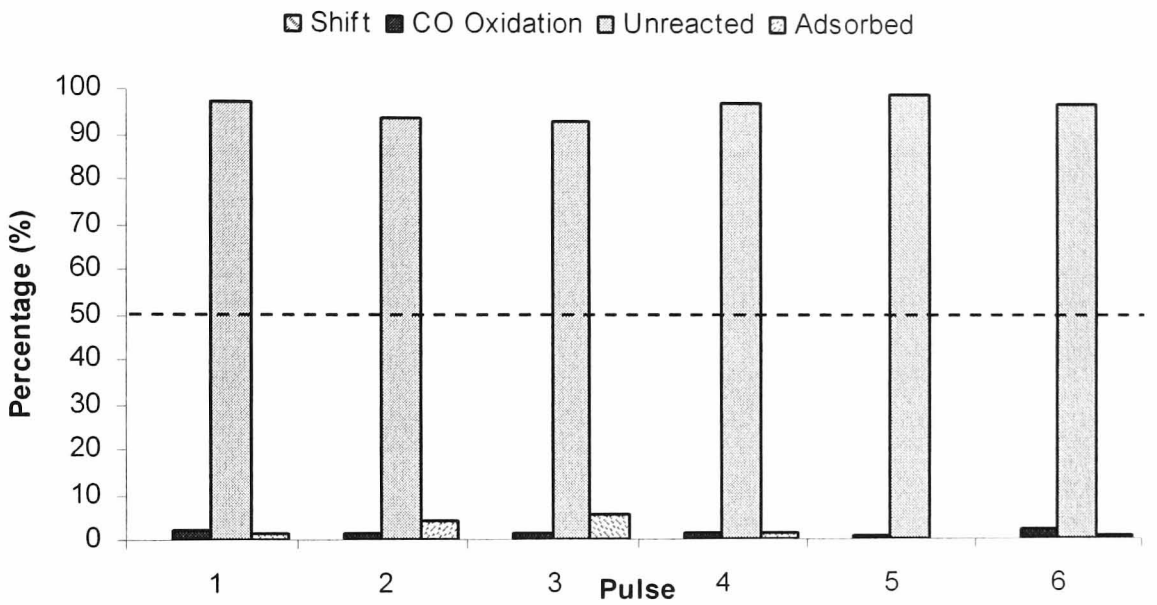

Similar results were observed over 5Ce/alumina (figure 3.4.6 and Table 3.4.4). However, as well as recovering all of the carbon monoxide over each pulse more water was recovered than with 5Ce/silica.

Figure 3.4.6. Shift reaction products for 5Ce/alumina.

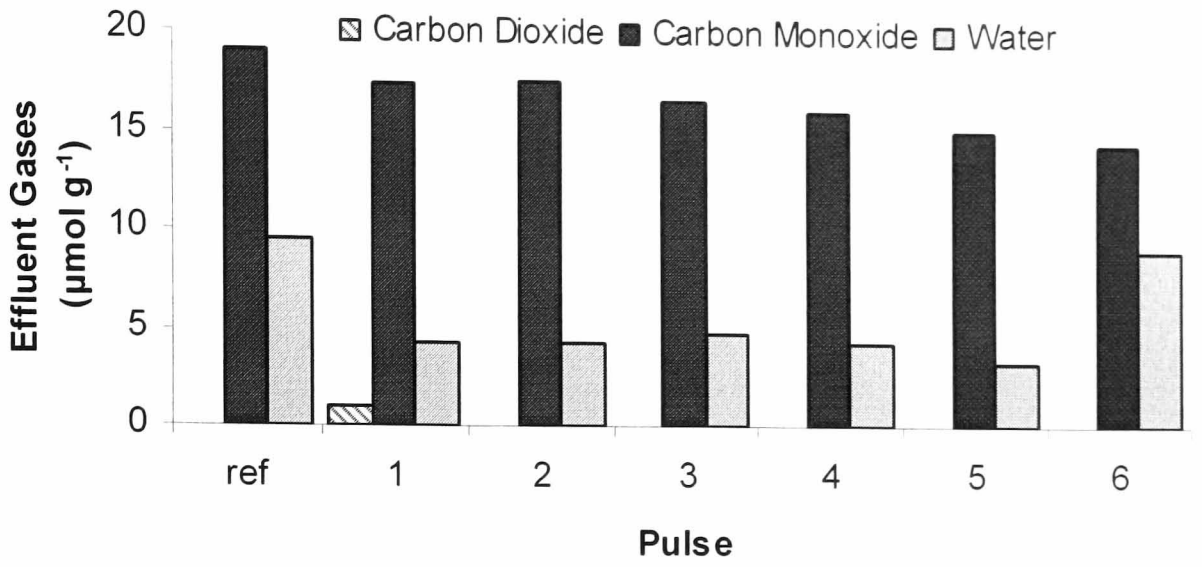

Table 3.4.4. Percentage of carbon and oxygen recovered across each pulse and conversion of reactants – 5Ce/alumina.

Pulse	*Conversion (%)*		*Mass Balance (%)*		*Effluent Gases (µmol gcatalyst^{-1})*		
	Carbon Monoxide	*Water*	*Carbon*	*Oxygen*	*Carbon Dioxide*	*Carbon Monoxide*	*Water*
1	5.0	54.2	100.0	85.2	0.9	17.4	4.2
2	0.0	52.1	100.0	82.6	0.0	17.6	4.2
3	0.4	42.4	99.6	85.6	0.0	16.5	4.8
4	0.2	47.2	99.8	84.2	0.0	16.1	4.3
5	2.7	57.0	97.3	79.2	0.0	15.1	3.3
6	2.6	-22.2	97.4	105.6	0.0	14.5	9.1

5Ce/alumina only produced carbon dioxide in the first pulse. From subsequent pulses unreacted carbon monoxide and water were detected. As for the 5Ce/silica catalyst, 5Ce/alumina was relatively unreactive towards the shift mixture. In the presence of water the carbon monoxide did not greatly improve the reduction of the CeO_2 on the catalyst surface. The main difference observed between the two catalysts was that 5Ce/alumina adsorbed less water, particularly in latter pulses. During the final pulse, more water was produced than that which was present in the reactants. It is possible that excess water was displaced from the surface during later pulses.

Figure 3.4.7. Separation of carbon monoxide uses for 5Ce/alumina.

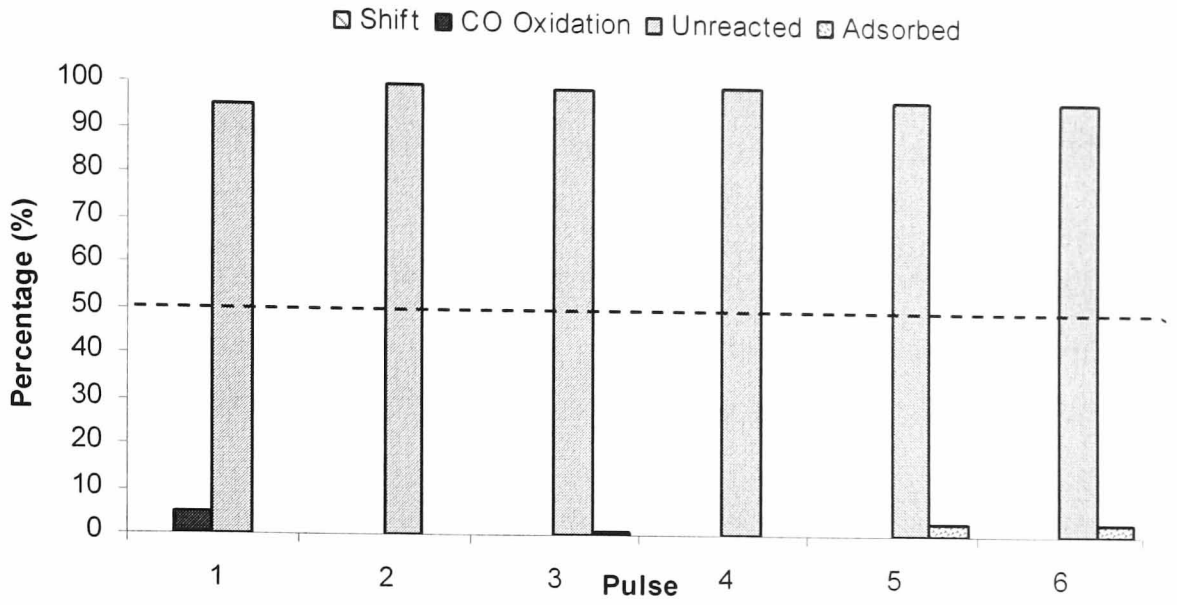

Characterisation of the Ce/support catalysts suggested that CeO_2 was present on the surface of the catalysts after reduction (TPR profiles, section 3.1.8). It was unlikely that reduced ceria was present, as the TPR of the catalysts showed that surface reduction did not begin until ~660 K (section 3.1.8). Although carbon monoxide is reportedly a better reducing agent for ceria [30, 35] conversion of carbon monoxide was very low. Literature reports that reduction of ceria by carbon monoxide can begin at temperatures as low as room temperature [35]. However thermodynamically, reduction of ceria by carbon monoxide is not favoured at 298 K and is an endothermic reaction.

$$2CeO_2 + CO \longrightarrow Ce_2O_3 + CO_2 \qquad \Delta H^\circ = 86.4\ kJmol^{-1}$$

$$\Delta G^\circ\ (298\ K) = 73.9\ kJmol^{-1}$$

Hence, it was unlikely that the supported ceria was reduced to Ce_2O_3. Reduction of CeO_2 by carbon monoxide is strongly dependent upon the textural and morphological properties of the ceria [231]. The more perfect the CeO_2 lattice, the more difficult it is to reduce [231]. Crystalline CeO_2 was the major crystalline phase detected by XRD of the unreduced Ce/alumina and post-reaction Ce/silica and Ce/alumina catalysts (section 3.1.6). Therefore, the cerium (IV) oxide present on the catalyst was not reduced by carbon monoxide in the presence of water.

Absence of reduced cerium oxide was reinforced by the fact that Ce^{3+} is able to adsorb carbon monoxide strongly [232]. In addition, literature reports that partially reduced

ceria samples can be utilised for the shift reaction [233]. Therefore, the cerium was in the Ce^{4+} oxidation state as little adsorption/reaction of carbon monoxide was detected. Literature reports suggest that carbon monoxide can be adsorbed by unreduced ceria to form bidentate carbonates at room temperature and polydentate species at higher temperatures [201]. However, the carbon mass balance for 5Ce/silica and 5Ce/alumina indicated that very little adsorption of carbon monoxide occurred. It was proposed that water forms surface hydroxy groups when adsorbed on unreduced ceria [201]. This is caused by dissociation of water on $Ce^{4+}O^{2-}$ sites to form two adsorbed hydroxy species [201]. The nature of the two different supports is also likely to influence the activity of the Ce/support catalysts. Hence, effects such as the differences in adsorption of water are probably due to the variations in the properties of the supports, as well as the differences in ceria dispersion on the supports.

3.4.1.2 Copper Catalysts

The 5Cu/silica and 5Cu/alumina catalysts produced a mixture of carbon monoxide, carbon dioxide and water on reaction with the water/carbon monoxide pulse (figures 4.5 and 4.6). Total conversion of carbon did not reach above 60 %. The oxygen mass balance was greater than the carbon mass balance, suggesting that either removal of oxygen from the surface of the catalyst had occurred or that carbon rich species were being adsorbed onto the catalyst surface.

Figure 3.4.8. Shift reaction products for 5Cu/silica.

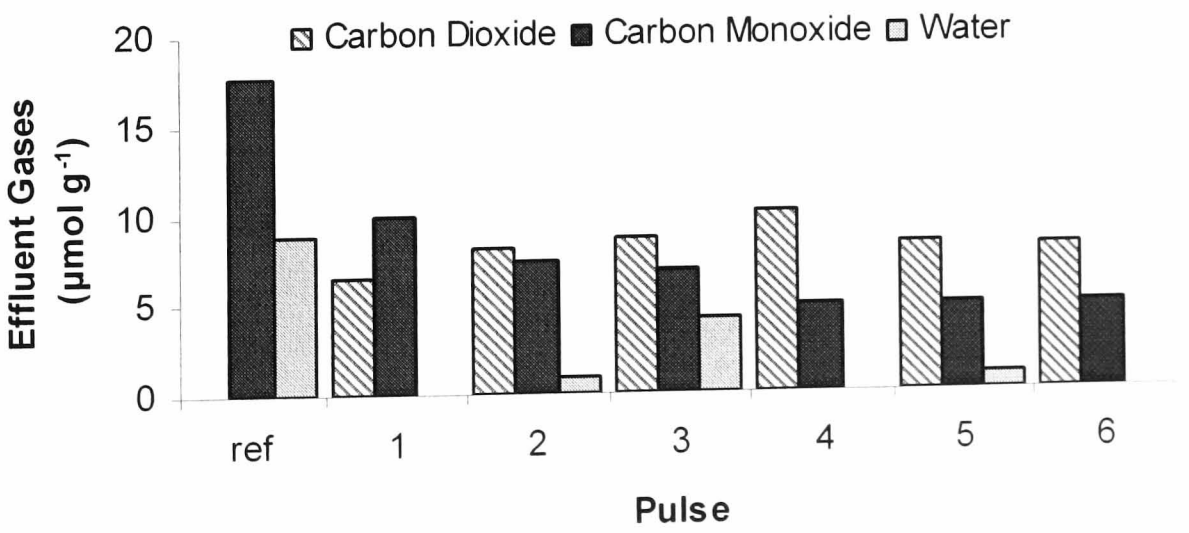

Table 3.4.5. Percentage of carbon and oxygen recovered across each pulse and conversion of reactants – 5Cu/silica.

Pulse	Conversion (%)		Mass Balance (%)		Effluent Gases (μmol gcatalyst^{-1}))		
	Carbon Monoxide	Water	Carbon	Oxygen	Carbon Dioxide	Carbon Monoxide	Water
1	41.6	100.0	96.8	90.2	6.5	9.9	0.0
2	54.5	89.8	95.4	100.3	8.1	7.4	0.8
3	56.6	47.9	98.8	120.2	8.7	6.8	4.1
4	67.1	100.0	100.0	111.4	10.1	4.9	0.0
5	65.8	87.3	91.5	103.4	8.3	4.9	0.9
6	64.4	100.0	93.7	101.1	8.0	4.9	0.0

Figure 3.4.9 shows that very little of the carbon monoxide was adsorbed. Hence, the high oxygen mass balance was due to removal of oxygen from the catalyst surface via carbon monoxide oxidation. Levels of carbon monoxide oxidation reach a maximum on the third pulse, and selectivity to the shift reaction reaches its peak on the following pulse. The decreasing trend in carbon monoxide oxidation towards the end of the reaction might indicate that the removal of oxygen from the surface is a transient process. At the same time, adsorption of carbon monoxide was also beginning to decrease.

Figure 3.4.9. Separation of carbon monoxide uses for 5Cu/silica.

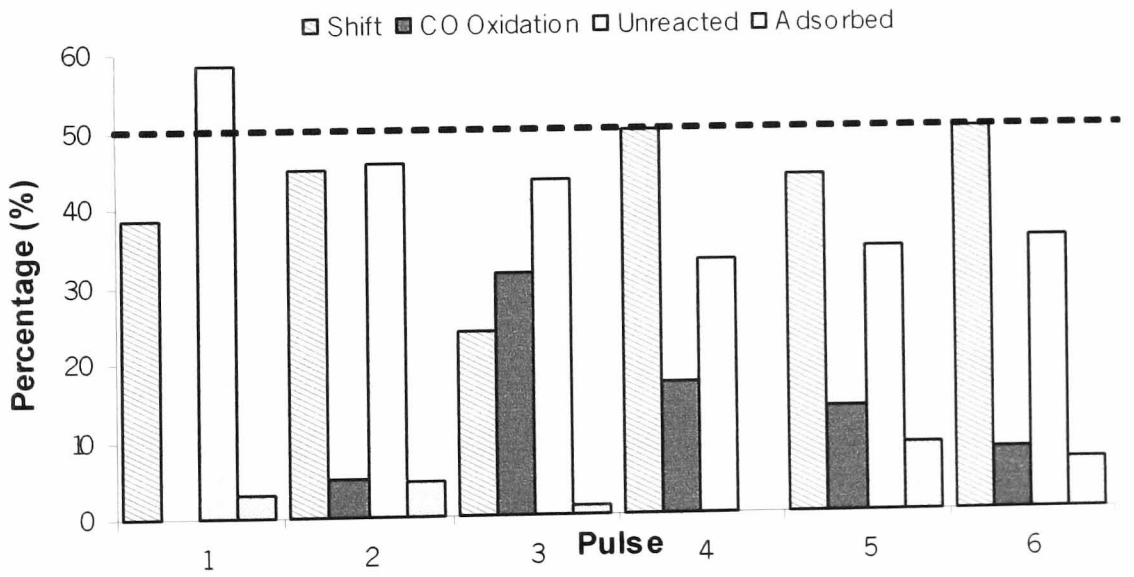

By changing the support, 5Cu/alumina showed an increase in unreacted carbon monoxide and water in the product gases. Conversion of the reactants was slightly

lower than for the 5Cu/silica catalyst; however the copper/support catalysts showed similar reactivity.

Figure 3.4.10. Shift reaction products for 5Cu/alumina.

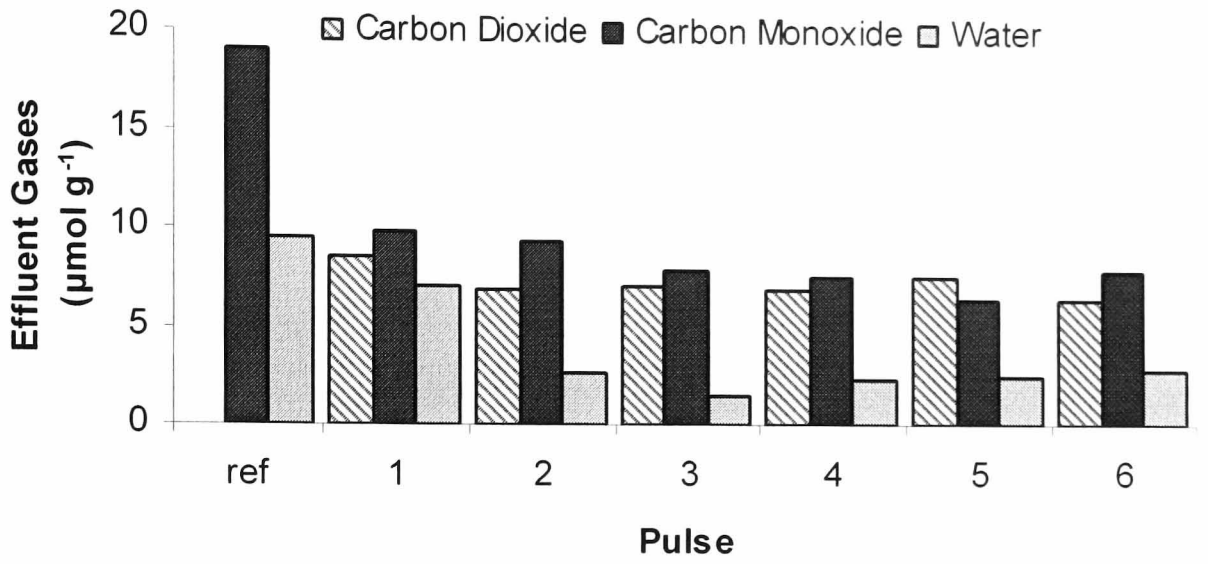

Table 3.4.6. Percentage of carbon and oxygen recovered across each pulse and conversion of reactants – 5Cu/alumina.

Pulse	*Conversion (%)*		*Mass Balance (%)*		*Effluent Gases (µmol gcatalyst^{-1})*		
	Carbon Monoxide	*Water*	*Carbon*	*Oxygen*	*Carbon Dioxide*	*Carbon Monoxide*	*Water*
1	46.2	22.9	100.0	123.2	8.5	9.8	7.1
2	47.2	70.8	92.2	97.5	6.9	9.3	2.6
3	53.6	82.1	88.3	92.8	7.1	7.8	1.5
4	53.6	71.2	89.1	97.5	6.9	7.5	2.3
5	58.9	68.0	89.5	102.6	7.5	6.4	2.5
6	47.7	63.2	95.5	104.8	6.5	7.8	2.7

The main reaction observed over the 5Cu/alumina catalyst was the shift reaction. The conversion of carbon monoxide did not reach above 60%, with the main side reaction being carbon monoxide oxidation. Very little of the carbon species were adsorbed by the catalyst.

Figure 3.4.11. Separation of carbon monoxide uses for 5Cu/alumina

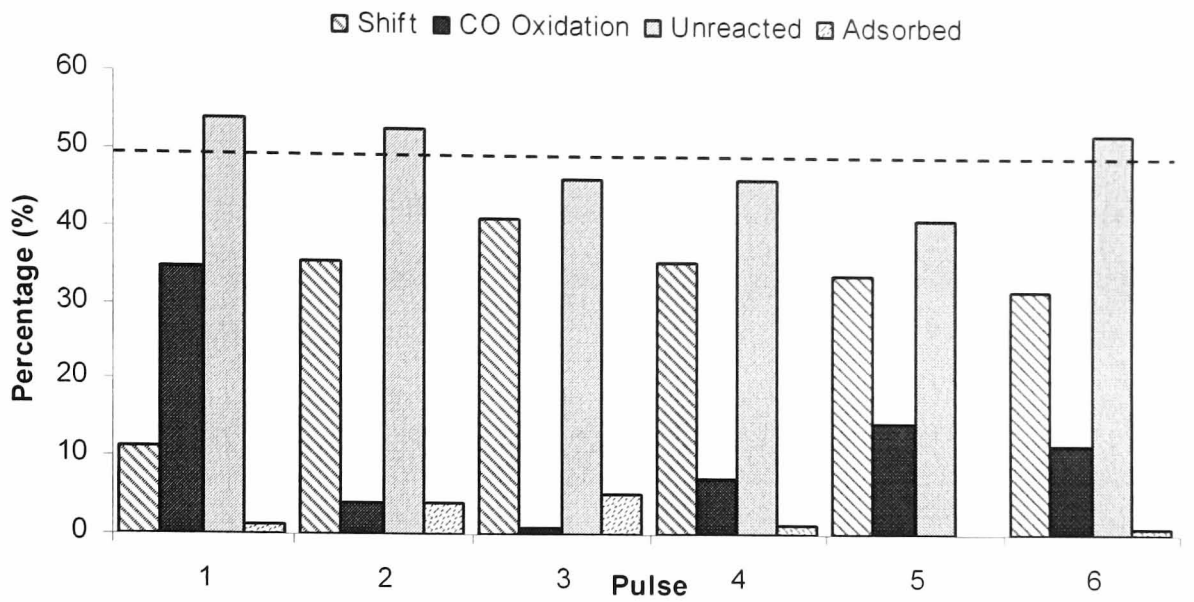

Conversion of carbon monoxide over 5Cu/silica was less than 60% and for 5Cu/alumina conversion was less than 50%. Conversion of water was higher across the silica-supported catalyst than the alumina supported catalyst. In contrast to 5Ce/silica the percentage of oxygen recovered after each pulse was higher than the percentage of carbon recovered for 5Ce/alumina. Hence, there was only a slight loss of carbon species to the catalyst surface and a gain in oxygen. The gain in oxygen may have been due to the presence of some unreduced copper on the catalyst, similarly to the methanol reactions (section 3.2.5). A methanol TPD study of CuO/Al_2O_3 catalysts showed that carbon dioxide and water could be formed as a result of oxidation by lattice oxygen of CuO [200]. The group detected a greater oxygen/carbon ratio in the products than reactants and this was attributed to oxygen extracted from CuO [200]. However, as temperature programmed reduction (TPR) shows T_{max} to be lower than 523 K for the 5% copper/support catalysts (section 3.1.8) the copper oxide present should have been fully reduced to copper metal after reduction to 523 K (section 2.5.1). Hence, the additional oxygen may have been due either to unreduced copper oxide or oxygen supplied by the support. *In-situ* Raman spectroscopy (section 3.1.2.7) showed that after reduction, the copper species present on the 5Cu/silica were reduced copper metal and Cu_2O.

$$Cu_2O + CO \longrightarrow 2Cu + CO_2 \qquad \Delta G° = -111\ kJmol^{-1}$$
$$\Delta H° = -114\ kJmol^{-1}$$

From the thermodynamic values, the reaction of copper (I) oxide with carbon monoxide to form copper and carbon dioxide was thermodynamically feasible. The shift reaction was studied over copper/silica catalysts using infrared studies [234]. Adsorption of carbon monoxide to form adsorbed carbonates was found to be an intermediate step in the shift reaction [234]. Millar and co-workers [234] also found that carbon monoxide reduced Cu^{+} sites to Cu^{0} (at 300 K). Hence, it was likely that any un-reduced copper oxide present on the Cu/support catalysts was further reduced by the excess carbon monoxide in the shift mixture.

Although there remain a number of authors who favour the formate mechanism [235-237] for the shift reaction, more recent work supports a redox mechanism [238, 239] over copper-based catalysts. However the results depend largely upon the composition of the catalyst examined and the reaction conditions chosen. One author [240] suggested that over copper/alumina catalysts the formate mechanism dominated for the reverse water gas shift reaction. This was also found for the reverse water gas shift mechanism on a copper/silica catalysts [241]. Hence, it was probable that the copper/support catalysts predominantly followed the formate mechanism for the forward water gas shift reaction.

3.4.1.3 Mixed Copper and Cerium Catalysts

The mixed loading copper and cerium catalysts (5Cu5Ce/silica, 5Cu1Ce/silica, 10Cu5Ce0.05Pd/silica and 5Cu5Ce/alumina) showed increased conversion of carbon monoxide when compared with either of the metals supported individually on silica or alumina. As conversion higher than 50% could not be attributed solely to the shift reaction, the excess carbon monoxide conversion was due to carbon monoxide adsorption and oxidation.

When compared with 5Cu/silica, the addition of 5% cerium in 5Cu5Ce/silica increased the carbon monoxide conversion from approximately 60% to 100%. The products of the reaction using the mixed catalyst were mainly carbon dioxide and unreacted water. Hydrogen was detected by mass spectrometry indicating that the shift reaction had taken place.

Figure 3.4.12. Shift reaction products for 5Cu5Ce/silica.

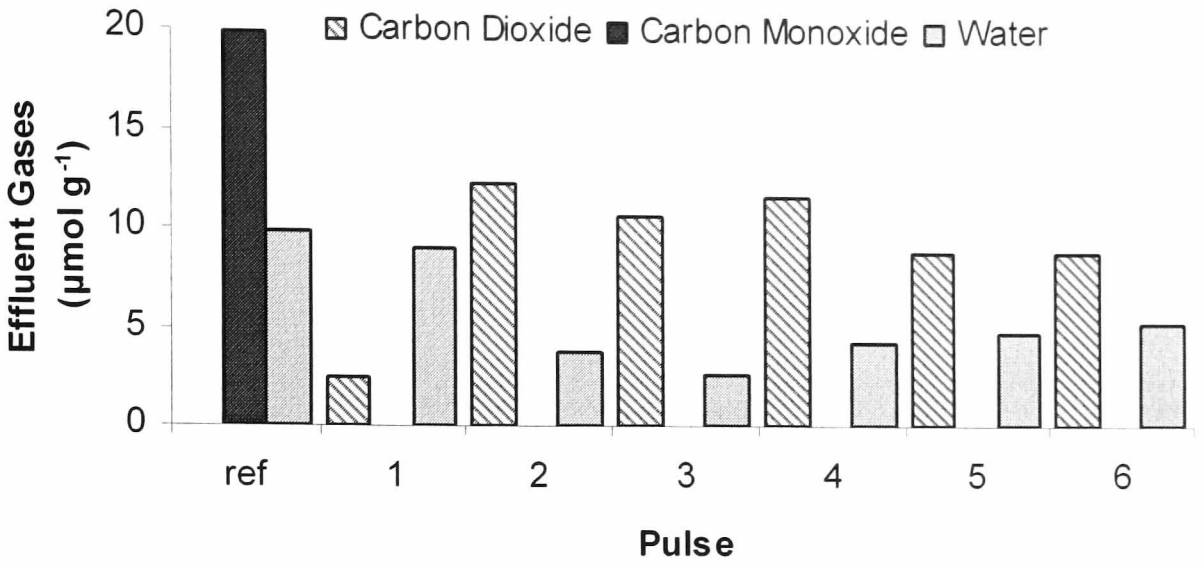

Table 3.4.7. Percentage of carbon and oxygen recovered across each pulse and conversion of reactants – 5Cu5Ce/silica.

Pulse	*Conversion (%)*		*Mass Balance (%)*		*Effluent Gases (µmol gcatalyst^{-1})*		
	Carbon Monoxide	*Water*	*Carbon*	*Oxygen*	*Carbon Dioxide*	*Carbon Monoxide*	*Water*
1	100.0	5.6	13.2	49.0	2.5	0.0	9.0
2	100.0	58.5	67.6	104.0	12.3	0.0	3.8
3	100.0	70.6	60.9	91.0	10.7	0.0	2.6
4	100.0	49.2	68.9	108.8	11.7	0.0	4.3
5	100.0	40.9	54.7	92.6	8.9	0.0	4.8
6	100.0	33.0	56.3	97.4	8.8	0.0	5.2

As the oxygen mass balance was higher than the carbon mass balance, this suggested that the surface of the catalyst was being reduced. This was confirmed by figure 3.4.13, which showed that carbon monoxide oxidation and adsorption of carbon monoxide (or carbon dioxide) were the main reactions occurring. The catalyst adsorbed almost 90 % of carbon monoxide from the first pulse without reaction. This suggests that in the case of 5Cu5Ce/silica, adsorption of carbon monoxide was required prior to the initiation of the shift reaction. In addition, the majority of carbon monoxide, which reacted in the first pulse, produced carbon dioxide by oxidation of the surface.

Figure 3.4.13. Separation of carbon monoxide uses for 5Cu5Ce/silica.

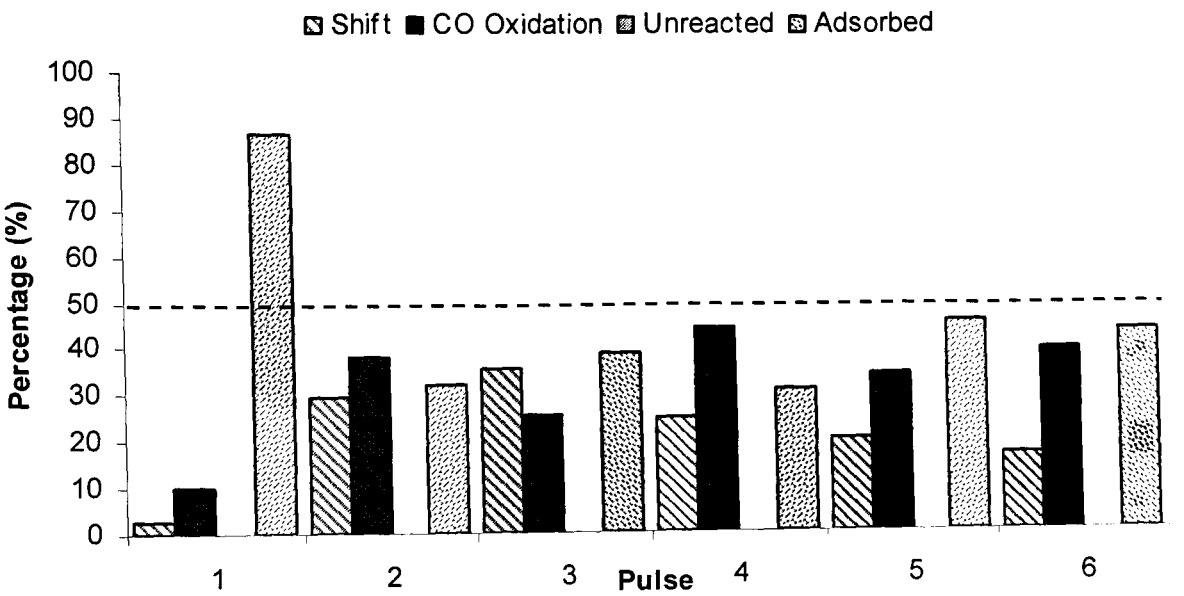

With a lower cerium loading, the conversion of carbon monoxide over the 5Cu1Ce/silica catalyst was reduced. Although carbon monoxide conversion decreased slightly, conversion of water increased to 100% in comparison with an average of 43% conversion for 5Cu5Ce/silica (figure 3.4.14).

Figure 3.4.14. Shift reaction products for 5Cu1Ce/silica.

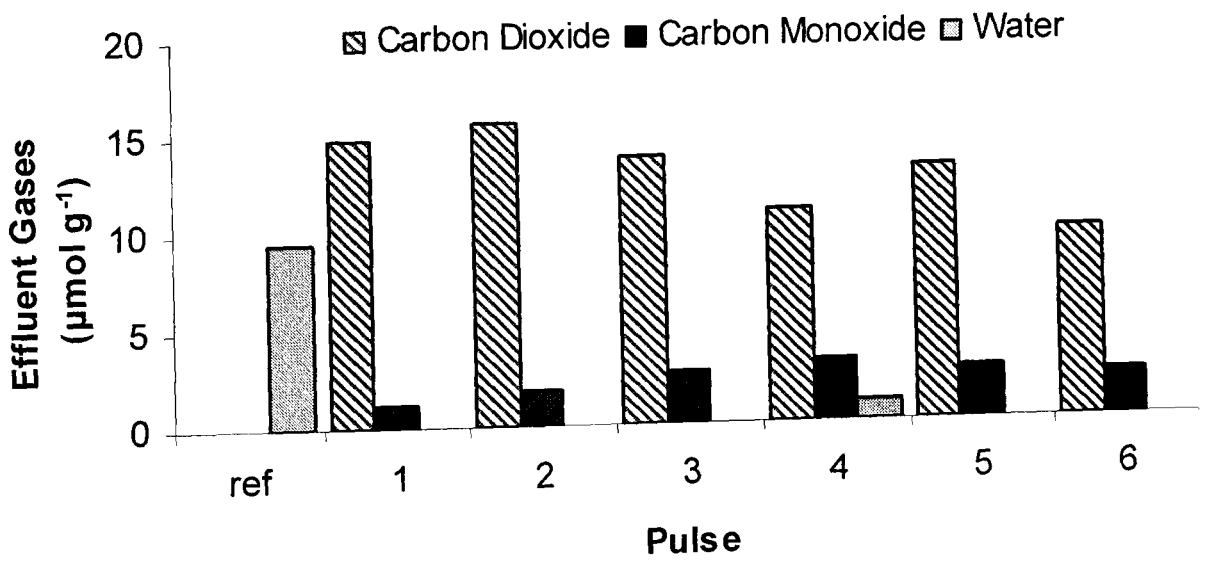

Table 3.4.8. Percentage of carbon and oxygen recovered across each pulse and conversion of reactants – 5Cu1Ce/silica.

Pulse	Conversion (%)		Mass Balance (%)		Effluent Gases (μmol $gcatalyst^{-1}$)		
	Carbon Monoxide	Water	Carbon	Oxygen	Carbon Dioxide	Carbon Monoxide	Water
1	93.2	100.0	87.7	112.4	14.8	1.2	0.0
2	89.9	100.0	99.4	125.7	15.7	1.8	0.0
3	84.3	100.0	97.0	118.8	13.8	2.7	0.0
4	80.4	88.5	87.1	106.9	11.0	3.2	0.9
5	83.1	100.0	100.0	122.1	13.1	2.7	0.0
6	84.7	100.0	80.5	97.2	9.9	2.3	0.0

The 5Cu1Ce/silica catalyst showed a high selectivity towards the shift reaction. In comparison with the products of the 5Cu5Ce/silica catalyst, less carbon monoxide was formed. In addition, there was a slight decrease in carbon monoxide oxidation as the number of pulses of reaction mixture increased. This might reflect a decreased availability of surface oxygen able to react with carbon monoxide, i.e. only a finite source of oxygen from either unreduced copper oxide or the ceria support is available. Carbon monoxide adsorption was lower than the quantity of carbon monoxide adsorbed by 5Cu5Ce/silica. This indicated that adsorption of carbon monoxide was related to the loading of cerium oxide. Hence, increased cerium loading led to an increase in sites available for carbon monoxide adsorption resulting in the formation of carbonates/carboxylates.

Figure 3.4.15. Separation of carbon monoxide uses for 5Cu1Ce/silica.

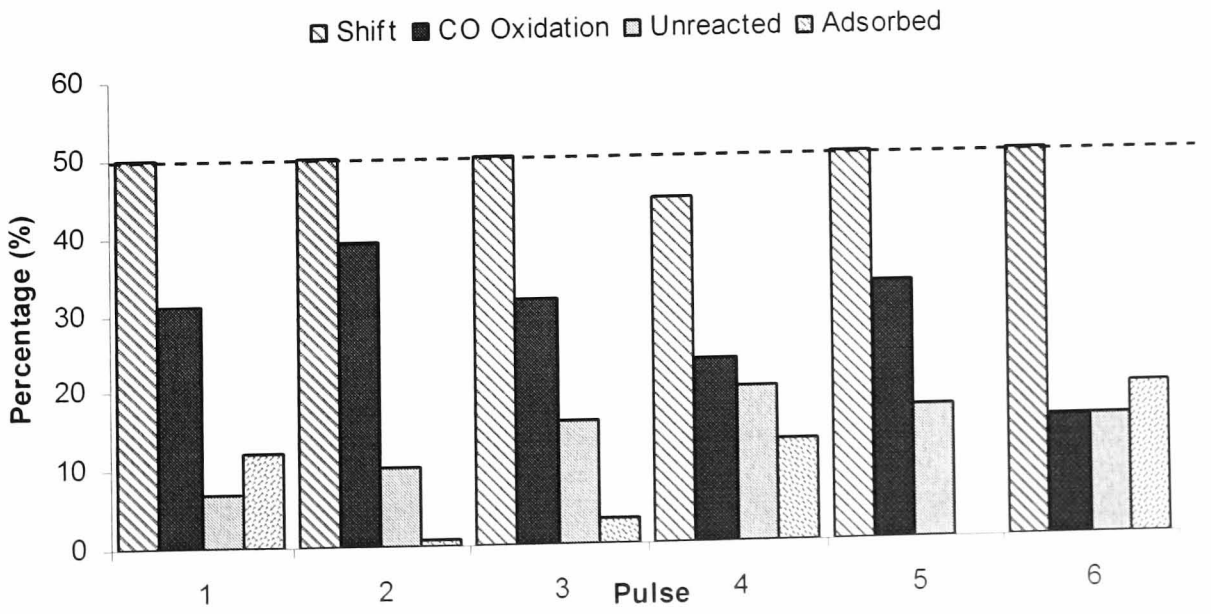

Figure 3.4.16 and table 3.4.9 show that carbon monoxide conversion was between 90 and 100% during the reaction with 10Cu5Ce0.05Pd/silica. The production of carbon dioxide peaked on the fourth pulse and began to decrease over the final pulses. As for 5Cu5Ce/silica and 5Cu1Ce/silica, the oxygen mass balance was greater than the carbon mass balance.

Figure 3.4.16. Shift reaction products for 10Cu5Ce0.05Pd/silica.

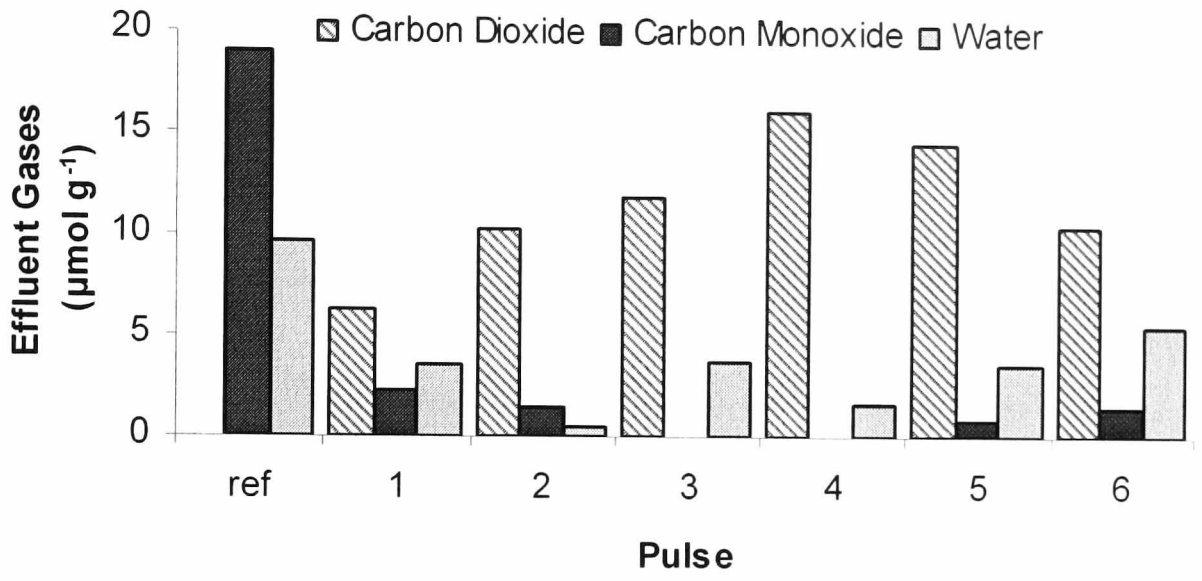

Table 3.4.9. Percentage of carbon and oxygen recovered across each pulse and conversion of reactants – 10Cu5Ce0.05Pd/silica.

Pulse	*Conversion (%)*		*Mass Balance (%)*		*Effluent Gases (µmol gcatalyst^{-1})*		
	Carbon Monoxide	*Water*	*Carbon*	*Oxygen*	*Carbon Dioxide*	*Carbon Monoxide*	*Water*
1	88.1	61.9	11.9	20.6	6.2	2.2	3.5
2	91.7	94.2	67.0	85.7	10.3	1.4	0.5
3	100.0	57.2	70.0	107.6	11.8	0.0	3.6
4	100.0	80.7	100.0	139.8	16.2	0.0	1.6
5	95.3	55.4	98.5	143.1	14.6	0.7	3.5
6	90.3	27.9	79.0	122.9	10.4	1.4	5.4

The 10Cu5Ce0.05Pd/silica catalyst was similar to the 5Cu5Ce/silica catalyst in that the catalyst adsorbed more than 50% of the first pulse of carbon monoxide. After the first pulse, adsorption decreased, as did the amount of carbon monoxide utilised in the shift reaction. However, over the last three pulses the quantity of carbon monoxide oxidised increased. This was unusual, as oxidation of products would have been expected to decline as availability of surface oxygen decreased.

Figure 3.4.17. Separation of carbon monoxide uses for 10Cu5Ce0.05Pd/silica.

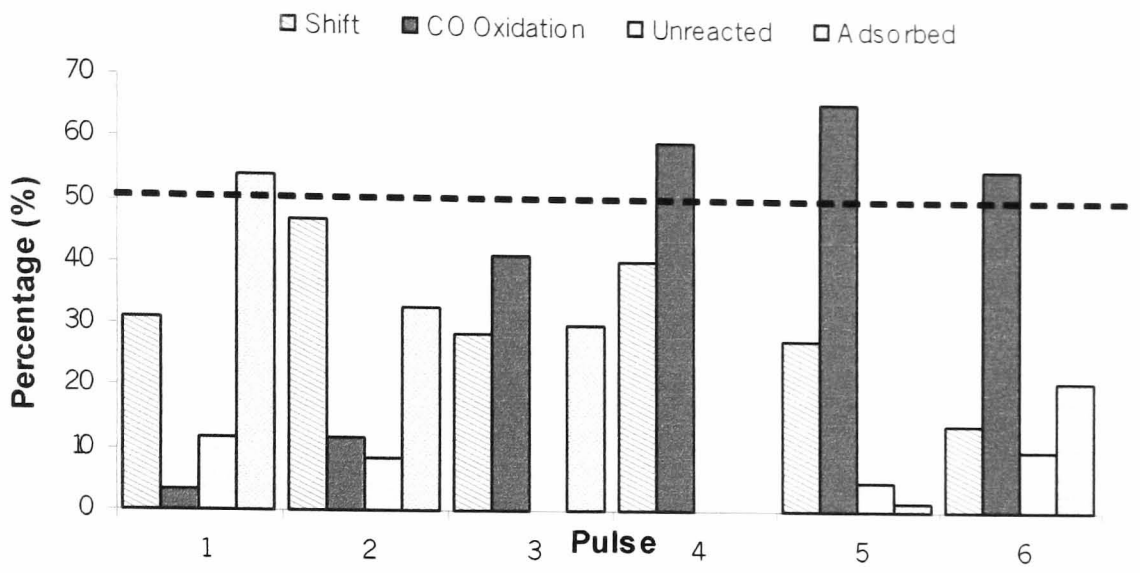

The final mixed catalyst examined was the 5Cu5Ce/alumina catalyst (figure 3.4.18). When compared with the results for the 5Cu5Ce/silica catalyst, the carbon monoxide conversion had increased, as had the formation of carbon dioxide. As expected, the high oxygen mass balance compared with that of carbon indicated that oxygen was being removed from the surface of the catalyst.

Figure 3.4.18. Shift reaction products for 5Cu5Ce/alumina.

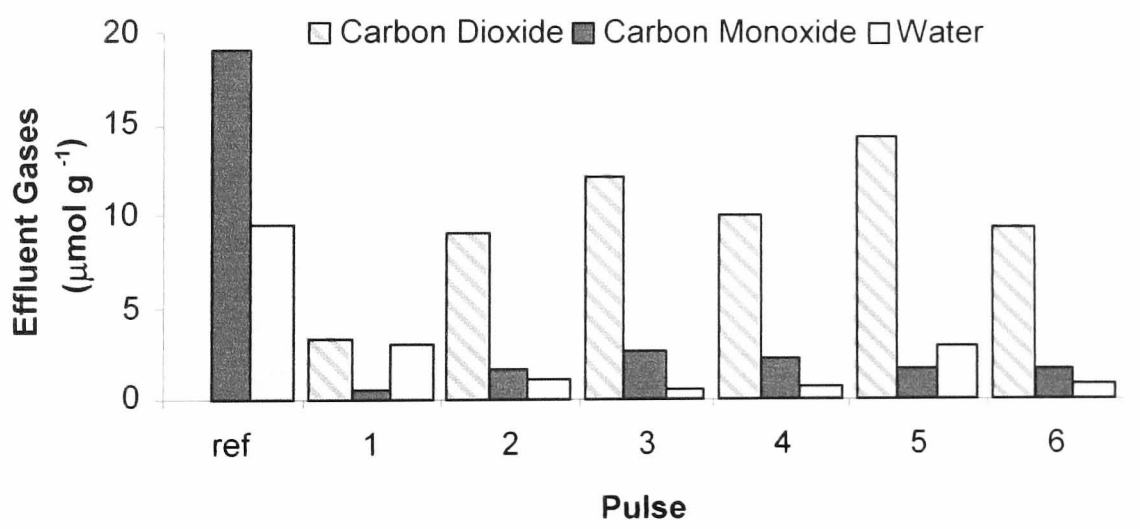

Table 3.4.10. Percentage of carbon and oxygen recovered across each pulse and conversion of reactants – 5Cu5Ce/alumina.

Pulse	Conversion (%)		Mass Balance (%)		Effluent Gases (μmol gcatalyst^{-1})		
	Carbon Monoxide	Water	Carbon	Oxygen	Carbon Dioxide	Carbon Monoxide	Water
1	97.4	68.2	20.6	36.3	3.3	0.5	2.9
2	90.5	88.2	60.2	78.0	8.9	1.7	1.0
3	84.5	95.0	87.1	107.5	12.1	2.6	0.4
4	86.8	92.5	74.4	92.9	10.0	2.1	0.6
5	89.3	63.8	101.7	140.6	14.2	1.7	2.8
6	88.9	89.5	73.5	94.1	9.4	1.7	0.8

The 5Cu5Ce/alumina catalyst was similar to the 5Cu5Ce/silica and 10Cu5Ce0.05Pd/silica catalysts that adsorbed the majority of carbon monoxide in the first pulse. Subsequent pulses showed that the quantity of carbon monoxide oxidised increased to a maximum on the fifth pulse. The amount of carbon monoxide utilised in the shift reaction remained relatively stable, while the adsorption of carbon monoxide decreased.

Figure 3.4.19. Separation of carbon monoxide uses for 5Cu5Ce/alumina.

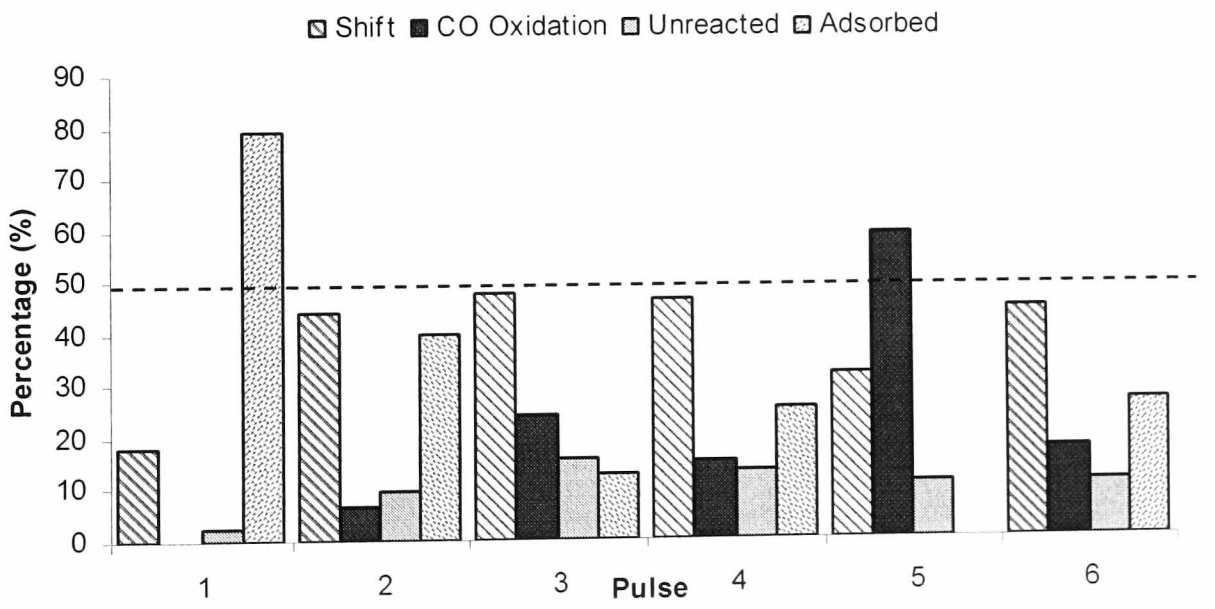

The main product over each of the mixed catalysts was carbon dioxide. Production of carbon dioxide was highest for 5Cu1Ce/silica and 10Cu5Ce0.05Pd/silica. Although all of the catalysts had carbon monoxide conversions greater than 80%, the conversion of water varied depending on the catalyst. 5Cu5Ce/silica was unusual in that conversion of carbon monoxide was 100%, while water conversion was much lower at ~50%. This

catalyst highlighted that water was not the only source of oxygen for the reactions and that oxygen was removed from the surface of the catalyst. Figure 3.4.3 highlights the increase in carbon monoxide oxidation on addition of a cerium component to a copper/support catalyst. Therefore, the effect cannot be completely attributed to the presence of copper oxide. It has been proposed that reduction of ceria by carbon monoxide involves adsorption of carbon monoxide onto the ceria surface, followed by reduction of surface oxygen to form oxygen vacancies [30]. In addition, reports have suggested that CeO_2 [30, 242] and CuO/CeO_2 [243] can be reduced at lower temperatures using carbon monoxide rather than hydrogen. This supports the theory that reduction of ceria by carbon monoxide was occurring. As a result, the availability of surface oxygen would decrease during the reaction.

Characterisation of 5Cu5Ce/silica by *in-situ* Raman (section 3.1.7.2) revealed that the catalyst was composed of reduced copper, copper (I) oxide and a partially reduced cerium oxide. On a (partially) reduced cerium oxide surface, Ce^{3+} species were shown to be active sites for CO_2 dissociation to form carbon monoxide [232]. Carbon monoxide was also found to be strongly adsorbed on Ce^{3+} [232]. Carbon dioxide can be adsorbed by ceria to form carboxylate and carbonate species, hence reducing the number of sites available for reaction [244]. Therefore adsorbed carbon species would have formed carbonates and carboxylates on the ceria of the mixed catalysts. It was found from TPR (section 3.1.8) that the presence of copper and cerium on the support led to partial reduction of the ceria. Creation of Ce^{3+} sites may have provided adsorption sites for the carbon species.

Sedmak *et al* [245] investigated $Cu_{0.1}Ce_{0.9}O_{2-y}$ catalysts and found that after removal of surface oxygen by carbon monoxide, subsurface lattice oxygen diffused to the surface and was similarly removed. When all surface and bulk oxygen was removed oxidation of carbon monoxide stopped [245]. A similar trend would be expected for the mixed copper and cerium catalysts. As there was not enough water in the mixture to replenish the oxygen atoms removed from the surface, the carbon monoxide oxidation reaction would eventually cease. This trend was evident for the catalyst containing the lowest loading of cerium (5Cu1Ce/silica), as the oxidation of carbon monoxide decreased across the pulses. All of the mixed catalysts showed a large difference between the oxygen and the carbon mass balances after each pulse. The figures confirmed that

oxygen was being removed from the catalyst surface. This effect was more pronounced on the mixed metal catalysts than the copper/support catalysts. This was due to the presence of cerium oxide in the catalysts, which is well known for its oxygen storage capacity [30]. Hence, there was evidence to suggest that carbon monoxide oxidation was a transient process and would cease when all excess oxygen was removed.

The shift reaction was the predominant reaction over the 5Cu1Ce/silica and 5Cu5Ce/alumina catalysts. Over 5Cu5Ce/silica and 10Cu5Ce0.05Pd/silica, carbon monoxide oxidation and adsorption were increased, probably due to the increased ceria loading. As well as supplying stored oxygen, the partially reduced ceria was able to provide adsorption sites for the formation of carbonate species. It is possible that the adsorbed carbonate species play a role in the shift mechanism over the mixed copper and cerium catalysts. The increase in adsorbed carbonate species might have reduced the ability ceria to be re-oxidised [105], in turn reducing the activity of the catalyst towards the shift reaction.

Hilaire and co-workers [105] studied a number of ceria-supported catalysts for the water gas shift reaction and the results of their study favoured the redox mechanism. The mechanism suggested that water oxidised the partially reduced ceria, which was then able to transfer oxygen to the supported transition metal to react with adsorbed carbon monoxide. Infrared data also indicated that the ceria surface was largely reduced and saturated with carbonate species [105]. Even though oxidation of palladium by ceria was not thermodynamically favoured, it was observed by XPS of palladium films supported on ceria [246]. Copper and nickel catalysts supported on ceria were also proposed to follow a redox mechanism [247]. Jacobs *et al* [101] used kinetic and infrared studies and determined that at high water to carbon monoxide ratios only a formate mechanism fitted the data. The report [101] also stated that information form Hilaire's report [100] supporting a redox mechanism, might indicate the presence of formate intermediates. The work of Hilaire and co-workers [100] was carried out at high carbon monoxide to water ratios, as in the current study. Regardless of the mechanism, it was clear that the ceria played an important role in the shift mechanism. The literature indicates that a ceria mediated formate reaction is most likely for catalysts with a transition metal supported on ceria. As TPR studies of the mixed metal catalysts

(section 3.1.8) highlighted the close interaction between copper and cerium of the mixed catalysts, it is likely that a similar mechanism occurred.

3.4.1.4 Commercial Catalyst

The commercial catalyst was one of the most successful shift catalysts of the series of catalysts examined. Almost all of the carbon monoxide was converted to carbon dioxide over each pulse and water was not observed in the exit gases.

Figure 3.4.20. Shift reaction products for commercial catalyst.

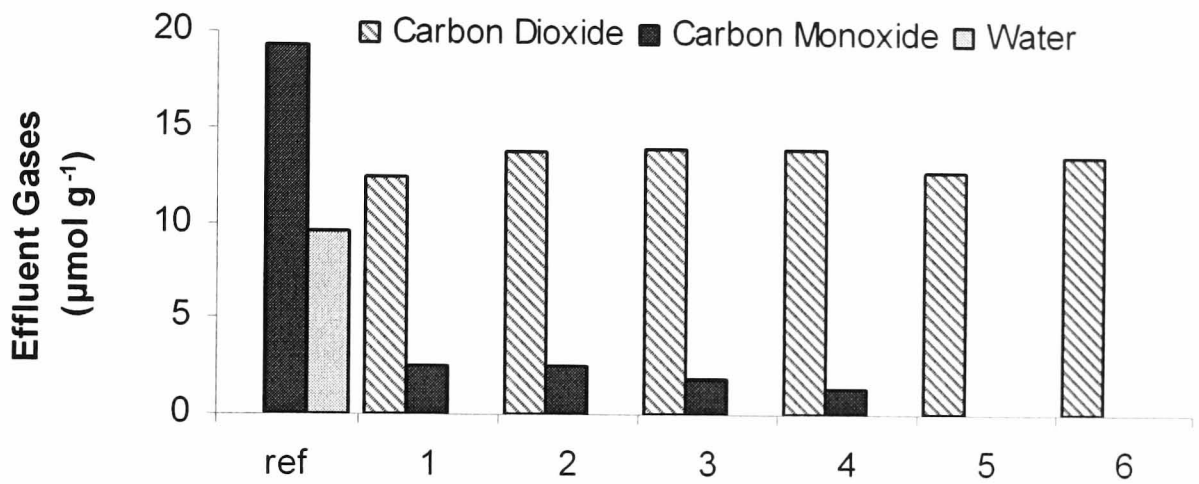

Table 3.4.11. Percentage of carbon and oxygen recovered across each pulse and conversion of reactants – commercial catalyst.

Pulse	*Conversion (%)*		*Mass Balance (%)*		*Effluent Gases (µmol gcatalyst^{-1})*		
	Carbon Monoxide	*Water*	*Carbon*	*Oxygen*	*Carbon Dioxide*	*Carbon Monoxide*	*Water*
1	86.1	100.0	81.8	99.7	12.5	2.6	0.0
2	85.5	100.0	92.4	113.6	13.8	2.6	0.0
3	88.7	100.0	93.1	116.6	13.9	1.9	0.0
4	92.1	100.0	93.8	119.8	14.0	1.3	0.0
5	100.0	100.0	81.5	108.7	12.8	0.0	0.0
6	100.0	100.0	90.7	120.9	13.6	0.0	0.0

Figure 3.4.21. Separation of carbon monoxide uses for commercial catalyst.

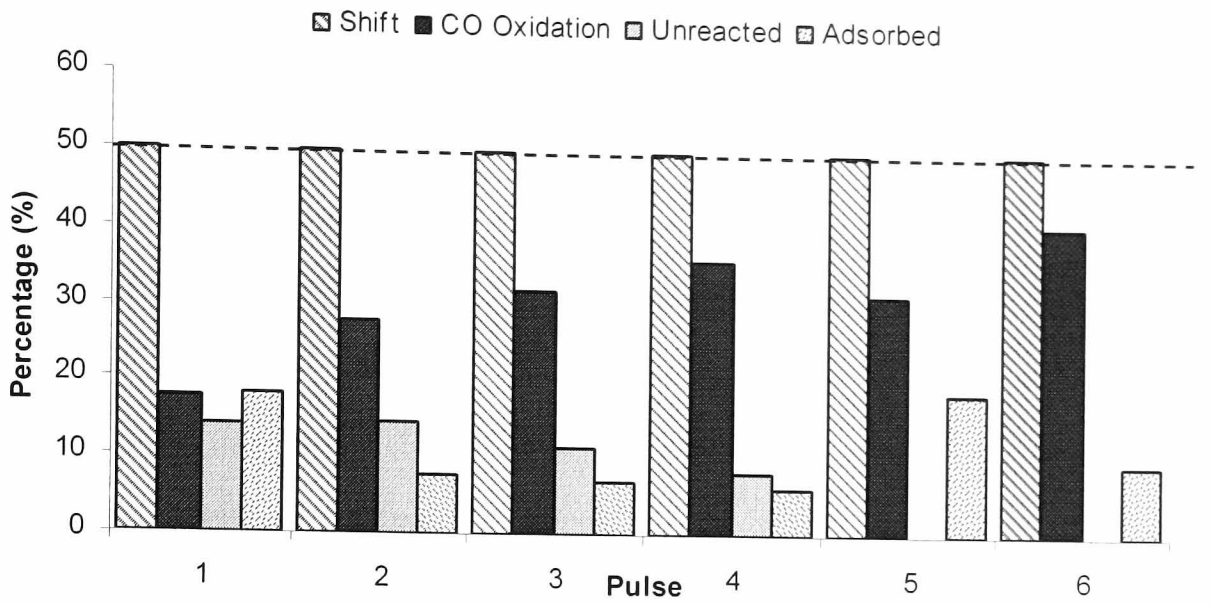

The commercial catalyst is composed of $Cu/ZnO/Al_2O_3$. The source of excess oxygen may have been due to the presence of zinc oxide in the catalysts. Cu/ZnO catalysts have been examined for the methanol decomposition reaction and it was found that the ZnO support had a detrimental effect on catalyst reactivity [188]. The group [188] suggested that loss of activity of Cu/ZnO catalysts was due to reduction of the ZnO phase, allowing dissolution of Zn into the copper phase under methanol decomposition conditions. They revealed that improved activity of copper-containing catalysts for methanol decomposition was observed in the absence of ZnO [188]. Hence, similar reduction of the zinc oxide phase would explain the increased oxygen mass balance during reaction with the shift mixture.

When compared with the commercial methanol synthesis catalyst, the catalysts that converted most carbon monoxide to carbon dioxide were the 5Cu1Ce/silica and 10Cu5Ce0.05Pd/silica catalysts. Addition of ceria to the catalysts increased conversion of carbon monoxide from the shift mixture. Although removal of surface oxygen was taking place, there was further evidence for the shift reaction occurring due to the hydrogen produced by all of the copper and cerium/support catalysts. Long-term stability of ceria and copper/support catalysts would require testing of the catalysts under continuous flow conditions. To investigate the role of surface oxygen further, attempts were made to improve the reduction of the catalysts surface by carbon monoxide pulses prior to reaction with the shift mixture.

3.4.2 Pre-Adsorption of Gases followed by Shift Mixture

A series of experiments were used to examine the effect of pre-adsorbing either carbon monoxide or oxygen onto the surface of the catalyst. The sequence of pulses was as follows: carbon monoxide, carbon monoxide and water (WGS mixture), oxygen and finally carbon monoxide and water (WGS mixture), as described in experimental section 2.5.3. The sequence of reactions was chosen to examine the effect if any, which would be observed by either reducing or increasing the quantity of surface oxygen available.

3.4.2.1 Carbon Monoxide Pre-adsorption

Four aliquots of carbon monoxide were pulsed over each of the reduced catalysts; the sum of the pulses was approximately 175.7 $\mu molg^{-1}$. The results from the reaction are shown in table 3.4.12. The table shows that 5Cu5Ce/silica and 10Cu5Ce0.05Pd/silica adsorbed the most carbon monoxide. Although 5Cu/silica, 5Cu1Ce/silica, 5Cu/alumina and the commercial catalysts had negative adsorption values, they were due to an accumulation of errors across the four pulses. As no reaction had been carried out prior to carbon monoxide pulsing, it was not possible that excess carbon monoxide could have been produced (as suggested by the negative values in table 3.4.12). Hence, negative adsorption values indicated that all of the carbon monoxide, which had reacted, was converted to carbon dioxide.

Table 3.4.12. Summary of carbon monoxide pulses over the catalysts.

Catalyst	*CO Out (μmol)*	*CO_2 Out (μmol)*	*CO Adsorbed (μmol)*
5Cu/silica	120	65	-8
5Cu5Ce/silica	88	55	48
10Cu5Ce0.05Pd/silica	65	35	78
5Cu1Ce/silica	118	75	-18
5Ce/silica	168	13	3
5Cu/alumina	170	23	-10
5Cu5Ce/alumina	88	65	23
5Ce/alumina	153	0	18
Commercial	138	43	-3

The cerium/support catalysts formed least carbon dioxide (<11.5 $\mu molg^{-1}$). Carbon monoxide is known to be a better reducing agent for ceria than hydrogen [30]. However carbon monoxide pulses were not able to reduce the ceria present on the silica support. Most of the carbon monoxide did not react. However there was a small quantity of the gas that was adsorbed by the catalyst. Hence, cerium reduction was not observed by using carbon monoxide pulses at 473 K and the CeO_2 on the support did not adsorb carbon monoxide.

Production of carbon dioxide varied widely across the different catalysts. Most carbon dioxide was produced from the mixed metal catalysts and the commercial catalyst. This was due to removal of oxygen from the catalyst surface to form carbon dioxide. Hence, the pulses of carbon monoxide improved the extent of reduction of the catalysts.

The theoretical value of carbon dioxide required to reduce all of the CeO_2 in 5Cu1Ce/silica to Ce_2O_3 was 35.7 $\mu molg^{-1}$. Hence, table 3.4.12 would indicate that enough carbon dioxide was produced to fully reduce the cerium oxide present. However the value of carbon dioxide produced for the 5Cu/silica catalyst was 65 $\mu molg^{-1}$. Hence even without the cerium oxide present there was a source of removable surface oxygen. However, this is in agreement with results from the methanol decomposition reactions where excess oxygen was removed from copper/support catalysts (see table 3.2.19, in section 3.2.5). Figure 3.4.21 shows that the production of carbon dioxide decreased initially before levelling out for the 5Cu1Ce/silica catalyst. This might have been due to initial removal of surface oxygen, followed by removal of bulk oxygen, which would require migration of oxygen to the surface.

Figure 3.4.21. Pulses of carbon monoxide over 5Cu1Ce/silica.

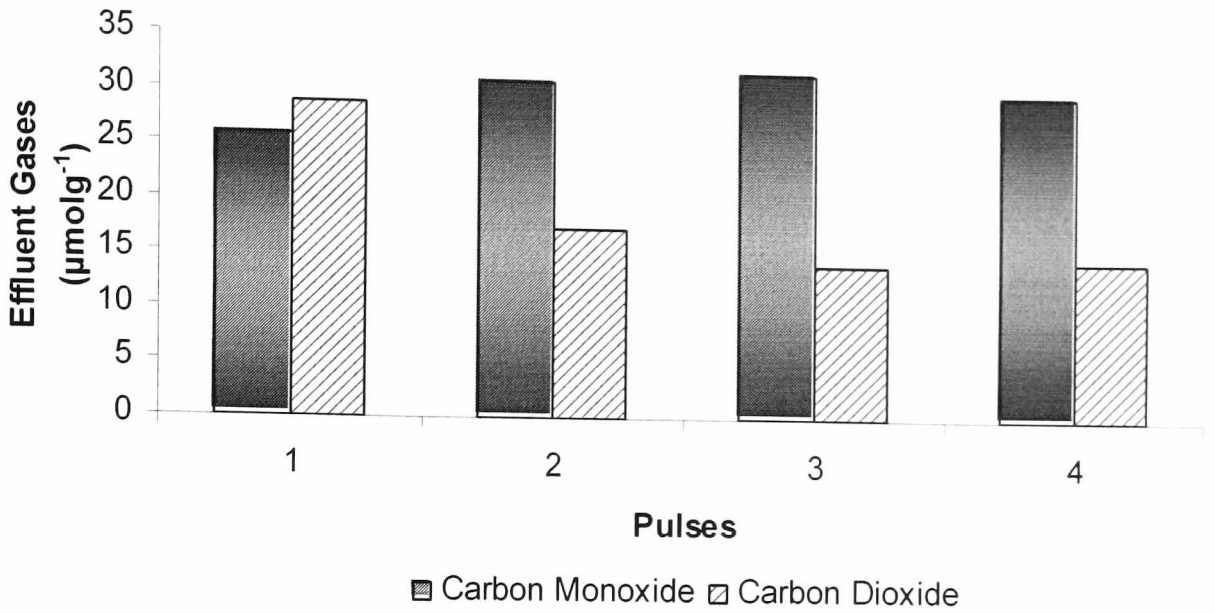

In-situ Raman spectra of 5Cu/silica and 5Cu5Ce/silica indicated that Cu_2O was present after the reduction process. Assuming that all of the copper in the 5Cu/silica catalyst had been present as Cu_2O, 393 $\mu molg^{-1}$ of carbon dioxide would have been required to reduce the copper to metal. Hence, the reaction of carbon monoxide with the copper/support or copper and cerium/support catalysts may have led to further reduction of the Cu_2O species present. For example, if as little as 16 % of the copper was present as Cu_2O after the reduction of 5Cu/silica, this would account for the formation of 65 $\mu molg^{-1}$ of carbon dioxide.

Although copper oxide may provide part of the source of oxygen for the mixed metal catalysts, it is probable that ceria also behaves as an oxygen source. Using catalysts with higher cerium loading and copper, it was possible that migration of oxygen from ceria to copper had occurred. Migration of oxygen to metal was detected over Rh/ceria catalysts at low temperatures [108]. The property was found to be dependent upon the interaction between the rhodium and ceria and did not occur with ceria alone [108]. Therefore, the interaction between the copper and cerium was an important factor affecting the reactivity of the catalysts. The importance of this interaction was recognised in the characterisation section (sections 3.1.7.2 and 3.1.8) where the presence of cerium oxide was found to improve the stability of a Cu_2O phase.

Addition of 5% cerium to the catalysts caused carbon monoxide to be adsorbed by the catalyst. In particular, 5Cu5Ce/silica and 10Cu5Ce0.05Pd/silica adsorbed most carbon

monoxide. This indicated that CeO_{2-x} provided an adsorption site for the formation of surface carbonates (as described in section 3.4.1.3).

3.4.2.2 Changes in Water Gas Shift (WGS) Reaction Behaviour

After pre-treatment with carbon monoxide, it was expected that less carbon monoxide from the shift mixture would be oxidised and that a greater percentage of the gas would be utilised in the shift reaction.

Figure 3.4.22. Conversion of CO during shift reaction after CO pre-treatment.

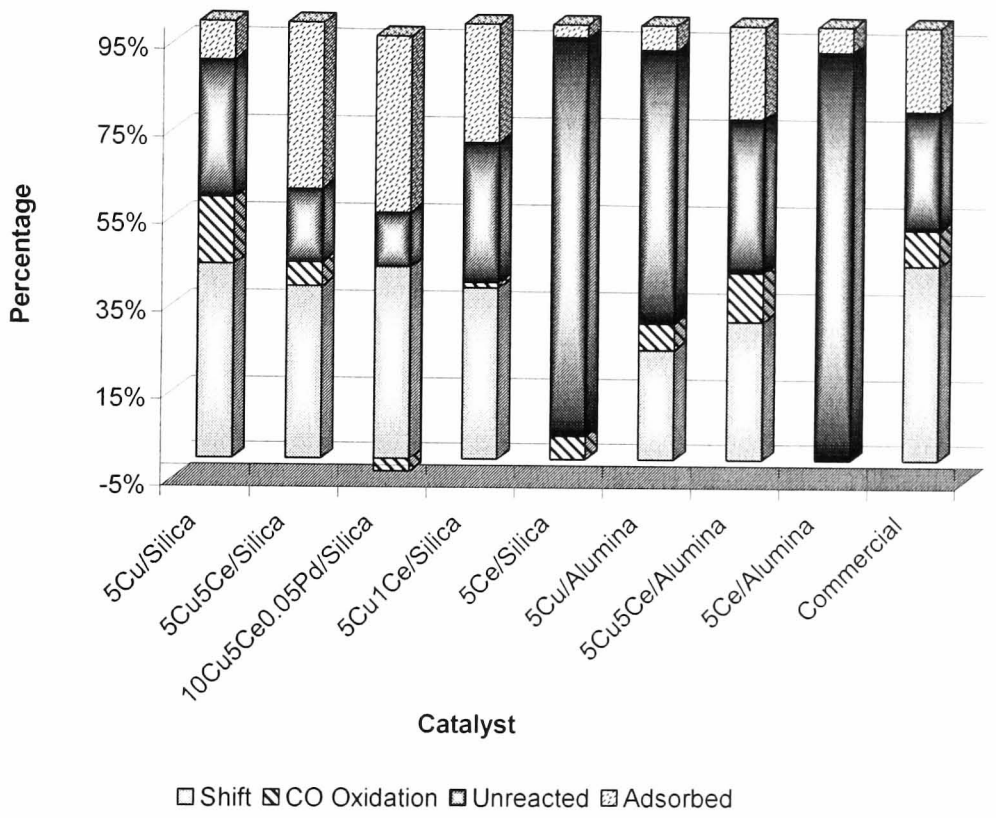

Table 3.4.13. Uses of carbon monoxide during reaction of catalyst with shift mixture, after carbon monoxide pulses.

Catalyst	*Uses of Carbon Monoxide (%)*			
	Shift	*Oxidised*	*Unreacted*	*Adsorbed*
5Cu/silica	44.6	15.3	31.4	8.8
5Cu5Ce/silica	39.6	5.6	16.8	38.1
10Cu5Ce0.05Pd/silica	46.9	-3.1	13.3	43.0
5Cu1Ce/silica	39.4	1.2	32.1	27.2
5Ce/silica	0.0	5.4	91.7	3.0
5Cu/alumina	25.4	6.1	62.7	5.7
5Cu5Ce/alumina	32.0	11.3	35.3	21.4
5Ce/alumina	0.0	0.0	94.2	5.8
Commercial	45.1	8.2	27.3	19.3

As expected, the average values of the reaction pulses showed a decrease in carbon monoxide oxidation for all of the copper and cerium/support catalysts, 5Cu/alumina and the commercial catalyst. Only 5Cu/silica showed a slight increase in carbon monoxide oxidation after the carbon monoxide pre-treatment. In addition, several catalysts showed improved reactivity towards the shift reaction, including 5Cu5Ce/silica and 10Cu5Ce0.05Pd/silica, both catalysts oxidised less carbon monoxide from the shift mixture. 10Cu5Ce0.05Pd/silica shows a slight negative value for carbon monoxide oxidation. This is due to an accumulation of errors and confirms that carbon monoxide oxidation was close to zero for this catalyst after carbon monoxide pre-treatment. The cerium/support catalysts were unreactive, as in previous shift reactions, hydrogen was not detected in the effluent gases and only a small amount of carbon monoxide was adsorbed. Hydrogen was however detected in the products of all remaining catalysts indicating that the shift reaction had occurred.

3.4.2.3 Exotherm on Reaction with Oxygen

The temperature increase on reaction of each catalyst with an aliquot of oxygen gas (~95 $\mu molg^{-1}$) is shown in table 3.4.14 and figure 3.4.23. The pulse size was chosen to ensure that the data recorder could detect any exotherm produced. The effluent gas from the reaction was composed of oxygen and no other products were detected.

Figure 3.4.23. Temperature exotherm produced on reaction of catalyst with oxygen pulse after shift reaction.

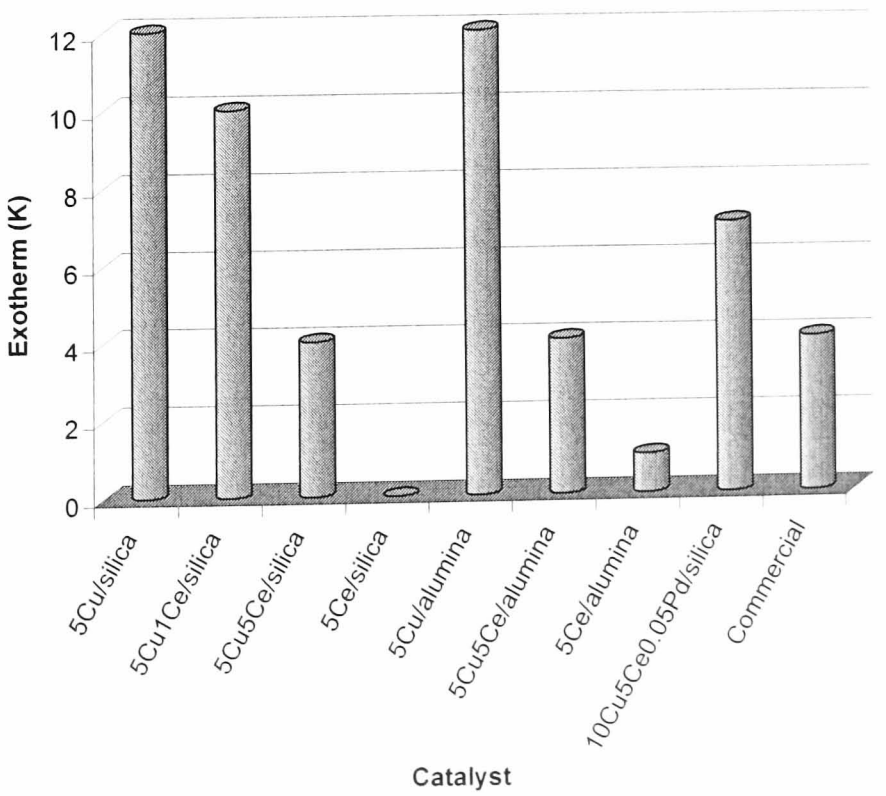

Table 3.4.14. Maximum exotherm produced by each catalyst on reaction with oxygen.

Catalyst	*Exotherm (K)*	*Oxygen Adsorbed ($\mu molg^{-1}$)*
5Cu/silica	12	98
5Cu1Ce/silica	10	97
10Cu5Ce0.05Pd/silica	7	93
5Cu5Ce/silica	4	74
5Ce/silica	0	4
5Cu/alumina	12	93
5Cu5Ce/alumina	4	92
5Ce/alumina	1	4
Commercial	4	94

The exotherm for the copper-containing catalysts was not related to the number of moles of oxygen adsorbed by the catalyst. However a trend was observed between metal loading and temperature rise. Irrespective of support, 5Cu/silica and 5Cu/alumina produced the same exotherm. The cerium/support catalysts were very unreactive and adsorbed less than 5% of the oxygen pulse, with no increase in temperature observed. This would confirm that the Ce/support catalysts were not reduced during the standard reduction procedure (section 2.5.1), as partially reduced cerium oxide would be re-oxidised by oxygen. Yao *et al* [33] observed a number of surface oxygen species during oxygen storage on ceria. These included surface peroxide and superoxides. The small quantity of oxygen adsorbed was likely to be due to formation of oxide species on the catalyst surface.

On combining cerium and copper in the catalysts, the temperature exotherm was reduced. Characterisation of the mixed metal catalysts showed that several species were present on the catalyst surface, including Cu_2O, Cu and CeO_{2-x} (Section 3.1). As the reaction exotherm was the same for catalysts with the same weight loading but different supports (figure 3.4.23), the effect was likely to be due to the active components on the catalyst and not to support influences. Differences may have been expected on changing the support as alumina has a higher heat capacity than silica (79.09 and 44.46 $JK^{-1}mol^{-1}$ respectively). As alumina has a higher heat capacity it would be expected to be better at dissipating heat. Presence of the partially reduced ceria appeared to reduce the temperature exotherm observed. Thermodynamic calculations for the possible reactions of oxygen with the catalyst components were:

$Cu + ½O_2 \longrightarrow CuO$ $\Delta H^\circ_r = -157.3\ kJmol^{-1}$, $\Delta G^\circ = -98.5\ kJmol^{-1}$

$Cu_2O + ½O_2 \longrightarrow 2CuO$ $\Delta H^\circ_r = -482.7\ kJmol^{-1}$, $\Delta G^\circ = -449.8\ kJmol^{-1}$

$Ce_2O_3 + ½O_2 \longrightarrow 2CeO_2$ $\Delta H^\circ_r = -369.4\ kJmol^{-1}$, $\Delta G^\circ = -331.1\ kJmol^{-1}$

Thermodynamically, reaction of Ce_2O_3 or Cu_2O with oxygen appeared to be the most favoured reactions. Although the reaction was more exothermic than the reaction of copper metal with oxygen, the larger heat capacity of the ceria would have reduced the temperature exotherm observed. Another possible reaction would have been the formation of super oxides on the unreduced ceria. However, this was unlikely to produce an exotherm, as the temperature change detected for the cerium/support catalysts was <1 K. It is possible however that once adsorbed onto the reduced cerium oxide; oxygen from the cerium oxide would be able to migrate back towards the copper to form Cu_2O. Migration of oxygen from ceria to metal was detected for Rh/ceria catalysts [108]. The thermodynamics of the reaction of ceria with copper are not favourable:

$2Cu + 2CeO_2 \longrightarrow Cu_2O + Ce_2O_3$ $\Delta H^\circ_r = 538.3\ kJmol^{-1}$, $\Delta G^\circ = 522.6\ kJmol^{-1}$

The oxidation of rhodium by ceria was also thermodynamically unfavourable [108]. It was suggested that the calculation does not take into account changes in energetics or contact between ceria and rhodium [108].

The high heat capacity of the ceria compared with copper improved heat dissipation, may have contributed to the reduction in the temperature exotherm detected. By increasing the loading of cerium in the catalyst there was a corresponding decrease in temperature exotherm. Ruettinger *et al* [102, 103] were able to prepare catalysts containing a precious metal (such as Rh, Pd or Pt) and a base metal component, which had a reduced temperature exotherm on exposure to air, when compared with copper/zinc oxide catalysts. In the series of catalysts examined one of the promoters examined was CeO_2 [103].

3.4.2.4 Activity after Oxygen Pulse

After one pulse of oxygen was passed across the catalyst an increase in carbon monoxide conversion was observed across all but the cerium catalysts. This was due to

removal of the surface oxygen by reaction with carbon monoxide. Figure 3.4.24 and table 3.4.15 show that after the oxygen pulse, the main reactions across the catalysts were back titration of the oxygen and formation of surface carbonate species. As hydrogen was not produced by any of the catalysts, the shift reaction did not take place. This suggested that after the oxygen pulse, the carbon monoxide from the reactant mixture was predominantly used to remove oxygen from the catalysts surface, i.e. the surface of the catalyst was oxidised and required reduction in order to be active towards the shift reaction.

Figure 3.4.24. Conversion of carbon monoxide during shift reaction, after an oxygen pulse.

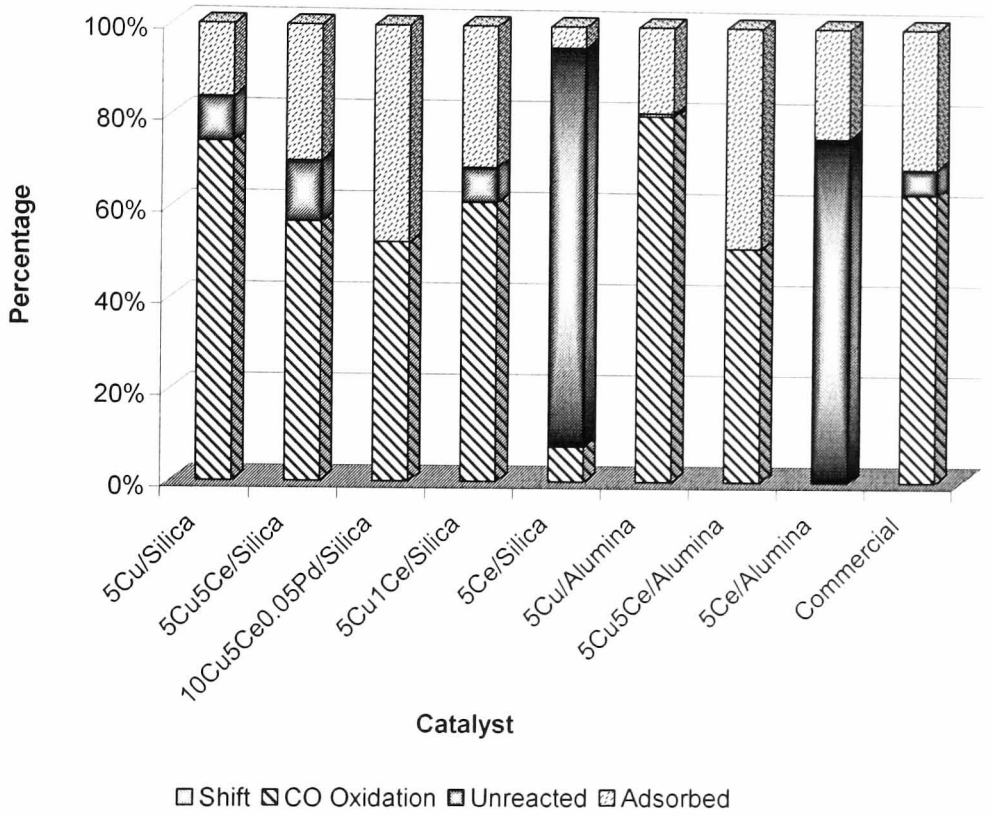

Table 3.4.15. Uses of carbon monoxide during reaction of catalyst with shift mixture, after oxygen pulse.

Catalyst	*Uses of Carbon Monoxide (%)*			
	Shift	*Oxidised*	*Unreacted*	*Adsorbed*
5Cu/silica	0.0	74.2	9.7	16.1
5Cu5Ce/silica	0.0	56.8	13.3	29.9
10Cu5Ce0.05Pd/silica	0.0	52.4	0.0	47.6
5Cu1Ce/silica	0.0	61.1	7.7	31.2
5Ce/silica	0.0	7.7	87.6	4.7
5Cu/alumina	0.0	80.4	0.6	19.0
5Cu5Ce/alumina	0.0	51.4	0.0	48.6
5Ce/alumina	0.0	0.0	75.7	24.3
Commercial	0.0	63.5	5.6	30.9

3.4.2.5 Water-Gas Shift Reactions

Although changes in activity can be compared using the carbon monoxide conversion, closer examination of the catalysts was required to compare differences in carbon dioxide production as well as water conversion and the amounts of carbon and oxygen recovered after each pulse. For each catalyst the shift reaction is shown after the carbon monoxide pulses, then after the oxygen pulse. The tables include values for carbon monoxide and water conversion as well as the oxygen and carbon mass balance over each pulse.

Cerium Catalysts

The 5Ce/silica catalysts showed that after the initial carbon monoxide pulses, the carbon monoxide and water conversion although initially low, increased after subsequent pulses of carbon monoxide/water mixture (figure 3.4.25). Calculation of the mass balance showed that almost all of the carbon species were recovered, whereas oxygen was retained by the surface of the catalyst. This is likely to have been due to adsorption of water by the ceria.

The conversion of carbon monoxide remained relatively low even after the oxygen pulse and water conversion also decreased over 5Ce/silica. A small amount of carbon monoxide oxidation occurred, however the products suggested that the shift reaction did not take place, as water conversion was low and hydrogen was not detected in the products. After the oxygen pulse, carbon monoxide conversion increased slightly and there was a small increase in the amount of carbon dioxide produced. 5Ce/silica adsorbed only 4 $\mu molg^{-1}$ of oxygen from the pulse. Hence, the increase in carbon dioxide production indicated that a small amount of oxygen was being removed from the surface. This was reflected in the oxygen and carbon mass balances, which showed that more oxygen was present in the products than carbon. Hydrogen was not detected in the exit gas during either stage of the reaction, confirming that the shift reaction did not occur.

Figure 3.4.25. Reaction of 5Ce/silica with shift mixture after CO pulses then after oxygen pulse.

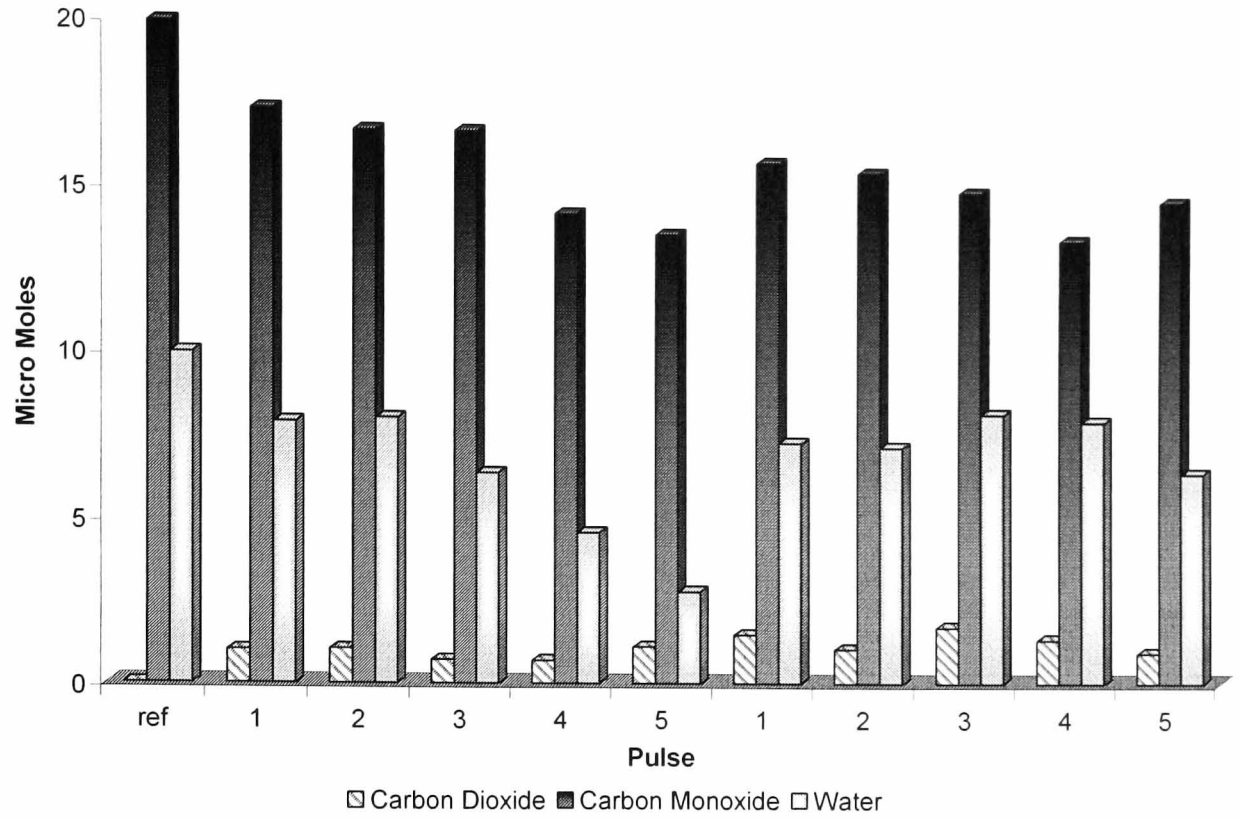

Table 3.4.16. Reaction products of 5Ce/silica with shift mixture after CO pulses then after oxygen pulse.

Pulse	*Conversion (%)*		*Mass Balance (%)*		*Effluent Gases ($\mu molg^{-1}$)*		
	CO	*H_2O*	*Carbon*	*Oxygen*	*CO_2*	*CO*	*H_2O*
1	8.9	16.9	96.4	95.5	1.0	17.3	7.9
2	7.8	11.4	98.0	98.7	1.0	16.7	8.0
3	4.1	26.7	100.0	93.8	0.7	16.7	6.4
4	10.1	42.0	94.3	85.2	0.7	14.2	4.6
5	10.8	63.3	96.5	81.4	1.1	13.6	2.8
1	14.2	20.6	93.9	94.4	1.5	15.8	7.3
2	12.5	18.9	93.4	93.2	1.0	15.5	7.2
3	12.0	3.1	98.1	104.5	1.7	14.9	8.2
4	17.2	1.8	91.0	98.9	1.3	13.5	8.0
5	6.0	17.5	100.0	98.1	0.9	14.7	6.4

The 5Ce/alumina catalyst (figure 3.4.26) was similar to the 5Ce/silica catalyst in that no shift reaction occurred. In addition no carbon dioxide was produced even after the oxygen pulse across the catalyst. This suggested that the small amount of oxygen adsorbed by the catalyst could not be easily removed by the carbon monoxide from the shift mixture. A similar quantity of oxygen was adsorbed by the 5Ce/alumina catalyst (4.3 $\mu molg^{-1}$). However, the mass balance of the oxygen remained less than the carbon mass balance even after adsorption of oxygen. Both the oxygen and carbon mass balance decreased after the oxygen pulse. This indicated that after adsorption of

oxygen, there was an increase in the quantity of carbonaceous species retained by the catalyst surface, i.e. carbon monoxide or carbon dioxide were adsorbed by the surface to form carbonates. Formation of carbonates on cerium containing catalysts has been reported previously in literature [232, 244].

Figure 3.4.26. Reaction of 5Ce/alumina with shift mixture after CO pulses then after oxygen pulse.

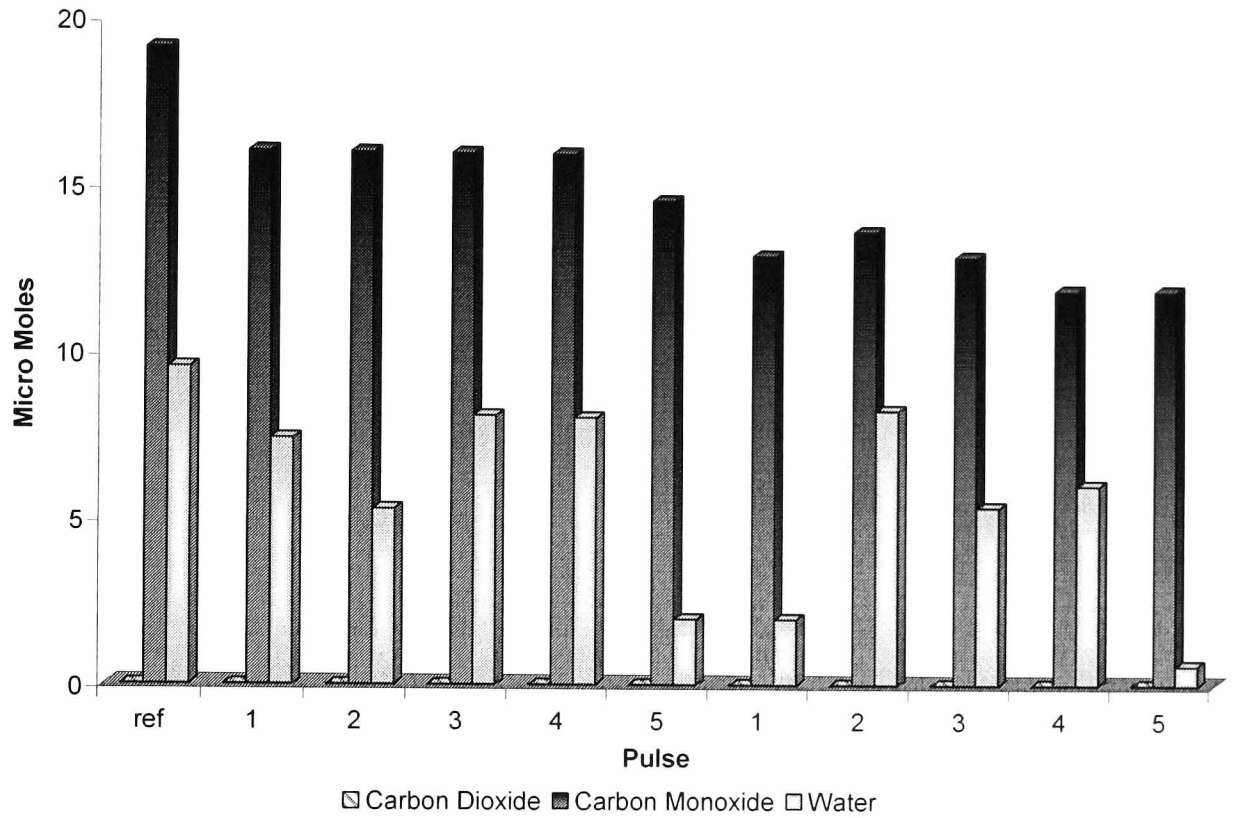

Table 3.4.17. Reaction products of 5Ce/alumina with shift mixture after CO pulses then after oxygen pulse.

Pulse	*Conversion (%)*		*Mass Balance (%)*		*Effluent Gases ($\mu molg^{-1}$)*		
	CO	*H_2O*	*Carbon*	*Oxygen*	*CO_2*	*CO*	*H_2O*
1	12.1	18.6	87.9	85.7	0.0	16.1	7.5
2	8.3	39.3	91.7	81.3	0.0	16.1	5.3
3	4.2	2.6	95.8	96.4	0.0	16.1	8.2
4	0.0	-0.9	100.0	100.3	0.0	16.1	8.1
5	4.5	74.1	95.5	72.3	0.0	14.7	2.0
1	28.7	78.2	71.3	54.8	0.0	13.1	2.0
2	21.6	4.9	78.4	84.0	0.0	13.8	8.4
3	22.8	35.8	77.2	72.8	0.0	13.1	5.4
4	25.7	24.7	74.3	74.6	0.0	12.1	6.1
5	23.0	92.4	77.0	53.9	0.0	12.1	0.6

The cerium/support catalysts highlighted the need for a transition metal to be present in order for the shift reaction to occur. The ceria on the support was relatively unreactive

under the testing conditions used. This was due to the absence of reduced cerium oxide. Shido and Iwasawa [233] reported that the water gas shift reaction only occurred on partially reduced ceria surfaces at temperatures of between 510 and 620 K. After reduction to 523 K, the ceria on the support was not reduced. Hence, the main reaction that occurred was adsorption of the reactants by the catalyst.

Copper Catalysts

Over the copper catalysts a mixture of carbon monoxide and carbon dioxide were produced during reaction with the shift mixture, similar to the shift reaction without carbon monoxide pulses (figure 3.4.27 and table 3.4.18). After the oxygen pulse, the main product was carbon dioxide, which suggested that the carbon monoxide was removing surface oxygen.

The 5Cu/silica catalyst shows the change in products after the oxygen pulse. The second set of shift pulses show an increase in carbon dioxide formation and unreacted water. At the same time the conversion of carbon monoxide increased after the oxygen pulse (figure 3.4.27 and table 3.4.18). There was also an increase in the difference between the oxygen and carbon mass balance after the oxygen pulse. This indicated an increased availability of surface oxygen. Although the production of carbon dioxide appeared to decrease, more pulses would be required to completely remove the oxygen adsorbed from the pulse and possibly allow conversion of carbon monoxide in the shift reaction.

Figure 3.4.27. Reaction of 5Cu/silica with shift mixture after CO pulses then after oxygen pulse.

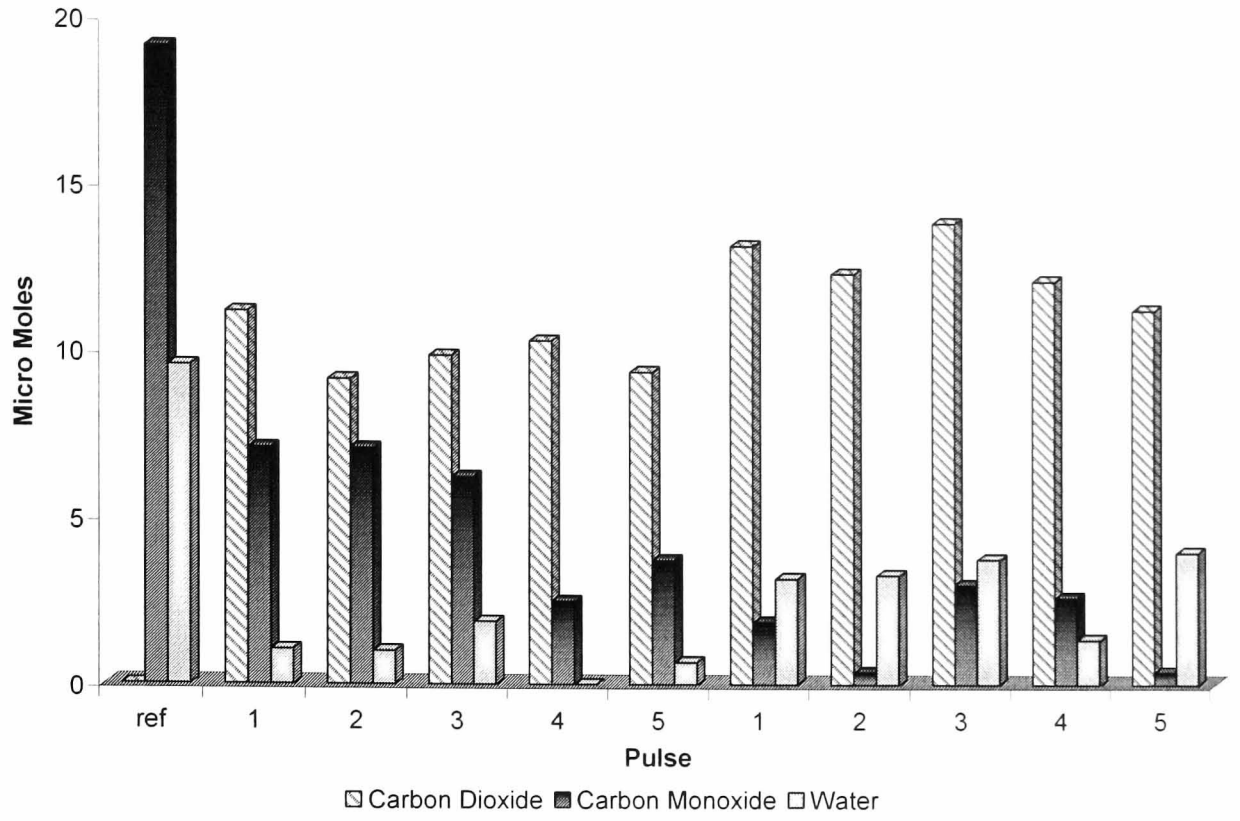

Table 3.4.18. Reaction products of 5Cu/silica with shift mixture after CO pulses then after oxygen pulse.

Pulse	*Conversion (%)*		*Mass Balance (%)*		*Effluent Gases ($\mu molg^{-1}$)*		
	CO	*H_2O*	*Carbon*	*Oxygen*	*CO_2*	*CO*	*H_2O*
1	61.13	88.55	100.0	111.2	11.2	7.1	1.0
2	59.59	88.59	92.6	100.3	9.2	7.1	1.0
3	62.73	77.44	96.2	110.9	9.9	6.3	1.9
4	84.26	100.00	80.9	97.3	10.4	2.5	0.0
5	75.41	91.22	86.4	101.8	9.5	3.8	0.7
1	89.80	65.46	81.7	113.7	13.3	1.9	3.2
2	97.87	62.80	72.1	107.1	12.5	0.4	3.3
3	82.23	55.40	100.0	136.4	14.1	3.0	3.8
4	83.85	83.35	90.9	116.0	12.3	2.7	1.4
5	97.59	48.70	74.9	115.4	11.4	0.4	4.0

The effect of the oxygen pulse was even more pronounced when the support was changed to alumina. The 5Cu/alumina catalyst changed from a carbon monoxide conversion of less than 50% after the carbon monoxide pulses to almost 100% after the oxygen pulse. This can be explained by the fact that carbon monoxide was reducing the surface, removing the excess oxygen present. The water conversion was low, suggesting that the oxygen adsorbed from the pulse was the main source of oxygen for the oxidation of carbon monoxide.

The initial set of shift pulses had high carbon and oxygen mass balances, which indicated that there was very little adsorption of the reactants by the catalyst. However, after the oxygen pulse the oxygen mass balance was approximately 50% higher than the carbon mass balance. Hence, removal of surface oxygen was the main reaction, with carbon species also being adsorbed onto the catalyst surface.

Figure 3.4.28. Reaction of 5Cu/alumina with shift mixture after CO pulses then after oxygen pulse.

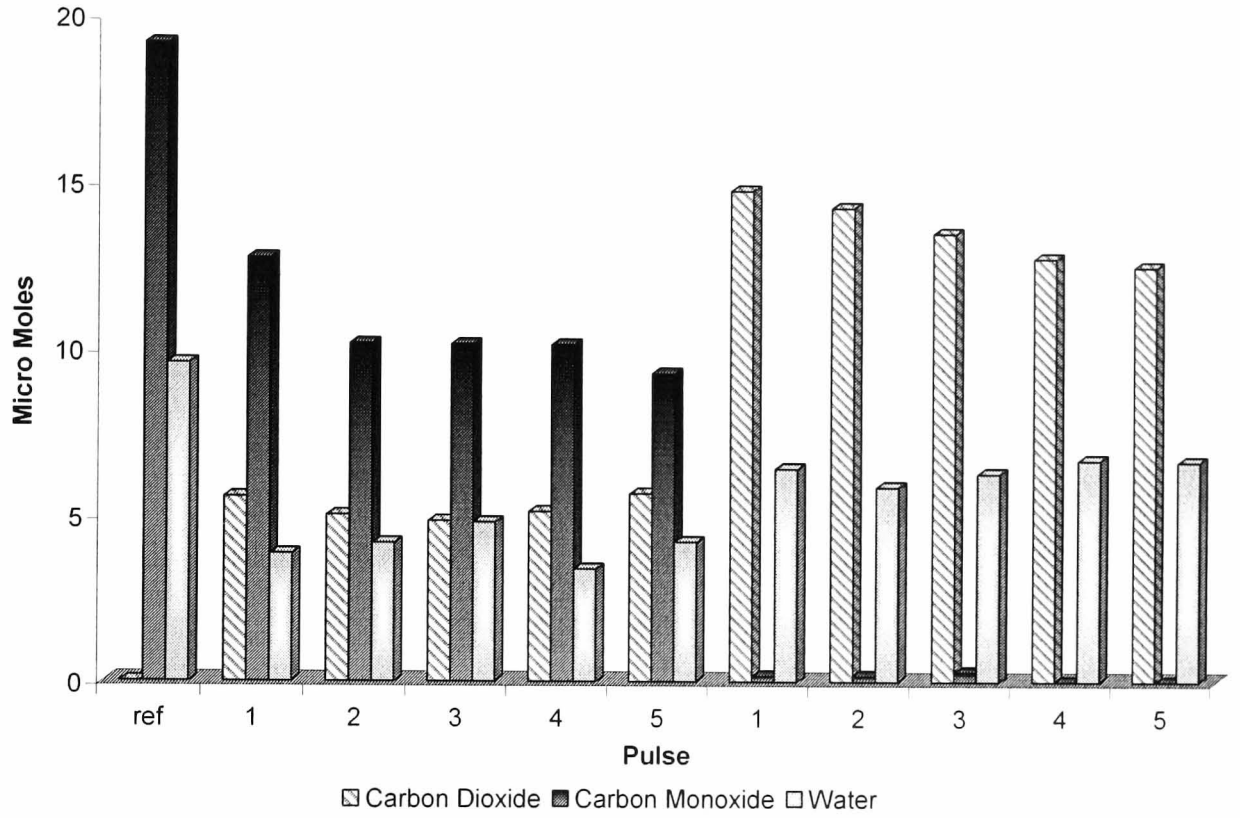

Table 3.4.19. Reaction products of 5Cu/alumina with shift mixture after CO pulses then after oxygen pulse.

Pulse	*Conversion (%)*		*Mass Balance (%)*		*Effluent Gases ($\mu molg^{-1}$)*		
	CO	*H_2O*	*Carbon*	*Oxygen*	*CO_2*	*CO*	*H_2O*
1	30.4	57.81	100.0	101.0	5.6	12.8	3.9
2	41.7	51.99	87.1	93.2	5.1	10.2	4.2
3	39.1	42.26	90.0	98.6	4.9	10.2	4.8
4	36.1	57.21	96.1	99.8	5.2	10.2	3.4
5	39.1	44.63	98.1	108.6	5.7	9.4	4.3
1	99.0	29.02	82.5	133.0	14.9	0.2	6.5
2	99.0	32.48	83.0	132.5	14.4	0.2	5.9
3	98.3	24.81	82.6	134.0	13.7	0.3	6.4
4	100.0	16.80	79.4	133.6	12.9	0.0	6.8
5	100.0	13.62	81.4	137.3	12.7	0.0	6.7

The reactivity of the copper/support catalysts towards the shift reaction was not improved by pre-treatment with carbon monoxide. However, the pre-treatment reduced the amount of excess oxygen detected in the products of the initial shift reaction. After treatment with oxygen, the shift reaction was no longer observed over the copper/support catalysts. The main reactions occurring in the second set of shift reactions were titration of oxygen from the surface and carbonate formation. Although the formation of carbon dioxide appeared to be decreasing across the pulses, it was unclear if the catalyst would have been active as shift catalysts after removal of the excess surface oxygen.

Copper and Cerium Mixed Catalysts

Over the mixed catalysts the carbon monoxide conversion decreased over the pulses while the water conversion remained high after the carbon monoxide pulses. After the oxygen pulse, carbon dioxide production increased and carbon monoxide was still produced by the 5Cu5Ce/silica and 5Cu1Ce/silica catalysts. 10Cu5Ce0.05Pd/silica and 5Cu5Ce/alumina produced no carbon monoxide in the exit gases. All of the catalysts produced an oxygen mass balance, which was 40-50% greater than the carbon mass balance after the oxygen pulse. This was due to removal of the adsorbed surface oxygen. As the carbon mass balance was below 100% this confirmed that carbon-containing species were also being adsorbed onto the catalyst surface.

Figure 3.4.29 shows an increase in the yield of carbon dioxide after treatment of the catalyst with a pulse of oxygen. The conversion of water also decreased. Production of carbon dioxide was lower than that of the 5Cu/silica catalyst. As the carbon monoxide conversions were similar, this indicated that the presence of partially reduced ceria encouraged adsorption of carbonate species on the catalyst surface. Table 3.4.20 shows that loss of carbon species was observed during both shift reactions however, as expected the oxygen mass balance increased after the oxygen pulse.

Figure 3.4.29. Reaction of 5Cu5Ce/silica with shift mixture after CO pulses then after oxygen pulse.

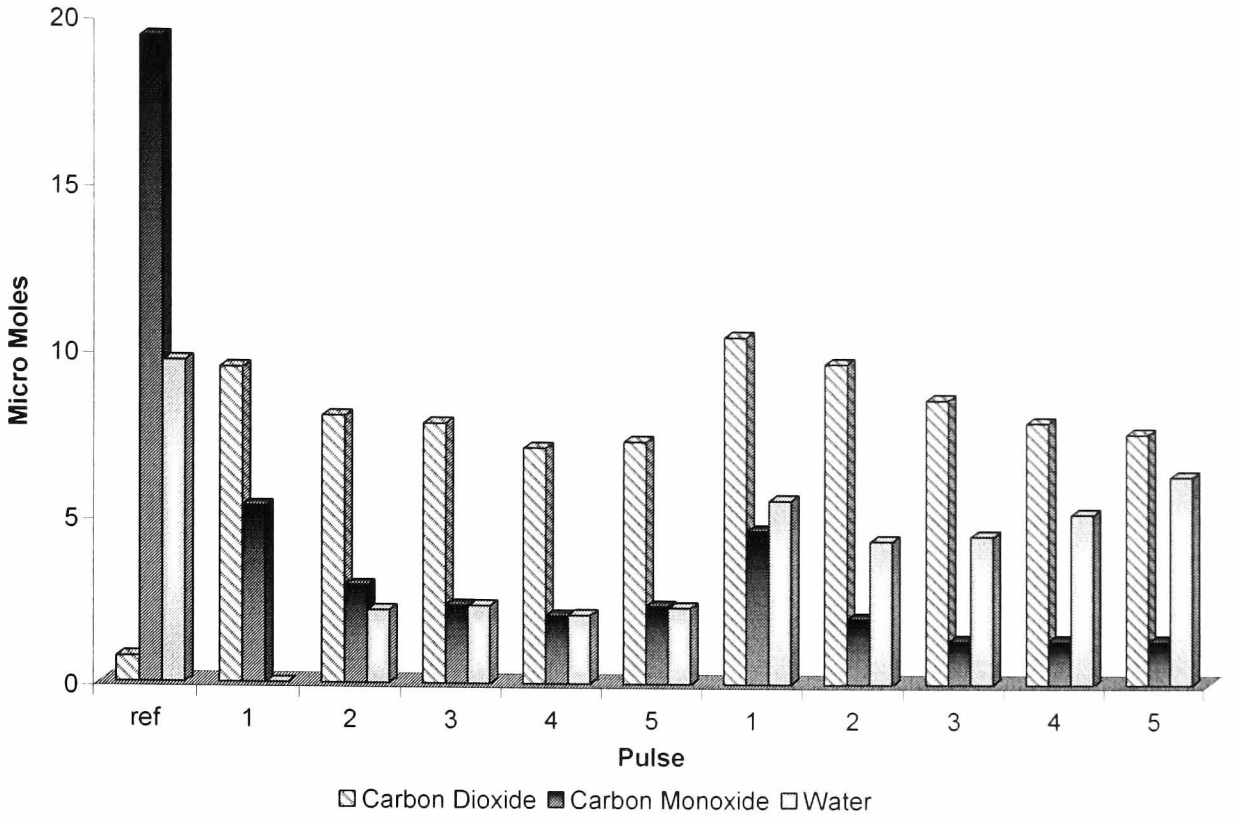

Table 3.4.20. Reaction products of 5Cu5Ce/silica with shift mixture after CO pulses then after oxygen pulse.

Pulse	*Conversion (%)*		*Mass Balance (%)*		*Effluent Gases ($\mu molg^{-1}$)*		
	CO	*H_2O*	*Carbon*	*Oxygen*	*CO_2*	*CO*	*H_2O*
1	72.5	100.0	76.5	83.7	9.5	5.3	0.0
2	84.0	76.1	59.7	76.9	8.1	3.0	2.2
3	86.6	73.4	58.0	77.3	7.9	2.4	2.4
4	87.7	75.2	54.8	73.2	7.2	2.1	2.1
5	85.3	71.2	60.4	80.4	7.4	2.4	2.3
1	72.5	34.1	89.6	123.1	10.6	4.7	5.6
2	87.7	46.4	72.2	106.0	9.8	2.0	4.4
3	91.5	42.1	64.0	99.0	8.7	1.3	4.5
4	91.1	30.7	62.2	100.1	8.0	1.3	5.2
5	90.7	11.5	62.6	106.7	7.7	1.3	6.4

The 5Cu1Ce/silica catalyst (figure 3.4.30 and table 3.4.21) show that pulsing carbon monoxide across the catalyst prior to the shift reaction mixture reduces the excess oxygen. The oxygen mass balance was only slightly higher than the carbon mass balance during the initial shift reaction. After the oxygen pulse the carbon mass balance decreased slightly while the oxygen mass balance increased. This indicated that there was an increased availability of surface oxygen species. In addition, the conversion of

water decreased, indicating that the catalyst was the main source of oxygen for carbon monoxide oxidation.

Figure 3.4.30. Reaction of 5Cu1Ce/silica with shift mixture after CO pulses then after oxygen pulse.

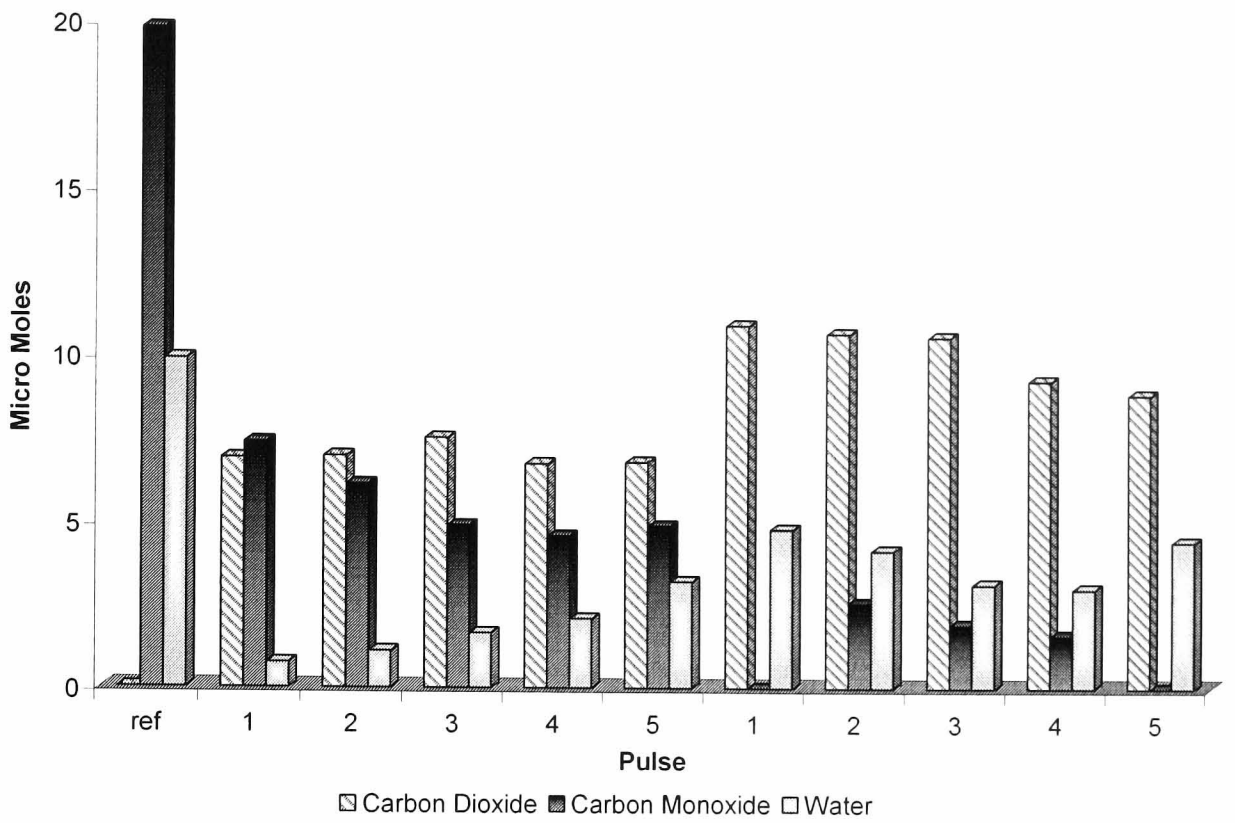

Table 3.4.21. Reaction products of 5Cu1Ce/silica with shift mixture after CO pulses then after oxygen pulse.

Pulse	*Conversion (%)*		*Mass Balance (%)*		*Effluent Gases ($\mu molg^{-1}$)*		
	CO	*H_2O*	*Carbon*	*Oxygen*	*CO_2*	*CO*	*H_2O*
1	60.9	92.0	75.7	77.5	7.0	7.4	0.8
2	65.9	87.7	72.8	78.5	7.0	6.2	1.1
3	71.5	80.8	72.1	83.6	7.6	5.0	1.7
4	72.1	74.6	32.0	32.5	6.8	4.7	2.1
5	68.9	59.2	74.3	91.9	6.9	5.0	3.3
1	100.0	46.8	60.4	98.3	11.1	0.0	4.9
2	85.3	52.1	76.2	107.8	10.8	2.6	4.2
3	88.5	62.3	75.0	104.9	10.7	1.9	3.2
4	90.0	62.3	68.4	97.1	9.4	1.6	3.0
5	100.0	41.9	58.1	96.8	9.0	0.0	4.5

The 10Cu5Ce0.05Pd/silica behaved similarly to the previous mixed metal catalysts (see figure 3.4.31 and table 3.4.22). Initial pulses of carbon monoxide reduced the surface oxygen available and after the oxygen pulse only carbon monoxide oxidation and

adsorption occurred. The main difference was that carbon monoxide conversion was 100 % after the oxygen pulse even though conversion of water was only ~60 %.

Figure 3.4.31. Reaction of 10Cu5Ce0.05Pd/silica with shift mixture after CO pulses then after oxygen pulse.

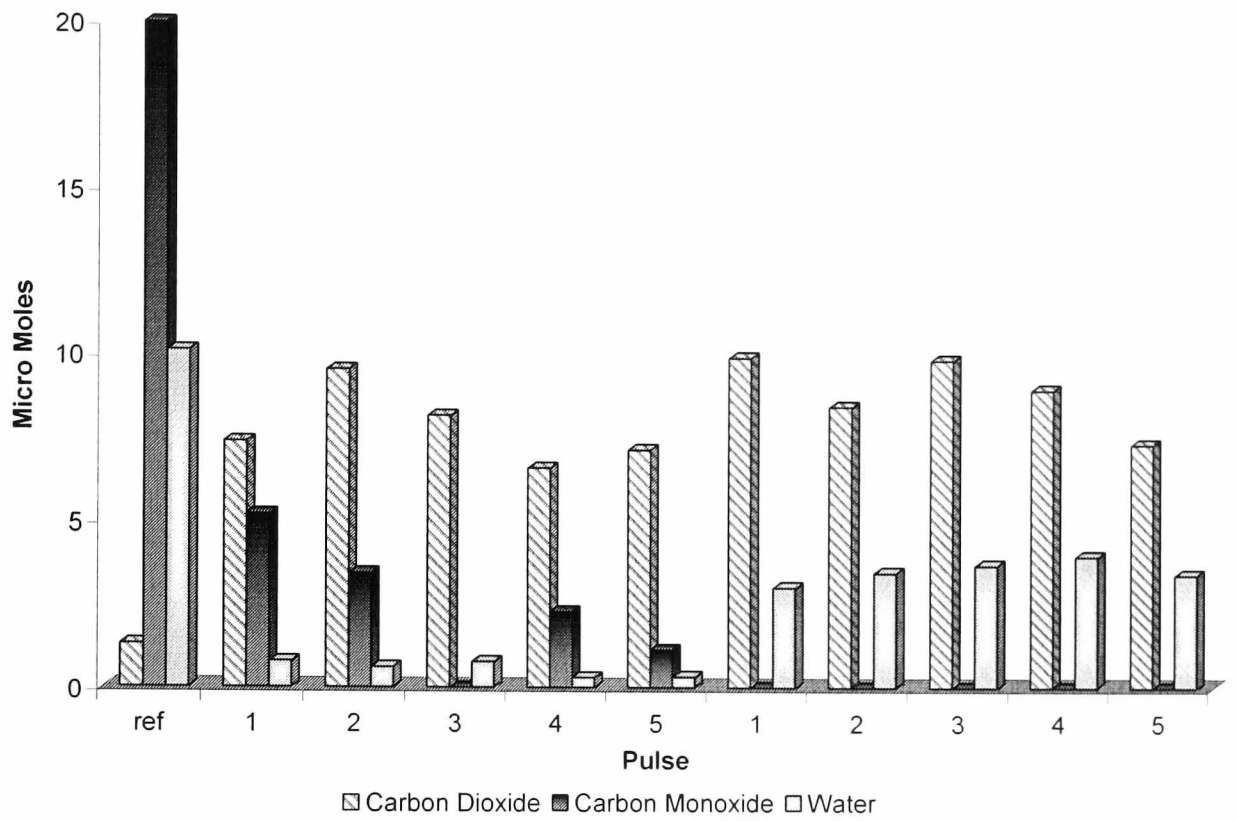

Table 3.4.22. Reaction products of 10Cu5Ce0.05Pd/silica with shift mixture after CO pulses then after oxygen pulse.

Pulse	*Conversion (%)*		*Mass Balance (%)*		*Effluent Gases ($\mu molg^{-1}$)*		
	CO	*H_2O*	*Carbon*	*Oxygen*	*CO_2*	*CO*	*H_2O*
1	73.2	91.9	64.8	71.2	7.4	5.2	0.8
2	81.3	93.4	70.4	83.6	9.6	3.5	0.6
3	100.0	91.2	46.1	64.4	8.2	0.0	0.8
4	86.4	96.4	52.6	62.2	6.6	2.3	0.3
5	92.9	96.0	51.2	64.9	7.2	1.2	0.3
1	100.0	66.8	54.4	83.6	10.0	0.0	3.1
2	100.0	60.2	48.3	77.7	8.5	0.0	3.5
3	100.0	55.9	58.8	93.1	9.9	0.0	3.7
4	100.0	50.8	55.5	90.4	9.0	0.0	4.0
5	100.0	55.9	47.2	77.7	7.4	0.0	3.5

By changing the support for the mixed metal catalysts to alumina, similar trends were observed. Figure 3.4.32 shows that the formation of carbon dioxide increases slightly after the oxygen pulse. The slight decline in carbon dioxide formation in the latter

pulses may reflect the reducing availability of excess oxygen; however prolonged testing would be required to examine this trend.

Figure 3.4.32. Reaction of 5Cu5Ce/alumina with shift mixture after CO pulses then after oxygen pulse.

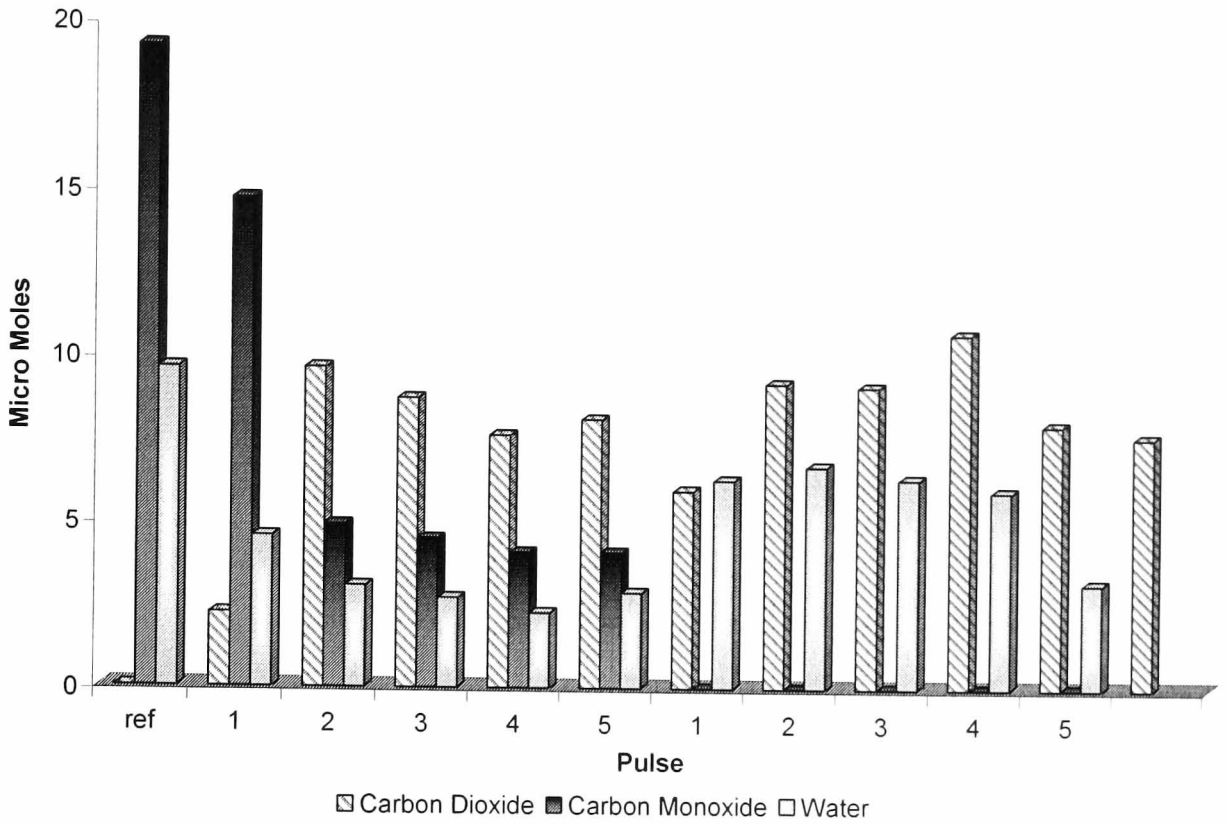

In contrast to the 5Cu/alumina catalyst (table 3.4.19), there was a decrease in carbon and oxygen mass balances. This suggests that a greater quantity of species is adsorbed by the mixed metal catalysts as shown in table 3.4.23.

Table 3.4.23. Reaction products of 5Cu5Ce/alumina with shift mixture after CO pulses then after oxygen pulse.

Pulse	*Conversion (%)*		*Mass Balance (%)*		*Effluent Gases ($\mu molg^{-1}$)*		
	CO	*H_2O*	*Carbon*	*Oxygen*	*CO_2*	*CO*	*H_2O*
1	20.0	50.6	92.1	85.9	2.2	14.8	4.6
2	72.2	65.3	82.5	103.0	9.7	4.9	3.1
3	73.3	68.0	78.5	97.6	8.8	4.5	2.7
4	74.8	72.2	72.3	88.9	7.7	4.1	2.3
5	73.7	63.0	78.7	99.8	8.2	4.1	2.9
1	100.0	32.9	49.2	88.0	9.3	0.0	6.3
2	100.0	25.6	50.7	92.4	9.2	0.0	6.8
3	100.0	26.7	62.3	107.5	10.9	0.0	6.4
4	100.0	27.8	48.4	88.6	8.1	0.0	6.0
5	100.0	60.0	48.2	77.6	7.7	0.0	3.2

Although the 5Cu/alumina and 5Cu5Ce/alumina catalysts behave differently after the carbon monoxide pre-treatment, after the oxygen pulses both catalysts show a high carbon monoxide conversion and similar water conversion values. Conversion of carbon monoxide and production of carbon dioxide was greatly enhanced using the alumina support when comparing the 5Cu5Ce/alumina and 5Cu5Ce/silica catalysts.

Commercial Methanol Synthesis Catalyst

An increase in unreacted carbon monoxide was observed for the first shift reaction after the carbon monoxide pulses when compared with the shift reaction alone, figure 3.4.33. As with the shift reaction alone the conversion of water remained high for each pulse. After the oxygen pulse the carbon dioxide production increased as the conversion of water decreased. As with the mixed catalysts the carbon balance decreased and oxygen mass balance increased after the oxygen pulse.

Figure 3.4.33. Reaction of Commercial catalyst with shift mixture after CO pulses then after oxygen pulse.

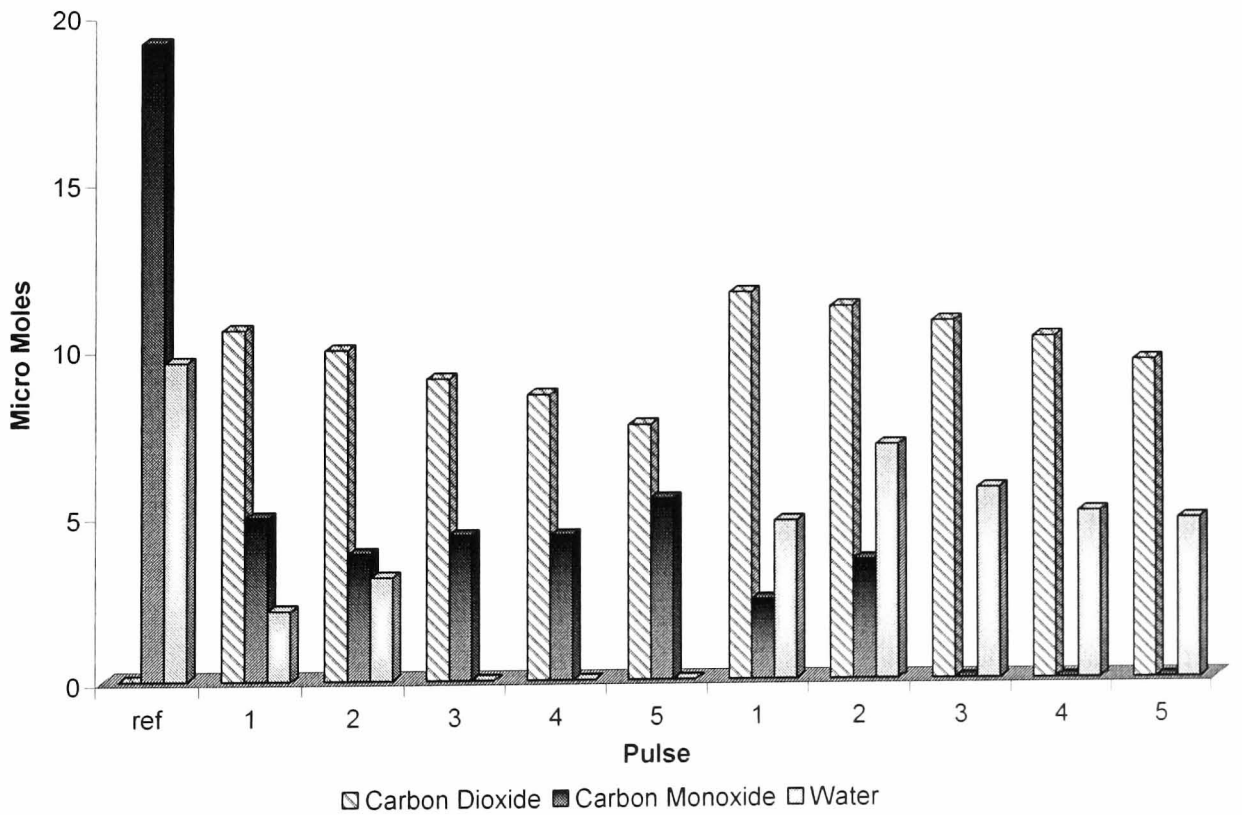

Table 3.4.24. Reaction products of commercial catalyst with shift mixture after CO pulses then after oxygen pulse.

Pulse	Conversion (%)		Mass Balance (%)		Effluent Gases ($\mu molg^{-1}$)		
	CO	H_2O	Carbon	Oxygen	CO_2	CO	H_2O
1	73.0	76.8	84.7	102.7	10.5	4.9	2.1
2	78.1	64.5	78.8	102.3	10.0	3.8	3.1
3	73.8	100.0	80.5	89.8	9.1	4.4	0.0
4	72.7	100.0	81.0	89.8	8.6	4.4	0.0
5	64.3	100.0	85.9	90.7	7.7	5.5	0.0
1	86.9	47.9	76.6	110.8	11.7	2.4	4.8
2	79.5	19.3	84.7	126.1	11.3	3.6	7.1
3	100.0	31.5	64.2	108.4	10.8	0.0	5.8
4	100.0	37.5	64.0	106.2	10.3	0.0	5.1
5	100.0	37.7	62.1	103.5	9.6	0.0	4.8

3.4.3 Summary of Catalyst Reactivity

Overall, the addition of cerium to copper-containing catalysts appeared to have a negative effect on the catalysts' reactivity as shift catalysts. However, addition of ceria reduced the temperature exotherm produced by the mixed catalysts on exposure to a pulse of oxygen. The low loading of cerium (5Cu1Ce/silica) appeared to have the benefits of maintaining high selectivity towards the shift reaction while lowering the temperature exotherm after air exposure. Increasing the cerium loading to 5% on the mixed catalysts led to an increase in the carbon monoxide oxidation and adsorption reactions. Hence, only a small weight percentage of cerium was required in the catalyst to produce beneficial effects.

By pre-treating the catalysts with either carbon monoxide or oxygen prior to the shift reaction, it was clear that the presence of surface oxygen greatly influenced the reaction products. Reducing the surface further using carbon monoxide, increased the selectivity of the carbon monoxide converted towards the shift reaction. After the oxygen pulse the main reaction was carbon monoxide oxidation. It is likely that removal of the complete surface layer of adsorbed oxygen would be necessary prior to the catalysts being active as shift catalysts. Several more pulses of carbon monoxide would have been necessary to reach this stage in the reaction; however this was not possible due to time constraints. Table 3.4.25 shows the average number of moles of gas present in the exit gas for each catalyst after carbon monoxide pulses then after an oxygen pulse.

Table 3.4.25. Average products observed in exit gases during shift reaction.

Catalyst	After Carbon Monoxide Pulses Effluent Gases ($\mu molg^{-1}$)			After Oxygen Pulse Effluent Gases ($\mu molg^{-1}$)		
	CO_2	CO	H_2O	CO_2	CO	H_2O
5Cu/Silica	10.0	5.4	0.9	12.7	1.7	3.2
5Cu5Ce/Silica	8.0	3.0	1.8	9.0	2.1	5.2
10Cu5Ce0.05Pd/Silica	7.8	2.4	0.6	8.7	0.0	3.6
5Cu1Ce/Silica	7.1	5.6	1.8	9.9	1.0	3.8
5Ce/Silica	0.9	15.7	5.9	1.3	14.9	7.4
5Cu/Alumina	5.3	10.6	4.1	13.4	0.1	6.3
5Cu5Ce/Alumina	7.1	6.0	3.0	8.8	0.0	5.6
5Ce/Alumina	0.0	15.8	6.2	0.0	12.6	4.1
Commercial	8.8	4.3	0.9	10.5	1.0	4.6

By looking at the values of carbon dioxide produced in the exit gases, it is clear that although the shift reaction does not take place after the oxygen pulse, even more carbon dioxide is produced (table 3.4.25). This is reiterated by the lower concentration of carbon monoxide in the exit gases which confirms that with the exception of the ceria/support catalysts the majority of carbon monoxide from the pulse is either oxidised or adsorbed by the catalyst. For all of the copper containing catalysts, the table shows an increase in unreacted water after the oxygen pulse. This suggests that water is not required as an oxidant as the surface is already saturated with oxygen. The carbon monoxide from the shift mixture was able to reduce the surface of the copper containing catalysts after the oxygen pulse. This was to be expected as results from methanol decomposition showed a similar trend (section 3.2.5). The results were also in agreement with *in-situ* techniques from the characterisation section which showed that copper oxide was present on the reduced 5Cu/silica (section 3.1.7.1). Formation of the copper oxide was increased on addition of ceria to the catalyst. Therefore, addition of a cerium component to the supported catalyst had the effect of improving the stability of the copper oxide. A similar trend has been observed during the shift reaction. Ability of the catalysts to oxidise carbon monoxide was greatly increased on addition of cerium to the catalyst.

The differences in the support again become apparent when examining the cerium/support catalysts. The results show that a small amount of oxygen can be

removed from 5Ce/silica after carbon monoxide pre-treatment whereas 5Ce/alumina remains relatively inactive. Even after oxygen pulsing 5Ce/alumina does not oxidise carbon monoxide. Hence, it is clear that the support chosen can affect the oxygen mobility of the catalyst.

3.5 Catalyst Ageing

When carrying out repeat reactions two years after making the catalysts, unusual results were observed. As a result, a series of reactions were carried out to investigate the difference in reactivity between the freshly prepared catalysts and the aged catalysts. after approximately two years. This phenomenon was observed previously with palladium/C30 silica [115] and with rhodium/silica [248] catalysts. Two copper/C10 catalysts were investigated for ageing effects, the 5Cu/silica and 5Cu5Ce/silica. The C10 silica support had been stored for several years prior to catalyst preparation. Catalysts were prepared by impregnation of the metal salts in aqueous solution, followed by drying at 333 K (section 2.1). After preparation, the copper based catalysts were active and produced reproducible results. By storing the catalysts in closed containers, changes were observed in their catalytic activity after a period of two years. The aged catalysts were tested for oxygen adsorption, methanol decomposition and hydrogenation activity.

3.5.1 Metal Dispersion

Oxygen chemisorptions were used to determine metal dispersion for both the 5Cu/silica and 5Cu5Ce/silica. It was expected that the change in activity of the catalysts would be reflected by a change in the catalysts' adsorption of oxygen, indicating a change in the metal surface area available for reaction.

Table 3.5.1. Metal dispersion as calculated in 2002 and 2004.

Catalyst	*March 2002* *Dispersion (%)*	*May 2004* *Dispersion (%)*
5Cu/silica	18.1	16.3
5Cu5Ce/silica	17.9	18.7

Table 3.5.1 shows that although the dispersion of the 5Cu/silica catalyst decreased, the dispersion of the 5Cu5Ce/silica catalyst increased slightly. It was therefore unclear from this method as to the extent of deactivation of the catalysts. The differences observed between the techniques of oxygen and N_2O chemisorptions in section 3.1.9 suggested that surface and bulk copper reacted with the oxygen pulses. During oxygen chemisorption, surface copper is readily oxidised, which is followed by slow migration

of oxygen into the bulk of the material [178]. Although there may be less surface copper available for adsorption on the aged catalysts, sub-surface metal could still be oxidised by diffusion of oxygen from the surface. Therefore the slight decrease in metal dispersion of the aged 5Cu/silica catalyst may reflect the problem of diffusion, i.e. only the sub-surface metal near surface oxidised copper will become oxidised by migration of the oxygen. The values of metal dispersion for 5Cu5Ce/silica before and after ageing were similar and increased slightly after ageing. This suggested that the total adsorption of oxygen by the surface and sub-surface metal had not changed greatly after ageing of the catalyst.

N_2O chemisorption may have provided greater information about changes to the actual surface metal area. However due to time limitations it was not possible to test the aged catalysts using N_2O chemisorption.

3.5.2 Methanol Decomposition

Pulse studies (section 2.5.2) were used to determine any change in reactivity of the catalyst since initial activity testing. Figure 3.5.1 and table 3.5.2 show the conversion and yield of products formed from the fresh 5Cu/silica. Carbon monoxide was the main product formed. Carbon dioxide and a small amount of methyl formate were produced. Although methanol conversion was high at ~99 %, the carbon mass balance showed that ~ 40 % of carbon species from each pulse were retained by the catalyst.

Figure 3.5.1. Methanol decomposition products using 5Cu/silica (March '02).

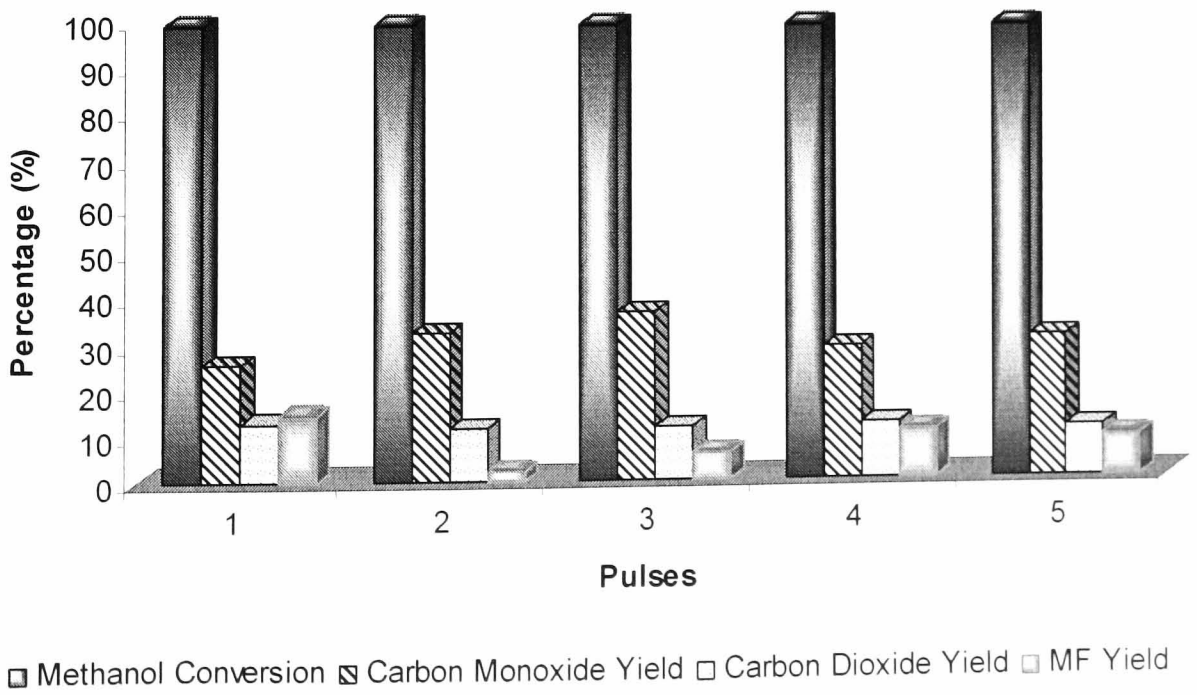

Table 3.5.2. Mass balance and yield of products during methanol decomposition, 5Cu/silica.

Pulse	Mass Balance (%)		Conversion (%)	Yield of Products (%)		
	Carbon	Oxygen		CO_2	CO	MF
1	68.7	81.6	98.8	12.9	25.6	14.5
2	49.5	61.0	98.9	11.6	32.5	2.2
3	61.1	72.8	98.8	11.7	36.5	5.8
4	63.4	75.4	98.9	12.0	28.9	10.7
5	60.7	71.7	98.9	11.0	30.7	9.0

After the catalyst had been stored for approximately two years, changes were observed to the products of methanol decomposition, figure 3.5.2 and table 3.5.3. Although conversion of methanol remained high at ~99 %, the ratio of products was greatly altered. The yield of carbon monoxide and carbon dioxide increased and methyl formate was no longer detected.

Figure 3.5.2. Methanol decomposition products using aged 5Cu/silica (April '04).

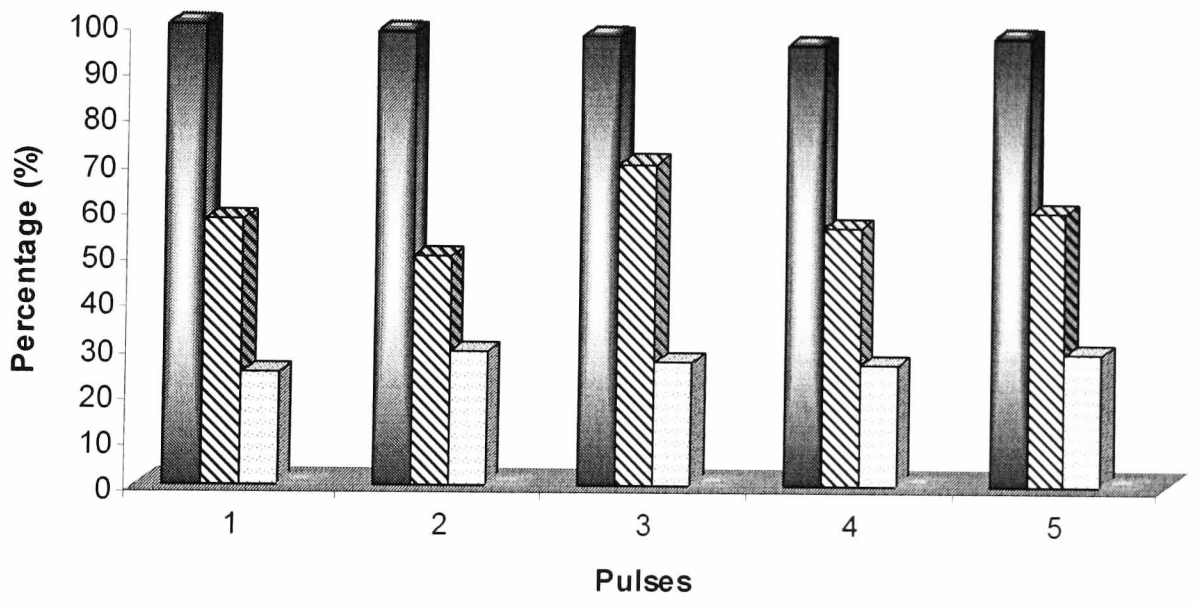

Table 3.5.3. Mass balance and yield of products during methanol decomposition, aged 5Cu/silica.

Pulse	Mass Balance (%)		Conversion (%)	Yield of Products (%)		
	Carbon	Oxygen		CO_2	CO	MF
1	82.4	107.0	99.8	24.6	57.6	0.0
2	80.4	109.9	99.0	29.4	50.0	0.0
3	99.8	127.2	98.0	27.4	70.5	0.0
4	86.5	113.1	96.7	26.6	56.7	0.0
5	91.2	120.4	98.6	29.2	60.6	0.0

The reactivity appeared to have altered after the ageing process as less carbon species were retained by the catalyst surface. The oxygen mass balance of the aged catalyst was greater than 100%. Therefore removal of surface oxygen occurred. This was similar to the effect observed for methanol decomposition over fresh 10Cu/silica (393 K) and 5Cu/alumina (see section 3.2.4 and 3.2.6). However, in general the removal of excess oxygen was more pronounced over catalysts, which contained copper and cerium components.

The ratio of carbon monoxide yield to carbon dioxide yield (averaged over the five pulses) changed slightly from 1:0.4, for the fresh 5Cu/silica, to 1:0.5, for the aged 5Cu/silica. This was combined with a loss of formation of methyl formate. The change in products indicated that there might have been a change in the decomposition mechanism. Fisher and Bell [196] proposed that over copper/silica catalysts, carbon dioxide and hydrogen were formed from the decomposition of formate species, while carbon monoxide and hydrogen were produced from the decomposition of methyl formate. The difference between a reduced and oxidised copper/silica catalyst was investigated using pulses of methanol [187]. It was found that the main carbon containing product was carbon monoxide over a reduced copper/silica catalyst, while the unreduced catalyst formed mainly carbon dioxide (at 523 K) [187].

The loss of methyl formate as a product after ageing might indicate a change in the mechanism for the production of carbon monoxide. Although it was suggested that carbon monoxide formation occurred by decomposition of methyl formate using copper/silica catalysts [196], it is possible that carbon monoxide can form without the methylformate intermediate. Hence, earlier intermediates such as adsorbed methoxide or formaldehyde may decompose to form carbon monoxide and hydrogen.

The 5Cu5Ce/silica catalyst was examined before and after ageing. The fresh sample had 100% methanol conversion, producing mainly carbon dioxide. Although the initial yield of carbon monoxide was low it increased as the number of methanol pulses increased (figure 3.5.3 and table 3.5.4).

Figure 3.5.3. Methanol decomposition products using 5Cu5Ce/silica (April '02).

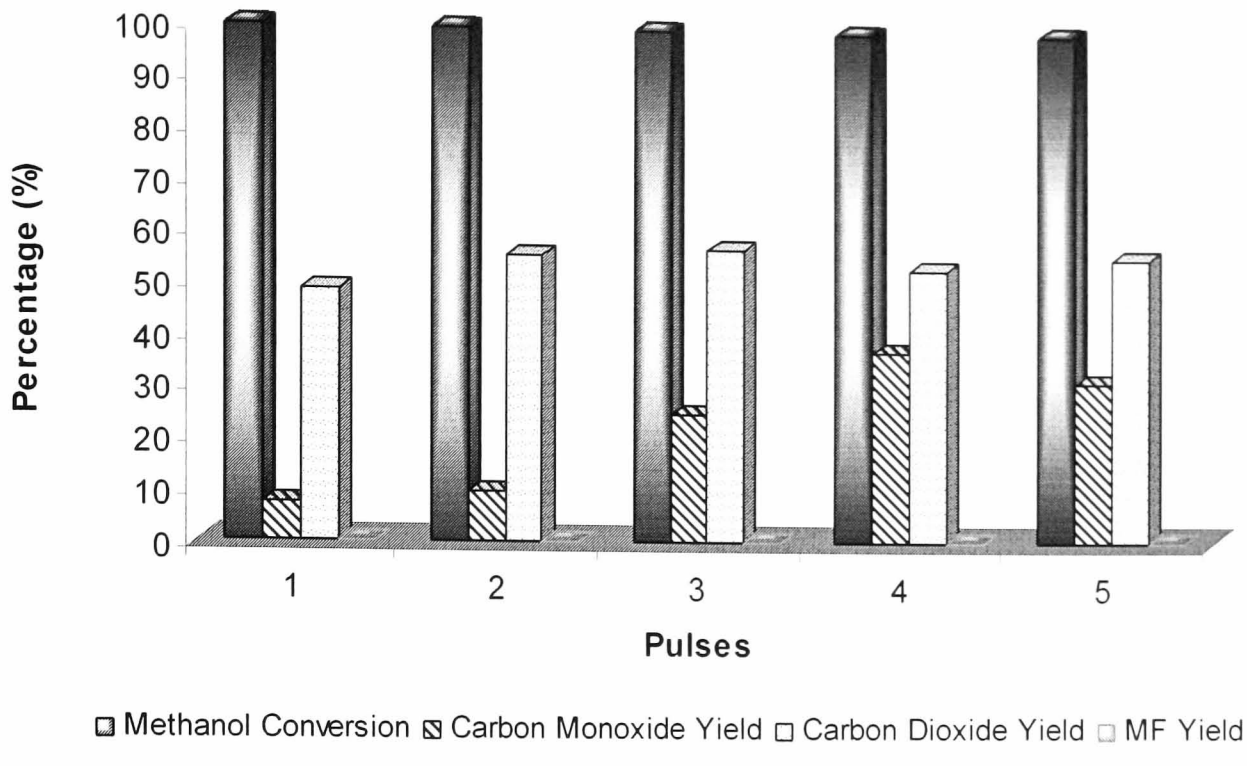

Table 3.5.4. Mass balance and yield of products during methanol decomposition, 5Cu5Ce/silica.

Pulse	*Mass Balance (%)*		*Conversion*	*Yield of Products (%)*		
	Carbon	*Oxygen*	*(%)*	CO_2	*CO*	*MF*
1	56.7	105.9	100.0	49.2	7.6	0.0
2	65.8	121.8	100.0	56.0	9.8	0.0
3	82.5	139.8	100.0	57.3	25.2	0.0
4	91.3	145.0	100.0	53.7	37.6	0.0
5	87.9	144.0	100.0	56.1	31.8	0.0

The reactivity of the aged 5Cu5Ce/silica fluctuated across the pulses. Unlike the fresh catalyst, which produced mainly carbon dioxide, the main product was carbon monoxide. Although some oxygen was lost from the catalyst surface the effect was not as pronounced as for the fresh catalyst. This indicated that a change in surface structure might have occurred during the ageing process, reducing the availability of surface oxygen.

Figure 3.5.4. Methanol decomposition products using aged 5Cu5Ce/silica (April '04).

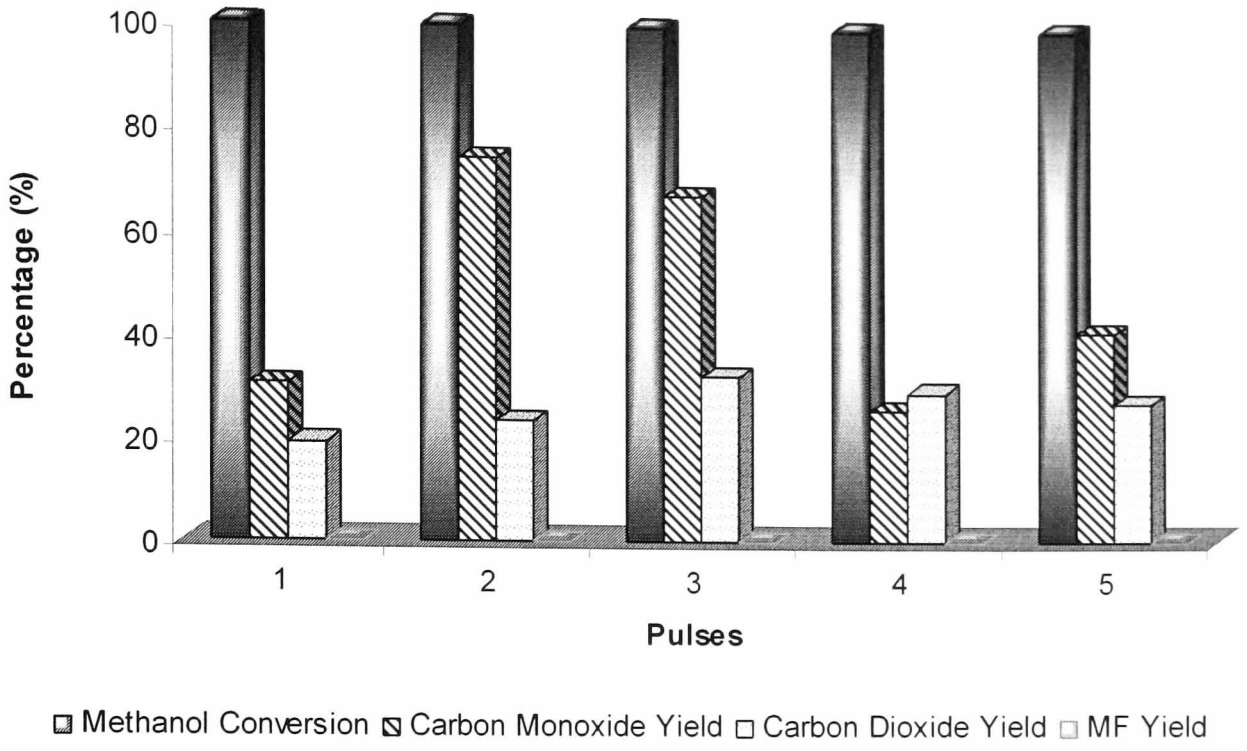

Table 3.5.5. Mass balance and yield of products during methanol decomposition, aged 5Cu5Ce/silica.

Pulse	Mass Balance (%)		Conversion (%)	Yield of Products (%)		
	Carbon	Oxygen		CO_2	CO	MF
1	49.7	68.9	100.0	19.2	30.5	0.0
2	98.3	121.9	100.0	23.6	74.7	0.0
3	99.9	132.2	100.0	32.4	67.5	0.0
4	55.4	84.8	100.0	29.4	26.0	0.0
5	68.5	95.8	100.0	27.3	41.1	0.0

The ratio of carbon monoxide to carbon dioxide (averaged from five pulses) changed from 1:2.7 to 1:0.6 after ageing. This was a dramatic switch in favour of carbon monoxide formation. The ratio of carbon oxides of the aged 5Cu5Ce/silica was similar to that of the aged 5Cu/silica. Methanol decomposition using the fresh 5Cu5Ce/silica catalyst indicated that excess surface oxygen was utilised during decomposition. It is likely that the ageing process reduced the availability or reactivity of the surface oxygen/hydroxyls. Therefore the active sites favoured the formation of carbon monoxide. It was suggested that surface oxygen/hydroxyls accelerate the formation of adsorbed methylene bisoxy ($CH_2(O)_2$) [194]. The methylene bisoxy decomposes to form a mono/bidentate formate, which can then decompose to form carbon dioxide and hydrogen [194, 196]. Therefore, it is probable that ageing of the catalyst decreased the concentration of surface oxygen/hydroxyl species on the catalyst surface.

3.5.3 Hydrogenation of 1,3-Butadiene

The hydrogenation of 1,3-butadiene was used as a test reaction to examine the 5Cu/silica and 5Cu5Ce/silica catalysts under continuous flow conditions (see experimental section 2.5.4). Both catalysts were examined in February 2003 then re-tested in March 2004. The reaction was carried out over catalysts at three different hydrogen to hydrocarbon ratios in the following sequence 1:4, 1:2, 1:1 and then 1:4. Between each reaction, hydrogen was used (at isothermal temperature) to clean the catalyst surface of any remaining hydrocarbon. The reaction temperature was 373 K throughout the reaction. Catalysts, which were active for 1,3-butadiene hydrogenation, produced a temperature exotherm during reaction. Hence, the reaction temperature increased slightly when reactant gases flowed over the catalyst.

The 5Cu/silica catalyst showed high conversion of 1,3-butadiene to products, figure 3.5.5. On the fresh catalyst this high conversion only began to decrease at the low hydrocarbon to hydrogen ratio (1:1). Trans but-2-ene was the predominant product produced with the exception of the 1:1 ratio, where but-1-ene was the main product. When the concentration of hydrogen was reduced the yield of butane and cis but-2-ene decreased. After returning to a hydrocarbon to hydrogen ratio of 1:4 the high conversion of the catalyst recovered. However, the ratio of products was different to that of the initial 1:4 ratio.

Figure 3.5.5. 1,3-Butadiene hydrogenation over 5Cu/silica (Feb '03).

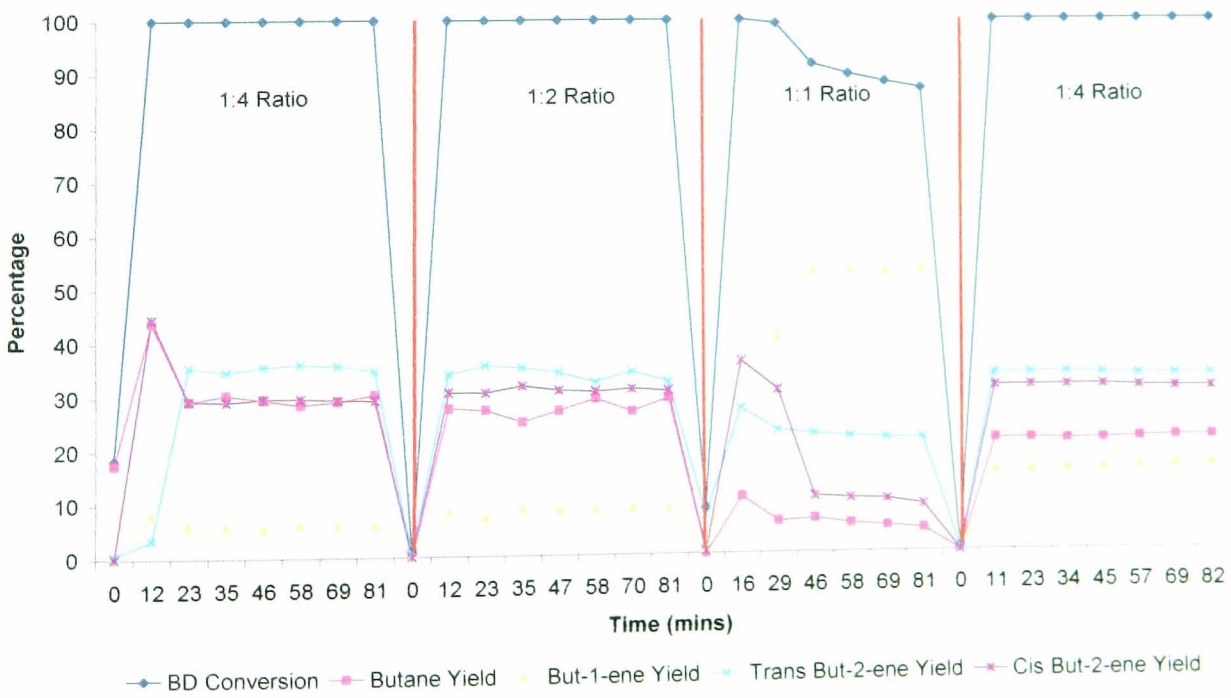

Koeppel and co-workers [249] found that copper/silica catalysts produced predominantly 1-butene during 1,3-butadiene hydrogenation. In addition, the group [249] found that conversion to butane was almost negligible. The standard reaction conditions used temperatures between 373 and 513 K and the ratio of reactant to hydrogen was 1:4 [249]. In addition, Koeppel [249] found that isomerisation during the hydrogenation reaction was negligible and that deactivation during 1,3-butadiene hydrogenation was also low. The results from reference [249] were similar to those found in this study for the 1:1 ratio of gases. However at higher hydrogen ratios (1:2 and 1:4) butane, cis-but-2-ene and trans-but-2-ene were produced and 1-butene yield was less than ~15 %. In addition, trans-but-2-ene was present at all stages of the reaction, suggesting that isomerisation was occurring.

After one year, there was a dramatic decrease in the activity of the catalyst towards hydrogenation, figure 3.5.6. The 1:4 ratio showed that but-1-ene yield increased as the yield of butane decreased. Although initial activity of the catalyst during the 1:4 reaction was high, subsequent gas ratios had very low conversions of 1,3-butadiene. Treatment of the catalyst with hydrogen between runs did not improve the conversion of the catalyst. During the repeat of the 1:4 reaction the conversion was lower than 3%.

Figure 3.5.6. 1,3-Butadiene hydrogenation over aged 5Cu/silica (Mar '04).

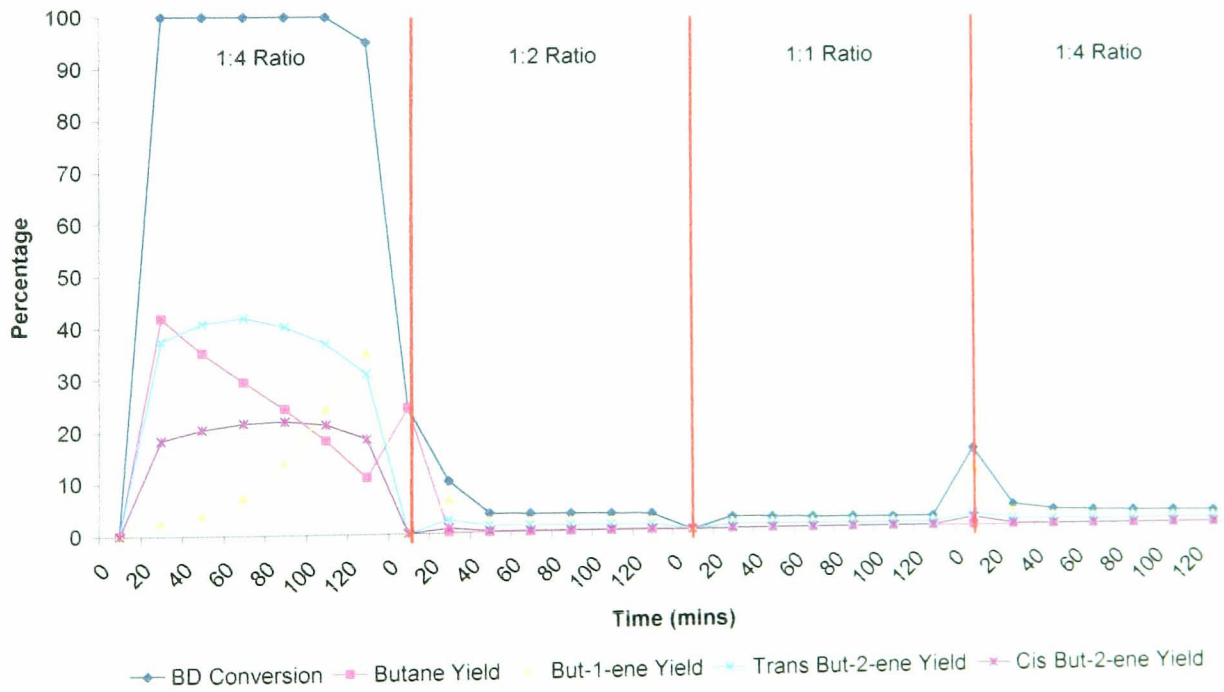

The fresh 5Cu5Ce/silica catalyst was examined for its hydrogenation activity. Addition of cerium to the copper catalyst appeared to have a detrimental effect on catalyst

activity, figure 3.5.7. The 5Cu5Ce/silica (fresh) deactivated more rapidly than 5Cu/silica (fresh) and on repeating the 1:4 ratio, less than 70% conversion was achieved. During the initial 1:4 reaction, the product ratio changed at 48 mins, at the same time the conversion began to decrease. Unlike 5Cu/silica (fresh), but-1-ene was the predominant product across all of the ratios after 48 minutes.

Figure 3.5.7. 1,3-Butadiene hydrogenation over 5Cu5Ce/silica (Feb '03).

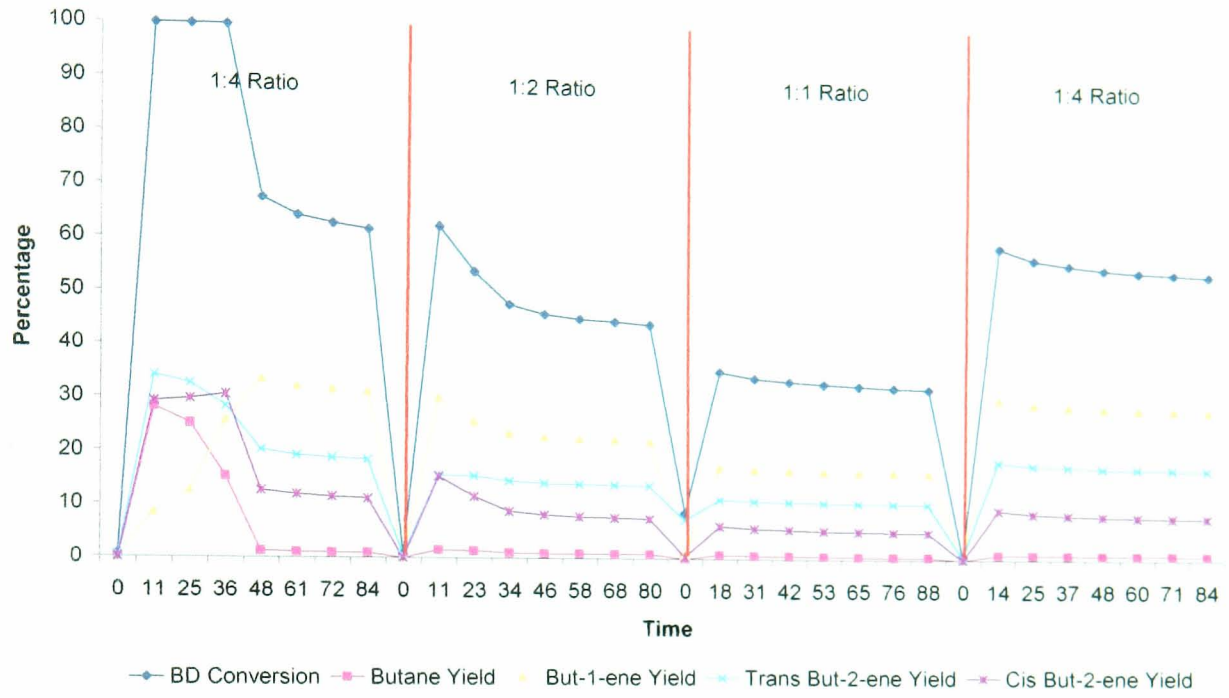

The aged 5Cu5Ce/silica catalyst was tested for 1,3-butadiene hydrogenation and was the least active of the catalysts examined. Initial reactivity declined rapidly and conversion fell below 4% after only 40 mins. Deactivation of the fresh 5Cu5Ce/silica catalyst was observed between 36 and 48 minutes (figure 3.5.7). Figure 3.5.8 showed that the reactivity did not improve on altering the hydrocarbon to hydrogen ratio. Cleaning the catalysts between runs with hydrogen did not improve the reactivity of the catalyst.

Figure 3.5.8. 1,3-Butadiene hydrogenation over aged 5Cu5Ce/silica (Mar '04).

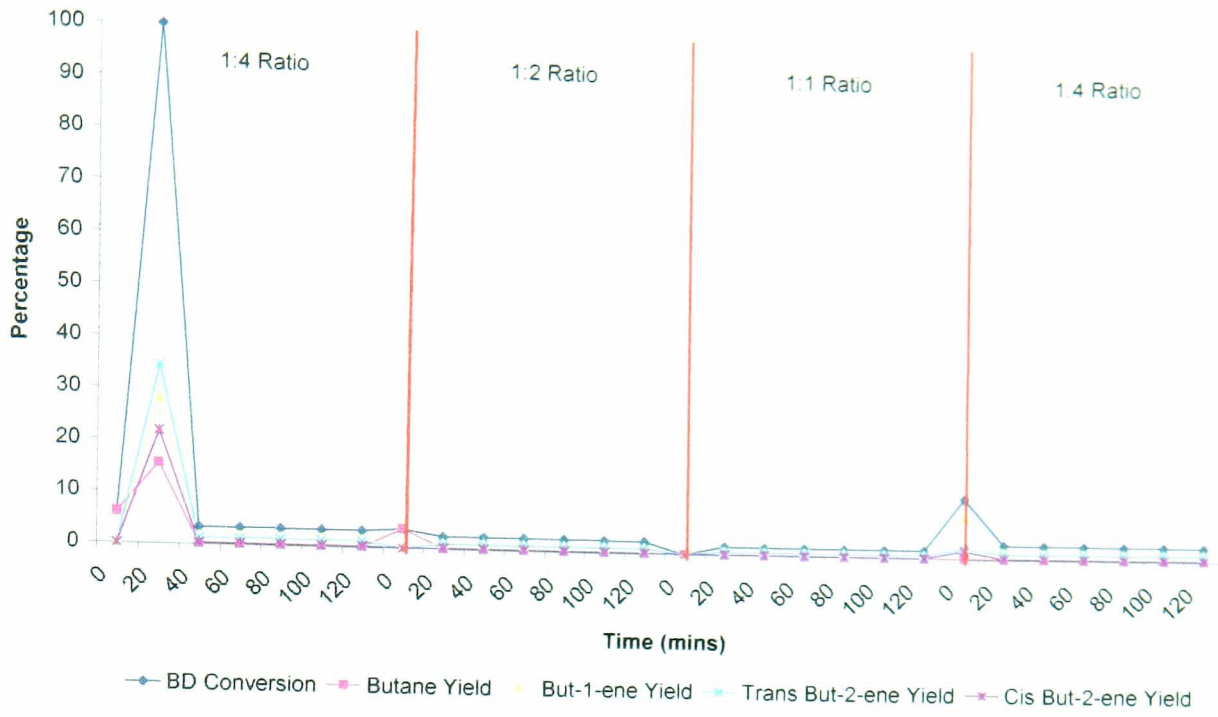

After being stored for approximately one year (in Feb '03) the copper/silica and copper and cerium/silica catalysts were still active for the hydrogenation reaction. However, after storage for a further year under the same conditions, the reactivity of the catalysts was severely retarded. Both the long term stability and activity of the catalysts were reduced due to the effects of catalyst ageing. The profiles of the 1,3-butadiene hydrogenations, at different ratios, using the fresh catalysts, provided information about the mechanism of the reaction. However, analysis of these results was out with the scope of this project. It was clear that after being stored for two years, the catalysts were no longer active for the hydrogenation reaction.

The ageing process was observed by N. Young [115], using palladium/C30 catalysts. TEM showed that palladium crystallites were located not on the silica surface but either on or within the matrix of a secondary more crystalline silica species present in the catalyst after ageing [115]. In addition, carbon monoxide chemisorption showed that the metal surface area of the aged catalysts had decreased [115]. The reason given for the changes to the catalyst was that encapsulation of metal particles occurred due to a restructuring of the support. As ageing of the catalyst was only observed for the palladium/silica catalyst and not the nickel/silica catalyst used in the study [115], it appeared that the choice of metal influenced whether or not the catalyst aged during storage. In addition, a loss of catalyst activity was reported for a Rh/silica hydrogenation catalyst which had been stored for 18 months [248].

Silicas prepared by low pressure chemical vapour deposition (LPCVD) or flame hydrolysis were found to be metastable, as once formed the siloxane rings or cages were unable to break Si-O-Si bonds to rearrange to a more stable configuration at low temperatures [25]. However sol-gel silicas were found to allow re-equilibration of metastable siloxane rings and cages by polymerisation and depolymerisation reactions [25]. Volume contraction during aging of sol-gel silicas reduced strain in the silica structure [25].

As a result of testing fresh and aged catalysts for methanol decomposition and 1,3-butadiene hydrogenation, it appeared that storage of the catalysts for two years had greatly changed the behaviour of the catalysts. Although still able to adsorb oxygen, the reactivity towards the hydrogenation of 1,3-butadiene had decreased and there was a change in the ratio of products formed by the decomposition of methanol. Although the oxygen chemisorptions showed little change in metal dispersion, the poor activity of the aged catalysts towards the hydrogenation reaction suggested that there was a reduction in the number of active sites for the hydrogenation reaction. The new sites were readily deactivated during the hydrogenation process, but the catalysts were still able to decompose methanol. However, the results indicated that the surface of both 5Cu/silica and 5Cu5Ce/silica had undergone changes. Hence the availability of surface oxygen/hydroxyls had altered.

As reported in section 3.1.7.2, the reduction process appeared to change not only the active species of the catalyst but to alter the structure of the catalyst support. Initially, the silica surface was composed of silanol groups and small strained rings (2- to 4- fold) [25]. Examination of the freshly prepared catalysts by Raman spectroscopy showed that all of the catalysts contained 3- and 4-membered rings (section 3.1.7.1). It has been suggested from NMR that porous silicas have a high content of 3-membered rings [26, 250]. From the *in-situ* Raman spectroscopy investigation (3.1.7.2) it appeared that encapsulation of the surface copper (and/or cerium) by the silica led to the formation of larger, more stable siloxane rings, after heating the catalyst in hydrogen. After reduction, the fresh catalysts were active for the 1,3-butadiene hydrogenation, whereas the aged catalysts rapidly deactivated. Even in the absence of hydrogen, it is probable that the slow re-arrangement of the surface structure during storage could have encapsulated the active metal species. Increased temperature during reduction increased

the rate of the ring expansion; the *in-situ* Raman spectroscopy studies followed the disappearance of the (3- and 4-fold) rings over a period of two hours. Hence two years of storage may have led to a similar process, encapsulating the active metal within larger siloxane rings (5-fold and greater). After reduction in hydrogen the reactivity of the aged catalysts had changed, indicating changes to the sites active for methanol decomposition and 1,3-butadiene hydrogenation.

After changes in catalytic activity were detected, no further testing of the silica-supported catalysts was carried out. Improved characterisation of the fresh and aged catalysts would be required to gain a full understanding of the processes occurring during the ageing process. In particular, N_2O chemisorption and Raman spectroscopy of the aged catalysts would provide more information about the metal surface area and the possible loss of 3- and 4-fold siloxane rings.

4 CONCLUSIONS

A series of copper and copper and cerium catalysts were successfully prepared and characterised. Initial attempts to explore the use of precursors other than nitrates proved difficult and no benefits were achieved by using alternative precursors.

Characterisation of the catalysts revealed that contrary to expectations, a reduction treatment to 523 K in hydrogen was not sufficient to completely reduce the copper species of a copper/support catalyst. *In-situ* Raman spectroscopy showed that copper (I) oxide was present after reduction of the 5Cu/silica catalyst. XRD patterns confirmed that non-crystalline materials were present on the surface of the catalyst both pre- and post-reaction.

The cerium/support catalysts proved to be non-facile materials to characterise. XRD showed that on the silica support the material was non-crystalline whereas on the alumina support some crystalline ceria was present prior to reduction. After reduction, crystalline ceria was present on both catalysts. Solid-state UV-Vis and Raman spectroscopy confirmed only that the nitrate species remained present on the support after drying the catalyst. Temperature programmed reduction confirmed that temperatures greater than 660 K are required to begin surface reduction.

Combining both copper and cerium on the catalysts changed the reactivity of both species. Characterisation of the mixed metal catalysts showed that the copper oxide formed had greater stability in the presence of ceria. This indicated a strong interaction between the two components, possibly similar to the synergetic effects, which have been reported for noble metal/ceria catalysts. In particular, in addition to added stability of the copper (I) oxide, *in-situ* Raman spectroscopy showed that the ceria had been partially reduced. This confirmed the close interaction between the two metals, with the possibility that the ceria is able to donate oxygen towards the copper to maintain the copper (I) oxide species.

For comparison a second support was also selected from which a range of catalysts was prepared. Characterisation showed differences even in the dried form of the catalyst. Solid state UV-Vis analysis showed that the main species present on the dried copper/silica catalyst was copper (II) nitrate hydrate as opposed to the copper (II) nitrate

hydroxide observed on the copper/alumina catalyst. This effect was also detected for the mixed metal catalysts.

After comparison with reference catalysts, methanol decomposition was found to be a useful method for examining possible applications of the prepared catalysts. All of the catalysts, which contained copper were active as decomposition catalysts. In the case of the silica-supported catalysts, the mixed metal catalysts showed an increase in the production of carbon dioxide with the exception of 5Cu1Ce/silica. It may be that addition of small amounts of cerium is sufficient to encourage selectivity towards the carbon monoxide. At higher cerium loadings the main effect is to supply surface oxygen, encouraging formation of carbon dioxide. With the alumina supported catalysts, the opposite trend was observed. 5Cu/alumina behaved similarly to the commercial catalyst, showing the highest selectivity towards carbon dioxide formation. On addition of cerium (i.e. 5Cu5Ce/alumina), carbon monoxide was detected in the products; however the main product remained carbon dioxide. The result of the investigation was that all of the catalysts prepared formed carbon dioxide, which would have behaved as a poison towards the copper/cerium alloy catalysts.

During the methanol decomposition reaction, excess oxygen was detected in the products of the mixed metal catalysts, 10Cu/silica and 5Cu/alumina. In the case of the copper catalysts, it is likely that unreduced copper species provide the main source of the excess oxygen. However, with the mixed metal catalysts it is likely that both unreduced copper oxide and ceria are being further reduced by the reaction mixture. As this effect is not observed for the cerium/support catalysts, this confirms that close interaction of the copper and cerium is required to observe this effect.

As the copper and cerium/support catalysts did not replicate the high activity/selectivity of the intermetallic alloy catalysts, attempts were made to investigate what was thought to be an active component of the alloy catalyst. Investigation of the cerium hydride showed that it was readily able to exchange hydrogen, was able to catalyse the hydrogenation of an alkyne and was unreactive towards carbon monoxide or carbon dioxide. As expected, on exposure to air/oxygen an increase in temperature was observed combined with the release of hydrogen. Investigation of methanol decomposition showed that the catalyst reacted irreversibly with methanol to produce

methane. This result provides an insight into the inability of the workers from the previous study to improve the stability of the catalysts. Even when poisoning and temperature effects were controlled deactivation of the alloy catalysts still occurred. It now appears that this was due to the poisoning effect of the reactant itself.

Testing the catalytic activity of the catalysts as shift catalysts confirmed the importance of surface oxygen species, in particular when carrying out pulse testing. The copper/support catalysts showed the highest selectivity towards the shift reaction. On addition of cerium to the copper/support catalysts, although still active for the shift reaction, carbon monoxide oxidation became the main reaction. An increase in adsorption of carbon containing species was observed on addition of cerium. This is most likely due to the formation of carbonates on the ceria. However, the ceria/support catalysts were relatively inactive towards the shift mixture, suggesting that only reduced ceria forms the adsorbed species. By pre-treating the catalysts with carbon monoxide and oxygen, differences were observed in the selectivity of the catalysts towards the shift reaction. Overall, carbon monoxide had the effect of further reducing the surface, hence enhancing the selectivity of the catalyst towards the shift reaction. After exposure to oxygen, the surface of the catalyst was oxidised. Hence, the carbon monoxide in the subsequent shift reaction mixture simply re-reduced the catalyst. In addition, the mixed catalysts produced less of an exotherm on exposure to oxygen. Hence, addition of ceria to copper containing catalysts may have a prospective use for reducing the exotherm of copper containing catalysts on exposure to air.

Unexpectedly, during the course of the study changes were observed in the activity of the copper/silica and copper and cerium/silica catalysts. By repeating previous characterisation processes such as oxygen chemisorption it appeared that there was little change in the behaviour of the catalysts. Testing with methanol pulses revealed changes in the product distribution of the catalysts in their fresh and aged states. However, the most dramatic changes were observed in the catalyst ability to hydrogenate 1,3-butadiene. Both aged catalysts showed severe loss in activity with rapid deactivation occurring during the reaction. It is likely that the ageing process occurs through a slow rearrangement of the silica ring structure. The resulting effect is encapsulation of the active metal species, which in turn has a strong effect on the catalytic properties of the material.

5 REFERENCES

1. J.M. Thomas and W.J. Thomas, *Principles and Practice of Heterogeneous Catalysis*, Weinheim: VCH Verlagsgesellschaft mbH (1997).
2. M.V. Twigg, *Catalyst Handbook*. Second ed, London: Manson Publishing (1996).
3. J.T. Richardson, *Principles of Catalysts Development*. Fundamental and Applied Catalysis, ed. M.V. Twigg and M.S. Spencer, New York and London: Plenum Press (1989).
4. M.V. Twigg and M.S. Spencer. *Topics in Catalysis*, **22**(3-4), 191 (2003).
5. D.A. Dowden. *La Chimica E L'Industria*, **55**(8), 639 (1973).
6. C.N. Satterfield, in *Heterogeneous Catalysis in Practice*. New York: McGraw-Hill, 214-221 (1980).
7. S.P.S. Andrew. *Chemtech*, **9**, 180 (1979).
8. E. Lieber and F.L. Morritz. *Adv. Catal.*, **5**, 417 (1953).
9. M. Komiyama. *Catal. Rev.*, **27**, 341 (1985).
10. R.L. Augustine, *Heterogeneous Catalysis for the Synthetic Chemist*, New York: Marcel Dekker, Inc (1996).
11. A.B. Stiles, *Catalyst Supports and Supported Catalysts*, Boston: Butterworths (1987).
12. R.K. Oberlander. *Appl. Ind. Catal.*, **3**, 63 (1984).
13. C. Morterra and G. Magnacca. *Catal. Today*, **27**, 497 (1996).
14. M. Che and C.O. Bennet. *Adv. Catal.*, **36**, 55 (1989).
15. H. Knözinger and P. Ratnasamy. *Catal. Rev. Sci. Eng.*, **17**, 31 (1978).
16. M. Trombetta, G. Busca, S. Rossini, V. Piccoli, U. Cornaro, A. Guercio, R. Cantani, and R.J. Willey. *J. Catal.*, **179**, 581 (1998).
17. B. Shi and B.H. Davis. *J. Catal.*, **157**, 359 (1995).
18. H. Knözinger. *Angew. Chem. Int. Ed. Engl.*, **7**, 791 (1968).
19. S.H. Cai and K. Sohlberg. *J. Mol. Catal. A: Chem.*, **193**, 157 (2003).
20. G. Busca. *Catal. Today*, **27**, 457 (1996).
21. V.S.Y. Lin, D.R. Radu, M.K. Han, W.H. Deng, S. Kuroki, B.H. Shanks, and M. Pruski. *J. Am. Chem. Soc.*, **124**, 9040 (2002).
22. K.C. Taylor. *Catal. Rev. Sci. Eng.*, **35**, 457 (1993).
23. R.W. McCabe, R.K. Usmen, K. Ober, and H.S. Gandhi. *J. Catal.*, **151**, 385 (1995).
24. G.C. Bond. *Appl. Catal.*, **71**, 1 (1991).

25. P.D. Maniar and A. Navrotsky. *J. of Non-Crystalline Solids*, **120**, 20 (1990).
26. L.F. Gladden, M. Vignaux, P. Chiaranussati, R.W. Griffiths, S.D. Jackson, J.R. Jones, A.P. Sharratt, F.J. Robertson, G. Webb, P. Chieux, and A.C. Hannon. *J. of Non-Crystalline Solids*, **139**, 47 (1992).
27. L.T. Zhuravlev. *Langmuir*, **3**, 316 (1987).
28. A. van Blaaderen and A.P.M. Kentgens. *J. Non-Cryst. Solids*, **149**, 161 (1992).
29. J.R. Anderson, in *Structure of Metallic Catalysts*. New York: Academic Press, 39 (1975).
30. A. Trovarelli. *Catal. Rev.*, **38**, 439 (1996).
31. D. Martin and D. Duprez. *J. Phys. Chem.*, **100**, 9429 (1996).
32. A. Badri, C. Binet, and J.-C. Lavalley. *J. Chem. Soc. Faraday Trans.*, **93**(6), 1159 (1997).
33. H.C. Yao and Y.F. Yu Yao. *J. Catal.*, **86**, 254 (1984).
34. A. Trovarelli, C. de Leitenburg, C. Dolcetti, and J. Llorca. *J. Catal.*, **151**, 111 (1995).
35. A. Badri, J. Lamotte, J.C. Lavalley, A. Laachir, V.Perrichon, and O. Touret. *Eur. J. Solid State Inorg. Chem.*, **28**, 445 (1991).
36. A. Laachir, V. Perrichon, A. Badri, J. Lamotte, E. Catherine, J.C. Lavalley, J.E. Fallah, L. Hilaire, F. Le Normand, E. Quéméré, G.N. Sauvion, and O. Touret. *J. Chem. Soc. Faraday Trans.*, **87**, 1601 (1991).
37. M. Ricken, J. Nölting, and I. Reiss. *J. Solid State Chem.*, **54**, 89 (1984).
38. W. Liu and M. Flytzani-Stephanopoulos. *J. Catal.*, **153**, 317 (1995).
39. A. Tscöhpe, W. Liu, M. Flytzani-Stephanopoulos, and J.Y. Ying. *J. Catal.*, **157**, 42 (1995).
40. J.C. Summers and S.A. Ausen. *J. Catal.*, **58**, 131 (1979).
41. G. Kim. *Ind. Eng. Chem. Prod. Res. Dev.*, **21**, 267 (1982).
42. P.J.A. Tijm, F.J. Waller, and D.M. Brown. *Appl. Catal. A*, **221**, 275 (2001).
43. J.P. Lange. *Catal. Today*, **64**, 3 (2001).
44. X.M. Liu, G.Q. Lu, Z.F. Yan, and J. Beltrmini. *Ind. Eng. Chem. Res.*, **42**, 6518 (2003).
45. G.C. Chinchen, K. Mansfield, and M.S. Spencer. *Chemtech*, **20**, 692 (1990).
46. K.C. Waugh. *Solid State Ionics*, **168**, 327 (2004).
47. G.C. Chinchen, P.J. Denny, J.R. Jennings, M.S. Spencer, and K.C. Waugh. *Appl. Catal.*, **36**, 1 (1988).

48. M. Kurtz, H. Wilmer, T. Genger, O. Hinrichsen, and M. Muhler. *Catal. Lett.*, **86**, 77 (2003).

49. S.P.S. Andrew. *Chem. Eng. Sci.*, **36**, 1431 (1981).

50. J.T. Gallagher and J.M. Kidd. UK Patent, 1 159 035

51. K. C. Waugh. *Catalysis Today*, **15**, 51 (1992).

52. M. Muhler, E. Tornqvist, L.P. Nielsen, B.D. Clausen, and H. Topsoe. *Catal. Lett.*, **25**, 1 (1994).

53. G.J. Millar, C.H. Rochester, and K.C. Waugh. *J. Chem. Soc. Faraday Trans.*, **87**, 1491 (1991).

54. A.Y. Rozovskii and G.I. Lin. *Topics in Catalysis*, **22**(3-4), 137 (2003).

55. M.S. Spencer. *Catal. Lett.*, **50**, 37 (1998).

56. J.L. Robbins, E. Iglesia, C.P. Kelkar, and B. DeRites. *Catal. Lett.*, **10**, 1 (1991).

57. J. Saussey and J.C. Lavalley. *J. Mol. Catal.*, **50**, 343 (1989).

58. M.E. Fakely, J.R. Jennings, and M.S. Spencer. *J. Catal.*, **118**, 483 (1989).

59. B. Imelik and J.C. Vedrine, *Catalyst Characterization*, New York: Plenum Press (1994).

60. R. Burch, S.E. Golunski, and M.S. Spencer. *J. Chem. Soc. Faraday Trans.*, **86**, 2683 (1990).

61. G.C. Bond, *Spillover of Adsorbed Species*, ed. G.M. Pajonk, S.J. Teichner, and J.E. Germain, Amsterdam: Elsevier Science Publishers B.V. (1983).

62. K.D. Jung and A.T. Bell. *J. Catal.*, **193**, 207 (2000).

63. J. Nakamura, Y. Choi, and T. Fujitani. *Topics in Catalysis*, **22**(3-4), 277 (2003).

64. A.J. Bridgewater, M.S. Wainwright, and D.J. Young. *Appl. Catal.*, **28**, 241 (1986).

65. J.B. Friedrich, M.S. Wainwright, and D.J. Young. *J. Catal.*, **80**, 1 (1983).

66. J.R. Mellor, N.J. Coville, A.C. Sofianos, and R.G. Copperthwaite. *Appl. Catal. A*, **164**, 171 (1997).

67. L. Ma, T. Tran, and M.S. Wainwright. *Topics in Catalysis*, **22**(3-4), 287 (2003).

68. W.G. Baglin, G.B. Atkinson, and L.J. Nicks. *Ind. Eng. Chem. Prod. Res. Dev.*, **20**, 87 (1981).

69. J.E. France and W.E. Wallace. in *12th Regional ACS Meeting*. 1980. Pitsburgh.

70. R.M. Nix, R.W. Judd, R.M. Lambert, J.R. Jennings, and G. Owen. *J. Catal.*, **118**, 175 (1989).

71. R.M. Nix, T. Rayment, R.M. Lambert, J.R. Jennings, and G. Owen. *J. Catal.*, **106**, 216 (1987).

72. G. Owen, C.M. Hawkes, D. Lloyd, J.R. Jennings, R.M. Lambert, and R.M. Nix. *Appl. Catal.*, **33**, 405 (1987).

73. C.M. Hay, J.R. Jennings, R.M. Lambert, R.M. Nix, G. Owen, and T. Rayment. *Appl. Catal.*, **37**, 291 (1988).

74. M.E. Fakley, J.R. Jennings, and M.A. Spencer. *J. Catal.*, **118**, 483 (1989).

75. J.R. Jennings, R.M. Lambert, R.M. Nix, G. Owen, and D.G. Parker. *Appl. Catal.*, **50**, 157 (1989).

76. W.J. Shen and Y. Matsumura. *Phys. Chem. Chem. Phys.*, **2**, 1519 (2000).

77. W.-J. Shen and Y. Matsumura. *J. Mol. Catal. A*, **153**, 165 (2000).

78. Y. Borodko and G.A. Somorjai. *Appl. Catal. A*, **186**, 355 (1999).

79. Y. Matsumura and W.-J. Shen. *Topics in Catalysis*, **22**(3-4), 271 (2003).

80. W.-J. Shen, M. Okumura, Y. Matsumura, and M. Haruta. *Appl. Catal. A*, **213**, 225 (2001).

81. S.W. Kaiser. European Patent, 0031 244

82. Y. Kikuzono, S. Kagami, S. Naito, T. Onishi, and K. Tamaru. *Faraday Disc. Chem. Soc.*, **72**, 143 (1981).

83. W.-J. Shen, Y. Ichihashi, H. Ando, M. Okamura, M. Haruta, and Y. Matsumura. *Appl. Catal. A*, **217**, 165 (2001).

84. W.-J. Shen, Y. Ichihashi, and Y. Matsumura. *Catal. Lett.*, **83**, 33 (2002).

85. Y. Matsumura, W.J. Shen, Y. Ichihashi, and H. Ando. *Catal. Lett.*, **68**, 181 (2000).

86. Y. Sakata, N. Kouda, Y. Sakata, and H. Imamura. *Studies in Surface Science and Catalysis*, **143**, 397 (2002).

87. D.S. Newsome. *Catal. Rev. Sci. Eng.*, **21**, 275 (1980).

88. *Introduction to Ammonia Manufacture*, in *http://www.synetix.com/ammonia/pdfs/ammonia.pdf*.

89. *http://www.synetix.com/ammonia/productinformation.htm*.

90. G.C. Chinchen, P.J. Denny, D.G. Parker, M.S. Spencer, and D.A. Whan. *Appl. Catal.*, **30**, 333 (1987).

91. C.-S. Chen, W. -H. Cheng, and S.-S. Lin. *Appl. Catal. A*, **238**, 55 (2003).

92. K.C. Waugh, G.J. Millar, and C.H. Rochester. *J. Chem. Soc. Faraday Trans.*, **88**, 1477 (1992).

93. C.T. Campbell and B.E. Koel. *Surf. Sci.*, **186**, 393 (1987).

94. J. Nakamura, J.M. Campbell, and C.T. Campbell. *J. Chem. Soc. Faraday Trans.*, **26**, 2725 (1990).

95. K. Klier, C.W. Young, and J.G. Nunan. *Ind. Eng. Fundam.*, **25**, 36 (1986).

96. G.C. Chinchen, C.M. Hay, H.D. Vandervell, and K.C. Waugh. *J. Catal.*, **103**, 79 (1987).

97. M.J.L. Gines, N. Amadeo, M. Laborde, and C.R. Apesteguia. *Appl. Catal. A*, **131**, 283 (1995).

98. R.A. Hadden, P.J. Lambert, and C. Ranson. *Appl. Catal. A*, **122**, L1 (1995).

99. I. Fishtik and R. Datta. *Surface Science*, **512**, 229 (2002).

100. S. Hilaire, X. Wang, T. Luo, R.J. Gorte, and J. Wagner. *Appl. Catal.*, **215**, 271 (2001).

101. G. Jacobs. *Appl. Catal.*, **258**, 203 (2004).

102. W. Ruettinger, O. Ilinich, and R.J. Farrauto. *Journal of Power Sources*, **118**, 61 (2003).

103. O. Korotkikh, W.F. Ruettinger, and R.J. Farrauto. US Patent, 6,562,315 (2003).

104. C. Wheeler, A. Jhalani, E.J. Klein, S. Tummala, and L.D. Schmidt. *J. Catal.*, **223**, 191 (2004).

105. S. Hilaire, X. Wang, T. Luo, R.J. Gorte, and J. Wagner. *Appl. Catal. A*, **258**, 271 (2004).

106. S. Sharma, S. Hilaire, J.M. Vohs, R.J. Gorte, and H.-W. Jen. *J. Catal.*, **190**, 199 (2000).

107. G. Jacobs, A. Crawford, L. Williams, P.M. Patterson, and B. Davis. *Appl. Catal. A*, **267**, 27 (2004).

108. G.S. Zafiris and R.J. Gorte. *J. Catal.*, **139**, 561 (1993).

109. N.F. Curtis and Y.M. Curtis. *Inorg. Chem.*, **4**, 805 (1965).

110. U. Chudasama and A.S. Anekar. *J. Mol. Catal.*, **55**, 199 (1989).

111. *CRC Handbook of Chemistry and Physics*. 67th ed, ed. R.C. Weast, M.J. Astle, and W.H. Beyer, Boca Raten, Florida: CRC Press Inc (1986).

112. *Brooks MFC Manual*.

113. S.D. Robertson, B.D. McNicol, J.H. de Baas, S.C. Kloet, and J.W. Jenkins. *J. of Catal.*, **37**, 424 (1975).

114. C.J.G. Van Der Grift, A. Mulder, and J.W. Geus. *Appl. Catal.*, **60**, 181 (1990).

115. N.C. Young. PhD Thesis, University of Glasgow (1995).

116. P.A. Webb and C. Orr, *Analytical Methods in Fine Partical Technology*, Norcross U.S.A.: Micromeritics Instrument Corp. (1997).

117. A. Guiner, *X-Ray Diffraction*, San Francisco and London: W.H. Freeman and Company (1963).

118. T. Toupance, M. Kermarec, and C. Louis. *J. Phys. Chem. B*, **104**, 965 (2000).

119. J.R. Anderson and K.C. Pratt, *Introduction to Characterization and Testing of Catalysts*, Australia: Academic Press (1985).

120. *Catalyst Characterization: Physical Techniques for Solid Materials*, B. Imelik and J.C. Vedrine, Editors. New York: Plenum Press, 417-444 (1994).

121. *Catalyst Characterization Science: Surface and Solid State Chemistry*, ed. M.L. Deviney and J.L. Gland, USA: American Chemical Society (1985).

122. *Catalysis and Surface Characterisation*, ed. T.J. Dines, C.H. Rochester, and J. Thomson, Cambridge: The Royal Society of Chemistry (1992).

123. F. Negrier, E. Marceau, and M. Che. *Chem. Comm.*, **11**, 1194 (2002).

124. C.J. Pouchert and J. Behnke, *Aldrich Library of 1H/13C NMR Spectra*, Milwaukee: Aldrich Chemical Co. (1993).

125. G.D. Fleming and R.E. Shepherd. *Spectrochimica Acta*, **43A**, 1141 (1987).

126. K. Nakamoto, *Infrared and Raman Spectra of Inorganic and Coordination Compounds*. 4th ed, USA: John Wiley and Sons (1986).

127. E. Farkas, E. A. Enyedy, G. Micera, and E. Garriba. *Polyhedron*, **19**, 1727 (2000).

128. A. Maes, R.A. Schoonheydt, A. Cremers, and J.B. Uytterhoeven. *J. Phys. Chem.*, **84**, 2795 (1980).

129. P. Peigneur, J.H. Lunsford, W. De Wilde, and A. Schoonheydt. *J. Phys. Chem.*, **81**, 1179 (1977).

130. G. Basu and S. Basu. *Anal. Chim. Acta*, **21**, 187 (1959).

131. B.J. Hathaway and D.E. Billing. *Co-ordination Chem. Rev.*, **5**, 143 (1970).

132. H.B. Jonassen, R.E. Reeves, and L. Segal. *J. Am. Chem. Soc.*, **77**, 2667 (1955).

133. L. Trouillet, T. Toupance, F. Villain, and C. Louis. *Phys. Chem. Chem. Phys.*, **2**, 2005 (2000).

134. J. Bjerrum and E.J. Nielson. *Acta Chem. Scand.*, **2**, 297 (1948).

135. Y. Omura, I. Nakagawa, and T. Shimanouchi. *Spectrochimica Acta*, **27A**, 2227 (1971).

136. J.M. Jehng, H. Hu, X. Gao, and I.E. Wachs. *Catalysis Today*, **28**, 335 (1996).

137. P.M. Castro and P.W. Jadodzinski. *Spectrochimica Acta*, **47A**(12), 1707 (1991).

138. M. Sakai, M. Hayakawa, N. Kuroda, Y. Nishina, and M. Yamashita. *J. Phys. Soc. Japan*, **60**, 1619 (1991).

139. S.D. Jackson, F.J. Robertson, and J. Willis. *J. Mol. Catal.*, **63**, 255 (1990).

140. R. Ganesan and B. Viswanathan. *J. Phys. Chem. B*, **108**, 7102 (2004).

141. I.A. Salen and M.S. El-Maazawi. *Chemosphere*, **41**, 1173 (2000).

142. A. Bensalem, J.C. Mueller, and F. Bozon-Verduraz. *J. Chem. Soc. Faraday Trans.*, **88**(1), 153 (1992).

143. M.C. Marion, E. Garbowski, and M. Primet. *J. Chem. Soc. Faraday Trans.*, **87**, 1795 (1991).

144. *Introduction to Zeolite Science and Practise*, ed. H. van Beklam, E.M. Flanigen, and J.C. Jansen, Amsterdam: Elsevier Science Publishers B.V. (1991).

145. *Powder Diffraction File (CD-ROM)*. 2000, International Centre for Diffraction Data: Newton Square, Pa.

146. S.A. Selim, H.A. Hassan, M. Abd-El-Kalik, and R.SH. Mikhail. *Thermochimica Acta*, **45**, 349 (1981).

147. M.A. Kohler, H.E. Curry-Hyde, A.E. Hughes, B.A. Sexton, and N.W. Cant. *J. Catal.*, **108**, 323 (1987).

148. P.W. Park and J.S. Ledford. *Catal. Lett.*, **50**, 41 (1998).

149. E.M. Lopasso, J.J. Andrade Gamboa, J.M. Astigueta, and D.M. Pasquevich. *J. Mater. Sci*, **32**, 3299 (1997).

150. M. Pijolat, M. Dauzat, and M. Soustelle. *Thermochimica Acta*, **122**, 71 (1987).

151. I.E. Wachs. *Topics in Catalysis*, **8**, 57 (1999).

152. L. Dixit, D.L. Gerrard, and H.J. Bowley. *Appl. Spect. Rev.*, **22**, 189 (1986).

153. J.M. Stencel, *Raman Spectroscopy for Catalysis*, New York: Van Nostrand Reinhold (1990).

154. I.E. Wachs. *Catalysis Today*, **27**, 437 (1996).

155. J.P. Mathieu and M. Lounsbury. *Discussions Faraday Soc.*, **9**, 196 (1950).

156. R. Ananthakrishan. *Proc. Indian Acad. Sci. A*, **5**, 447 (1937).

157. L.T. Zhuravlev. *Colloids and Surfaces A*, **173**, 1 (2000).

158. A. Jagminas, G. Niaura, J. Kuzmarksyte, and R. Butkiene. *Appl. Surf. Sci.*, **225**, 302 (2004).

159. L. Dong, Y. Hu, D. Lu, B. Xu, Z. Hu, and Y. Chen. *J. Phys. Chem. B*, **104**, 78 (2000).

160. M.S.P. Francisco, V.R. Mastelaro, P.A.P. Nascente, and A.O. Florentino. *J. Phys. Chem. B*, **105**, 10515 (2001).

161. L.F. Gladden, M. Vignaux, R.W. Griffiths, S.D. Jackson, J.R. Jones, A.P. Sharratt, F.J. Robertson, and G. Webb. *Physica B*, **180-181**, 785 (1992).
162. W. Liu and M. Flytzani-Stephanopoulos. *Chem. Eng. J.*, **64**, 283 (1996).
163. M. Fernández-García, E. Gómez Rebollo, A. Guerro Ruiz, J.C. Conesa, and J. Soria. *J. Catal.*, **172**, 146 (1997).
164. X.M. Lin, L.P. Li, G.S. Li, and W.H. Su. *Materials Chemistry and Physics*, **69**, 236 (2001).
165. A.G. Dedov, A.S. Loktev, I.I. Moiseev, A. Aboukais, J.-F. Lamonier, and I.N. Filimonov. *Appl. Catal. A*, **245**, 209 (2003).
166. W. Shan, W. Shen, and C. Li. *Chem. Mater.*, **15**, 4761 (2003).
167. J.B. Wang, H.-K. Lee, and T.-J. Huang. *Catal. Lett.*, **83**, 79 (2002).
168. L.E. Briand, A.M. Hirt, and I.E. Wachs. *J. Catal.*, **202**, (2001).
169. N.W. Hurst, S.J. Gentry, A. Jones, and B.D. McNicol. *Catal. Rev. -Sci. Eng.*, **24**, 233 (1982).
170. C. Decarne, E. Abi-Aad, B.G. Kostyuk, V.V. Lunin, and A. Aboukaïs. *J. Mater. Sci*, **39**, 2349 (2004).
171. A. Chambers, S.D. Jackson, D. Stirling, and G. Webb. *J. Catal.*, **168**, 301 (1997).
172. V. Higgs and J. Pritchard. *Appl. Catal.*, **25**, 149 (1986).
173. *CRC Chemical and Physical Data Handbook.*
174. P.-O. Larsson and A. Andersson. *Appl. Catal. B*, **24**, 175 (2000).
175. G.C. Bond, S.N. Namijo, and J.S. Wakeman. *J. Mol. Catal.*, **64**(3), 305 (1991).
176. J.J.F. Scholten, A.P. Pijpers, and A.M.L. Hustings. *Catal. Rev.-Sci. Eng.*, **27**, 151 (1985).
177. G.E. Parris and K. Klier. *J. Catal.*, **97**, 374 (1986).
178. E. Giamello, B. Fubini, P. Lauro, and A. Bossi. *J. Catal.*, **87**, 433 (1984).
179. S.D. Jackson, A.W. Owens, and M.W. Roberts. *Indian J. Tech.*, **30**, 85 (1992).
180. C.J.G. Van Der Grift, A.F.H. Wielers, B.P.J. Joghi, J. Van Beijnum, M. De Boer, M. Versluijs-Helder, and J.W. Geus. *J. Catal.*, **131**, 178 (1991).
181. T.J. Osinga, B.G. Linsen, and W.P. Van Beek. *J. Catal.*, **7**, 277 (1967).
182. J.W. Evans, M.S. Wainwright, A.J. Bridgewater, and D.J. Young. *Appl. Catal.*, **7**, 75 (1983).
183. A. Martínez-Arias. *J. Phys. Chem. B*, **104**(4038), (2000).
184. C. Lamonier, A. Ponchel, A. D'Huysser, and L. Jalowiecki-Duhamel. *Catal. Today*, **50**, 247 (1999).

185. G. Owen, C.M. Hawkes, D. Lloyd, J.R. Jennings, R.M. Lambert, and R.M. Nix. *Appl. Catal.*, **58**, 69 (1990).

186. Y. Matsumura, K. Kagawa, Y. Usami, M. Kawazoe, H. Sakurai, and M. Haruta. *J. Chem. Soc, Chem. Comm.*, 657 (1997).

187. S.D. Jackson, D.S. Anderson, G.J. Kelly, T. Lear, D. Lennon, and S.R. Watson. *Topics in Catalysis*, **22**(3-4), 173 (2003).

188. W.H. Cheng. *Appl. Catal. A*, **130**, 13 (1995).

189. Y. Choi and H.G. Stenger. *Appl. Catal. B*, **38**, 259 (2002).

190. W.H. Cheng, C.Y. Shiau, T.H. Liu, H.L. Tung, J.F. Lu, and C.C. Hsu. *Appl. Catal. A*, **170**, 215 (1998).

191. W.-H. Cheng, C.-Y. Shiau, T.H. Liu, H.L. Tung, H.H. Chen, J.-F. Lu, and C.C. Hsu. *Appl. Catal. B*, **18**, 63 (1998).

192. S. Imamura, H. Yamane, H. Kanai, T. Shibata, K. Utani, and K. Hamanda. *Journal of the Japan Petroleum Institute*, **45**, 187 (2002).

193. S. Shiizaki, I. Nagashima, Y. Matsumura, and M. Haruta. *Catal. Lett.*, **56**, 227 (1998).

194. D.B. Clarke, D.-K. Lee, M.J. Sandoval, and A.T. Bell. *J. Catal.*, **150**, 81 (1994).

195. M.S. Spencer. *Catal. Lett.*, **60**, 45 (1999).

196. I.A. Fisher and A.T. Bell. *J. Catal.*, **184**, 357 (1999).

197. M.A. Peña, J.P. Gómez, and J.L.G. Fierro. *Appl. Catal. A*, **144**, 7 (1996).

198. W.R.A.M. Robinson and J.C. Mol. *Appl. Catal.*, **44**(1-2), 165 (1988).

199. A. Gotti and R. Prins. *J. Catal.*, **178**, 511 (1998).

200. E.M. Cordi, P.J. O'Neil, and J.L. Falconer. *Appl. Catal. B*, **14**, 23 (1997).

201. C. Binet, M. Daturi, and J.-C. Lavalley. *Catalysis Today*, **50**, 207 (1999).

202. R.M. Ferrizz, G.S. Wong, T. Egami, and J.M. Vohs. *Langmuir*, **17**, 2464 (2001).

203. R. Craciun. *Solid State Ionics*, **110**, 83 (1998).

204. Y. Liu, T. Hayakawa, K. Suzuki, S. Hamakawa, T. Tsunoda, T. Ishii, and M. Kumagai. *Appl. Catal. A*, **223**, 137 (2002).

205. W.-J. Shen, Y. Ichihashi, and Y. Matsumura. *Catal. Lett.*, **79**, 125 (2002).

206. W.-J. Shen, Y. Ichihashi, M. Okumura, and Y. Matsumura. *Catal. Lett.*, **64**, 23 (2000).

207. R.N.R. Mulford and C.E. Holley. *J. Phys. Chem.*, **59**, 1222 (1955).

208. W.L. Korst and J.C. Warf. *Inorg. Chem.*, **5**(10), 1719 (1966).

209. Y.-H. Fan, M.-X. Wu, Q. Wu, S.-J. Liao, and J. Xu. *Chinese J. Chem.*, **20**, 1450 (2002).

210. W. Mueller, J.P. Blackledge, and G.G. Libowitz, *Metal Hydrides*. 1968, Academic Press: New York and London.

211. K.H. Gayer and W.G. Bos. *J. Phys. Chem.*, **68**, 2569 (1964).

212. M. Hadano, N. Urashihara, S. Terada, D. Katsuya, and H. Uchida. *J. Alloys Comp.*, **330-332**, 498 (2002).

213. D. Teschner, A. Wootsch, T. Röder, K. Matsuek, and Z. Paál. *Solid State Ionics*, **142**, 709 (2001).

214. M. Hadano, N. Urashihara, T. Inoue, and H. Uchida. *J. Alloys Comp.*, **293-295**, 403 (1999).

215. M. Brill, J. Bloch, D. Shmariahu, and M.H. Mintz. *J. Alloys Comp.*, **231**, 368 (1995).

216. D. Sarussi, I. Jacob, J. Bloch, N. Shamir, and M.H. Mintz. *J. Alloys Comp.*, **191**, 91 (1993).

217. Y. Maruyama, S. Motohashi, N. Sakai, M. Tanaka, H. Ogata, and Y. Kubazono. *Synthetic Metals*, **135-136**, 737 (2003).

218. K.I. Hardcastle and J.C. Warf. *Inorg. Chem.*, **5**, 1728 (1966).

219. C.E. Holley, R.N.R. Mulford, and F.H. Ellinger. *J. Phys. Chem.*, **59**, 1226 (1955).

220. R. Burtovyy and M. Tkacz. *Solid State Communications*, **131**, 169 (2004).

221. A. Wurtz. *Comp. Rend.*, **18**, 702 (1884).

222. *Metal Hydrides*, ed. W.M. Mueller, J.P. Blackledge, and G.G. Libowitz, New York and London: Academic Press (1968).

223. N.P. Fitzsimons, W. Jones, and P.J. Herley. *J. Chem. Soc. Faraday Trans.*, **91**, 713 (1995).

224. N.P. Fitzsimons, W. Jones, and P.J. Herley. *Catal. Lett.*, **15**, 83 (1992).

225. Z. Paál and P.G. Menon, *Hydrogen Effects in Catalysis*, New York: Marcel Dekker Inc. (1988).

226. L.K. Heung and G.G. Wicks. *J. Alloys Comp.*, **293-295**, 446 (1999).

227. H. Imamura, T. Konishi, Y. Sakata, and S. Tsuchiya. *J. Chem. Soc. Faraday Trans.*, **88**(15), 2251 (1992).

228. H. Imamura, T. Konishi, Y. Tokunaga, Y. Sakata, and S. Tsuchiya. *Bull. Chem. Soc. Jpn.*, **65**, 244 (1992).

229. H. Imamura, K. Igawa, Y. Sakata, and S. Tsuchiya. *Bull. Chem. Soc. Jpn.*, **69**, 325 (1996).

230. H. Imamura, M. Suzuki, Y. Sakata, and S. Tsuchiya. *J. Alloys Comp.*, **303-304**, 514 (2000).

231. C. Padeste, N.W. Cant, and D.L. Trimm. *Catal. Lett.*, **18**, 305 (1993).

232. W.-J. Shen, Y. Ichihashi, H. Ando, Y. Matsumura, M. Okumura, and M. Haruta. *Appl. Catal. A*, **217**(1-2), 231 (2001).

233. T. Shido and Y. Iwasawa. *J. Catal.*, **136**(2), 493 (1992).

234. G.J. Millar, C.H. Rochester, and K.C. Waugh. *J. Chem. Soc. Faraday Trans.*, **87**(9), 1467 (1991).

235. T. van Herwijnen and W.A. de Jong. *J. Catal.*, **63**, 83 (1980).

236. T. Salmi and R. Hakkarainer. *Appl. Catal.*, **49**, 285 (1989).

237. T. Takagua, G. Pleizer, and Y. Amenomiya. *Appl. Catal.*, **18**, 285 (1985).

238. S. Fujita, M. Usui, and N. Takezawa. *J. Catal.*, **134**, 220 (1990).

239. C.V. Ovesen, P. Stoltze, J.K. Norksov, and C.T. Campbell. *J. Catal.*, **134**, 445 (1992).

240. C.-S. Chen, W.-H. Cheng, and S.-S. Lin. *Catal. Lett.*, **68**, 45 (2000).

241. C.-S. Chen and W.-H. Cheng. *Catal. Lett.*, **83**(3-4), 121 (2002).

242. C. Li, Y. Sakata, T. Arai, K. Domen, K.-I. Maruya, and T. Onishi. *J. Chem. Soc. Faraday Trans.*, **85**, 929 (1989).

243. A. Martinez-Arias, M. Fernandez-Garcia, O. Galvez, J.M. Coronado, J.A. Anderson, J.C. Conesa, J. Soria, and G. Munuera. *J. Catal.*, **195**, 207 (2000).

244. R. Rajasree, J.H.B.J. Hoebink, and J.C. Schouten. *J. Catal.*, **223**, 36 (2004).

245. G. Sedmak, S. Hocevar, and J. Levec. *J. Catal.*, **222**, 87 (2004).

246. M.Y. Smirnov and G.W. Graham. *Catal. Lett.*, **72**, 39 (2001).

247. Y. Li, Q. Fu, and M. Flytzani-Stephanopoulos. *Appl. Catal. B*, **27**, 179 (2000).

248. K.T. Hindle. PhD Thesis, University of Glasgow (2004).

249. R.A. Koeppel, J.T. Wehrli, M.S. Wainwright, D.L. Trimm, and N.W. Cant. *Appl. Catal. A*, **120**, 163 (1994).

250. C.J. Brinker, R.K. Brow, D.R. Tallant, and R.J. Kirkpatrick. *J. of Non-Crystalline Solids*, **120**, 26 (1990).